The role of cortical layer 6b in local and global brain state control

Elise Meijer

St John's College
Department of Physiology, Anatomy and Genetics
University of Oxford

Thesis submitted for the degree of Doctor of Philosophy

Trinity Term 2023

The role of cortical layer 6b in local and global brain state control

Abstract

Layer 6b (L6b) is the deepest cortical layer, is found in many species and partially derived from subplate. Evolutionary conversation of subplate-derived cells into adulthood and abnormalities in their human homologue, interstitial white matter neurons, in neuropsychiatric disorders suggest functional importance, but their function is currently unknown. It has been shown in somatosensory cortex that subsets of L6b receive long-range intracortical input and project selectively to higher order thalamus. Moreover, L6b subpopulations can be activated by orexin in vitro. Therefore, L6b could play a role in brain state control, potentially via an orexin-gated mechanism.

In this project, I performed continuous EEG/EMG recordings in freely moving Drd1a-Cre;Snap25$^{fl/fl}$;TdTom, "L6b silenced" mice, in which regulated synaptic vesicle release is selectively ablated from a subset of L6b. Distribution of vigilance states and sleep fragmentation were unchanged, but there was a reduction in theta power during wakefulness and REM, and a reduction in 3-30 Hz frontal EEG power during NREM. After sleep deprivation, EEG slow wave activity dissipated at a lower rate. Silencing L6b also changed in vivo responses to orexin. Orexin A increased maximal wakefulness episodes duration, and this increase was larger in L6b silenced animals. In NREM, orexin A and B increased sleep-wake attempts in both genotypes, and orexin A caused a relative increase in 3-30 Hz frontal EEG spectral power in both genotypes, which extended to 0.5-3.0 Hz only in L6b silenced animals. In an auditory oddball paradigm, I found increased within-paradigm and decreased between-paradigm adaptation in L6b silenced animals, as well as an overall reduction of early peak amplitudes.

Altogether, the findings in this project demonstrate that L6b has a role in sleep-wake regulation, sleep homeostasis and adaptation, and that there is an interaction between L6b and orexin signalling in vivo. These findings contribute to establishing the role of L6b in brain state control.

Acknowledgements

First and foremost, I would like to thank Prof Zoltán Molnár and Prof Vlad Vyazovskiy for being excellent supervisors. Zoltán, you suggested this project and I am so happy you did. Your enthusiasm is endless and your drive to bring scientists together has brought many enjoyable discussions. Vlad, thank you for your advice, patience, and support, for giving direction when needed but also freedom to try things out by myself.

I would also like to thank Anna Hoerder-Suabedissen and Tomoko Yamagata as you both helped with shaping the first steps of this project. Anna, I am very grateful for learning from you, for your knowledge, kindness, and dry humour. Tomoko, you helped me set up my first EMG/EEG recordings and your joy in doing experiments is contagious. I would also like to thank Prof Matthew Larkum, Dr Tim Zolnik and prof Britta Eickholt, for hosting me in Berlin for three months. The research visit to your lab was stimulating and inspiring.

Thank you to all members of the Molnár and Vyazovskiy labs. In specific, Sara 'the best friend to miss a plane with', Auguste, Atreyi and Marissa: you made the experience so much more fun. Lukas, thank you for your help with getting started in the world of sleep, in the lab, and in Oxford.

Beyond the lab, I would like to thank Maja, partner in crime for planning hiking trips and my favourite stroke's woman in St John's College Boat Club. To Gemma, Pol, and Bruno, thank you for being fantastic housemates during the pandemic. From taskmaster New Year's Eve to coffee breaks and drinks in South Park, you have kept me sane in those weird corona years.

I would also like to thank my current colleagues at the department of Ophthalmology in Utrecht, as you made the transition back into clinical medicine so much smoother and more enjoyable.

Friends from medicine: Remi, Simone, Gautam, Floor, Siri, Timon, Dorine and Nina: thank you for all the fun adventures all over the world, for the spontaneous dinners during medical school and thereafter, and for hosting me when I was in Utrecht during the DPhil. I hope we experience many more adventures together.

Thank you Rishi, for being such a support in the past few years, by celebrating the end of a round of surgeries together and by being a buddy on weekend trips to the BSB - and happily also elsewhere. I am so happy you came into my life. Thank you as well to my family. Mum, dad, Aldert you have always been there when I needed you and I could not have done this without you.

I would also like to thank Prof David Corey, Bence György and Maryna Ivanchenko, since my master's project in your lab fuelled my enthusiasm in science and drive to pursue a career as a clinician-scientist. I am very grateful to the O'Sullivan Family Charitable Trust and St John's College Oxford for funding my DPhil, and the University of Oxford Scatcherd European Scholarship for financially supporting my visit to Berlin.

I would also like to thank Prof Antoine Adamantidis and Prof Randy Bruno for agreeing to be my examiners.

Declaration and attributions

I declare that no part of this thesis has been, or is being, submitted for any qualification other than the degree of Doctor of Philosophy at the University of Oxford.

Research presented in this thesis was carried out under the supervision of Prof Zoltán Molnár and Prof Vladyslav Vyazovskiy. All work presented is my own except were explicitly stated in the text as detailed below:

For the surgeries and the sleep deprivation experiment presented in Chapter 3, I was assisted by members of the Vyazovskiy lab. A special notion to Sian Wilcox, who looked after my animals when I was not able to visit the laboratory because of a covid infection. The circadian screen in Chapter 3 has been performed by Dr Luiz Guidi, in collaboration with Prof Peter Oliver. I reanalysed the blinded raw data that I received from Dr Luiz Guidi with guidance and advice from Dr Lewis Taylor and Prof Peter Oliver.

Dr Atreyi Chakrabarty gave me instructions on implanting cannulas for intracranial infusions and setting up the infusion system for Chapter 4. She and other members of the Vyazovskiy laboratory assisted with surgeries. The pilot food intake measurements in Chapter 4 were performed together with Marissa Mueller, who was involved in the orexin experiment as part of her MSc in Neuroscience dissertation project. She also assisted with implantation surgeries and intracerebroventricular injections.

Table of Contents

Table of Figures

List of tables

Abbreviations

ACh	Acetylcholine
AEP	Auditory evoked potential
ABR	Auditory brainstem response
ANOVA	Analysis of Variance
ATP	Adenosine triphosphate
BSB	Biomedical Sciences Building
CA3	Cornu ammonis region of hippocampus
CAG	Cytomegalovirus enhancer fused to chicken beta-actin promoter
CCK	Cholecystokinin
CCK1R	Cholecystokinin receptor type 1
CCK2R	Cholecystokinin receptor type 2
Cplx3	Complexin 3
CRY	Cryptochrome
CSF	Cerebrospinal fluid
Ctgf	Connective tissue growth factor
DAPI	4′,6-diamidino-2- phenylindole
DEV	Deviant tone
DMH	Dorsomedial hypothalamus
DORA	Dual-receptor antagonist
DR	Dorsal raphe nucleus
Drd1a	Dopamine receptor 1a
EEG	Electro-encephalogram
EMG	Electro-myography
EPSC	Excitatory postsynaptic potential
ERP	Event-related potential
FIJI	Fiji is Just ImageJ
GABA	gamma-amino butyric acid
GPCR	G-Protein coupled receptor
ICV	Intracerebroventricular
IWNs	Interstitial white matter neurons
KO	Knockout
L1	Cortical layer 1
L2/3	Cortical layer 2/3
L4	Cortical layer 4
L5	Cortical layer 5
L6	Cortical layer 6
L6a	Cortical layer 6a
L6b	Cortical layer 6b
LC	Locus coeruleus
LDT	Laterodorsal tegmental nucleus
LFP	Local field potential
LH	Lateral hypothalamus
Lpar1	Lysophosphatidic acid receptor 1
M1	Primary motor cortex
MCH	Melanocortin concentrating hormone
ML	Midline
MMN	Mismatch negativity
moxD1	Monooxydase Dbh-like 1
MUA	Multi-unit activity
NPY	Neuropeptide Y

NREM	Non-rapid eye movement sleep
NTSR1	Neurotensin receptor type 1
NTSR2	Neurotensin receptor type 2
Nurr1	Orphan nuclear receptor 1
Nxph3	Neuroexophillin 3
ORXA	Orexin A
ORXB	Orexin B
OX1R	Orexin receptor type 1
OX2R	Orexin receptor type 2
P1	Postnatal day 1
PBS	Phosphate buffered saline
PBSA	Phosphate buffered saline with 0.05% azide
PER	Period
PFC	Prefrontal cortex
PIL	Personal license
PPL	Project license
Pom	Posterior medial nucleus
PPT	Pedunculopontine tegmental nucleus
PV	Parvalbumin
REM	Rapid eye movement sleep
RS	Repetition suppression
S1	Primary somatosensory cortex
S2	Secondary somatosensory cortex
SCN	Suprachiasmatic nucleus
SD	Sleep deprivation
SEM	Standard error of the mean
SLD	Sub laterodorsal region
SNARE	N-ethylamide-sensitive factor attachment protein receptor
SNAP25	Synaptosomal Associated Proteins of 25 kiloDalton
SPZ	Subparaventricular zone
SSA	Stimulus-specific adaptation
SST	Somatostatin
STD	Standard tone
SWA	Slow-wave activity (0.5-4.0 Hz)
SWE	Slow wave energy (SWA x Time)
SWS	Slow wave sleep
TDT	Tucker Davis Technologies
TdTom	TdTomato
Tmem163	Transmembrane protein 163
TMN	Tuberomammillary nucleus
TRN	Reticular thalamic nucleus
V1	Primary visual cortex
VIP	Vasoactive intestinal protein
vlPAG	Ventrolateral periaqueductal grey
VLPO	Ventrolateral preoptic nucleus
VPM	Ventroposterior medial
WT	Wildtype animals (Drd1a-Cre$^{-/-}$;TdTom;Sanp25$^{fl/fl}$, C57BL6 background)

1 General introduction

1.1 Introduction

A fundamental property of the neocortex or isocortex is its laminated structure, a characteristic that was already delineated in the anatomical drawings by Ramon y Cajál and Lorente de Nó over a century ago (Lorente de Nó, 1922; Ramon Y Cajál, 1904). Anatomy reflects function, and the cortical lamination that is visible in histological samples indicates the presence of distinct functional entities. It is because of historical reasons that we define six cortical layers, from layer 1 (L1) externally to layer 6 (L6) internally, but in early anatomical studies, seven layers were distinguished (Lorente de Nó, 1922; Ramon Y Cajál, 1904). In current descriptions of the cortex, the innermost "7th layer" is only giving a status of sublayer within layer 6, layer 6b (L6b), and it is often overlooked in functional schemes of cortical processing. However, L6b is unique amongst cortical layers, both for its developmental origin, but also in its responsiveness to neuromodulators and intracortical and subcortical connectivity (Feldmeyer, 2023; Molnár, 2019; Thomson, 2010). In this thesis, I describe my investigation of the role of the enigmatic cortical L6b in sleep-wake regulation and brain state control, with electrophysiological recordings in a mouse model in which the function of L6b is chronically silenced.

In this *General Introduction* chapter, I first give a general overview of sleep, including the electrophysiological definitions of different stages of sleep. I next describe the neurobiological mechanisms known to underly sleep, and brain structures involved in the regulation of sleep and wakefulness. In the following section, I briefly review the mechanisms that have been implicated in the regulation of sleep amount, timing, and intensity. After this general introduction into the

field of sleep, I will focus on cortical L6b, and describe its developmental origin, composition, connectivity, and responsiveness to specific neuromodulators. I will conclude this chapter with formulating a hypothesis on the functional role of L6b and stating the aims for this DPhil project.

1.2 Sleep

Sleep is a paradox in evolutionary biology, occurring in one form or another in all organisms studied so far, but at the same time being evolutionary expensive, increasing the risk of predation and other dangers, and reducing the time that can be spent in other activities that are important for survival such as feeding, mating, and learning (Anafi et al., 2019; Campbell and Tobler, 1984). The function of sleep is a matter of debate, but in all organisms studied so far, control mechanisms exist to compensate for a lack of sleep (Achermann and Borbély, 2003; Borbély, 1982) and it is often argued that a complete absence of sleep will have detrimental, eventually fatal, consequences (Cirelli and Tononi, 2008; Rechtschaffen and Bergmann, 2002).

Sleep can be defined behaviourally, as a reversible state of quiescence characterised by reduced responsiveness to external stimuli, typically spent in a species-specific posture and engaged in at a species-specific time of 24h (Campbell and Tobler 1984). A more objective way of defining sleep in humans and experimental animals requires recording of electrophysiological signals from the brain, as described below, which allows distinction between wakefulness, NREM and REM sleep, which will be described below, and can give insights into the mechanisms underlying the different sleep-wake states.

1.2.1 Recording states of sleep and wakefulness

The electro-encephalogram (EEG) was first recorded in humans by the German Psychiatrist Berger in 1924 and is a measurement of the electrical potential difference between two electrodes places resulting from the summation of all ionic processes occurring in the brain tissue in the proximity of the electrodes (Berger, 1929; Buzsáki et al., 2012). For recording an EEG, surface electrodes are positioned on the scalp, and electric potentials are recorded at a “global”

level, i.e., as a sum of signals from large brain regions. EEGs can be recorded in humans or model animals and show sleep-wake state specific patterns (Berger, 1929; Buzsáki et al., 2012). Electrical potentials can also be recorded from within the brain, for example, with a silicon probes in the cortex or a subcortical structure, that have one or more electrodes to record potentials from a local area, local field potential (LFP). Waveforms can be extracted from these signals, resulting in a measure of firing of a neuronal population, or multi-unit activity (MUA). Zooming in further, signals can be recorded intracellularly, with in vivo or in vitro patch-clamp recordings (Buzsáki et al., 2012).

For the definition of sleep-wake states, it is most common to record global or local field potentials with EEG or LFP, respectively, in combination with a registration of muscle activity with electromyography (EMG). With EMG, active movements can be quantified, as well as sleep-linked atonia, which is detected as an absence of postural tone (Sulaman et al., 2023).

In humans, sleep consists of cycles of three stages of non-rapid eye movement (NREM) sleep, NREM1-3, and one stage of rapid eye movement (REM) sleep (Adamantidis et al., 2019). In mice, which are used in the research presented in this thesis, only one stage of NREM sleep is defined, which can be followed by REM or ended with a transition back to wakefulness (Adamantidis et al., 2019; Thomas et al., 2022; Traut et al., 2023).

Sleep-wake state specific activity patterns can be referred to as brain states in general, as cortical states when they are recorded from cortex, or as vigilance states or sleep-wake states when they refer to the global behavioural sleep-wake state of an animal (Harris and Thiele, 2011; Tantirigama et al., 2020).

The activity pattern linked to wakefulness consists of irregular population activity in EEG/LFP recordings that shows high-frequency, low-voltage oscillations, and a predominantly active EMG (Figure 1.1). During NREM sleep, EEG/LFP show low-frequency, high-amplitude waves; the EMG is quiet, apart from the heart rate that may become apparent in the absence of skeletal muscle activity. During REM sleep, EEG/LFP show a pattern that resembles wakefulness, with smaller-amplitude, higher-frequency oscillations. Characteristic of REM sleep are theta-

frequency (5-10 Hz) oscillations generated in the hippocampus. Theta oscillations can also occur in wakefulness but the EMG, which shows muscle activity during theta rich wakefulness and is quiet because of muscle atonia during REM sleep, allowing differentiation between these states. A deviation from this principle is phasic REM sleep, when regular bursts of muscle activity are visible on the EMG (Adamantidis et al., 2019).

Vigilance states exhibit the patterns shown below for wakefulness, NREM and REM sleep at a global, brain wide level. However, with LFP and MUA, it has been shown that local vigilance states are not always consistent with global vigilance states. For instance, during wakefulness, local sleep oscillations have been recorded in rats (Vyazovskiy et al., 2011) and humans (Huber et al., 2004). Moreover, some animals only sleep with parts of their brain, such as dolphins which produce delta waves in only half of their brain during NREM sleep (Mukhametov et al., 1977). The occurrence of local brain states has been explained with local differences in sleep-wake history, activating sleep homeostatic mechanisms (Krueger et al., 2008), which will be described further in section 1.2.4.

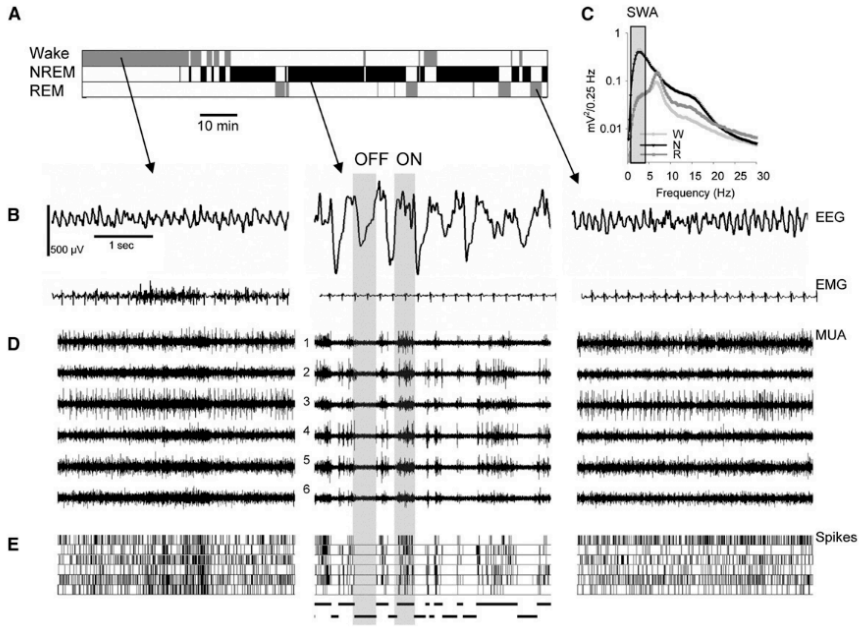

Figure 1.1: Electrophysiological patterns across vigilance states. Representative traces from a single rat. (A) 24-hour hypnogram. (B) EEG and EMG traces in Wake (left), NREM (middle), REM (right). (C) 24-hour EEG spectral power, with slow wave activity (SWA) in the 0.5-4 Hz range indicated as a shaded area. (D) raw multiunit activity (E) raster plots of spiking activity. From Vyazovskiy et al 2009.

1.2.2 Sleep-wake oscillations

Fourier transformation of field potentials reveals their frequency components; defined frequency bands have been linked to activity in specific neuronal populations. I will give an overview of the major oscillations observed during sleep and wakefulness - with an emphasis on the oscillations detected during NREM sleep.

NREM sleep

Slow waves (0.5-4.0 Hz) are the hallmark electrographical feature of NREM sleep or slow wave sleep (SWS). Slow waves can be subdivided into slow oscillations (<1 Hz) and delta waves (1-4 Hz) (Steriade et al., 1993a), but their distinction and the underlying mechanisms remain a matter of discussion, so they are often considered together as "slow waves".

Slow waves are the result of synchronous firing of populations of cortical and thalamic neurons and originate more often in the prefrontal and orbitofrontal regions, from where they travel in an anteroposterior direction (Massimini et al., 2004; Steriade et al., 1993b, 2001; Vyazovskiy et al., 2009). A slow wave consist of an UP phase, when neurons are depolarised, and a DOWN phase, during which neurons are hyperpolarised (Poulet and Petersen, 2008), and these membrane states coincide with the ON phase of neuronal firing and the OFF phase of neuronal quiescence, respectively (Csercsa et al., 2010; Vyazovskiy et al., 2009)(Figure 1.1D,E).

In search for the origin of the slow wave, signals have been recorded from deafferented cortical slabs; the detection of slow waves in these samples suggested that slow waves arise from the cortex (Timofeev et al., 2000). However, blocking the output from the thalamus to the cortex also markedly reduces the occurrence of slow waves (David et al., 2013), demonstrating that both thalamic and cortical neuronal populations contribute to the generation of slow waves. Intrinsically bursting, bistable neuronal populations have been detected in L2/3, L5 and L6b of the neocortex, and these may initiate or at least participate in slow waves (Le Bon-Jego and Yuste, 2007; Mao et al., 2001; Wenger Combremont et al., 2016a). At the thalamic level, midline and

dorsal thalamic nuclei may have an important contribution in the timing and synchrony of cortical slow waves (Gent et al., 2018).

Phase-locked with slow waves are sleep spindles (Figure 1.2B). These waxing-and-waning bursts of activity oscillate at 10-15 Hz, the sigma frequency range, and arise from interaction between thalamus, reticular thalamic nucleus (TRN) and cortex (Adamantidis et al., 2019). Sleep spindles are generated in a process involving intrinsically firing inhibitory neurons in the TRN that send bursts of activity to first order or sensory thalamic nuclei (Crunelli et al., 2006; Steriade et al., 1993c)(Figure 1.2A). This results in strong hyperpolarization in thalamic neurons, which triggers a depolarising I_h current, leading to opening of T-type Ca^{2+} channels, resulting in a low-threshold Ca^{2+} spike, and a burst of action potentials from the sensory thalamic neurons to L4 of the cortex. After 0.5-2 seconds, the sleep spindle is ended by input from the cortex (Bonjean et al., 2011).

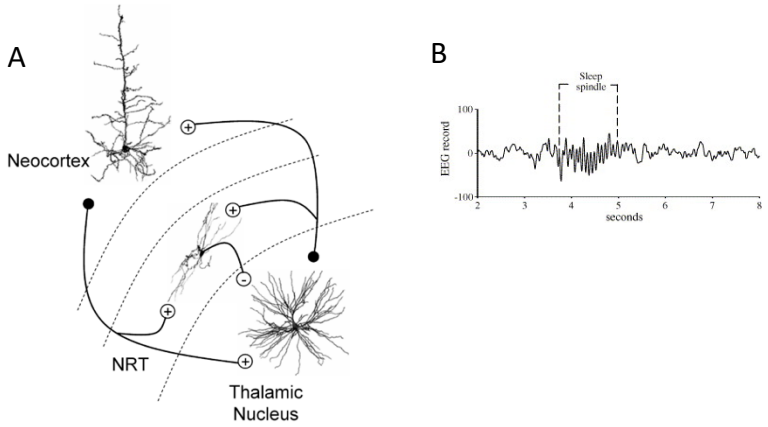

Figure 1.2 Sleep spindles.
(A) Sleep spindles are generated by an interaction between inhibitory thalamic reticular nucleus (in this Figure shown as NRT) neurons, that evoke burst firing in excitatory thalamic neurons. These neurons activate cortical neurons in L4, which project to TRN and thalamus to terminate the spindle Figure from Crunelli et al 2006.
(B) Example of a sleep spindle on an EEG recording. Figure from Ventouras et al 2005.

The functional role of sleep spindles is not fully established. They occur more frequently around NREM-REM transitions and may contribute to these transitions (Bandarabadi et al., 2020). They have also been linked to sensory disconnection and memory consolidation, with the degree of coupling between slow waves and sleep spindles being the most important predictor of memory consolidation (Hahn et al., 2019; Helfrich et al., 2018). Spindle-slow wave coupling is thought to involve a prefrontal circuit, and sleep spindle deficits are found in schizophrenia patients who also have abnormalities in TRN, thalamus and prefrontal cortex (PFC) coupling (Ferrarelli and Tononi, 2017). It is likely that sleep spindles cannot be regarded as a dichotomous event with a single function but that their effects are diverse and depend on their electrophysiological appearance, or 'oscillatory quality', which also determines the degree of coupling of slow waves and spindles (Blanco-Duque et al., 2023). In humans, a classification has been made between slow (9-13 Hz) and fast (13-16 Hz) sleep spindles, recruiting frontal and hippocampal areas, respectively (Schabus et al., 2007).

Memory consolidations is also thought to involve sharp wave ripples (SWRs), which consist of a sharp nonperiodic wave and a fast periodic ripple (150-200 Hz). SWRs play a role in hippocampus-cortex synchronization, which contributes to the consolidation of declarative memories (Khodagholy et al., 2017).

Infraslow oscillations have a frequency of <0.1 Hz and occur in cortex, thalamus, basal ganglia, hippocampus, and locus coeruleus (Adamantidis et al., 2019). Infraslow oscillations at the specific 0.02 Hz frequency show correlation with sleep spindles and contribute to NREM sleep stability. During the UP phase of 0.02 Hz waves, animals are less likely to wake up from auditory stimulation, and during the DOWN phase, they are more likely to do so (Lecci et al., 2017).

K-complexes are 9-16 Hz oscillations are irregularly occurring waves that can be elicited by environmental stimuli and derive their name from the effect of auditory stimuli of 'knocks' by researchers (Adamantidis et al., 2019) K complexes are a reflection of coupling between sleep spindles, slow waves and slow oscillations and are thought to contribute to sleep stability (Amzica and Steriade, 2002; Loomis et al., 1935).

REM sleep

REM sleep is also named paradoxical sleep, because of the apparent paradox of a behaviourally asleep animal with a highly active brain, showing high-frequency, low-amplitude oscillations (Jouvet, 1959). The characteristic brain waves of this state are theta oscillations, which are 6-9 Hz waveforms (Figure 1.1B) that are generated in an interaction between the entorhinal cortex and the CA3 region of the hippocampus (Buszáki, 2002) and have been linked to memory consolidation and emotional processing during REM sleep (Boyce et al., 2016; Hutchison and Rathore, 2015).

Phase-locked with theta oscillations are gamma oscillations that have a frequency between 30-100 Hz, although in different studies several subdivisions have been made within the 30-100 Hz range. Gamma oscillations are regarded as an expression of neocortical GABAergic firing and have been linked with higher order cognitive processing (Fellous and Sejnowski, 2000).

Wakefulness

Some of the oscillations that occur during sleep also occur during wakefulness, but the exact shape of the waveforms and their functional significance can differ between brain states. For example, theta and gamma oscillations are not only observed in REM but also in wakefulness and in the latter reflect a substate of exploratory wakefulness and higher cognitive processing, respectively (Bragin et al., 1995; Buszáki, 2002; Vassalli and Franken, 2017). Other waveforms recorded during wakefulness include alpha waves (9-12 Hz) which are observed in the absence of sensory input when awake subjects close their eyes and are linked to perception preparation (Bazanova and Vernon, 2014; Busch et al., 2009), and beta waves (13-30 Hz), which are linked to the continuation of ongoing actions (Engel and Fries, 2010).

1.2.3 Neurobiology of brain state transitions

Transitions between wakefulness and sleep are tightly regulated, to ensure rapid and complete transitions according to environmental demands. Several theoretical models have been proposed

to explain sleep-wake transitions, which I discuss below, including the brain state stabilizing influence of orexin.

The "flip-flop" model

In the 'flip-flop model', vigilance state control is compared to an electrical switch, and sleep-wake transitions are regulated by the interplay of subcortical nuclei that are mutually inhibiting, thus allowing only one state to exist at a time (Saper et al., 2001).

In this model, wakefulness is initiated with activation of the ascending arousal system. In foundational experiments, Moruzzi and Magoun observed that electrical stimulation of the reticular formation in the brainstem results in desynchronization of the cortex such as seen in wakefulness (Moruzzi and Magoun, 1949). Later on, specific nuclei were identified (Figure 1.3).

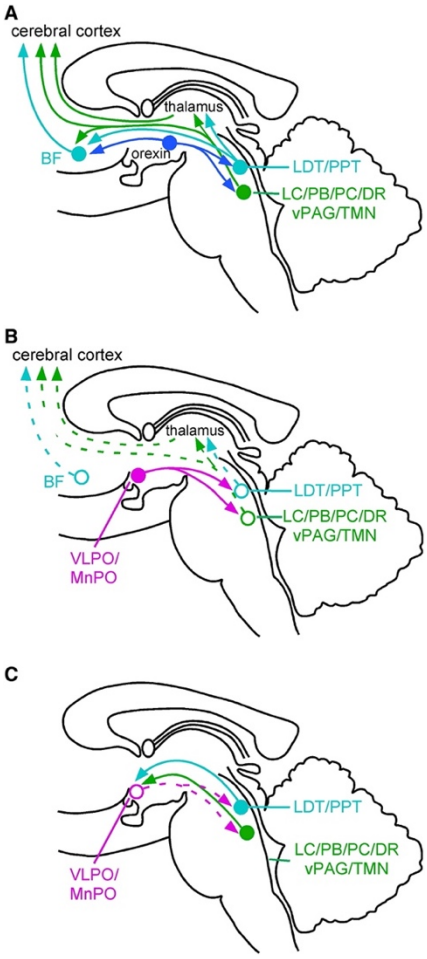

Figure 1.3: The sleep wake switch. (A) Wake active nuclei of the ascending arousal system, with a branch from LDT/PPT (green) to thalamus, basal forebrain and cortex, and a branch from the monoaminergic nuclei (aqua) to thalamus, basal forebrain, and cortex. Orexin further promotes wakefulness. (B) The sleep active VLPO inhibits the ascending arousal system. (C) The mutually inhibiting nuclei ensure rapid and complete sleep state switching. Figure from Saper et al 2010.

A first branch of the ascending arousal system starts in the brainstem, in the cholinergic laterodorsal tegmental (LDT) and pedunculopontine tegmental (PPT) nuclei which project to thalamus, TRN, lateral hypothalamus (LH), and basal forebrain (Satoh and Fibiger, 1986) (Figure 1.3A, aqua). A second branch starts at the monoaminergic nuclei in the brainstem: the locus coeruleus (LC) releasing noradrenaline, the tuberomammillary nucleus (TMN) releasing histamine, the dorsal raphe (DR) nucleus releasing serotonin and the ventrolateral periaquaductal grey (vlPAG) releasing dopamine (Figure 1.3A, green). The monoaminergic nuclei innervate the LH, basal forebrain, and cerebral cortex (Saper et al., 2010). Next, the LH releases orexin and melanocortin-concentrating hormone (MCH), and the basal forebrain releases acetylcholine (Saper et al., 2010). Thus, the cortex is innervated directly but also indirectly, via the basal forebrain and LH, and this indirect route provides an amplification mechanism (Saper et al., 2010). The side branches to the TRN and midline thalamic nuclei also activate the cortex (Moruzzi and Magoun, 1949; Saper et al., 2010).

During sleep, the ventrolateral preoptic nucleus (VLPO) becomes most active (Figure 1.3B, magenta). It is located at the anterior side of the hypothalamus and produces both GABA and galanin, which inhibit the nuclei of the ascending reticular arousing system, both the PPT/LDT branch and the monoaminergic branch (Sherin et al., 1996, 1998). The VLPO predominantly promotes NREM sleep, but experimental lesioning of the VLPO in rats leads to a robust reduction of both NREM and REM sleep (Lu et al., 2000; Sherin et al., 1996). At the end of a sleep episode, PPT/LDT and monoaminergic nuclei inhibit the VLPO and promote the transition back to wakefulness (Saper et al., 2010)(Figure 1.3C)..

Within sleep, transitions between NREM and REM sleep are regulated with another reciprocal switch system. With cFos labelling it has been shown that the extended VLPO promotes the onset of REM sleep (Lu et al., 2002). Within the extended VLPO, the GABAergic neurons in the vlPAG, LPT and sublaterodorsal region (SLD) play a key role (Figure 1.4A). To stay in NREM sleep, the vlPAG and LPT fire and inhibit the SLD, while during REM sleep, the SLD fires and inhibits the vPAG and LPT. NREM-REM transitions are further influenced by activity in the VLPO, orexin

neurons, LC and DR and the LDT/PPT (Figure 1.4B). REM sleep atonia is established by the effect of glutamatergic neurons of the SLD on spinal and medullary interneurons, and the transition to an EEG theta rhythm through ascending projections from glutamatergic SLD neurons to parabrachial nucleus and basal forebrain that drive cortical desynchronisation (Figure 1.4C)(Saper et al., 2010).

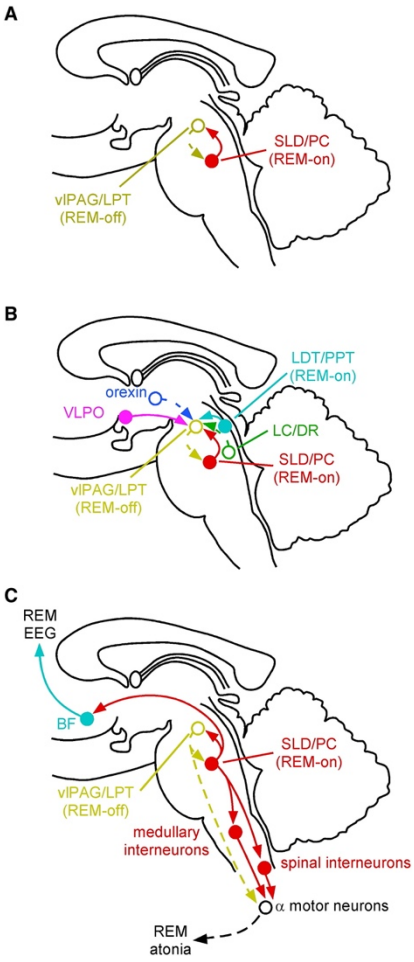

Figure 1.4 The regulation of transitions between NREM and REM sleep.
(A) REM-on neurons in the SLD/PC (red) and REM-off neurons in the vlPAG/LPT (gold) mutually inhibit each other, ensuring complete transition between NREM and REM.
(B) LC/DR, orexin, LDT/PPT, VLPO influence the switch to be towards REM-on or REM-off.
(C) a distinct population of glutamatergic neurons in the SLD (red) activates inhibitory neurons in the brain stem, leading to REM sleep atonia. Ascending glutamatergic projections from PC cause cortical desynchronisation and generation of theta rhythm. Figure from Saper et al 2010.

Orexin as a stabiliser of sleep wake states

The risk with a prompt sleep-wake switch is the possibility of unwanted and frequent transitions, which can occur when one side of the switch is broken, as each state will be closer to the pivot point (Saper et al., 2005). For instance, animal with VLPO lesions do not only exhibit less sleep, but also more frequent transitions between sleep and wake (Lu et al., 2000).

Orexin (also named: hypocretin; I use orexin throughout this DPhil thesis for no particular reason) neurons promote wakefulness, but also project to both sleep and wake active nuclei and in this way stabilize the 'flip-flop' switch (Figure 1.3). The effects of orexin on state stabilisation become apparent in narcolepsy patients, who often have a reduced number of orexin neurons in the lateral hypothalamus and in 90% of cases have reduced orexin A levels in the cerebrospinal fluid (Nishino et al., 2000; Peyron et al., 2000; Thannickal et al., 2000). Narcolepsy symptoms consist of excessive daytime sleepiness, sudden onset of sleep from wakefulness, cataplexy (sudden loss of muscle tone during wakefulness), sleep paralysis and hypnagogic hallucinations. A secondary diagnostic criterium is a lower concentration of orexin A in cerebrospinal fluid (Sakurai, 2007). Since narcolepsy patients do not experience a change in the total daily time spent awake or asleep, but rather suffer from unwanted transitions between sleep-wake states, narcolepsy is regarded as a disease of state instability (Sakurai, 2007).

The stabilizing function of orexin neurons is related to their connectivity. There are mutual projections between the VLPO and orexin neurons, but the VLPO does not express orexin receptors (Chou et al., 2002; Marcus et al., 2001; Sakurai et al., 2005; Yoshida et al., 2006). This causes the sleep promoting VLPO neurons to inhibit wakefulness through orexin but does not allow orexin neurons to promote sleep. The resultant consolidated wakefulness will then via sleep homeostatic mechanisms result in consolidated sleep (Saper et al., 2005).

The thalamocortical model

The 'flip flop model' describes how prompt and brain wide transitions between states of sleep and wakefulness can be established, but cannot explain how sleep-wake history plays a role in

likelihood of transitions, nor does it explain how local sleep or at least slow waves can occur in an otherwise awake brain (Krueger et al., 2008; Vyazovskiy et al., 2011).

It has been suggested that sleep may not be regulated by the interplay between subcortical nuclei, but that it is governed at a local level, by interactions between thalamus and cortex. In the thalamocortical model of sleep-wake regulation, it is postulated that local thalamocortical network activity determines the necessity of a state transition (Krueger and Obál, 1993; Krueger et al., 2008; Thomas et al., 2020). L5 neurons could be a driving factor for the initiation of local and consecutively global sleep, supported by the observation that mice with a functionally silenced population in L5 pyramidal neurons sleep markedly less than their control littermates (Krone et al., 2020). Moreover, two recent studies have assigned an important contribution in sleep regulation to PFC, both by driving sleep preparatory behaviours and by initiating REM sleep (Hong et al., 2023; Tossell et al., 2023). Whether thalamocortical network activity or subcortical neuromodulation is determining in state transitions is an open question.

1.2.4 Homeostatic and circadian regulation of sleep

After periods of prolonged wakefulness, the following sleep shows an increase in SWA and is more consolidated. The electrophysiological signature of this process is an exponential increase in low frequency activity during wakefulness and a consecutive exponential decline in SWA during NREM sleep (Guillaumin et al., 2018a; Krone et al., 2021; Milinski et al., 2021; Thomas et al., 2020; Vyazovskiy and Tobler, 2005; Vyazovskiy et al., 2009). The process is referred to as sleep homeostasis, or process S, and possible underlying mechanisms are still under active investigation (Borbély, 1982; Borbély et al., 2016; Daan et al., 1984).

The sleep homeostat could be set by the levels of brain energy stores (Scharf et al 2008), such as, adenosine, the metabolic end product of adenosine triphosphate (ATP) hydrolysis (Krueger et al., 2008; Obál and Krueger, 2003; Porkka-Heiskanen et al., 2004). Another theory suggests that the mechanism behind sleep homeostasis lies in cellular metabolism (Vyazovskiy and Harris, 2013). According to a third theory, the synaptic homeostasis hypothesis, the function

of sleep is to reduce the number of synapses formed during wakefulness, in order to only preserve essentials connections. In this explanation, sleep intensity is an expression of the number of synapses, which will diminish over time with the duration of sleep (Cirelli and Tononi, 2008). A fourth theory suggests phosphorylation as a sleep debt tracking mechanism (Tone et al., 2022).

Whether homeostatic control of sleep is based on metabolic, cellular, or synaptic processes (or all), sleep need is not only controlled by preceding sleep-wake history but also by the circadian rhythm, or process C (Daan et al., 1984). Several circadian oscillators are found in different organs throughout the body and serve a local pacemaker function, but these eventually rely on the 'master clock' of circadian pacemaker cells which is located in the suprachiasmatic nucleus (SCN) in the hypothalamus (Reppert and Weaver, 2002).

The molecular mechanism of the intrinsic pacemaker properties of the fly analogue of the SCN received the 2017 Nobel prize in Physiology or Medicine (Bargiello et al., 1984; Hardin et al., 1990; Liu et al., 1992; Price et al., 1998; Siwicki et al., 1988; Vosshall et al., 1994; Zehring et al., 1984). The core molecular clock is a transcriptional-translational loop and consists of the transcription factors CLOCK-BMAL1 that induce the expression of their own negative regulators Period (PER) / Cryptochrome (CRY). Once PER/CRY levels drop, CLOCK/BMAL1 can induce another round of expression, continuing the molecular cycle (Patke et al., 2020). The SCN receives input from specialised retinal ganglion cells during the light phase and projects to the subparaventricular zone (SPZ). The SPZ innervates the ventral dorsomedial hypothalamus (DMH) which promotes wakefulness by inhibiting the VLPO, and by stimulating orexin neurons in the LH (Deurveilher and Semba, 2005; Lu et al., 2001). Process S and process C interact extensively to allow dynamic adaptation to a changing environment, with experimental manipulations of circadian clock genes directly affecting sleep-wake regulation (Borbély et al., 2016; Laposky et al., 2005; Maywood et al., 2021; Wisor et al., 2002).

1.3 Cortical layer 6b

In this second part of the introduction, I describe the development, connectivity, responsiveness to neuromodulators, and a putative role in deviance detection of cortical L6b.

1.3.1 Developmental origin of L6b

Subplate neurons are amongst the earliest generated neurons in the cerebral cortex (Kostovic and Rakic, 1980, 1990). They are components of the subplate zone, which contains an extensive extracellular matrix and is therefore anatomically distinguishable in some species including human and mice (Kostović, 2020) (Figure 1.5). Cortical plate neurons are formed in the ventricular zone and migrate outwards via radial glial cells, which moves the subplate inwards (Bystron et al., 2008; Hoerder-Suabedissen and Molnár, 2015). During development, subplate neurons have an important role in the establishment of thalamo-cortico-thalamic networks, through the formation of transient connections with thalamocortical axons and also by forming a waiting compartment for afferent axons (Allendoerfer and Shatz, 1994; McConnell et al., 1989; Molnár and Blakemore, 1995; Molnár et al., 1998). When cortical development is completed, most subplate neurons die, but 10-20% survive and remain present as functional neurons into adulthood (Allendoerfer and Shatz, 1994; Price et al., 1997; Torres-Reveron and Friedlander, 2007). In mice, the remaining subplate neurons form a condensed cell layer at the bottom of the cortex named L6b; regarded as the human homologue are cell bodies interspersed between the white matter fibres below the cortex, interstitial white matter neurons (IWNs) (Duque et al., 2016; Kostović and Judaš, 2010; Kostovic and Rakic, 1980). Not all neurons in L6b are derived from the subplate; some neurons are formed later in cortical development (Marx and Feldmeyer, 2013). L6b or IWNs have been identified in many different species and this conservation suggests and evolutionary advantage of the survival of subplate neurons into adulthood (Bhagwandin et al., 2020; Reep, 2000; Swiegers et al., 2019, 2021a, 2021b).

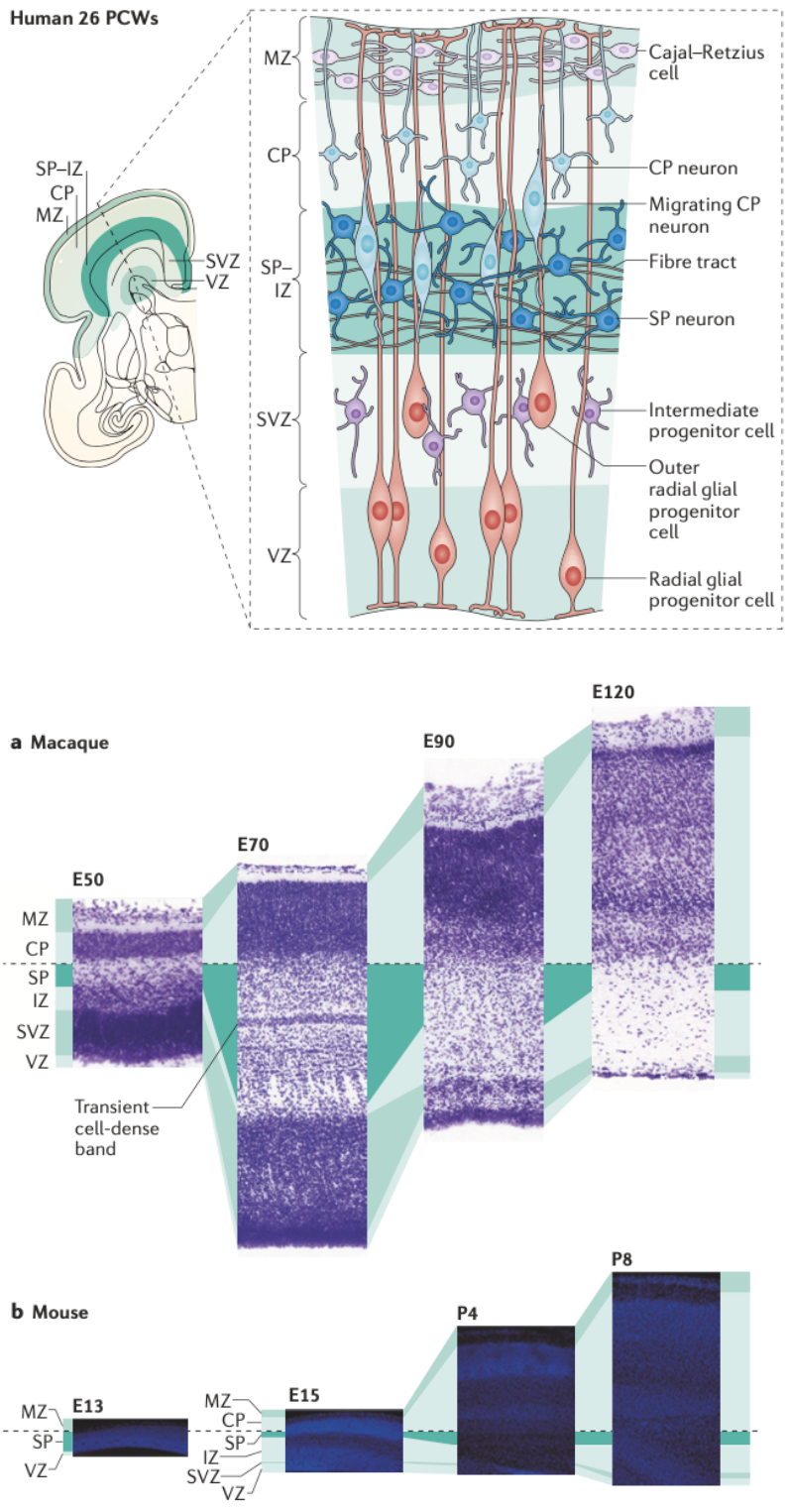

Figure 1.5: Development of the neocortex in mice and humans. (top) schematic representation of cortical development at 24 weeks post conception in humans. (bottom) histological images showing the changes in the composition of the neocortex in the course of development in macaque (a) and mouse (b). From Hoerder-Suabedissen & Molnár 2015.

1.3.2 Cellular composition of layer 6b

L6b, historically also referred to as multiform layer, is a heterogenous layer, with excitatory and inhibitory neurons that are diverse in their developmental origin, gene expression, morphology, connectivity, and responsiveness to various neurotransmitters (Kanold and Luhmann, 2010).

Most neurons in L6b are excitatory and with electrophysiology and biocytin filling followed by reconstruction and cluster analysis, five excitatory cell types have been described in L6b of rat somatosensory barrel cortex: pyramidal cells, inverted pyramidal cells, horizontal pyramidal cells, tangential pyramidal cells, and multipolar cells (Marx et al., 2017)(Figure 1.6).

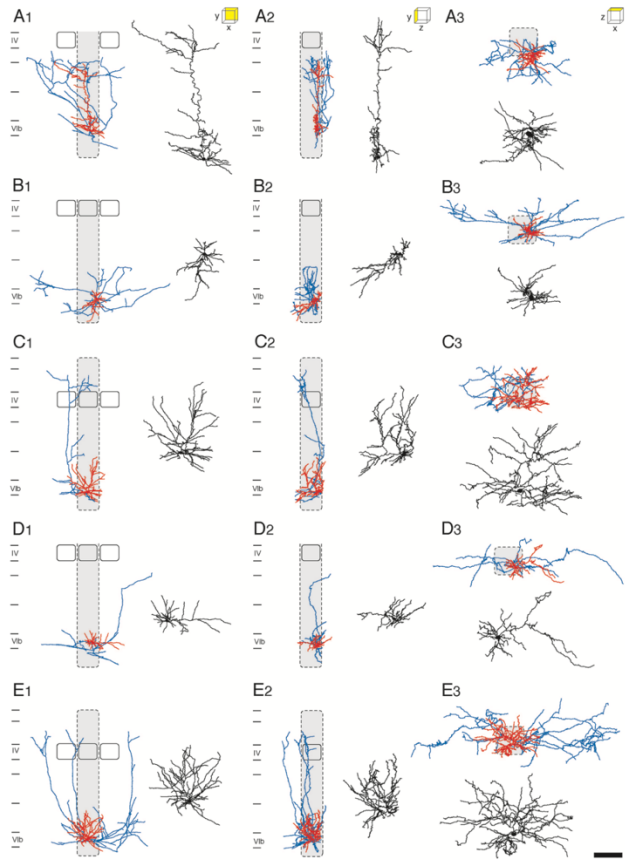

Figure 1.6: Excitatory cell types in layer 6b. Examples of individual neurons of each subgroup (rows) in three perspectives (columns). (A) pyramidal neuron, (B) inverted neuron, (C) tangentially oriented neuron, (D) horizontal neuron, (E) multipolar neuron. Dendrites shown in red, axons shown in blue. Coloured reconstructions, neuron at its location within the cortex with axonal projection shown. Black reconstructions, somatodendritic segment of same neuron depicted with a two-fold magnification. Scale bar: 300 um (A1-E2), 200 um (A3-E3), 150 um (somatodendritic magnification A1-E2), 100um (somatodendritic magnification A3-E3).
From Marx & Feldmeyer 2003.

Inhibitory cell types have also been studied in somatosensory cortex, albeit in the entirety of L6 and not in L6b in specific. Based on electrophysiological properties, dendritic morphology, and marker gene expression, four inhibitory neuron types have been identified: neuropeptide Y (NPY), parvalbumin (PV), somatostatin (SST) and vasoactive intestinal protein (VIP) expressing interneurons. NPY expressing neurons take up half of all inhibitory neurons in L6 and are especially concentrated in the lower part of L6, presumably L6b (Perrenoud et al., 2013). While during development the subplate provides a permissive environment for the tangential migration of GABAergic interneurons and contains a large number of them, the adult L6b contains the smallest proportion of GABAergic interneurons (Boon et al., 2019).

1.3.3 Genetic markers of L6b

Several genetic markers have been identified for L6b. Connective tissue growth factor (Ctgf) seems the most specific, at least in sensory cortices (Heuer 2003). Other markers that have been identified are orphan nuclear receptor 1 (Nurr1), Neurexophillin 3 (Nxph3), Lysophosphatidic acid receptor 1 (Lpar1), Transmembrane protein 163 (Tmem163), Complexin 3 (Cplx 3) and monooxydase Dbh-like 1 (moxD1) (Arimatsu et al., 2003; Beglopoulos et al., 2005; Hoerder-Suabedissen and Molnár, 2013; Hoerder-Suabedissen et al., 2009). Based on marker expression, L6b takes up about 15% of L6, but based on morphology and projection pattern the L6b component of L6 may be larger (Hoerder-Suabedissen et al., 2018; Lorente de Nó, 1922; Marx and Feldmeyer, 2013; Perrenoud et al., 2013; Valverde et al., 1989) and based on projection pattern too (Hoerder-Suabedissen et al., 2018). In entorhinal cortex, which is part of the evolutionary older archicortex, Ctgf and Cplx3 label the full width of L6 and not just L6b; L6b in that part of the cortex may take up the full width of L6 (Ben-Simon et al., 2022).

Single cell transcriptomic analysis of L6b neurons has identified 6 glutamatergic subgroups within L6b, but currently there is no consensus on how these subgroups match up with the subgroups identified based on somatodendritic morphology or based on connectomics (Henning et al., 2023).

1.3.4 Cre lines to study subpopulations of projection neurons in cortical L6b

Specific Cre driver lines to target subpopulations of cortical L6b have only recently been developed. In my study, I used a dopamine receptor 1a (Drd1a) Cre line, (Tg(Drd1a-cre)FK164Gsat/Mmucd)(Hoerder-Suabedissen et al., 2018). In this mouse line, Cre expression is mostly restricted to its cortical expression pattern, with only limited expression in subcortical areas including only scattered cells in striatum, and some expression in hippocampus, medial pretectal area and cerebellum (Hoerder-Suabedissen et al., 2018)(Supplementary Figure S3.2). In the FK164 Drd1a-Cre line, Cre expression starts during the first postnatal week, beginning in medial and anterior cortex at P1 and continuing more caudally and laterally until P8, when the expression in cell bodies reaches the adult pattern (Hoerder-Suabedissen et al., 2018). Of the neurons in L6b in S1, 25% or even 40% are Drd1a-Cre positive (Hoerder-Suabedissen et al., 2018; Zolnik et al., 2020); the percentages of Drd1a Cre cells in areas other than S1 and M1 may be lower (Mueller, Szabó, Molnár, unpublished). The expression of Drd1a-Cre is restricted to L6b in primary somatosensory (S1), primary visual (V1) and primary motor (M1) cortex (Hoerder-Suabedissen et al., 2018; Zolnik et al., 2020) and restricted to deep layers in PFC (gensat.org).

In terms of co-expression of other subplate markers, Drd1a-Cre positive cells do not express Lpar1 (Hoerder-Suabedissen and Molnár, 2013) but do express Golli-tau (Jacobs et al., 2007), whereas not all Golli-tau expressing cells co-express Drd1a-Cre (Hoerder-Suabedissen et al., 2018). Of the Drd1a-Cre expressing cells, about one-third expresses Ctgf, Neuroserpin or Cplx3 (Hoerder-Suabedissen et al., 2018; Zolnik et al., 2020). Drd1a-Cre neurons are excitatory neurons and are a mix of pyramidal and non-pyramidal cells (Zolnik et al., 2020). Henning *et al.* suggested that only one of the 6 transcriptomic clusters of excitatory L6b neurons expresses receptors for orexin (Henning et al., 2023) and in vitro electrophysiological recordings from Drd1a-Cre+ cells indicated that a large proportion of the Drd1a-Cre+ neurons in L6b are orexin sensitive (Tim Zolnik, unpublished observations in S1 and Rajeevan Therpurakal, unpublished observations in PFC). This made the Drd1a-Cre line particularly suitable for my own studies.

Another Cre driver line that can be used for selective targeting of L6b is the Ctgf-Cre line (CtgfTg2-Cre line). In this line, Cre expression is restricted to L6b and subplate during development (Heuer et al., 2003). In the PFC in adulthood, however, Cre expression is localized to cortical L2/3 (Hoerder-Suabedissen, Szabó, Berry, Sharott, unpublished; gensat.org). Moreover, since Ctgf is expressed in the embryonic ventricular zone within cortical neuronal progenitors (Wang et al., 2010), a direct cross with this driver line is not possible for achieving selective reporter gene expression. With an inducible Ctgf-Cre line, Zolnik *et al.* have been able to target L6b cells in adult mice and they found that Ctgf-Cre expressing neurons form 25% of neurons in L6b, are excitatory neurons, and are mostly non-pyramidal cells (Zolnik et al., 2020).

1.3.5 Connectivity of L6b

Consistent with the cellular, morphological, transcriptomic, and developmental variations in L6b, multiple projections patterns have been reported for L6b (Feldmeyer, 2023).

At the most local, within-layer and within-area, level, connections may be stronger for inhibitory than for excitatory neurons. Excitatory neurons can form connections with other L6b excitatory neurons and interneurons, but these have relatively low efficacy (Marx et al., 2017). Similarly, Drd1a-Cre positive and Ctgf-Cre positive neurons in S1 receive input from other L6b neurons but this input is sparse and weak (Zolnik et al., 2020). Based on morphology, deep L6 inhibitory neurons in S1 and prefrontal cortex (PFC) seem well-suited for local connectivity, having dense axonal collaterals (Ding et al., 2021; Marx & Feldmeyer, 2013).

At the cortical column level, there are anatomical projections from L6b in S1 to all other cortical layers, although these may vary in density and strength (Marx and Feldmeyer, 2013; Viswanathan et al., 2017). Functionally, in S1, local L4 input to L6b is strong but indirect, L2/3 input is present, and local L5 input elicits responses in L6b but those are much weaker than long-range connections (Zolnik et al., 2020). Inhibitory neurons from L1 also connect to L6b (Zolnik et al 2020) and vice versa, L6b neurons project to local L1 (Clancy and Cauller, 1999; Ledderose et al., 2023; Marx and Feldmeyer, 2013; Zolnik et al., 2020). Recent findings suggest that a

subpopulation of Drd1a neurons in L6b projects to L1, while another subpopulation of Drd1a neurons in L6b projects to L5 and higher order thalamus and that these subpopulations have different functional roles (Zolnik et al., 2023).

Long-range connectivity of L6b can be divided in two categories, cortico-cortical and cortico-thalamic (Figure 1.7). Cortico-cortical connections became apparent in autoradiography and histological studies and are thought to be formed by horizontally and tangentially oriented excitatory neurons in L6b (Prieto and Winer, 1999; Valverde et al., 1989). Retrograde tracing confirmed long-range cortico-cortical projections from L6b (Vandevelde et al., 1996). With combined immunohistochemistry and retrograde tracing, it was found that Nurr1 positive cells in L6b project to corticocortical rather than subcortical targets and that this population of L6b is restricted to interhemispheric connections. It was suggested that different subpopulations of L6b may be involved in different circuits (Arimatsu et al., 2003). The specific anatomic and functional connectivity in different subpopulations of L6b was studied with monosynaptic rabies tracing and channelrhodopsin-assisted circuit mapping from Ctgf-Cre and Drd1a-Cre from S1 (Zolnik et al., 2020). Here it was found that the predominant long-range input to L6b in S1 is L5 in ipsilateral motor cortex, but that there are also considerate connections from S2 and from the collateral S1. Input from all areas is mostly from neurons in deeper cortical layers, such as from contralateral pyramidal neurons in L5 (Hay et al., 2015; Zolnik et al., 2020). Zolnik *et al*. found that 13.2% of long-range connections to Drd1a positive and Ctgf positive neurons was derived from the contralateral hemisphere, which disagrees with the earlier study on Nurr1 positive neurons (Arimatsu et al., 2003; Zolnik et al., 2020). This inconsistency in interhemispheric connectivity could be explained by the different subpopulations of L6b that were studied.

L6b is also integrated in thalamocortical networks. Drd1a-Cre positive neurons in L6b project to thalamus, but selectively to higher order nuclei of the thalamus, which are involved in higher order processing and brain state control (Hoerder-Suabedissen et al., 2018; Viswanathan et al., 2017). Non-pyramidal neurons in L6b innervate thalamus only sparsely, suggesting a cell type specific innervation pattern (Prieto and Winer, 1999).

In the other direction, there are few direct projections from VPM or POm to L6b in S1 (Meyer et al., 2010; Wimmer et al., 2010). Likewise, monosynaptic rabies tracing showed that subcortical input to L6b contributes only 1% of long-range input to L6b, as opposed to cortico-cortical input which forms 95% of long-range input to L6b (Zolnik et al., 2020).

The sparsity of thalamocortical projections does not exclude the possibility of functionally important cortico-thalamo-cortical loops involving L6b, such as the one proposed by Hay *et al.* in which L6b potentiates thalamocortical projections in L6a in the presence of orexin (Hay et al., 2015). Also, it should be noted that amongst the sparce long-range subcortical input to L6b, input from higher order thalamus is the predominant one (Zolnik et al., 2020). Moreover, recent findings show that L6b can activate L5 and higher-order thalamus in vitro, indicating that L6b may be involved in activating higher-order cortico-thalamo-cortical loops in vivo (Zolnik et al., 2023). The dynamics of these loops require further study, such as whether thalamus-L6b projections synapse in L6b apicals in L5a or elsewhere.

Lastly, L6b projects to hippocampus and may be part of a network involved in spatial learning and memory. In entorhinal cortex, an evolutionary old area of the cortex, the entire width of L6 shows characteristics of L6b and these neurons project to all areas of hippocampus, most strongly to CA3. When these L6b neurons are optogenetically activated, EPSCs recorded from hippocampus suggest functional significance, and when they are optogenetically silenced, animals show reduced spatial learning and memory, suggesting that these differences are behaviourally relevant (Ben-Simon et al., 2022).

Altogether, L6b is embedded in various direct cortico-cortical, transthalamic cortico-cortical, and cortico-hippocampal networks. It is likely that these projection patterns reflect different L6b populations, and that L6b populations are differentially integrated depending on cortical area.

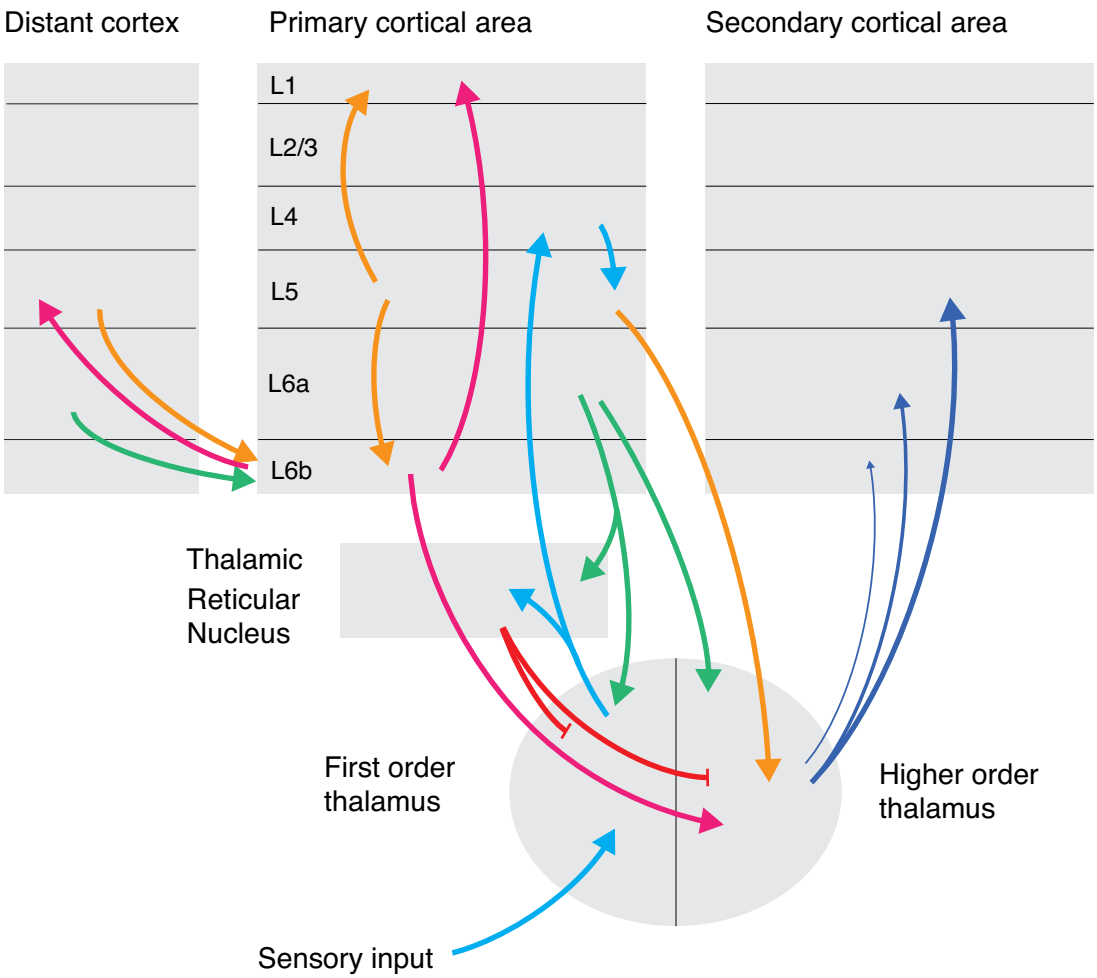

Figure 1.7: Simplified schematic of transthalamic and direct cortico-cortical networks involving layer 6b. Sensory information reaches the cortex via first order thalamic nuclei and arrives in L4 (light blue). From L4, it is transmitted to other layers for further processing including L5, the main output layer of the cortex (light blue). L5 sends powerful driver projections that end in large boutons in higher order thalamus (orange) and this projection is reciprocal, forming a transthalamic cortico-cortical loop (navy blue). There are some projections from higher order thalamus to L1 and L6a (navy blue) and sparse projections from higher order thalamus to L6b (thin navy blue). L6a projects to both first order and higher order thalamic nuclei and modules thalamocortical transmission (green). L6a projections give side branches to TRN in contrast to L6b and L5 projections. Only frontal cortical layer 5 projections give some collaterals to TRN. TRN GABAergic neurons inhibit both first order and higher order thalamus, providing a mechanism for sensory decoupling (red). L6b receives intracortical input, predominantly from L5 (orange) and L6a (dark green) but also other cortical layers. L6b projects to L1, near and distant other layers, with a large component to L5, and to higher order thalamus (magenta). For clarity, projections from L6b to other layers than L1 and long-range L5 are not shown; neither are the projections to local and secondary cortex, such as local projections to L6a and L6b interneurons. Projection patterns of individual neurons depend on L6b cell type, and there may be two broad categories of cortico-cortically projecting and thalamocortical L6b neurons. L1-L6b, cortical layer 1 – 6b. TRN, thalamic reticular nucleus.

1.3.6 Neuromodulation of L6b

Neurons in L6b are responsive to various neurotransmitters and neuropeptides, with a cell type dependent response, and for some combinations, interactions between multiple neuromodulatory systems have been observed. This may enable L6b to sense and integrate homeostatic information (Feldmeyer, 2023).

Orexin

In Chapter 4, I describe orexin expression, orexin receptor expression and orexin effects on sleep and wakefulness in more detail, but below I give a short overview of the in vitro effects of orexin on L6b. Orexin, is mostly known for its subcortical effects (see also Chapter 4), but its receptors are expressed in cortex too and in cortex, its effects are thought to be area specific.

In PFC, orexin 1 receptor (OX1R) is most strongly expressed, and orexin A (ORXA) can powerfully activate layer 2/3 and layer 5 (Lambe and Aghajanian, 2003; Li et al., 2010; Song et al., 2006; Xia et al., 2005; Yan et al., 2012a).

In somatosensory cortex, motor cortex, primary visual cortex and cingulate cortex, on the other hand, robust activation by both subtypes of orexin, ORXA and orexin B (ORXB), have been demonstrated for L6b but no other cortical layers and this is thought to result from activation of orexin type 2 receptors (OX2R) (Bayer et al., 2004; Wenger Combremont et al., 2016b, 2016a). The effect is postsynaptic and dependent on closure of a potassium conductance.

Within L6b, orexin can activate multiple cell types. A population of multipolar, spontaneously slow bursting non-pyramidal neurons has been identified that are spontaneously slow bursting (Wenger Combremont et al., 2016a). These neurons can be activated by orexin and other neurotransmitters of arousal, including histamine and noradrenaline, which decreases burst firing and promotes cortical synchronization, which could be a mechanism for sleep-wake transitions (Wenger Combremont et al., 2016a). Fast-spiking PV interneurons in L6b are only indirectly activated after orexin bath application, possibly in response to directly excited L6b pyramidal neurons projecting to interneurons (Wenger Combremont et al., 2016b).

Moreover, orexin can depolarise and excite the nonspecific centromedial and rhomboid thalamic nuclei, which are involved in promotion of wakefulness through widespread cortical projections (Bayer et al, 2002). Optogenetic activation of thalamocortical rhomboid nucleus neurons in rat brain slices results in excitatory currents in L6 neurons in the parietal cortex, the main recipient cortical area of rhomboid nucleus. Interestingly, the responses of L6a neurons to photoactivation of thalamocortical rhomboid nucleus axons are enhanced by bath application of orexin, not only with an increase in number of action potentials but also in timing precision. Since L6b but not L6a is thought to be activated by orexin, this finding suggests that orexin activation of L6b promotes responsiveness of L6a to thalamocortical input (Hay et al., 2015).

Lastly, thalamocortical terminals in the PFC can be presynaptically activated by orexin and elicit antidromic bursting in the thalamus during wakefulness, which may contribute to attention and vigilance (Lambe and Aghajanian, 2003).

Acetylcholine

Acetylcholine (ACh) is a prominent neurotransmitter of the arousal system and is produced predominantly by the basal forebrain (Saper et al., 2005). Direct effects of nicotine on L6b have been observed, although only in synergism with orexin. Nicotine applications leads to prolonged firing of L6b neurons and potentiates the response of these neurons to orexin, but at the same time nicotine is dependent on orexin to elicit activation of L6b (Hay et al., 2015). Fast-spiking interneurons in L6b are not dependent on orexin and can be activated by acetylcholine directly (Wenger Combremont et al., 2016b).

Neurotensin

Neurotensin plays a role in various homeostatic behaviours including sleep, locomotion, food and fluid intake, and the regulation of body temperature. It does this via two GPCRs, the neurotensin receptor 1 (NTSR1) and 2 (NTSR2). The Ntsr1 receptor is expressed in L6 corticothalamic

neurons that project to the ventroposterior medial (VPM) nucleus of the thalamus, which identifies a population of L6a neurons and is therefore used as marker for L6a (Bortone et al., 2014; Guo et al., 2017; Olsen et al., 2012). Neurotensin can excite both slow-bursting neurons and fast-spiking interneurons in L6b (Wenger Combremont et al., 2016b, 2016a). In corticothalamic slices, neurotensin application also reduces the occurrence of slow oscillatory activity and increases the spike timing precision after thalamocortical stimulation. Whole-cell recordings showed that neurotensin reduces the activity of excitatory neurons and increases the activity of inhibitory neurons. Neurotensin colocalizes with tyrosine hydroxylase, which is an enzyme in the dopamine synthesis pathway, suggesting a potential synergistic role of the dopaminergic and neurotensin systems (Case et al., 2017).

Dopamine

Dopamine is produced by the substantia nigra – ventral tegmental area complex and hypothalamus and dopaminergic axons project widely, including to the neocortex. There are two types of dopamine receptors, the excitatory D1 like receptors (Drd1, Drd5) and the inhibitory D2 like receptors (Drd2, Drd3, Drd4). D1 like receptors are strongly expressed in the deeper layers of the neocortex (Berger, 1991). Because of the enrichment of Drd1a specifically in L6b, a Drd1-Cre mouse line is used as a driver line for L6b research, which is modified to have relatively specific expression of Drd1a in the cerebral cortex (Hoerder-Suabedissen et al., 2018). It is likely that the dopaminergic system has a functional effect on L6b neurons. As described before, neurotensin colocalizes with tyrosine hydroxylase from the dopamine synthesis pathway suggesting co-release dependent on context (Case et al., 2017). Moreover, dopamine can directly activate slow bursting neurons in L6b (Wenger Combremont et al., 2016a).

Cholecystokinin

Cholecystokinin (CCK) was identified as a gut peptide but was later found to be highly expressed in the brain, especially in neocortex, including its two receptor types, cholecystokinin receptor 1

(CCK1R) and cholecystokinin receptor 2 (CCK2R). Both CCK and its receptors CCK1R and CCK2R are expressed in the deep layers of the cortex, and CCK can cause robust and long-lasting action potentials in excitatory L6b neurons in S1 (Chung et al., 2009).

Summarizing, multiple neurotransmitters can activate L6b neurons, directly or indirectly, and all neurotransmitters that have been investigated in this context so far are arousal-promoting. Different neuromodulatory systems may be integrated in L6b and promote synergistic effects in situations where increased attention or arousal is required.

1.3.7 Layer 6b and deviance detection

Sensory information from the environment reaches the cortex via the sensory organs, through their respective brainstem nuclei, and the modality-specific relay nuclei of the thalamus. The first order, or relay nuclei project to neurons in L4 in their respective primary sensory cortical area, which innervate secondary sensory areas for further processing (Harris and Shepherd, 2015).

Not every stimulus should be perceived with the same intensity, as some should carry more weight, because they are more salient towards survival or other evolutionary needs. Changes in the environment are especially salient, and therefore different deviant detection methods are wired in the sensory process via two parallel processes, sensory adaptation in lower processing steps and top-down prediction error signalling from the cerebral cortex.

In one form of predictive coding, information passes through neuronal nodes that are organised in a hierarchical order, and only perceptive information that does not match a prediction is passed on to the following node. Predictive coding is the result of cortico-cortical and cortico-thalamo-cortical networks and involves suppression of predicted information and facilitation of deviant information, or error messages (Shipp, 2016). The rationale is that higher order cortical networks generate prediction models and that these models are compared to lower-order incoming information. Only incoming information that is different from the predicted model is passed forward in the hierarchy to the next node of comparison.

The lowest node in this stream is the input from thalamus to cortical layer 4. Higher-order models are generated from cortico-thalamic input. In transthalamic cortico-cortical connections, corticothalamic input is provided by the deep layer neurons of the neocortex in L5 and L6 (Antunes and Malmierca, 2021; Sherman et al., 2014). L5 pyramidal neurons, the main output cells of the brain, project to subcortical targets but also send projections to the thalamus. These projections are specific to higher order nuclei of the thalamus, which are the nuclei that are involved in higher order processing (Bourassa and Deschênes, 1995; Sherman et al., 2014).

L5 corticothalamic boutons are on average large, and they are described as drivers, referring to their similarities to feedforward projections from the sensory system that can drive information transmission in the thalamus (Bajo et al., 1995; Sherman and Guillery, 1996).

L6a thalamocortical excitatory neurons, on the other hand, have projections that innervate both first order or relay thalamic nuclei, and higher order nuclei (Bajo et al., 1995; Bourassa and Deschênes, 1995). Their axonal boutons are smaller in size, and they are described as modulators, that do not change the contents of the information, but rather modify the strength of transmission (Bajo et al., 1995; Bourassa and Deschênes, 1995; Sherman and Guillery, 1996). L6a CT neurons are excitatory neurons but can exert modulation in either direction, because they have direct projections to the thalamus for excitatory effects but also parallel projections to the TRN for inhibitory effects. TRN neurons project to thalamic neurons which allows di-synaptic inhibition of target thalamic neurons (Antunes and Malmierca, 2021; Guo et al., 2017).

In transthalamic cortico-cortical networks in predictive processing, it is possible that L6a neurons take on a prediction error coding role, since they can both enhance and suppress information transfer through their projections to thalamic nuclei and TRN, respectively. This allows them to compare information to existing models and modulate whether to pass on the information or suppress transmission. In such a scenario, L5 neurons, having driving properties that place them on a lower hierarchical position, are more likely to generate predictive models rather than to compare them to incoming information (Antunes and Malmierca, 2021).

A subpopulation of L6b neurons that are labelled in the Drd1a-Cre mouse line form a different population from either of the above, projecting selectively to higher order nuclei of the thalamus and not to first order thalamic nuclei or TRN, but having smaller axonal boutons than L5 neurons (Hoerder-Suabedissen et al., 2018). This makes L6b neurons a unique subpopulation amongst the infragranular populations.

The sensitivity of L6b to orexin and other neuromodulators might equip L6b with an additional level of control, in which information about the internal and external environment is integrated. In S1, optogenetic stimulation of Drd1-Cre thalamocortical neurons increases spiking activity after whisker deflections in the POm, the higher order nucleus of somatosensory perception in mice. This happens only to the first whisker deflection of a train of deflections, after which adaptation occurs rapidly (Ansorge et al., 2020). This finding suggests that the L6b subpopulation can enhance higher order thalamic activity in specific behavioural contexts. The photoactivation of the Drd1a-Cre positive Layer 6b neurons in S1 had little effect on activity in other cortical areas, suggesting a more important role of transthalamic circuits rather than corticocortical circuits in this context (Ansorge et al., 2020). A possible advantage of transthalamic circuits for predictive processing could be the integration of input from both distant cortical areas and from different modalities in multimodality thalamic nuclei (Antunes and Malmierca, 2021).

On the other hand, cortico-cortically projecting L6b neurons could also play a role in detecting changes in the environment. There are several subtypes of L6b neurons. Some L6b neurons project to L1 in somatosensory barrel cortex, in visual cortex, in sensory, motor, and frontal cortex (Clancy and Cauller, 1999; Zolnik et al., 2020). At least in S1, the L6b neurons engaging in this projection are the Drd1a-Cre expressing neurons (Zolnik et al., 2020). L1 inhibitory neurons have been demonstrated to be key mediators of generating a ‘mismatch response’ to deviant stimuli (Lakatos et al., 2020). However, it would be unclear which neuronal populations would innervate L6b in this scenario.

The mismatch response to a deviant auditory stimulus in the prefrontal cortex is likely to be based on prediction error signalling (Casado-Román et al., 2020). Narcolepsy patients show altered frontal evoked responses in pre-attentive and attentive tasks (Naumann et al., 2001) and orexin administration enhances performance in attention tasks in rats (Lambe et al., 2005). Since L6b is the main cortical population responsive to orexin (Bayer et al., 2004), the effect of orexin on pre-attentive processing and attention in prefrontal and frontal cortex could be, at least partially, mediated through L6b. Altogether, a role of L6b in signalling changes in the environment could be possible based on its projection pattern and would be consistent with the vigilance promoting effects of neuromodulators.

1.3.8 Clinical implications of studying L6b

Some of the susceptibility genes of autism and schizophrenia are transiently expressed in subplate during development (Hoerder-Suabedissen and Molnár, 2015; Hoerder-Suabedissen et al., 2009). Abnormal distribution and numbers of IWNs have been described in autism and schizophrenia (Akbarian et al., 1996; Bailey et al., 1998; Casanova, 2015; Duchatel et al., 2019). Detection of sensory stimuli and brain state control are altered in these conditions (Adler et al., 1982; Bailey et al., 1998; Boutros et al., 2004; Casanova, 2015; Duchatel et al., 2019; Miano and Ferri, 2010; Shelley et al., 1999; Siegel et al., 1984; Waite et al., 2016), and it is an interesting possibility that the abnormal subplate remnant circuits are responsible for the altered perception, state control and sleep in autism and schizophrenia. This translational potential provides additional motivation to further understand the role of these circuits in normal and pathological development.

1.4 Hypothesis and project aims

L6b is comprised of neurons that can be considered as the remnants of the subplate, a key structure in cortical development. In all species studied (Bhagwandin et al., 2020; Swiegers et al., 2019, 2021a, 2021b), some subplate cells survive into adulthood as L6b (rat and mouse) or as interstitial white matter neurons (primates and carnivores)(Kostovic and Rakic, 1980). This evolutionary conservation suggests a functional benefit of survival of subplate cells into adulthood. L6b has several subtypes; some are well-connected, both with long-range projections to other cortical layers, and some with projections selectively to higher order nuclei of the thalamus. Moreover, multiple cell types in L6b can be directly activated by orexin in vitro(Bayer et al., 2004; Hay et al., 2015; Wenger Combremont et al., 2016b, 2016a) . These properties combined make L6b a suitable player in the regulation of brain state transitions, since it can integrate information over large cortical areas and from the presence of orexin and signal the integrated message to higher order thalamic nuclei, which can initiate cortical arousal and brain state transitions. This could place L6b in networks of brain state control, in sleep wake regulation and possibly also in deviance detection. Multiple cell types of L6b can be activated by orexin in vitro, suggesting that orexin also has an effect on L6b in vivo, and in line with this, some of the effects on to the cerebral cortex of orexin could be mediated through L6b.

Project aims

1. To investigate the sleep-wake phenotype of mice with a chronic manipulation of neocortical layer 6b Drd1a-Cre pyramidal neurons
2. To investigate the effects of orexin on sleep-wake regulation in mice with a chronic manipulation of neocortical layer 6b Drd1a-Cre pyramidal neurons
3. To investigate deviance detection in an auditory oddball paradigm in mice with a chronic manipulation of neocortical layer 6b Drd1a-Cre pyramidal neurons

2 General methods

In this Chapter, I describe the general methods for *in vivo* continuous electrophysiological recordings, offline signal processing, and statistical approaches that were used in the research presented. Methods specific to subprojects are described in the methods' sections of the respective chapters.

All experiments were performed in accordance with the United Kingdom Animal (Scientific Procedures) Act 1986 and local ethical review under personal license (PIL) and Vyazovskiy and Molnár project licences (PPL) granted by the United Kingdom Home Office. Ethical approval was provided by the Ethical Review Panel at the University of Oxford. Animal holding and experimentation was located at the Biomedical Sciences Building (BSB), University of Oxford.

2.1 Animal housing and husbandry

Mouse breeding was performed at the dedicated breeding facility in the BSB. The breeding scheme of the layer 6b silenced mouse (Drd1a-Cre:Snap25$^{fl/fl}$:TdTom) colony is described in the methods section of Chapter 3 (3.2.1). Briefly, Tg(Drd1a-cre)FK164Gsat/Mmucd (*Drd1a-Cre*; MMRRC)) and *Snap25fl/fl* were crossed to B6;129S6-Gt(ROSA)26Sortm14(CAG-tdTomato)Hze/J (*Ai14*) mice. The Ai14 reporter strain has a STOP-floxed copy of a CAG-promoter driven red fluorescent protein gene (TdTomato), which allows selective visualisation of Cre expressing cells (Hoerder-Suabedissen et al., 2019)

Animals were group-housed and kept on a 7AM-7PM light dark cycle, with water and food available ad libitum. Animals that were assigned for surgery followed by electrophysiological recordings were transferred to Level 1 of the BSB when they reached an age of 6-10 weeks. On Level 1, animals were kept on a 9AM-9PM light-dark cycle. Three days before surgery, animals received non-medicated mash and jelly, to allow habituation to mash for postoperative food

intake and jelly for postoperative drug administration. On the day of surgery, animals were transferred to the surgery room on Level 3. After surgery, animals were returned to Level 1 for postoperative care and management. After recovery, animals were transferred to the recording setup on Level 3. On all levels of the BSB, room temperature and humidity were maintained at 20 ± 1°C and 60 ± 10%, respectively.

2.2 Surgical procedures and postoperative care

Surgical implantation of EEG/EMG recording electrodes was carried out as previously described (Krone et al., 2021; McKillop et al., 2021). Immediately prior to surgery, animals were weighed for preparation of the surgical analgesics Metacam (meloxicam, 5 mg/kg, Boehringer Ingelheim Ltd., Bracknell, UK) and vetergesic (buprenorphine, 0.1 mg/kg, Sogeval UK Ltd., York, UK). At the start of surgery, mice were anesthetized with isoflurane (3-5%), mixed with oxygen (3-4 L/min) in an induction chamber. When the righting reflex was lost, animals were transferred to a heat mat, with anaesthesia via a nose mask (2-3% isoflurane, 1-1.5L/min oxygen), where the skin on the head was shaved with clippers, and metacam and vetergesic were administered subcutaneously (s.c.). Next, the animal was positioned in the stereotactic frame (David Kopf Instruments, California, USA; Model 900 Small Animal Stereotaxic Instrument) and anaesthesia administered through a nose mask at maintenance dose (isoflurane 1-2.5%, oxygen 1-1.5 L/min). A rectal thermometer linked to a feedback heat map system was inserted for maintenance of body temperature (35-36 °C) (Homeothermic monitoring system, Harvard Apparatus, Cambridge, MA, USA), and the eyes were protected with lubricating eye gel (Viscotears, Alcon Laboratories Limited, Hemel Hempstead, UK). Hydration was provided through s.c. injection of sterile saline (0.1 ml at the start of surgery). Breathing rate, temperature and depth of anaesthesia were monitored constantly, and anaesthesia was adjusted if needed. Surgical instruments were laid out in a sterile area and the animal was covered with sterile drapes. The skin on the head was cleaned with three consecutive washes of povidone-iodine and 70% ethanol. Next, an incision was made over the midline skin of the head of the mouse. The skin was retracted, and connective tissue was

removed, through carefully scratching, and application of etching gel, which was washed off with sterile saline. Bregma was localized and the positions of the electrodes were marked with a sterilized marker, with the frontal EEG 2 mm anteroposterior (AP), +2 mm to the right of the midline (ML), occipital EEG -3.5mm AP and +2.5mm ML. At the marked positions, with a microdrill a hole was created in the skull without entering the brain. A third hole was made above the cerebellum for the reference screw. Next, the EEG/EMG headstage was positioned with the bone screws into the holes using a small screwdriver. The headstage was secured with dental cement (Super bond, Prestige Dental Products Ltd, Bradford, UK). After the dental cement had solidified, the EMGs were implanted into the nuchal muscles and the EMGs were secured to the rest of the headstage with acrylic dental cement (Simplex Rapid, Associated Dental Products Ltd, Swindon, UK). If needed, the skin was closed with a suture (Ethicon-W9915, Henry Schein, Gillingham UK). Animals received additional saline (0.1ml/hour of surgery) and were weighed immediately after the surgery; the headstage weight was <10% of presurgical body weight in all animals. The animal was transferred to a heated recovery box, where it was monitored until it showed a righting reflex which took usually less than 10 minutes. The animal was then transferred to a preheated IVC with white surgical bedding and placed on a heat mat during the first night.

During the first five days after surgery, animals were examined and weighed daily. Their condition was recorded on a score sheet, including body weight, spontaneous behaviour, provoked behaviour, breathing, and the mouse grimace scale. Postoperative analgesia was provided through jellies mixed with oral Metacam (meloxicam, 5 mg/kg, Boehringer Ingelheim Ltd., Bracknell, UK) where needed, and animals that required analgesia based on postoperative scores but did not show interest to medicated jellies were injected with injectable Metacam. In the first days after surgery, food was enriched with mash and plain jelly, trail mix and water-soaked pellets. When general condition and body weight had returned to baseline, food was reverted to regular pellets, that were supplied ad libitum on the floor of the cage until the end of the experiment.

2.3 Electrophysiological recordings

2.3.1 EEG/EMG head stages

I custom-made EEG/EMG head stages. For the EEGs, three 2cm-long stainless-steel wires were stripped at the ends and soldered onto the three anterior pins on the right side of an 8-pin 90 degrees connector (Pinnacle Technology Inc, Kansas, USA, model 8415-SM). At the other ends, 0.5cm of the wire was stripped and wrapped 2-3 times tightly around a stainless-steel bone screw (Fine Science Tools, 19010-10, InterFocus Ltd, Cambridge, UK) that had been clipped off and sanded with sandpaper to limit penetration into the brain. For the EMGs, two 2.5cm long wires were stripped at the ends and soldered onto the posterior two pins of the 8-pin connector. At the other ends, the wires were folded into a loop and the loops were soldered into a smooth blob. Connections were conductivity-tested and electrically isolated with a layer of dental cement (Simplex Rapid dental acrylic cement (Associated Dental Products Ltd, Swindon, UK) (Figure 2.1).

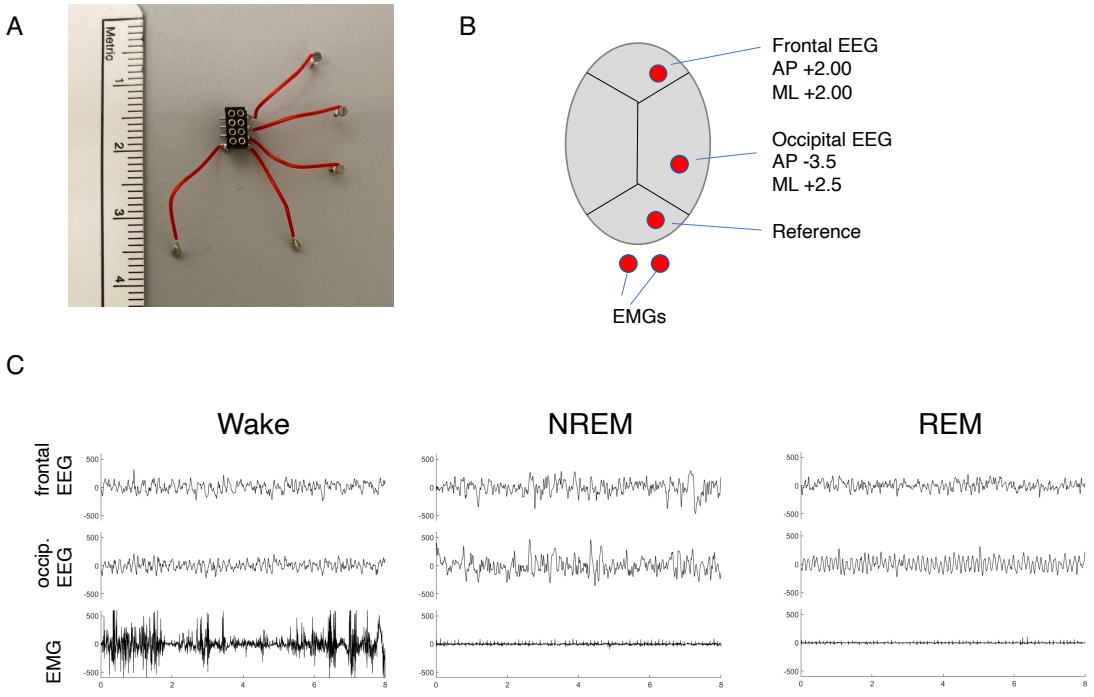

Figure 2.1: EEG/EMG recording in mice.
A) Headstage, consisting of 3 EEG recording electrodes and 2 EMG recording electrodes connected via stainless steel wire and solder to an 8-pin connector. B) Location of EEG and EMG electrodes after implantation, coordinates with reference to Bregma. AP, anterioposterior direction, ML, midline direction. C) Example traces of EEG/EMG recordings (in µV) in a mouse.

2.3.2 EEG/EMG Cables

Custom-made EEG/EMG recording cables consisted of two parts which together formed a recording cable pair for each animal. The first part consisted of small plug cables that were plugged into the splitterbox for recording four derivations per animal (frontal to cerebellar, occipital to cerebellar, frontal to occipital (backup, in case of damage to cerebellar connection), and EMG1 to EMG2). The plugs were soldered onto a rainbow cable (612-6372, RS Components, London UK) which connected to the second part of the cable set. The second part consisted of a rainbow cable with a complimentary end (612-6423, RS Components), soldered onto a silver cable. The silver cable was soldered onto a headstage with straight pins (Pinnacle Technology Inc, Kansas, USA, model 8415), that fit into the headstage implanted in the animal.

2.3.3 Recording setup

After recovery from surgery, animals were transferred to the recording room, with a constant light-dark cycle (9AM light on, 9PM lights off). In the recording room, animals were housed in individual custom-made Plexiglas cages (35x35x50cm^3) with bedding, nesting material and a water bottle. Food was supplied ad libitum on the floor of the cage. Two Plexiglas cages were placed in each sound-attenuated recording chamber (Campden Instruments, Loughborough, UK). The recording chambers were lit with an LED strip attached to the top of the chamber (light levels 120-180 lux), which was connected to a timer on the same light-dark schedule as the room. Chambers were ventilated through a fan mounted on the side wall of the chamber that was electrically shielded with aluminium foil. A hole in the top of the chamber allowed insertion of EEG/EMG cables and positioning of webcams (Logitech, C270, Lausanne, Switzerland) for remote monitoring.

2.4 Experimental timeline

After animals were moved to the recording room on level 3, they were first left undisturbed for a day, for habituation to the cage and the chamber. The following day, they were connected to

EEG/EMG cables and the signals were checked in the Synapse recording software setup (Synapse, Tucker Davis Technologies, Florida USA). If the signals were not of sufficient quality, other headstage cables or splitterbox cables were tested in a systemic order, and grounding of the chamber and its components were checked to reduce noise. Once signals were deemed of sufficient quality, several days of test recordings followed. Throughout the experiment, animals were closely monitored for signs of distress and for having twisted cables. A few days later, when animals were habituated to the cables, a baseline recording followed. During this recording, animals were briefly checked at 9AM, just before starting the recording, and the rest of the day the chamber was left closed and the animals undisturbed. The recording was ended the next day at 9AM, and the animals were checked again and intermittently through webcam view. Typically, experiments lasted 1-3 weeks, and had 2-3 days in between experimental days other than baseline recording days. When the experiment had been completed, the integrity of recording files was verified, the animals were disconnected from the EEG/EMG cables, animals were terminally anesthetised and perfused (see section 2.7) and brains were obtained for histology. Splitterbox cables were typically reused, for headstage cables I generally made a new set for every block of recordings.

2.5 Data acquisition

Data was acquired with a 128-channel neurophysiology recording system with an RZ2 processor (Tucker Davis Technologies (TDT), Florida, USA), connected to a computer installed with the TDT Synapse software (Tucker Davis Technologies) and stored locally. The EEG/EMG cables were connected to a splitterbox in a configuration for analogue referencing (frontal-cerebellar, occipital-cerebellar, a backup derivation frontal-occipital, and EMG1-EMG2). EEG/EMG signals were preamplified by a PZ5 preamplifier and sampled at a sampling rate of 305 Hz (Chapter 4) or 1017.3 Hz (Chapter 3, 5) and filtered with an anti-aliasing filter at 45% sampling rate. EEG/EMG recordings were continuous, apart from a brief manual restart at 9AM every morning.

2.6 Signal processing

EEG and EMG signals were processed offline with custom-written Matlab scripts. First, signals were resampled to 256 Hz. Next, signals were filtered with a Chebyshev type II filter, 0.3 Hz-100 Hz for EEG signals and 3-100 Hz for EMG signals. The resampled, filtered signals were then converted into European Data Format (.edf) files and blinded for manual assignment of vigilance states in 4-seconds epochs in SleepSign (Kissei Comptech Co Ltd, Nagano, Japan). Vigilance states were scored as non-rapid eye movement (NREM) sleep, rapid eye movement (REM) sleep or Wakefulness, based on visual inspection of the frontal and occipital EEG and the EMG (Figure 1). Brief episodes of movements during sleep (up to 4 epochs) were scored as movement rather than wakefulness. Episodes of NREM and wakefulness were considered as uninterrupted if interruptions were 16s or shorter, episodes of REM were considered as uninterrupted if interruptions were 8s or shorter. Epochs with large movement and other noise were scored as artefacts of the respective vigilance state, which were included in vigilance state analysis but not spectral analysis.

For spectral analysis, two methods of calculating spectra were compared. First, spectra were calculated within SleepSign software. After sleep scoring was completed, continuous Fast Fourier Transforms (cFFT) were computed within the software, using a Hanning window and 0.25 Hz resolution, and cFFTs were exported with a 0-30 Hz window. The second method involved calculating spectra directly from raw data in Matlab, applying the PWelch function:

[pxx f] = pwelch(**data, window , noverlap , NFFT , Fs , 'spectrumType'**)

- window: Hanning and number of samples per window (sampling rate / frequency bin size)
- noverlap: overlap between adjacent windows, 0
- NFFT: length of a window
- Fs: sampling rate
- spectrumType: power spectral density (PSD)

In the output, pxx is the power spectral density that is estimated for each frequency bin, and f is the centre frequency for each frequency bin.

The PWelch method is provisionally most accurate, because it divides the signal into shorter fragments of which the results are averaged, reducing variance. With my data, I found that PWelch generated spectra with higher absolute power but with a similar shape compared to the SleepSign-generated spectra (Figure 2.2). For all spectral analysis presented in this thesis, I used the PWelch function in Matlab.

For examining temporal dynamics of spectra around NREM-REM transitions and after sleep deprivation (Chapter 3), spectra were also calculated with PWelch in Matlab, but instead of using as data input a matrix of all epochs of a vigilance state combined, power spectral density was calculated per epoch, resulting in a matrix with dimensions epochs x frequency bins.

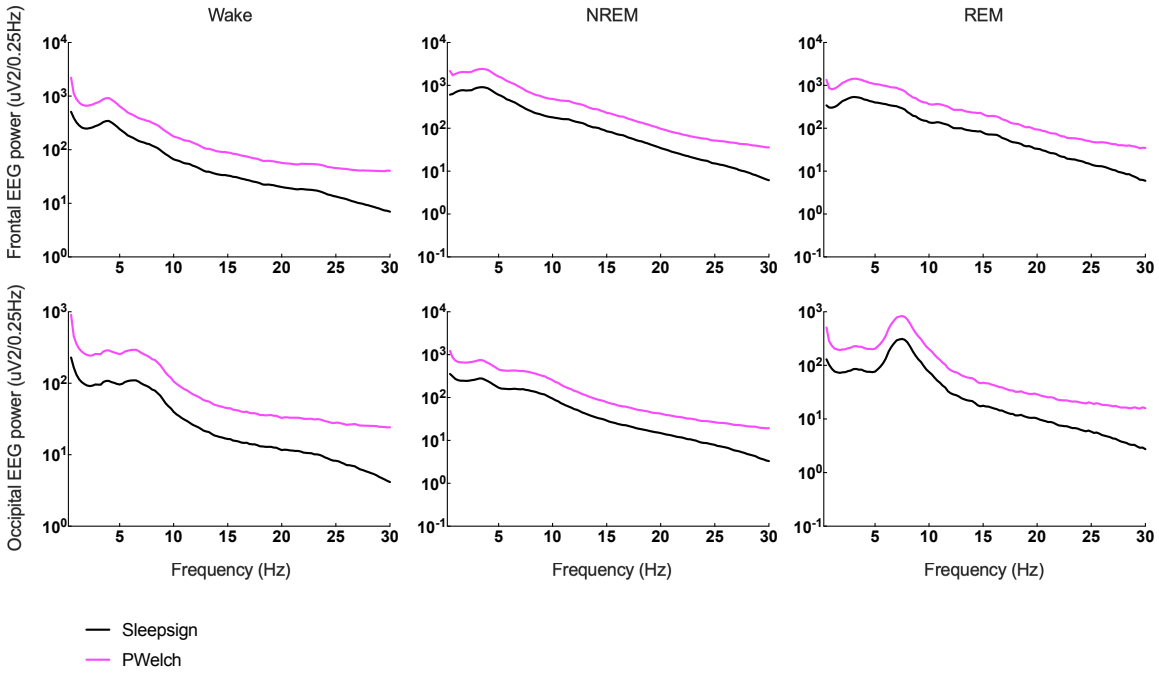

Figure 2.2: Comparison of two methods of calculating Fast Fourier transforms.
Fourier transforms calculated in SleepSign (black trace) and with the PWelch function in Matlab (magenta) in a single animal during Wake, NREM and REM sleep for the frontal and occipital EEG. The PWelch method results in higher EEG power estimates but the shape of the spectra is comparable between both methods.

For calculating EEG power in frequency bands, the Matlab function bandpower was used:

Bp = bandpower(**pxx, f , freqBand , spectrumType**)

- **pxx**: spectral power density with 0.25 Hz bins
- **f**: spectral bins in spectrum loaded, 513 frequency bins from 0-128 Hz
- **freqBand**: frequency band limits, e.g. [1 4] for 1-4 Hz delta power
- **spectrumType**: power spectral density (PSD)

Theta peaks were calculated by plotting the spectrum pxx, finding the maximum value within the defined theta peak window (3.5-9 Hz for wakefulness, 4.5-9 Hz for REM) and determining the frequency at which the maximum value occurred.

2.7 Statistics

Data was analysed with Matlab and GraphPad Prism. Unless otherwise indicated, all reported averages are mean ± standard error of the mean (SEM) values, and for all statistical tests, alpha was set at 0.05. Throughout this thesis, the applied statistical test is stated in the text and numbers of animals contributing to the data are stated in the figure legends.

Differences between L6b silenced and WT animals were investigated with unpaired two-tailed t tests if there was a single value per animal. One exception to this was the NREM latency that was calculated for sleep phenotyping in Chapter 3, where values were obviously not normally distributed, and a Mann Whitney U test was performed instead.

When there were multiple values per animal, genotypes were compared with two-way Analyses of Variance (ANOVAs) with genotype as column factor and sleep architecture parameters, epochs, or EEG frequency bin as row factor. When there were missing values, a Mixed Effects ANOVA was applied instead of a two-way ANOVA. Equal variability of differences between the groups was not assumed, and therefore the Geisser-Greenhouse correction was applied for all two-way ANOVAs and mixed effects analyses. Significant two-way interactions were followed up with post-hoc comparisons, with Bonferroni correction (0.05/number of observations), except for post-hoc comparisons of EEG spectra, where no correction was applied, as adjusting

for 119 frequency bins (0.25 Hz bins between 0.5-30 Hz) would be too conservative (Krone et al 2021). When there were more than two conditions compared, three-way ANOVA was applied. For EEG spectral analysis, EEG spectra of individual animals were either log transformed or normalised to baseline or vehicle spectra before statistical testing.

For the preliminary survival analysis in Chapter 4, the maximal duration of wakefulness episodes was determined per animal and per condition, and the difference in maximal wakefulness between conditions (orexin and vehicle) was compared between genotype groups with a log rank test in GraphPad Prism.

2.8 Histology

After completion of the experiment, animals were deeply anaesthetised with a lethal dose of pentobarbitone (obtained from the BSB) and after the toe pinch reflex and corneal reflex had disappeared, perfused with 0.1 M Phosphate Buffered Saline (PBS), followed by 4% formaldehyde (F8775; Sigma-Aldrich) in 0.1 M PBS. Headstages were pulled off and brains were extracted, post-fixed in 4% PFA for 24 hours at 4 °C, and transferred to 0.05% PBS-azide (PBSA) for long-term storage at 4 °C. Brains were sectioned into 50µm-thick coronal sections using a vibroslicer (Leica VT1000s). Free floating sections were collected and stored in PBSA. Nuclei were stained with 4′,6-diamidino-2- phenylindole (DAPI) for visualisation of tissue structure. The sections were mounted in mounting medium (Fluorsave, VWR, Lutterworth UK) on a microscope slide (Thermoscientific superfrost, RF12312108, Loughborouw, UK) and covered with a cover slid (VWR coverglasses, 24 x 50mm, 531-0146, Lutterworth UK). The brain sections were imaged with an epifluorescence microscope mounted with a camera (Leica Digital Module R, (DMR) with DFC500) or confocal microscope (Zeiss LSM710). Images were processed in Fiji is Just ImageJ (FIJI, Schindelin et al 2012) by background subtraction, brightness, and contrast adjustments, and merging of images from different fluorescent channels. Further processing, such as adding labels and indicating histological or anatomical boundaries, were carried out in Adobe Illustrator (Adobe Illustrator 2021, San Jose, California, USA).

3 Sleep architecture and sleep regulation in 'layer 6b silenced' mice

3.1 Introduction

In this Chapter, I describe my investigation of sleep-wake architecture, EEG oscillations and homeostatic sleep regulation in Drd1a-Cre;Ai14;Snap25$^{fl/fl}$, or 'layer 6b (L6b) silenced' mice. In the L6b silenced mouse, there is a selective elimination of regulated synaptic vesicle release from around birth in a subpopulation of excitatory neurons in cortical L6b, which allows the study of the functional role of these neurons (Figure 3.1).

I performed continuous EEG/EMG recordings in freely moving L6b silenced and control animals during an undisturbed 24-h baseline day, followed by sleep deprivation (SD), to investigate whether L6b silencing results in changes in sleep architecture and the homeostatic regulation of sleep. In addition, circadian phenotyping was undertaken to address whether any sleep-related changes are mediated by the circadian clock.

3.1.1 SNAP25

Synaptic vesicles can be released from neurons through spontaneous (Dagani and D'Angelo, 1992; Katz and Miledi, 1963) and regulated (Südhof and Rothman, 2009) synaptic vesicle release, and each of these processes is facilitated through a specific set of proteins. Regulated synaptic vesicle release, which follows depolarisation of the presynaptic terminal, is mediated by the N-ethylamide-sensitive factor attachment protein receptor (SNARE) complex that has components in the synaptic vesicle membrane and in the cell membrane of the presynaptic terminal. After

depolarisation of the presynaptic neuron, voltage gated calcium channels open, leading to calcium influx. This causes SNARE proteins associated with the synaptic vesicle to interact with SNARE proteins in the plasma membrane, promoting and fuelling the fusion of the respective membranes and the release of neurotransmitter from the synaptic vesicle. The neurotransmitters then bind to receptors on the postsynaptic neuron, transmitting the signal downstream (Rizo and Südhof, 2012; Söllner et al., 1993).

SNAP25 (Synaptosomal Associated Proteins of 25 kiloDalton) proteins are SNARE complex proteins that are associated with the plasma membrane, and they mediate regulated synaptic vesicle release, by forming a complex with synaptobrevin in the synaptic vesicle membrane and syntaxin-1 in the plasma membrane (Hanson et al., 1997; Poirier et al., 1998; Sutton et al., 1998). In culture, genetic deletion of *Snap25* leads to condensation of the cis-Golgi system, which results in cell death from the third division onwards, although some cells survive past the first week (Santos et al., 2017). Moreover, loss of *Snap25* in vitro reduces neuronal arborisation and completely eliminates regulated synaptic vesicle release (Bronk et al., 2007; Delgado-Martínez et al., 2007; Tafoya et al., 2008; Washbourne et al., 2002). Spontaneous vesicle release was found to occur with a reduced frequency in cultured Snap25 KO neurons in vitro but in vivo was unaltered in *Snap25* KO mice (Bronk et al., 2007; Delgado-Martínez et al., 2007; Tafoya et al., 2008; Washbourne et al., 2002). In vivo, the absence of regulated synaptic vesicle release at the neuromuscular junction in *Snap25* KO mice results in lethality at birth (Washbourne et al., 2002).

Whereas in vivo whole-mouse manipulation of *Snap25* is impossible because of the perinatal lethality, *Snap25* can be targeted in specific cell populations without causing lethality. Elimination of functional *Snap25* from specific populations of cortical projection neurons by Cre mediated excision in cortical L5 (Rbp4-Cre), L6a (Ntsr1-Cre) and L6b (Drd1a-Cre) reduces fusion of synaptic vesicles with the presynaptic terminal and shows normal initial cortical development (Hoerder-Suabedissen et al., 2019; Korrell et al., 2019). Eventually, this manipulation results in neuronal degeneration, with the time course of degeneration varying per targeted neuronal

population. In the L5 silenced (Rbp4-Cre;Ai14;Snap25$^{fl/fl}$) mouse, degeneration starts at the earliest age, from 8 months of age, whereas in the L6b silenced (Drd1a-Cre;Ai14;Snap25$^{fl/fl}$) mouse, there is synaptic loss and fibre loss, but no degeneration was observed until 9 months of age, the oldest time point investigated (Hoerder-Suabedissen et al., 2019). Thus, in my study, Drd1a-Cre neurons are present in L6b and are expected to show no signs of neurodegeneration, but have no functional synaptic transmission, effectively eliminating these neurons and their downstream effectors, a situation we refer to as 'synaptic silencing'.

3.1.2 The Drd1a-Cre driver line

In the Tg (Drd1a-cre)FK164Gsat/Mmucd mouse (Drd1a Cre) line, Cre recombinase is expressed relatively selectively in neocortical L6b from the time of birth (Gerfen et al., 2013). Expression is specific to cortical excitatory neurons and is observed in 25-40% of neurons in L6b (Hoerder-Suabedissen et al., 2018; Zolnik et al., 2020). Drd1a-Cre cells often have a pyramidal shape, but are also observed with other morphologies, such as multipolar and with a tangential orientation (Hoerder-Suabedissen et al., 2018). Monosynaptic rabies virus tracing experiments in primary somatosensory cortex using Drd1a-Cre neurons as starter cells showed that they receive predominantly long-range intracortical input (Zolnik et al., 2020) and anterograde Cre dependent adeno associated virus tracing indicated that they project to L1 and L5 of the cortex, and selectively to higher order (e.g. lateral posterior (LP) and posterior (Po) nuclei) but not first order (e.g. dorsal lateral geniculate nucleus, ventrobasal nucleus, medial geniculate nucleus) nuclei of the thalamus (Hoerder-Suabedissen et al., 2018). The L6b projections do not form collaterals to the thalamic reticular nucleus (TRN), and they form small boutons at their targets (Hoerder-Suabedissen et al., 2018). Cortically, expression of Drd1a-Cre is most prominent in L6b but also observed in L6a and occasionally in L5, especially in anterior and medial cortical areas (Hoerder-Suabedissen et al., 2018). Subcortically, sparse expression is found in hippocampus and striatum, and denser expression in several midbrain nuclei and in the cerebellum (Hoerder-Suabedissen et al., 2018)(Supplementary Figure S3.2).

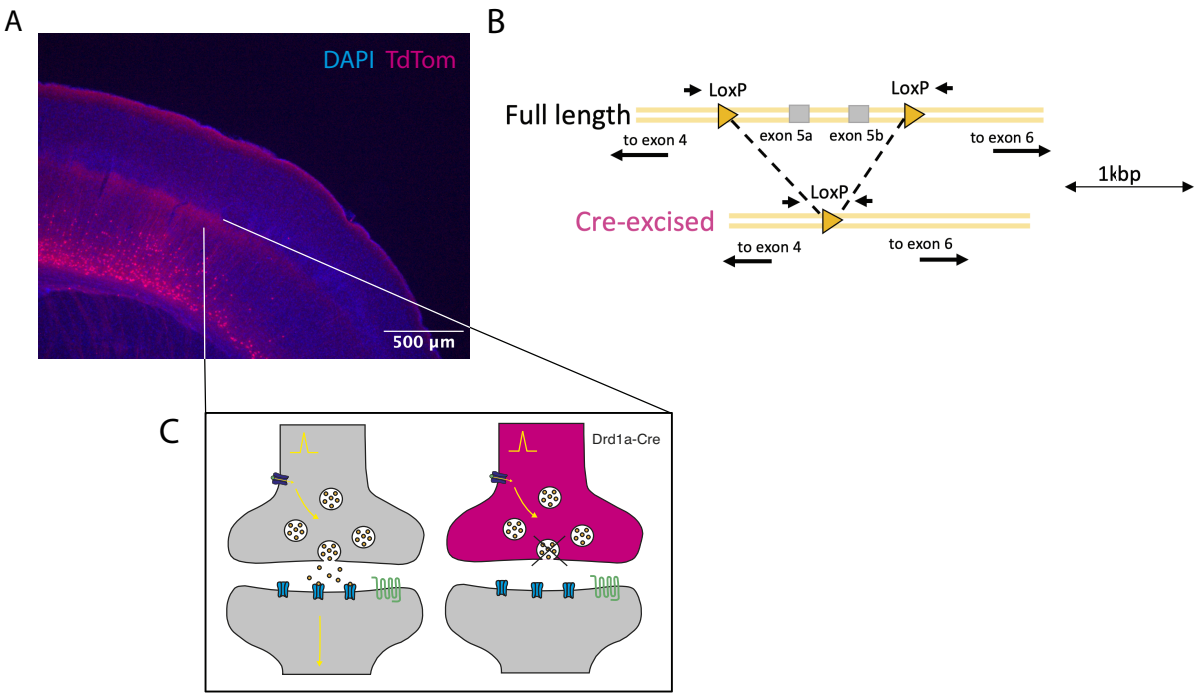

Figure 3.1 The 'layer 6b silenced' mouse. (A) Cre expression in Drd1a-Cre;Snap25fl/fl;TdTom ('L6b silenced') mice express is mostly restricted to cortical L6. Cre expressing cells co-express TdTomato, allowing visualisation of these cells. (B) When Cre is present, exon 5a/5b of the *Snap25* gene are excised , resulting in a truncated, non-functional variant of Snap25. (C) In the absence of functional Snap25, synaptic transmission is blocked.

3.1.3 Hypothesis

L6b might have a unique role in cortical processing and brain state regulation that is different from L6a and L5. The selective projections from Drd1a-Cre neurons to higher order but not first order thalamic nuclei and the lack of collaterals to the TRN distinguishes L6b from L6a neurons, which project to both first order and higher order nuclei with small projections that have a modulating effect, and also have collaterals in TRN (Bajo et al., 1995; Bourassa and Deschênes, 1995; Guo et al., 2017; Hoerder-Suabedissen et al., 2018; Sherman and Guillery, 1996). Based on its thalamic projection pattern, L6b is more comparable to L5 than to L6a, but axonal projections from L6b are on average not as large as L5 boutons, and the responsiveness to neuromodulators is also dissimilar between L6b and L5 (Bayer et al., 2004; Hoerder-Suabedissen et al., 2018).

In vitro, L6b can be directly activated by orexin, and because of this, L6b has been suggested to stimulate arousal and wakefulness via an orexin-activated gated mechanism (Bayer et al., 2004; Hay et al., 2015; Wenger Combremont et al., 2016a).

Orexin neurons have widespread projections to the brainstem nuclei of the ascending arousal system, thalamus, and cortex and promote wakefulness (Peyron et al., 1998). In PFC, orexin can activate L2/3 and L5 (Li et al., 2010; Song et al., 2006; Xia et al., 2005; Yan et al., 2012a), but in primary somatosensory, primary visual, motor, and cingulate cortex selectively activates L6b (Bayer et al., 2004; Wenger Combremont et al., 2016b, 2016a). In thalamus, orexin more powerfully activates higher thalamic nuclei, which are a projection target of L6b (Bayer et al., 2002; Hoerder-Suabedissen et al., 2018; Lambe and Aghajanian, 2003).

Orexin does not only have a wake-promoting but also a state-stabilizing effect, since genetic removal of orexin or orexin receptors leads to sleep fragmentation in laboratory animals (Chemelli et al., 1999; Hara et al., 2001; Lin et al., 1999). Moreover, decreased orexin levels are correlated with narcolepsy in humans, which is a disease of sleep-wake instability characterised by rapid-onset sleep attacks intruded into wake and frequent arousals from sleep (Nishino et al., 2000; Peyron et al., 2000; Thannickal et al., 2000).

If activation of cortical L6b is important for the effects of orexin on sleep-wake regulation, silencing L6b could mimic or partially mimic the effects of orexin or orexin receptor deletion in cortex, with a reduction in arousal behaviour and impaired sleep-wake consolidation.

Since the L6b silenced mouse is a unique model not used by any other group, the study was exploratory in nature, using group size comparable to studies in literature. I performed continuous EEG/EMG recordings in freely moving L6b silenced (n=9) and Cre negative control (n=7) animals. I analysed the distribution of vigilance states across 24 hours, not limited to but with attention to parameters of sleep fragmentation. I conducted EEG power spectral analysis for each vigilance state. The animals were subjected to SD to investigate homeostatic regulation of sleep. Lastly, I reanalysed an existing data set for a circadian screen that has been performed in a seperate cohort of L6b silenced animals.

3.2 Methods

3.2.1 Layer 6b silenced mice breeding

For the establishment of the colony, C57BL6-Snap25tm3mcw (Snap25$^{fl/fl}$) mice were crossed with C57BL6;129S6-Gt(ROSA)26Sortm14(CAG-tdTomato)Hze/J (Ai14) mice until both alleles were present homozygously. In the homozygous animals, exon 5a/5b of the *Snap25* gene is floxed and excised in cells that express Cre, rendering a truncated, dysfunctional protein, and omitting regulated vesicle release (Figure 3.1)(Hoerder-Suabedissen et al., 2018). Concomitantly, a stop sequence is excised, and the reporter TdTomato is expressed, for visualisation of silenced neurons (Figure 3.1). Snap25$^{fl/fl}$;Ai14/Ai14 mice were crossed with the driver line (Tg(Drd1a-cre)FK164Gsat/Mmucd (Drd1a-Cre::MMRRC)), where Cre is expressed predominantly in L6b starting from the time of birth (Hoerder-Suabedissen et al., 2018). I maintained the colony by crossing Cre$^{/+}$::Ai14/Ai14::Snap25$^{fl/fl}$ females to Ai14/Ai14::Snap25$^{fl/fl}$ males.

For colony maintenance, the genotype of pups was determined by assessing TdTomato expression in young (~P14) animals with fluorescent goggles in the breeding facility. For experimental animals, the genotype was confirmed by polymerase chain reaction (PCR) from ear clips in-house or through Transnetyx (Transnetyx Inc, Cordova, Tennessee, USA). For the experimental EEG/EMG cohort, young male animals were used (L6b silenced (n=9), Controls (n=7)), where possible littermates. Only male animals were used, because the role of L6b may vary with sex, and therefore group sizes would need to be much larger than desired from an initial, exploratory study. Although the age at the start of the recording was comparable between the genotypes (controls 11±0.48 weeks vs L6b silenced 10.6±0.39 weeks $t_{(14)}$=0.6966,p=0.4974), the L6b silenced animals had a lower body weight (controls 23±0.67 g vs L6b silenced 21±0.47 g, $t_{(14)}$=2.530, p=0.024). A lower body weight compared to Cre negative control animals has also been observed in Rbp4-Cre;Snap25$^{fl/fl}$;TdTom, or 'L5 silenced' mice (Hoerder-Suabedissen et al., 2019). Implant weights were surprisingly comparable (controls 0.94±0.04g, L6b silenced 0.94±0.04g).

3.2.2 Experimental procedures

A detailed description of the surgical implantation of EEG/EMG devices, electrophysiological recording setup, data acquisition, sleep state annotation, data analysis, statistical procedures, and histology can be found in the in Chapter 2 – General Methods.

3.2.3 Sleep deprivation procedure

For sleep deprivation (SD), animals were kept awake from light onset for the duration of 6 hours, during the time when mice in laboratory conditions are predominantly asleep. At light onset (9AM), the chambers were opened, and nests were removed from the cages. Next, animals were continuously observed by an experimenter for the full 6 hours, and when an animal seemed to be falling asleep based on posture and/or online EEG/EMG traces, a novel object was introduced into the cage. This is a common procedure for SD in rodents, and keeps animals awake successfully in an ethologically relevant manner that is less stressful than other methods of SD (McKillop et al., 2018). After 6 hours, the objects were taken out of the cages, the nests were reintroduced, and the chambers were closed.

3.2.4 Data analysis

Data analysis is described in Chapter 2 – General methods. In the current section, I specify the mode of spectral calculations. For state-specific spectral analysis, Fourier transforms were generated in Matlab with the PWelch function, across all epochs with the same vigilance state assignment (Chapter 2 – General Methods). For analysis of spectra around the NREM-REM transition and analysis of sleep homeostatic regulation, Fourier transforms were also generated in Matlab with the PWelch function, but calculated per epoch, to allow investigation of temporal dynamics. Spectra were either log transformed (24-hour spectra) or normalised (NREM-REM transition spectra normalised to 24-hour NREM baseline spectra, SD spectra normalised to 24-hour NREM/Wake baseline spectra) before statistical comparison.

3.2.5 Excluded EEG/EMG data from pilot experiment

In 2015, a pilot EEG sleep study was performed by Associate Professor Tomoko Yamagata, in a small cohort of L6b silenced animals (n=2) and a control animal (n=1). In the pilot, no major effects on distribution of vigilance states were identified, but the cohort size was too small to conduct spectral analysis and no detailed investigation of the effects of SD was undertaken. Yet, the foundations for the study of sleep wake regulation in L6b silenced were laid, and we decided to revive this project and repeat the experiment with a cohort size conventional in neurophysiological rodent sleep studies at the start of my DPhil. To decide whether I could include the previously recorded data, I compared the spectra exported from SleepSign from the 2015 cohort and my current 2022 cohort. I found that the spectra of the 2015 study were significantly different from the current 2022 study (Supplementary Figure S3.1). For the 2015 animals, there was also not sufficient data for control animals, and inclusion of just L6b silenced animals' data would lead to unbalanced group sizes. Considering these aspects, I decided not to include the data from the 2015 pilot study in my analyses and focus only on the current cohort.

3.2.6 Excluded EEG/EMG data from the current experiment

For the current cohort, the occipital EEG channel in one control animal (C7) was of low quality and excluded from spectral analysis for both baseline and SD day. The occipital EEG channels of one additional control animal (D6) and a L6b silenced animal (D5) were excluded only for SD. In two (different) animals, the EMG signals were of insufficient quality to reliably score bouts of movement, so these animals were excluded from analysis of brief awakenings. The reduced quality of some channels was most likely due to impaired conduction in the head stage wires after multiple days of implantation; especially the EMG wires, which are implanted in the neck muscles, are prone to deterioration over time. Artifact 4s-epochs were scored as artifact of their respective vigilance state and included in sleep-wake architecture analysis but excluded from EEG spectral analysis. The percentage of artifact epochs across the 24-hour file was comparable between genotypes (Controls 2.80±1.43%, L6b silenced 2.09±0.729, $t_{(14)}$=0.4706, p=0.65).

3.2.7 Circadian screen

This experiment has been performed in 2015 by Dr Luiz Guidi and Professor Peter Oliver in a separate cohort of L6b silenced animals that was generated by Dr Anna Hoerder-Suabedissen. I received the blinded raw data from Luiz and reanalysed the data.

Experimental setup

For the circadian experiment, young adult male L6b silenced (n=6) and control animals (n=7) were used, that had been raised in 12h:12h light-dark schedules with food and water ad libitum. Upon start of the experiment, they were moved to individual cages inside light-tight chambers to allow better control of the light-dark schedule. Home cage activity was assessed with running wheels, of which rotations were recorded with a 1-minute resolution in ClockLab (ActiMetrics Inc, Wilmette, Illinois, USA, version 6.1.02).

Experimental schedule

Baseline rhythmicity was investigated with a 12h:12h light-dark schedule, with lights on at 5:00AM (Figure 3.2). After 21 days, the light schedule was changed to constant darkness for 10 days, for assessment of the innate active period, alpha. Next, animals were kept in constant light for 16 days, aimed at characterising properties of the circadian clock in constant conditions. Lastly, a 6-hour phase-advance protocol was applied, in which lights were turned off at 11:00AM, corresponding to 6h after light onset, and on at 11:00PM, and recordings continued for 10 days.

Excluded data

During the 12h:12h light-dark condition, the first two days were excluded for all animals because the animals were not stably entrained yet, and the last day was excluded for all animals because the data was missing as a result of a computer crashes. For both the constant dark and the constant light paradigm, one day was excluded for all animals because of missing data. For the constant light condition, data from one control animal was excluded for technical reasons.

Data analysis

I received raw data blinded per genotype as 'cat' and 'dog'. Unblinding was performed after completion of analysis and verified with the original investigators. I reanalysed all raw data in Clocklab and further processed the results in Matlab and GraphPad Prism.

Statistics

All comparisons in the circadian screen report the results of a two-tailed unpaired t test, except for the phase advance paradigm, where the genotypes are compared with a two-way ANOVA.

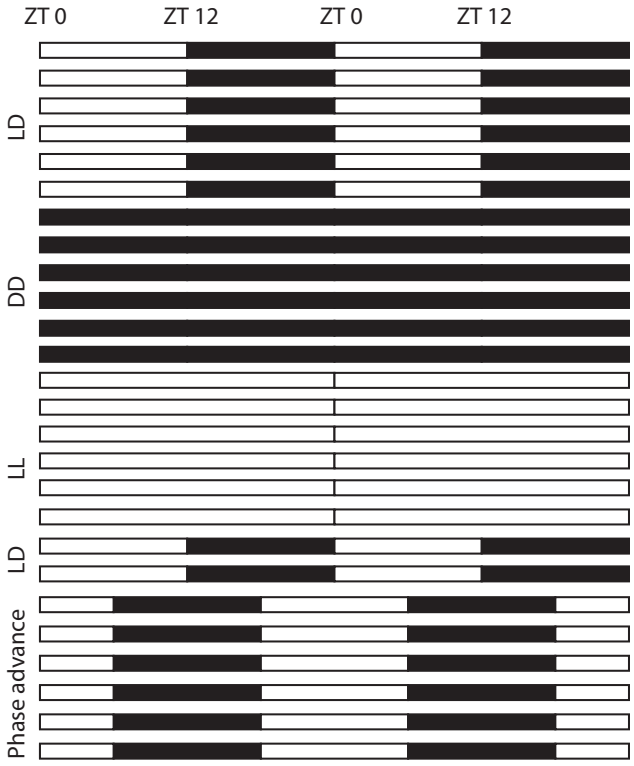

Figure 3.2: Schematic overview of the circadian experiment.
Each bar shows two consecutive days of 24 hours. The number of bars per condition is kept constant for ease of visualisation and does not precisely correspond to the exact number of days per condition. First, animals were exposed to a 12:12h light-dark schedule for 21 days (LD). Then, animals were kept in constant darkness for 10 days (DD). Next, the lights were constantly turned on for 16 days (LL). The animals were then exposed to a few days of a 12:12h light dark schedule again (LD), after which the phase of the light schedule was advanced for 6 hours and kept on this schedule for another 10 days (phase advance).

3.3 Results

In this experiment, I conducted continuous EEG/EMG recordings in L6b silenced mice, in which regulated synaptic transmission is ablated from Drd1a-Cre positive cortical neurons by Cre dependent deletion of exon 5a/5b of the *Snap25* gene (Hoerder-Suabedissen et al., 2019).

3.3.1 Baseline sleep-wake regulation in L6b silenced mice

Blinded scoring of vigilance states was performed manually in 4s-epochs following convention in EEG sleep studies (Yamagata et al., 2021). Epochs with irregular low-amplitude EEG activity and low or high EMG activity were scored as wakefulness; epochs with high-amplitude, low-frequency EEG waves and heartbeat-only EMG activity, were scored as NREM; epochs with regular low-amplitude, 4-10 Hz EEG activity and heartbeat-only EMG activity were scored as REM (Figure 3.2). NREM episodes interrupted by short bouts of movement on the EMG (≤16s) were considered as single episodes and these brief awakenings were scored as 'movement'. Raw traces were comparable between genotypes, facilitating unbiased scoring (Figure 3.3).

Hypnograms show that during the light phase, more time is spent asleep, and during the dark phase, wakefulness predominates, as is expected from nocturnal animals (Figure 3.4). The time course of NREM sleep slow wave activity (SWA, 0.5-4 Hz) in the frontal EEG showed a typical build-up and decline of SWA during sleep. EMG activity is high during wakefulness, and low during sleep (Figure 3.5A). During NREM sleep, EEG power is increased in the lower frequencies (0.5-4 Hz), and during wakefulness, EEG power becomes more prominent in the theta-frequency range (4-10 Hz), especially in the occipital EEG (Figure 3.5B,C).

In all animals, the EEG spectral power density showed a typical pattern of high SWA (0.5-4 Hz) during epochs scored as NREM sleep, a prominent theta peak (4-10 Hz) during epochs scored REM sleep, and mixed frequencies during epochs scored as wakefulness (Figure 3.5C). The high levels of SWA during NREM sleep are most pronounced in the frontal EEG, reflecting more frequent occurrence of slow waves in anterior brain areas. The theta peak is most pronounced in the occipital EEG, as the occipital EEG electrode is closest to the hippocampus in rodents.

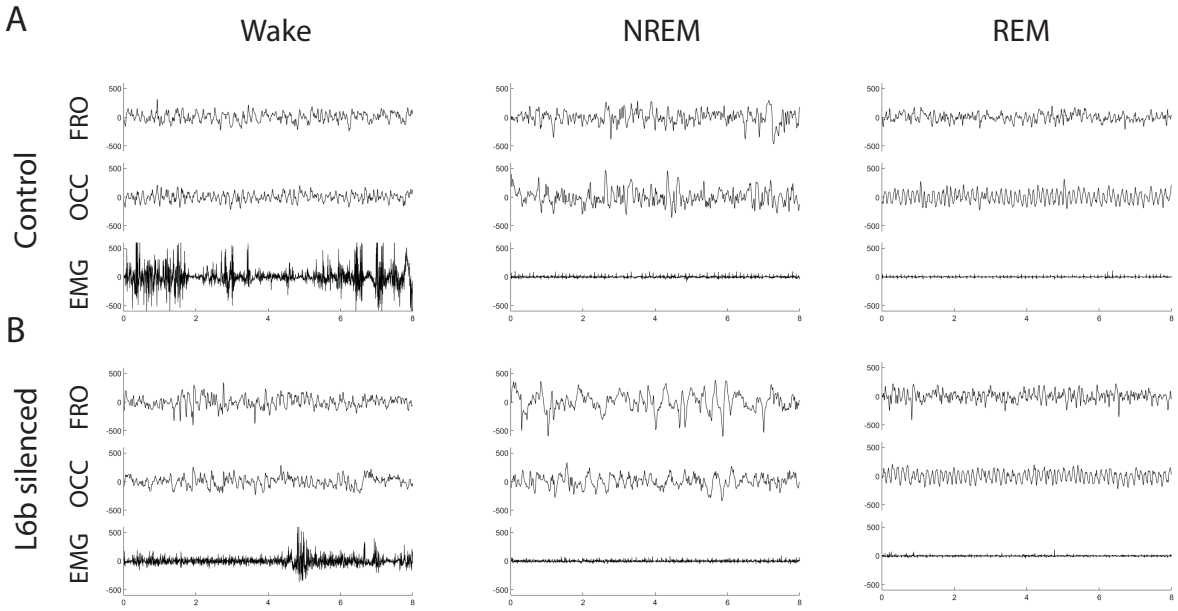

Figure 3.3: Example EEG/EMG traces in a L6b silenced and control animal. An 8 second trace is shown for the frontal EEG, occipital EEG and EMG during Wake, NREM and REM in a representative control (A) and a L6b silenced animal (B).

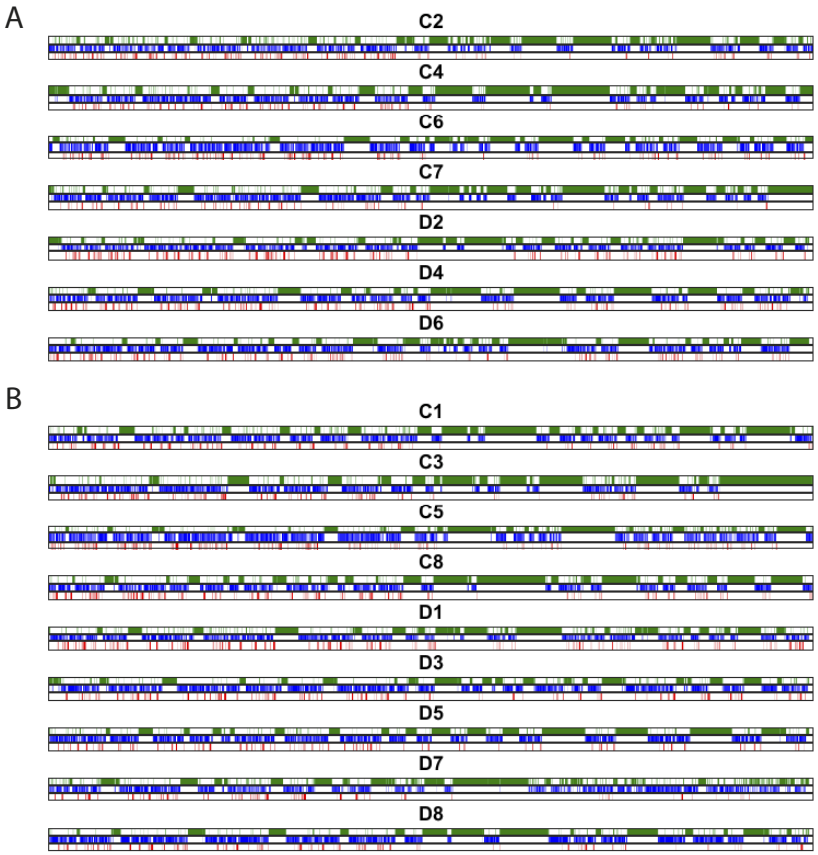

Figure 3.4: Hypnograms of all animals. Hypnograms across 24 hours show no obvious differences in the distribution of wakefulness (green), NREM sleep (blue) and REM sleep (red) between control animals (A) and L6b silenced animals (B).

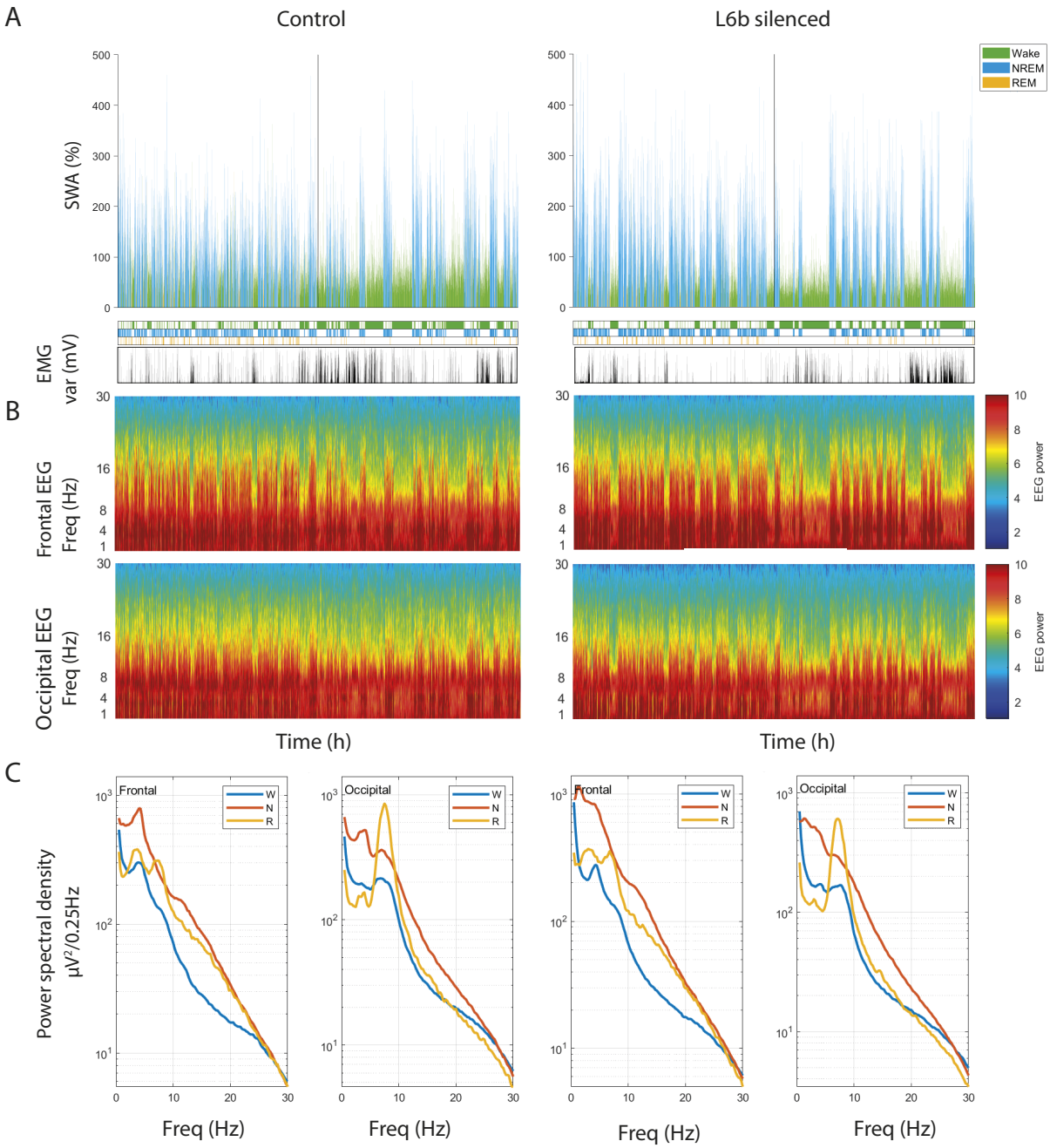

Figure 3.5: Spectral characteristics in example animals.
(A) Representative SWA, hypnogram and EMG variance in a representative control (left) and L6b silenced (right) animal. SWA shows a typical pattern of exponential increase and decrease during NREM, visible by the comparison of SWA and the hypnogram plotted below. EMG activity is highest during wakefulness and lowest during NREM and REM.
(B) Power spectral density across 24 hours in a representative control (left) and L6b silenced (right) animal.
(C) Power spectral density per vigilance state averaged over 24 hours in a representative control (left) and L6b silenced (right) animal.

3.3.2 Daily sleep-wake architecture

On visual inspection of all hypnograms, no major differences were apparent between the two genotypes (Figure 3.4). Across 24 hours, L6b silenced and control animals spent comparable time in wakefulness (controls 42.5±1.30% vs L6b silenced 41.3±1.82%, $t_{(14)}$=0.5059, p=0.6208), NREM (controls 45.0±0.799% vs L6b silenced 46.6±1.55%, $t_{(14)}$=0.8672, p=0.4005) and REM sleep (controls 7.97±0.710% vs L6b silenced 7.41±0.407%, t(14)=0.7262, p=0.4797)(Figure 3.6C).

The hourly time courses of Wake, NREM and REM showed a typical pattern for nocturnal animals, with most time in NREM sleep during the light phase and most time in wakefulness during the dark phase with no difference between genotype-grouped averages (Figure 3.6A)(Time x Genotype interaction, Wake $F_{(23,322)}$=0.8239 p=0.7008; NREM F(23,322)=0.8173 p=0.7094; REM $F_{(23,322)}$=0.6488, p=0.8925). The hourly time course of REM sleep as a percentage of total sleep was also not different (Time x Genotype interaction, $F_{(23,322)}$=1.133, p=0.3075), indicating that L6b silencing does not selective suppress or enhance REM sleep (Figure 3.6B).

If sleep-wake states are unstable, total time spent in each of the vigilance states can be unchanged whereas episodes will be shorter in duration and occur more frequently. The genotypes showed comparable hourly episode counts in each of the vigilance states throughout the day (Time x Genotype interaction, Wake $F_{(23,322)}$=0.8667, p=0.6440; NREM $F_{(23,322)}$=0.9279, p=0.5609; REM $F_{(23,322)}$=1.092, p=0.3527) (Figure 3.5D). The average duration of individual episodes of Wake (controls 14.3±1.29 min vs L6b silenced 14.7±1.43 min, $t_{(14)}$=0.1663, p=0.8703), NREM (controls 4.28±0.200 min vs L6b silenced 4.50±0.298 min, $t_{(14)}$=0.5671, p=0.5796) and REM sleep (controls 1.04±0.0344 min vs L6b silenced 1.10±0.0523 min, $t_{(14)}$=0.9792, p=0.3441) were also unchanged (Figure 3.6E), as was the number of brief awakenings (≤16s) from NREM sleep (controls 51.1±2.04 h^{-1} vs L6b silenced 51.6±3.97h^{-1}, $t_{(12)}$=0.1205, p=0.9061)(Figure 3.6F). Lastly, the NREM latency was not different between the genotypes (controls median 1.2 min, L6b silenced median 0.13 min, Mann Whitney U 26.50, p=0.6156)(Figure 3.6G). Altogether, these findings indicate that L6b silencing does not affect sleep-wake stability.

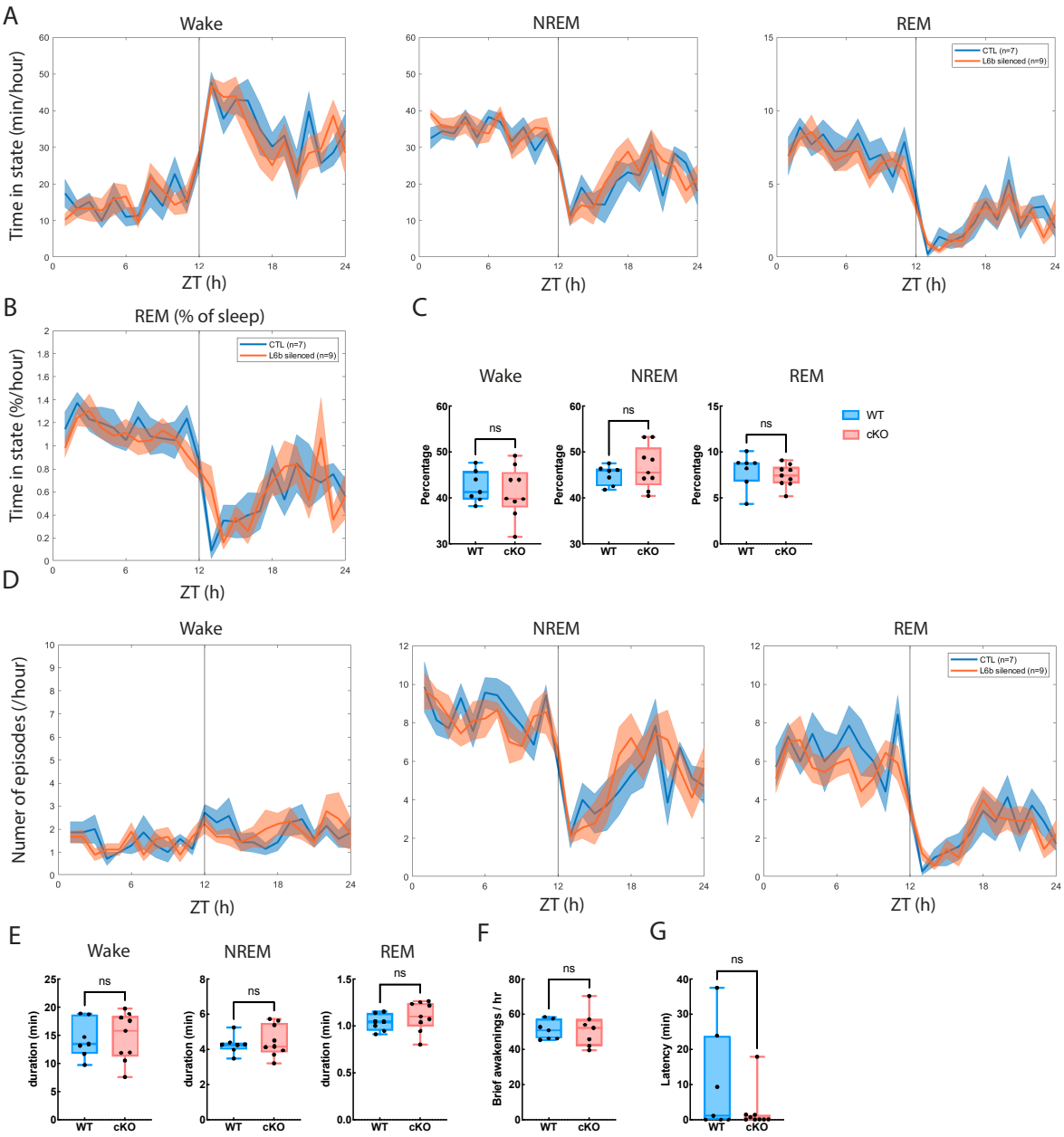

Figure 3.6: Daily sleep architecture.

(A) Hourly time course of wakefulness, NREM and REM sleep was not different between L6b silenced (n=9) and control (n=7) animals.

(B) Hourly time course of REM as a percentage of total REM sleep was also not altered in L6b silenced animals, indicating no selective suppression of REM sleep.

(C) Total percentage of time spent in Wake, NREM and REM over 24 hours was similar in L6b silenced and control animals.

(D) The number of episodes of wake, NREM and REM per hour was not affected by silencing L6b.

(E) Average episode duration was not changed in L6b silenced animals.

(F) The number of brief awakenings per hour of NREM sleep was not different between L6b silenced (n=7) and control (n=7) animals.

(G) The latency to NREM sleep was highly variable and therefore tested with a nonparametric test, that showed no significant differences between L6b silenced (n=9) and control animals (n=7).

3.3.3 Spectra during wakefulness

After examining daily sleep-wake architecture, I investigated the effect of L6b silencing on EEG spectra. L6b silencing did not alter spectral power density in the frontal EEG during wakefulness although there was a decrease in the theta power range in posthoc comparisons (Two-way ANOVA, Genotype x Frequency, $F_{(117,1638)}$=0.399, p>0.9999, posthoc comparison significant for 8.0-11 Hz, 12-12.75 Hz) (Figure 3.7A). When band power in the theta frequency range (4.5-10 Hz) was calculated, there was no significant difference between genotypes (absolute EEG power, $t_{(13.71)}$=1.494, p=0.1579, as percentage of total 1-30 Hz power ($t_{(13.52)}$=0.7057, p=0.4924, unpaired Welch's t test)(Figure 3.7E,F).

In the occipital EEG, L6b silencing significantly changed spectral power density during wakefulness, due to a reduction in the theta frequency range (Two-way ANOVA, Genotype x Frequency, $F_{(117,1521)}$=2.176, p<0.0001, posthoc comparison significant for 8.75-13.5 Hz, 14.0-15.0 Hz). Yet, when band power was calculated for the frequency range (4.5-10 Hz), there was no significant difference between the genotypes (absolute band power: $t_{(12.98)}$=1.406, p=0.1833; as percentage of total 1-30 Hz power $t_{(11.97)}$=1.146, p=0.2742), Welch's t test)(Figure 3.7 G,H).

The difference in spectral power that was observed between occipital EEG spectra (Figure 3.7B) may result from a slowing of theta oscillations (Figure 3.7J, theta peak frequency WT 7.42±0.300 Hz vs L6b silenced 5.78 ± 0.485 Hz, Welch's t test, $t_{(12.40)}$=2.873, p=0.0136) since the theta peak amplitude was not different (Figure 3.7I, $t_{(10.78)}$=0.9218, p=0.3768).

EEG spectral power in the gamma range (30-100 Hz) originates from activity in cortical networks and the amplitude of gamma oscillations is phase-locked with the phase of theta oscillations and this coupling is stronger during REM sleep (Scheffzük et al., 2011). To test whether changes occurred in the gamma frequency range, I analysed the EEG spectral power across the full spectrum recorded (up to 128 Hz), instead of using an upper limit of 30 Hz as I did in other analyses (Figure 3.7B,D). The 49-51.5 Hz frequency range was excluded from spectral analysis. I found that L6b silencing did not change gamma frequency spectral power density in the frontal or occipital EEG derivation during wakefulness.

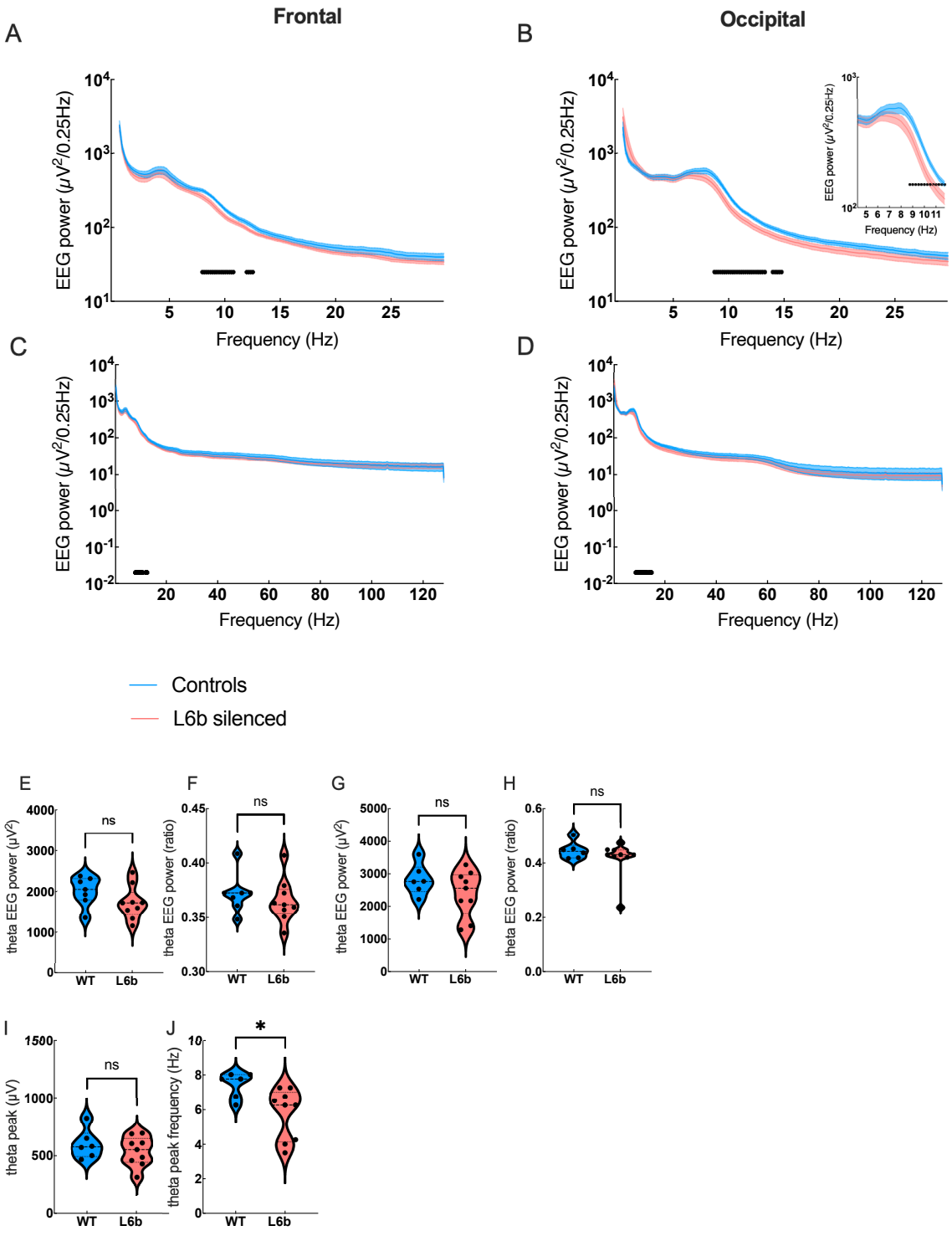

Figure 3.7: Spectral power density during wakefulness.
(A) EEG spectral power in the frontal EEG in L6b silenced (n=9) and control (n=7) animals. Black asterisks indicate frequency bins that were significantly different in posthoc comparison between the genotype groups. (B) EEG spectral power in the occipital EEG in L6b silenced (n=9) and control (n=6) animals. Inset shows changes in theta frequency range in more detail. (C) EEG spectral power in the frontal EEG with frequency range extended to 128 Hz. (D) EEG spectral in the occipital EEG with frequency range extended to 128 Hz. (E) Frontal EEG spectral power in the theta frequency band (4.5-10 Hz), absolute power and (F) power relative to total power in the 1-30 Hz spectrum. (G) Occipital EEG spectral power in the theta frequency band (4.5-10 Hz), absolute power and (H) relative to total power in the 1-30 Hz spectrum. (I) Peak value in the theta frequency range (4.5-10 Hz) in the occipital EEG and (J) peak frequency.

3.3.4 Spectra during REM sleep

REM sleep is also called paradoxical sleep because it is behaviourally characterised as sleep, but the EEG shows a pattern of cortical activation. L6b silencing affected EEG spectra during REM sleep, with a reduction in frontal EEG spectral power density in the theta and beta frequency ranges (Two-way ANOVA, Genotype x Frequency, $F_{(117,1638)}$=4.300, p<0.0001, posthoc comparison significant between 8-10 Hz and 14.75-30 Hz), which led to an overall spectral power reduction in the frontal EEG (Two-way ANOVA, Genotype, $F_{(1,14)}$=4.775, p=0.0464)(Figure 3.8A).

When I performed comparisons across the entire 0.5-128 Hz range, I found that frontal EEG power in the gamma frequency range was decreased in L6b silenced animals during wakefulness (Two-way ANOVA, Genotype x Frequency, $F_{(500,7000)}$=1.563, p<0.0001, posthoc comparison significant between 8-10 Hz, 14.75-107.5 Hz)(Figure 3.8C).

The decrease in theta power that was seen in the frontal EEG was also observed in the occipital EEG (Two-way ANOVA, Genotype x Frequency, $F_{(117,1521)}$=4.455, p<0.0001, posthoc comparison significant between 8.5-10 Hz)(Figure 3.8B), as well as a decrease in gamma power (Two-way ANOVA, Genotype x Frequency, $F_{(500,6500)}$=6.284, p<0.0001, posthoc comparison significant between 8.5-10 Hz, 69.75-128 Hz)(Figure 3.8D).

The EEG power decrease in the occipital EEG that was detected in the 8.5-10 Hz frequency range was the result of a slowing of theta power (Figure 3.8 B, G-H)(theta peak frequency controls 7.58 ± 0.0833 Hz vs L6b silenced 7.11 ± 0.0735 Hz, $t_{(11.47)}$=4.250, p=0.0012, Welch's t test) rather than an absolute decrease in theta power, which was not difference between genotypes (Welch's t test of absolute 4.5-10 Hz power in the occipital EEG, $t_{(12.37)}$=0.7076, p=0.4923)(Figure 3.8E,F).

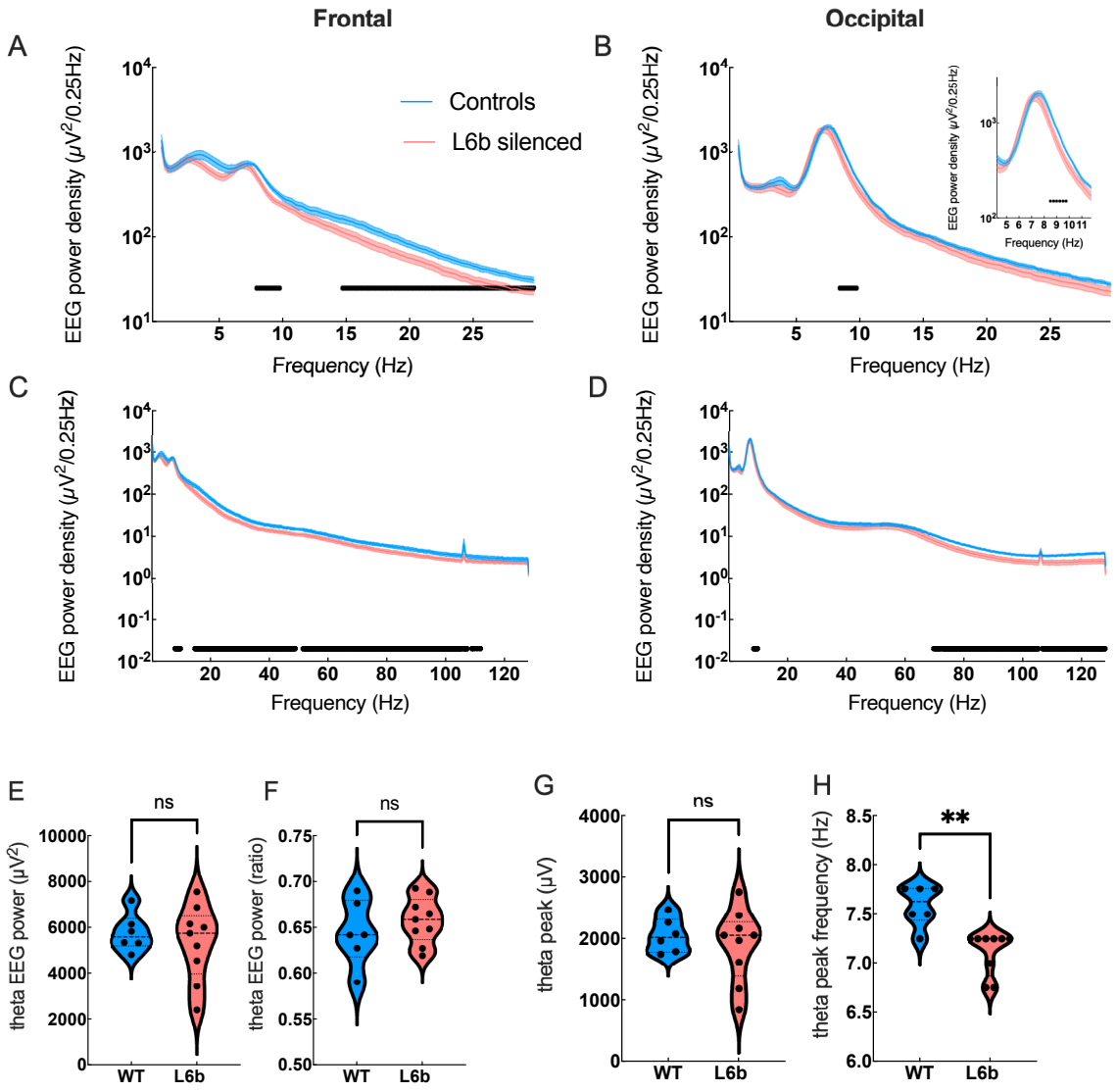

Figure 3.8: Spectral power density during REM sleep.
(A) EEG spectral power in the frontal EEG in L6b silenced (n=9) and control (n=7) animals. Black asterisks indicate frequency bins that were significantly different in posthoc comparison between the genotype groups.
(B) EEG spectral power in the occipital EEG in L6b silenced (n=9) and control (n=6) animals. Inset shows changes in theta frequency range in more detail.
(C) EEG spectral power in the frontal EEG with frequency range extended to 128 Hz.
(D) EEG spectral in the occipital EEG with frequency range extended to 128 Hz.
(E) EEG power in the theta frequency range (4.5-10 Hz) in the occipital EEG in L6b silenced and (n=9) and control (n=6) animals.
(F) EEG power in the theta frequency range (4.5-10 Hz) in the occipital EEG in L6b silenced and (n=9) and control (n=6) animals, expressed as a ratio of total 1-30 Hz occipital EEG power.
(G) EEG power at the peak theta frequency (4.5-10 Hz) in the occipital EEG in L6b silenced (n=9) and control (n=6) animals.
(H) Frequency of the theta peak (4.5-10 Hz) in the occipital EEG in L6b silenced (n=9) and control (n=6) animals.

3.3.5 Spectra during NREM sleep

During NREM sleep, L6b silencing caused a marked reduction in frontal EEG spectral density across nearly the entire frequency range, between 3-30 Hz (Two-way ANOVA, Genotype x Frequency, $F_{(117,1638)}$=8.105, p<0.0001, posthoc comparison significant between 3-30 Hz), causing an overall genotype effect (Two-way ANOVA, Genotype, $F_{(1,14)}$=10.42, p=0.0061)(Figure 3.9A). The frontal EEG power reduction extended into the gamma frequency range (Two-way ANOVA, Genotype x Frequency, $F_{(500,7000)}$=5.566, p<0.0001, posthoc comparison significant between 3-67.75 Hz)(Figure 3.9C).

At closer inspection, no change in absolute frontal EEG band power in the delta frequency range (1-4 Hz) became apparent in L6b silenced animals ($t_{(11.20)}$=1.321, p=0.2130, Welch's t test)(Figure 3.9E). When power in the delta range was normalised to the total 1-30 Hz power, the contribution of delta power seemed increased in L6b silenced animals ($t_{(13.80)}$=2.626, p=0.0201, Welch's t test(Figure 3.9F)), likely resultant from changes in other oscillations in the slower frequency range. Indeed, sigma EEG power (10.5-16 Hz) was reduced in L6b silenced animals, both when examined absolute frontal EEG power in this range ($t_{(13.33)}$=3.735, p=0.0024, Welch's t test)(Figure 3.9G) and when examined as a fraction of total 1-30 Hz frontal EEG power ($t_{(10.01)}$=3.471, p=0.0060, Welch's t test)(Figure 3.9H).

In the occipital EEG (Figure 3.9B,D), L6b silencing had an interaction with the EEG spectral power distribution but this was not localized to a specific frequency range (Two-way ANOVA, Genotype x Frequency, $F_{(117,1521)}$=3.847, p<0.0001, no significant differences in posthoc comparison)(Figure 3.9B). When the frequency range was extended, a significant decrease in high gamma power was observed in L6b silenced animals (Two-way ANOVA, Genotype x Frequency, $F_{(500,6500)}$=1.131, p=0.0274, posthoc comparison significant between 84.25-128 Hz)(Figure 3.9D).

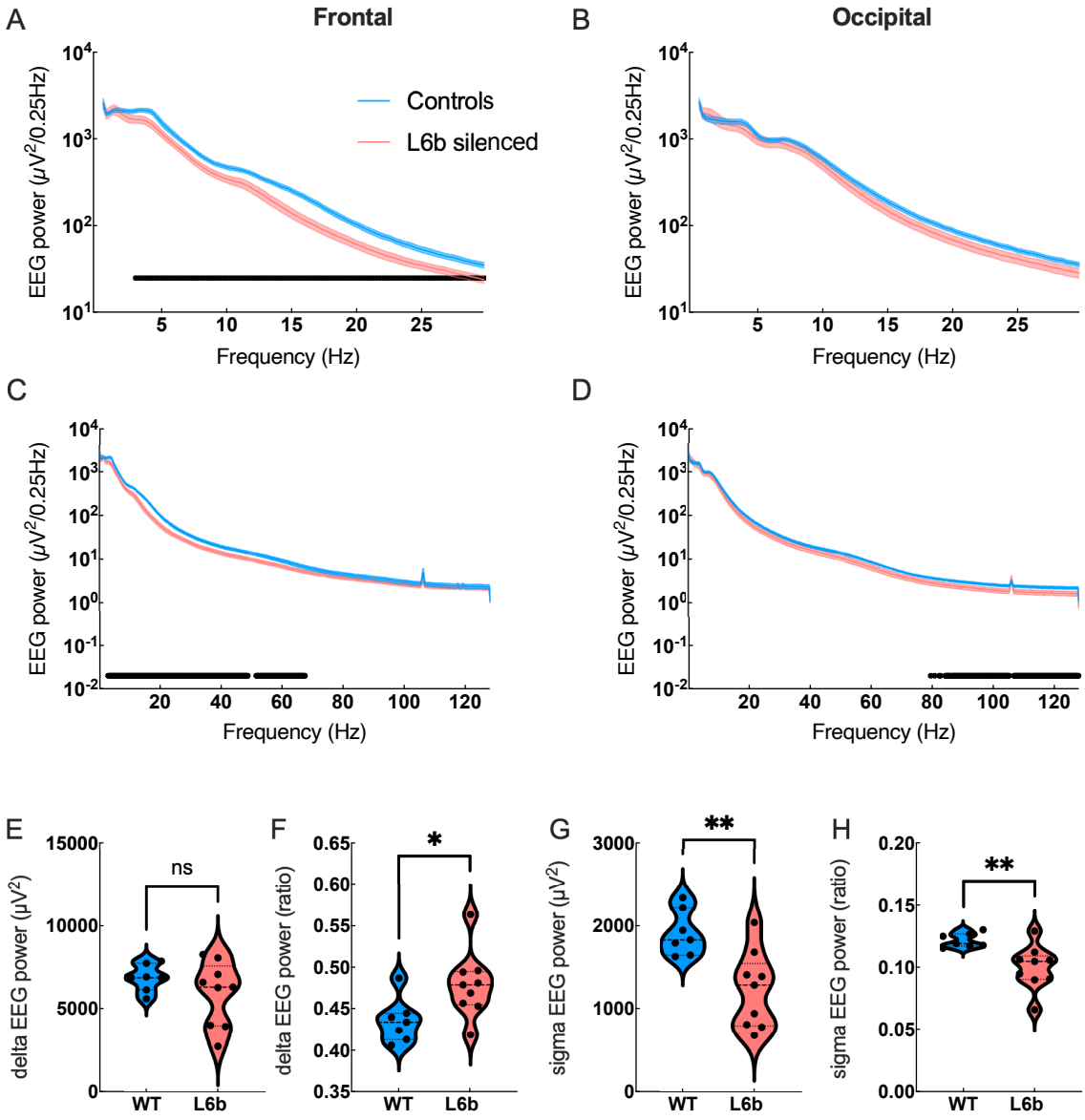

Figure 3.9: Spectral power density during NREM sleep.
(A) EEG spectral power in the frontal EEG in L6b silenced (n=9) and control (n=7) animals. Black asterisks indicate frequency bins that were significantly different in posthoc comparison between the genotype groups.
(B) EEG spectral power in the occipital EEG in L6b silenced (n=9) and control (n=6) animals.
(C) EEG spectral power in the frontal EEG with frequency range extended to 128 Hz.
(D) EEG spectral in the occipital EEG with frequency range extended to 128 Hz.
(E) EEG power in the delta frequency range (1-4 Hz) in the frontal EEG in L6b silenced (n=9) and control (n=7) animals.
(F) EEG power in the delta frequency range (1-4 Hz) in the frontal EEG in L6b silenced (n=9) and control (n=7) animals, expressed as a ratio of total 1-30 Hz frontal EEG spectral power.
(G) EEG power in the sigma frequency range (10.5-16 Hz) in the frontal EEG in L6b silenced (n=9) and control (n=7) animals.
(H) EEG power in the sigma frequency range (10.5-16 Hz) in the frontal EEG in L6b silenced (n=9) and control (n=7) animals, expressed as a ratio of total 1-30 Hz frontal EEG spectral power.

3.3.6 Spectra around NREM-REM transitions

The frequency range in which EEG spectral power density was reduced after L6b silencing included the sigma frequency range (10-16 Hz), the frequency range of sleep spindles. Because sleep spindles are observed with a higher density around NREM-REM transitions (Bandarabadi et al., 2020), I further examined EEG spectral changes around these transitions. I combined EEG spectra surrounding all NREM-REM transitions on baseline day per genotype (Figure 3.10A-D) and calculated spectra in L6b silenced animals as a ratio of spectra in control animals (Figure 3.10E,F). L6b silenced animals showed a pronounced reduction in 10-25 Hz frontal EEG spectral power in NREM epochs preceding the NREM-REM transition. The power reduction appeared as two hotspots on the spectrogram, which may reflect an underlying effect on infraslow oscillations.

Although the EEG power reduction in the sigma frequency range was distinctly visible around the NREM-REM transition, it was not specific to NREM episodes before NREM-REM transitions. When the EEG spectral power in the 32 seconds of NREM preceding NREM-REM transitions was normalised to overall NREM spectral power density on baseline day, no difference between genotypes was observed anymore (Figure 3.10G)(Two-way ANOVA, Frequency x Genotype: $F_{(118,1652)}$=1.183, p=0.0942).

In the occipital EEG, an increase in spectral power density during the 32 seconds of NREM sleep immediately preceding the transition to REM sleep was visible around 6-7 Hz, which was statistically significant (Figure 3.10H)(Two-way, ANOVA, Frequency x Genotype, $F_{(118,1652)}$=1.235, p=0.0492). During subsequent REM sleep, an increase between 6-8 Hz and a decrease between 8-10 Hz spectral power density became apparent (Figure 3.10F), which is consistent with the theta peak shift that was observed when the full day was analysed (Figure 3.8B).

Figure 3.10: Spectral changes around the NREM-REM transition. (next page)
Spectral changes from 2 minutes before until 1 minute after the NREM-REM transition.
(A) Spectral power density in the frontal EEG in control animals (n=7) (B) Spectral power density in the occipital EEG in control animals. (C) Spectral power density in the frontal EEG in L6b silenced animals (n=9). (D) Spectral power density in the occipital EEG in L6b silenced animals. (E) L6b silenced spectral power normalised to controls' spectral power in frontal EEG and (F) in occipital EEG. (G) Spectral power in the 32s before the NREM-REM transition normalised to total baseline NREM spectral power in the frontal EEG and (H) in the occipital EEG.

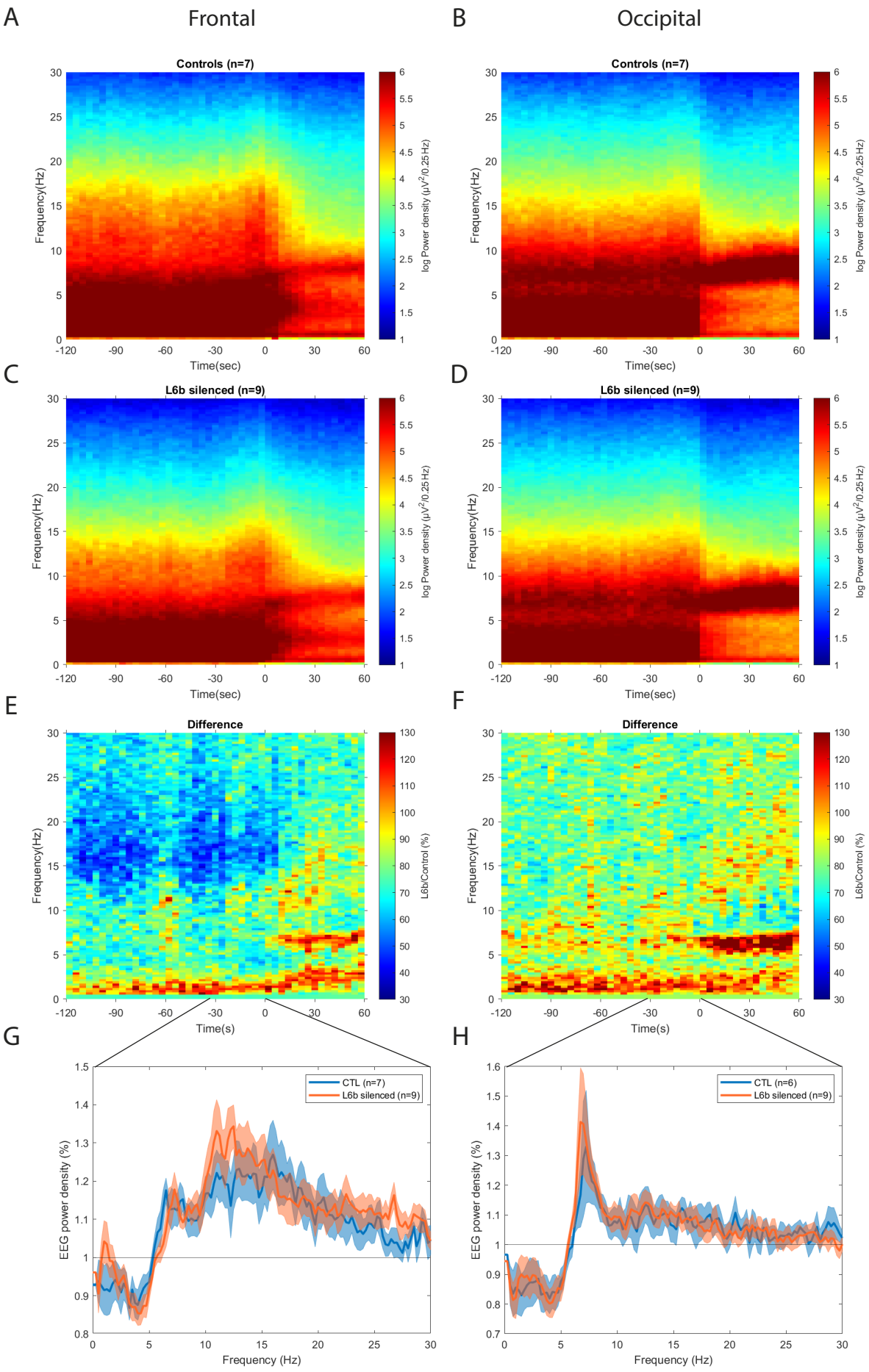
A
Frontal
B
Occipital
Controls (n=7)
L6b silenced (n=9)
Difference
Frequency(Hz)
Time(sec)
log Power density (μV²/0.25Hz)
C
D
E
F
Time(s)
L6b/Control (%)
G
H
CTL (n=7)
CTL (n=6)
L6b silenced (n=9)
EEG power density (%)
Frequency (Hz)

3.3.7 Response to sleep deprivation

In the second part of this experiment, I investigated homeostatic sleep regulation in L6b silenced animals, by performing SD, a widely used tool to investigate the effects of physiologically increased sleep pressure and the dynamics of the homeostatic process that compensates for this manipulation. Typically, longer waking time leads to reduced sleep latency, longer and more consolidated sleep, and increased levels of SWA, which dissipate gradually over the following hours (see Chapter 1, section 1.2.5). SWA is regarded as an electrophysiological measure of sleep debt and its build-up and decline as markers of the sleep homeostatic process, or Process S (Achermann and Borbély, 2003; Borbély, 1982; Daan et al., 1984; Guillaumin et al., 2018b).

In this experiment, SD was performed for 6 hours starting from light onset, which corresponds to a relatively inactive phase in laboratory mice. SD was successful in all animals, with only minimal sleep observed during the 6 hours SD procedure (controls 15.0±3.73 min vs L6b silenced 14.3±3.97 min, $t_{(14)}$=0.1240, p=0.9030). Animals fell asleep soon after the end of SD and the latency to the first consolidated NREM sleep was not significantly different between the genotypes (controls, 6.75±2.92 min, L6b silenced 11.2±2.56 min, $t_{(14)}$=1.153, p=0.2680).

Time course of NREM SWA after SD

A typical time course of increased SWA after SD that dissipated in subsequent NREM sleep was seen in both L6b silenced and control animals, but the rate of SWA dissipation was clearly attenuated in L6b silenced animals (Figure 3.11A). When I plotted the time course of SWA during recovery sleep in individual animals and fitted an exponential curve (Figure 3.11C), I found that the time constant of NREM SWA dissipation was indeed significantly lower in L6b silenced animals compared to controls in the frontal EEG (controls -0.57 ± 0.060 h^{-1} vs L6b silenced -0.28 ± 0.029 h^{-1}, $t_{(8.723)}$=4.286, p=0.0022, unpaired Welch's t test)(Figure 3.11D).

As expected, the rate of SWA dissipation was lower in the occipital EEG compared to the frontal EEG (Figure 3.11B). Occipital EEG SWA dissipation rate was not different between genotypes (controls -0.33 ± 0.026 h^{-1} vs L6b silenced -0.34 ± 0.029 h^{-1}, $t_{(10.73)}$=0.2732, p=0.79).

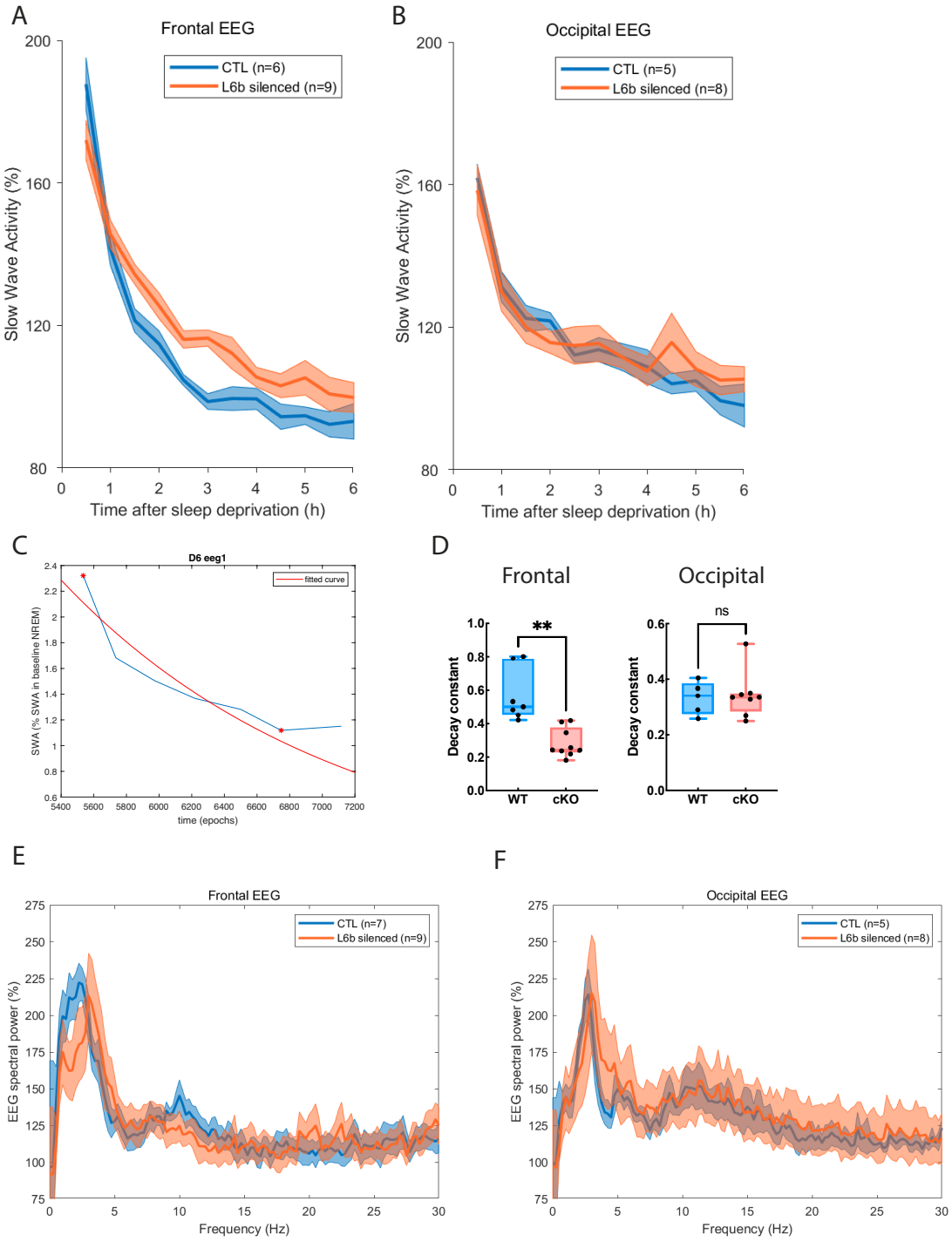

Figure 3.11: Homeostatic regulation of sleep.
(A) Decline in SWA (0.5-4.0 Hz) in the frontal EEG from the end of SD for the next 6 hours, in half hour bins. SWA is normalised to SWA averaged across all NREM epochs on baseline day.
(B) Decline in SWA (0.5-4.0 Hz) in the occipital EEG from the end of SD for the next 6 hours, in half hour bins. SWA is normalised to SWA averaged across all NREM epochs on baseline day.
(C) Example in one animal of how the SWA decline rate was estimated. The time course of SWA was plotted for a single animal (blue), the minimum and maximum value were automatically identified, and an exponential fit was determined based on these two coordinates (red).
(D) Comparison of decay constant in L6b silenced and control animals. Decay constant was negative but here plotted as absolute values to emphasize the reduction in decay rate in L6b silenced mice.
(E) EEG power during the first 30 min of NREM in the frontal EEG and (F) in the occipital EEG.

Spectra during NREM after SD

Normalisation of frontal EEG spectral power density during the first 30 min of NREM sleep following SD to frequency bin-wise averaged NREM sleep on baseline day indicated that SD caused a relative increase in frontal EEG spectral power density in the delta frequency range, as expected. However, in L6b silenced animals the relative increase in delta range frontal EEG power appeared blunted for the lower frequencies (Figure 3.11E)(Two-way ANOVA, Genotype x Frequency, $F_{(118,1652)}$=1.502, p=0.0006, posthoc comparison not significant differences for individual frequency bins), although there was no overall reduction in frontal EEG spectral power density in L6b silenced animals (Two-way ANOVA, Genotype, $F_{(1,14)}$=0.1606, p=0.9009). These results indicate that the reduction in 3-5 Hz frontal EEG spectral power density that was found in L6b silenced animals during baseline recordings persisted after SD but was not further affected by SD. There were no differences between the genotypes in relative occipital EEG spectral power density during the first 30 min of NREM sleep following SD (Figure 3.11F)(Two-way ANOVA, Genotype x Frequency, $F_{(118,1298)}$=0.6552, p=0.9981; Genotype, $F_{(1,11)}$=0.04015, p=0.8448).

Slow wave energy

To further investigate the dynamics of sleep regulatory mechanisms, I calculated Slow Wave Energy (SWE), which is the cumulative sum of delta power over all epochs scored as NREM sleep (Figure 3.12). I found that the time course of SWE on SD day was not changed by silencing L6b, neither when SWE was calculated for the frontal EEG (two-way ANOVA, Genotype x Time, $F_{(23,322)}$=1.326, p=0.1472, although posthoc comparison showed a lower SWE at 8-9 hours, which corresponds to 2-3 hours after the end of SD), nor for the occipital EEG (two-way ANOVA, Genotype x Time, $F_{(23,253)}$=0.6169, p=0.9157, no significant differences in posthoc comparisons).

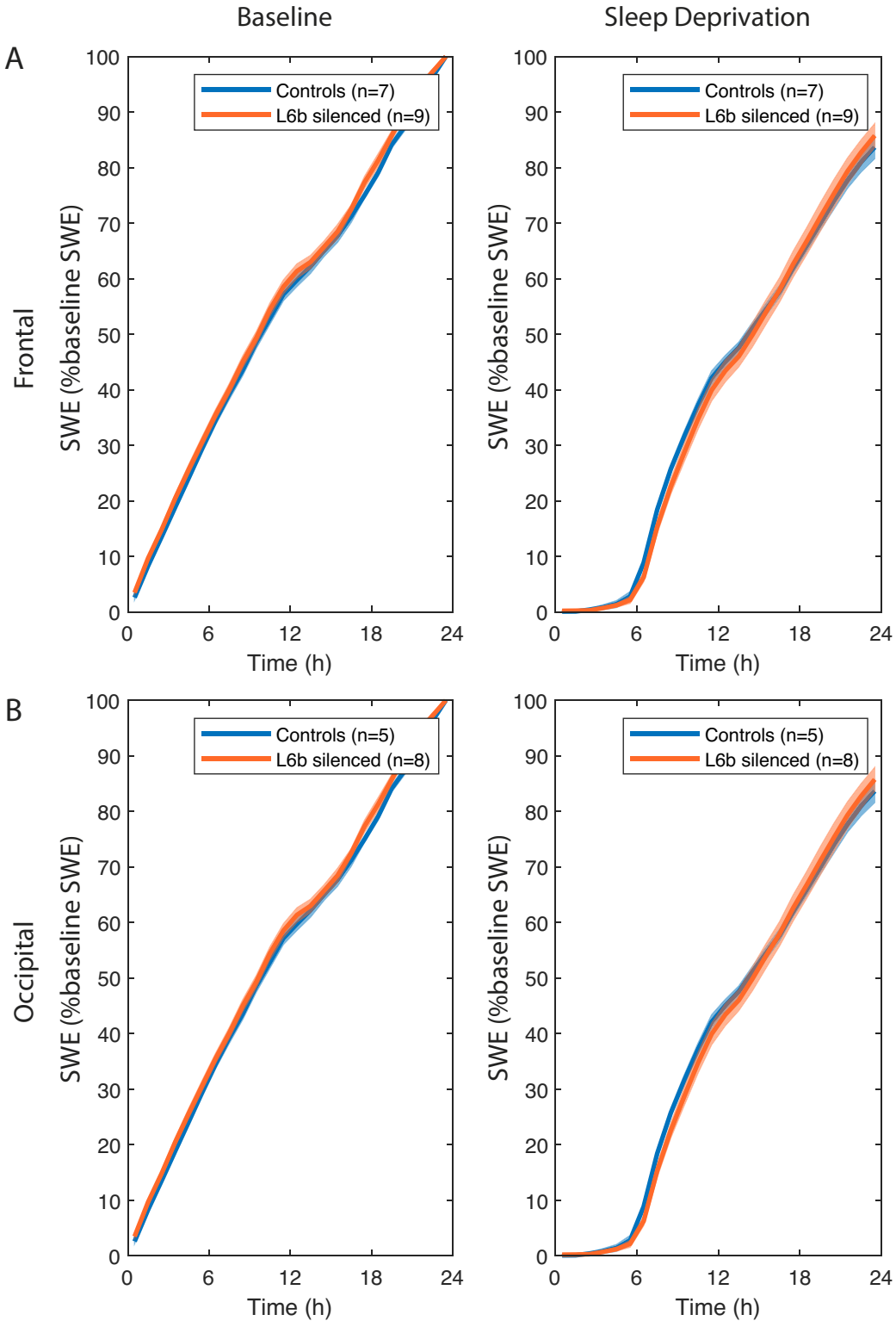

Figure 3.12: Slow wave energy.
(A) Cumulative SWE (SWA x Time) in the frontal EEG across the baseline day (left) and sleep deprivation day (right) in L6b silenced (n=9) and control (n=7) animals.
(B) Cumulative SWE in the occipital EEG across baseline day (left) and sleep deprivation day (right) in L6b silenced (n=8) and control (n=5) animals.

Intensity of wakefulness during sleep deprivation

Build-up and decline of sleep debt are related to the intensity of wakefulness, so I also explored the intensity of wakefulness during SD by comparing EEG spectra (Vassalli and Franken, 2017; Vyazovskiy and Tobler, 2005; Yamagata et al., 2021). When wakefulness spectra during SD were normalised to wakefulness spectra during the baseline day, a relative increase in theta frequency EEG power was visible in both the frontal and occipital EEG (Figure 3.13), with no significant difference between genotypes when comparisons were made across the full frequency range (Frequency x Genotype, $F_{(118,1652)}$=0.8614, p=0.8517, although significant differences for 9.5-10.25 Hz in posthoc comparison). Band power comparisons for the high theta range (7.5-10 Hz) however, revealed significant differences ((Baseline vs SD) x Genotype interaction, $F_{(1,14)}$=24.46, p=0.0002). In the occipital EEG, theta power changes were also not picked up by ANOVA (Occipital EEG: Two-way ANOVA, Frequency x Genotype, $F_{(118,1298)}$=1.928, p<0.0001, posthoc comparison only significant for 0.75-1.25 Hz, likely artefactual). Band power calculations indicated that the high theta power increase was significantly smaller in L6b silenced animals ((Baseline vs SD) x Genotype interaction, $F_{(1,11)}$=14.12, p=0.0032)(Figure 3.13C,D).

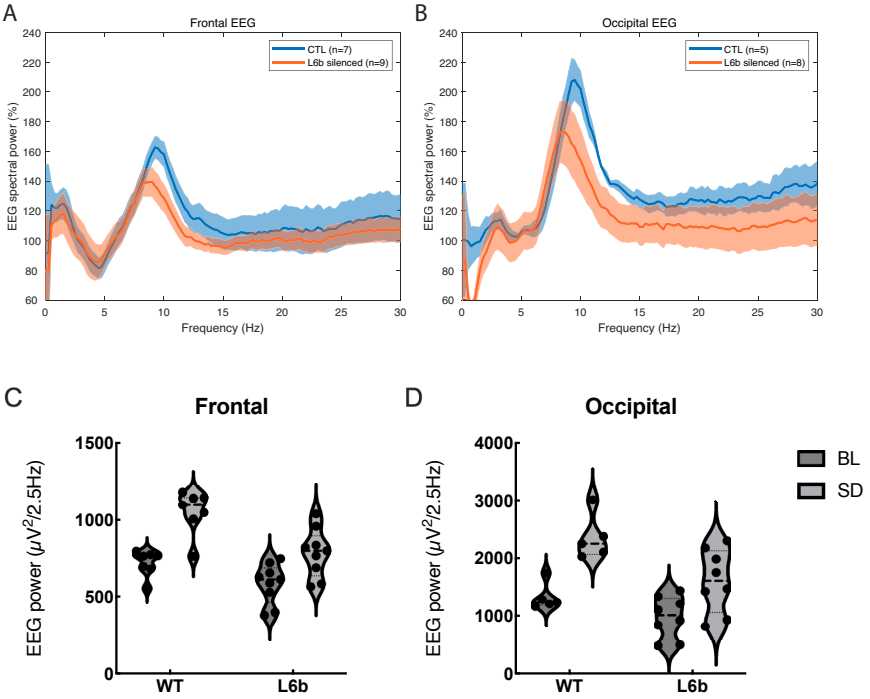

Figure 3.13: Spectra during sleep deprivation. (A) Spectral power density in the frontal EEG in L6b silenced (n=6) and control (n=7) animals. (B) Spectral power density in the occipital EEG in L6b silenced (n=8) and control (n=5) animals. (C) Band power in high theta (7.5-10 Hz) frequency band in the frontal EEG. (D) Band power in the high theta frequency band in the occipital EEG. BL, wake episodes during 24-hour baseline; SD, wake episodes during 6-hour sleep deprivation.

3.3.8 Circadian screen

To start my examination of circadian regulation in L6b silenced animals, I assessed Cre expression in key centres of circadian regulation in Drd1a-Cre;Snap25$^{fl/fl}$;TdTom animals. It has been reported before that there are no Drd1a-Cre expressing cells in the eyes and retina of the mouse line that was used in this study (Hoerder-Suabedissen et al., 2018). I also did not find Cre expressing cells in the suprachiasmatic nucleus (SCN) (Figure 3.14)(Paxinos and Franklin, 2003).

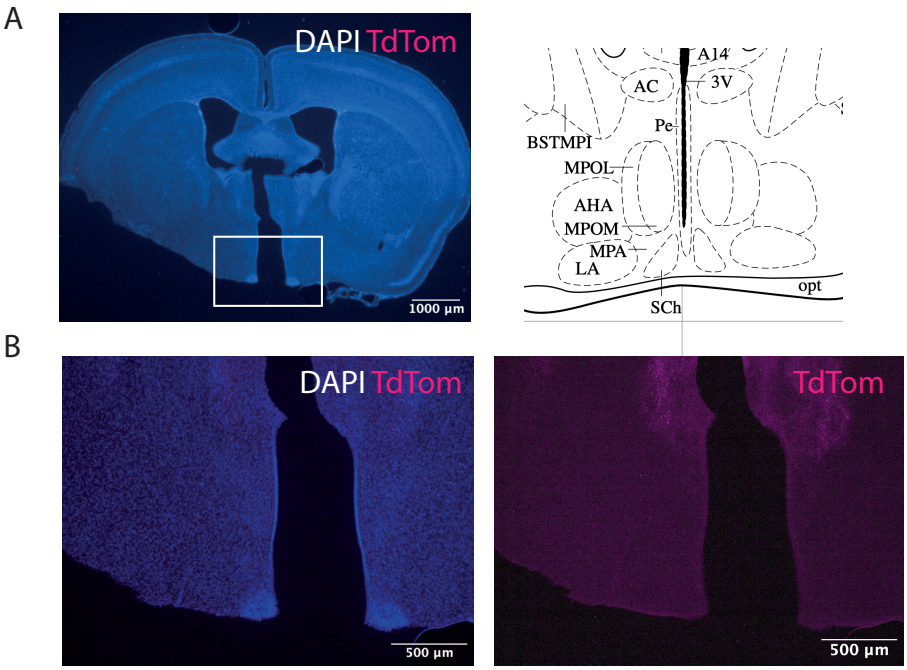

Figure 3.14: Absence of Cre expressing cells in the suprachiasmatic nucleus of L6b silenced animals. Images show representative images from a single Cre positive animal. There are no Cre expressing cells in the SCN of Drd1a-Cre;Snap25$^{fl/fl}$;TdTom animals, indicated by the absence TdTomato reporter expression in the SCN. A, overview of section with 1.6X fluorescence micrograph, the white square indicates the magnified area in B which shows the SCN. B, there is no TdTomato expression in the SCN. The upper right image shows the SCN area at this anteroposterior level from the Paxinos mouse brain atlas. Scale bar, A, 1000µ, B, 500 µm.

To investigate circadian regulation in L6b silenced animals functionally, a circadian screen has been performed in a separate cohort of young, male wildtype (n=7) and L6b silenced (n=6) animals using running wheels and varying light-dark conditions. The screen has been performed by Dr Luiz Guidi and Professor Peter Oliver and I reanalysed the raw data.

Light-dark

First, a 12:12 light-dark schedule was applied, to assess baseline circadian entrainment (Figure 3.15A,B). As expected, the period was close to 24h in both genotypes (wildtypes 24.0 ± 0.006 h, L6b silenced 24.0 ± 0.01 h, $t_{(11)}$=0.1422, p=0.8895). The amount of time spent actively, Alpha, as counted by engaging in wheel running, was significantly longer in L6b silenced animals (wildtypes 12.5 ± 0.156 h vs L6b silenced 13.4 ± 0.349 h, $t_{(11)}$=2.463, p=0.0315). The number of activity bouts per day, the duration of activity bouts and number of activity counts per bout were not changed by L6b silencing. However, the number of activity counts per day appeared reduced in L6b silenced animals and this effect was nearly significant when examined across the entire day ($t_{(11)}$=2.108, p=0.0588), significant when examined across the light phase only ($t_{(11)}$=2.988, p=0.0124) and not significant for the dark phase only ($t_{(11)}$=1.804, p=0.0987).

Constant darkness

Next, animals were kept in constant darkness, to study the main active period duration, Alpha, in the absence of Zeitgebers such as a light-dark schedule (Figure 3.15C,D). In constant darkness, the period was shorter than 24h and not different between genotypes (wildtypes 23.8 ± 0.0605 h vs L6b silenced 23.6 ± 0.0626 h, $t_{(11)}$=1.721, p=0.1133). Alpha increased with constant darkness and was not significantly different between the genotypes (wildtypes 16.2 ± 0.583 h vs L6b silenced 14.9 ± 0.737 h, $t_{(11)}$=1.457, p=0.1731). The number of bouts per day, the duration of individual bouts and the number of activity counts per bout were not different between the genotypes, but the number of activity counts per day again showed a trend towards lower activity in L6b silenced animals ($t_{(11)}$=2.045, p=0.0656).

Constant light

The following schedule was constant light (Figure 3.15E,F). Constant light increased the period, and this increase was significantly larger in L6b silenced animals (wildtypes 25.3 ± 0.191 h vs L6b silenced 24.8 ± 0.137 h, $t_{(10)}$=2.350, p=0.0406). L6b silenced animals showed fewer activity bouts per day ($t_{(10)}$=2.291, p=0.0449) and again fewer activity counts per day ($t_{(10)}$=2.257, p=0.0476).

Phase advance

Finally, a jet lag paradigm was applied, in which light offset was advanced by 6 hours, to study the rate of adjustment to the new light schedule (Figure 3.15G,H). The rate of adjustment was comparable between the genotypes (two-way ANOVA, Time x Genotype, $F_{(9,99)}$=0.4807, p=0.8845).

In summary, L6b silenced animals showed an increased active phase duration in 12:12h light-dark conditions and were less active across all light conditions. A constant light schedule led to an increase in period length and this increase was larger in L6b silenced animals.

Figure 3.15: Circadian screen in layer 6b silenced and wildtype animals (next page).
The experiment started with a 12:12 light-dark schedule, (A1) an example wildtype animal and (A2) an example L6b silenced animal. (B1-B8) measures of circadian regulation during 12:12h light-dark schedule.
Constant darkness, (C1) in an example wildtype animal and (C2) in an example L6b silenced animal. (D1-D6) measures of circadian regulation during constant darkness.
Constant light, (E1) in an example wildtype animal and (E2) in an example L6b silenced animal. (F1-F5) measures of circadian regulation during constant darkness.
6-hour Phase advance, (G1) in an example wildtype animal) and (G2) in an example L6b silenced animal. (H) Phase adjustment from the onset of the phase advance schedule.
Comparisons show the result of a two-sided unpaired t test with alpha 0.05 or a two-way ANOVA (phase adjustment, H) between wildtype animals (n=7) and L6b silenced animals (n=6). When an effect was nearly significant, instead of n.s., the p value is indicated.
In the example actograms shown (A1-2,C1-2,E1-2,G1-2), activity counts in the L6b silenced animal appear clustered at the start of the active phase compared to the example control animal. In future analysis, this will be further explored at a genotype-grouped level.

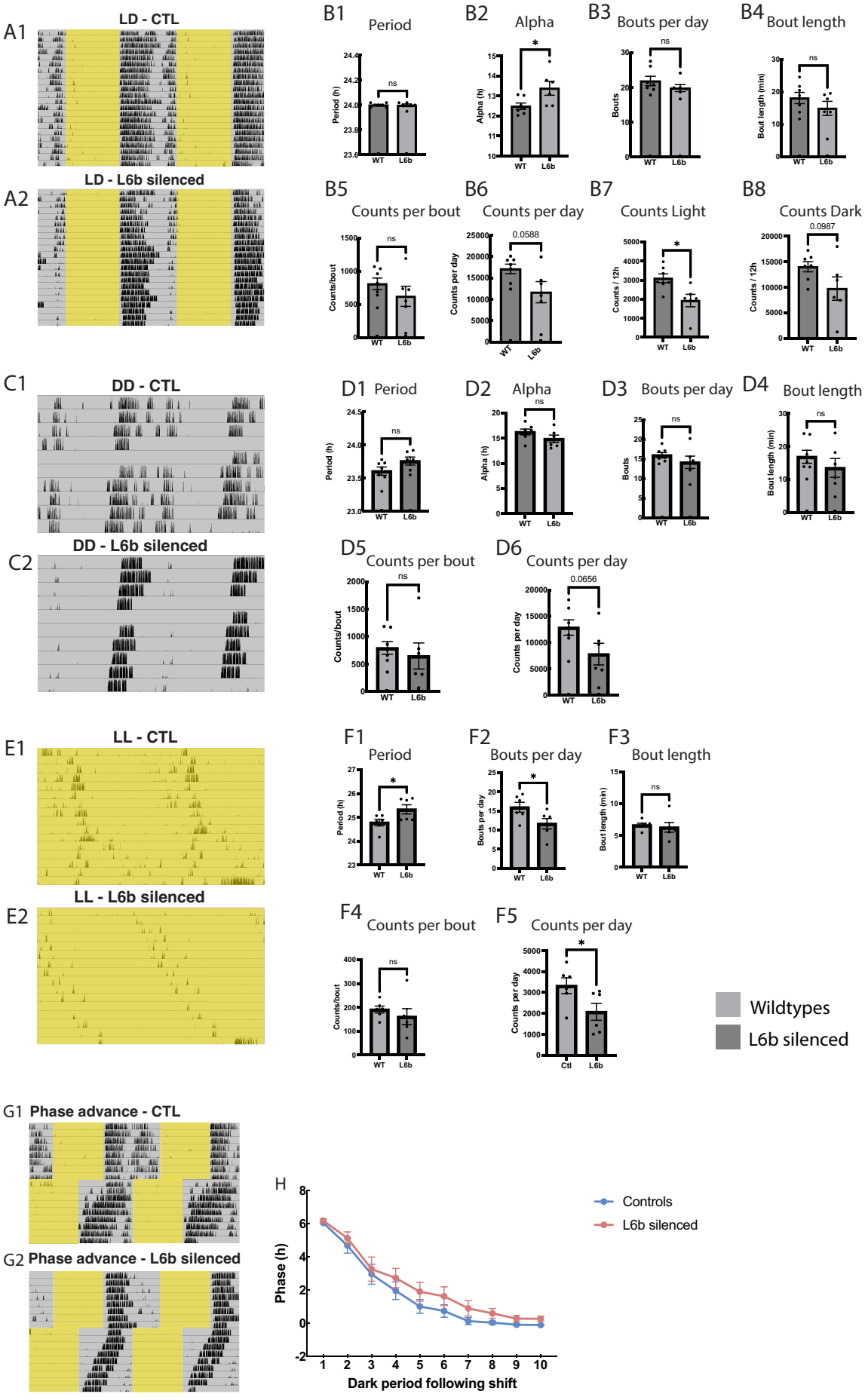
A1
LD - CTL
A2
LD - L6b silenced
B1
Period
B2
Alpha
B3
Bouts per day
B4
Bout length
B5
Counts per bout
B6
Counts per day
B7
Counts Light
B8
Counts Dark
C1
DD - CTL
C2
DD - L6b silenced
D1
Period
D2
Alpha
D3
Bouts per day
D4
Bout length
D5
Counts per bout
D6
Counts per day
E1
LL - CTL
E2
LL - L6b silenced
F1
Period
F2
Bouts per day
F3
Bout length
F4
Counts per bout
F5
Counts per day
Wildtypes
L6b silenced
G1 Phase advance - CTL
G2 Phase advance - L6b silenced
H
Controls
L6b silenced
Phase (h)
Dark period following shift

3.4 Discussion

3.4.1 Summary of results

In this experiment, I investigated sleep-wake regulation in mice with a conditional ablation of *Snap25* from the Drd1a positive subset of cortical L6b neurons, resulting in dysfunctional synaptic transmission from these neurons. I performed continuous EEG/EMG recordings on a baseline and an SD day and assessed daily sleep architecture and homeostatic regulation of sleep.

I found that there were no differences in the diurnal distribution of vigilance states, the frequency and duration of wakefulness, NREM and REM episodes, and the number of brief awakenings from NREM sleep, suggesting that sleep stability was not affected by L6b silencing.

However, EEG spectral power was reduced in specific frequency bands in L6b silenced animals. In baseline recordings, there was a reduction in theta power in wakefulness, a reduction in theta and gamma power during REM sleep, and a reduction in 3-30 Hz and the gamma frequency range during NREM sleep. In wakefulness during SD, there was a blunted increase in theta power, and after SD, SWA dissipated at a lower rate in L6b silenced animals.

In a separate cohort of L6b silenced and control animals, a circadian screen was performed, and it was found that L6b silenced animals had an increased active phase during a 12:12h light-dark schedule and showed a decrease in wheel-running activity during a 12:12h light dark schedule, constant darkness, and constant light. Constant light increased the period duration and did so to a greater extent in L6b silenced animals. L6b silencing did not affect adaptation to a phase advance paradigm.

3.4.2 Implications

Our initial interest for investigating the role of L6b in sleep-wake regulation was based on its sensitivity to orexin (Bayer et al., 2004; Wenger Combremont et al., 2016b, 2016a). Orexin promotes arousal and stabilizes sleep wake states (Chemelli et al., 1999; Hara et al., 2001; Lin et al., 1999; Nishino et al., 2000; Peyron et al., 2000; Thannickal et al., 2000). If cortical L6b would

be important for orexinergic sleep-wake regulation, L6b silencing would result in a phenotype mimicking reduced orexin signalling, with impaired arousal and sleep-wake stability (Chemelli et al., 1999; Hara et al., 2001; Lin et al., 1999; Nishino et al., 2000; Peyron et al., 2000; Thannickal et al., 2000). The absence of such a phenotype in L6b silenced mice is not surprising, since orexin neurons project to multiple nuclei that are important in sleep-wake regulation, such as locus coeruleus, the nuclei of the reticular activating system and higher order thalamus and these projections may have a stronger effect on global brain state (Horvath et al., 1999; Peyron et al., 1998; Van Den Pol, 1999)(Figure 4.1B).

Even though it is impossible to identify orexin-mediated effects in the spectral changes observed in L6b silenced animals, an involvement of orexin is conceivable. It has been shown that orexin is required for the expression of theta-rich wakefulness in mice (Vassalli and Franken, 2017). In my findings, across all vigilance states, EEG spectral power was reduced in the theta range, and this could be a result of an impairment of orexin signalling through L6b. Whether silencing Drd1a-Cre L6b neurons changes the effects of orexin administration on EEG spectra in vivo, is the topic of the next chapter (Chapter 4 - In vivo effects of orexin in L6b silenced mice).

It is unlikely that changes in theta oscillations in L6b silenced animals are caused by off-target expression of Drd1a-Cre in hippocampus, since Drd1a-Cre cells are at most sparsely expressed in hippocampus (Hoerder-Suabedissen et al., 2018). Interestingly, excitatory neurons in the deepest layer of the entorhinal cortex, that are likely of the same population as L6b, project to and can drive hippocampus (Ben-Simon et al., 2022). Moreover, silencing these L6b neurons in entorhinal cortex prevents spatial learning, implying functional significance of this L6b-hippocampal circuit. The study by Ben-Simons *et al.* was carried out with an inducible Ctgf-Cre driver line and not the Drd1a-Cre driver line (Ben-Simon et al., 2022). However, these two L6b populations partially overlap, at least in somatosensory cortex, where it was found that one-third of Drd1a-Cre neurons also express Ctgf (Zolnik et al., 2020).

Changes in theta-frequency EEG oscillations in L6b silenced animals could relate to changes in coupling with other oscillations. In L6b silenced mice, there was a reduction in power

spectral density in the 3-5 Hz frequency range and oscillations in this range have been linked to entrainment to respiration (Biskamp et al., 2017; Chi et al., 2016; Jessberger et al., 2016). A breathing-related rhythm expressed in the PFC, the prefrontal respiratory rhythm, is phase-locked with hippocampal theta-activity and modulates prefrontal gamma oscillations (Biskamp et al., 2017). The reduction in delta, theta, and gamma frequency EEG spectra in L6b silenced mice could reflect L6b involvement in a breathing-related circuit, although I have not investigated breathing rate in my experiment. A direct effect of non-brain expression of Drd1a Cre on respiration seems unlikely since in Drd1a-Cre;Ai40 animals, Cre expression has been observed in lungs but only in small patches, and not in the intercostal muscles involved in the mechanics of respiration (Hoerder-Suabedissen et al., 2019).

Another finding was that the theta peak frequency was reduced in L6b silenced animals during wakefulness and REM sleep. Interestingly, such changes have also been observed with hyperdopaminergic states (Dzirasa et al., 2009). Since the L6b silenced mouse is effectively a knockout of dopamine receptor expressing neurons (Drd1a Cre line FK164) from the time of birth, this finding may indicate a change in dopaminergic signalling in the cortex, with a possible compensatory increase resulting from a reduction in receptor signalling.

The reduction in the 3-5 Hz frontal EEG power during NREM sleep, along with the reduced SWA dissipation rate following SD, could also reflect a reduced build-up of sleep pressure, suggesting an involvement of L6b in the homeostatic regulation of sleep (Achermann and Borbély, 2003; Borbély, 1982; Daan et al., 1984; Guillaumin et al., 2018b). Changes in sleep homeostatic regulation occurred at the EEG level but studying L6b activity with LFP recordings in different cortical areas could shed light on area-specific effects and the link between global brain state control and local cortical dynamics. Another possibility is that L6b plays a role in low frequency oscillations and that these are affected by silencing L6b without affecting sleep homeostatic mechanisms.

Decreased NREM SWA in L6b silenced animals could, in theory, be a result of a nonspecific reduction in the number of active synapses which would, according to the synaptic homeostasis

hypothesis of sleep (see Chapter 1 – General Introduction), lead to a decrease in sleep intensity. However, since L6b neurons are relatively few in number, the decrease in the number of active synapses is unlikely to result in pronounced changes in EEG spectra. Moreover, the effects of L6b silencing were very different from the effects of L5 silencing, which led to a marked decrease in time spent asleep, impaired sleep homeostatic regulation and changes in layer-specific dynamics in LFP recordings rather than changes in spectral EEG power (Krone et al., 2021). Therefore, it is more likely that a specific network dysfunction causes the sleep phenotype in L6b silenced animals rather than a nonspecific reduction in the number of synapses.

The reduction in the sigma frequency range during NREM sleep could indicate that L6b has a role in a sleep spindle-generating or regulating network. Sleep spindles are generated by mutual inhibition and rebound excitation between thalamus, the TRN and cortex (see Chapter 1, General Introduction). Whereas Drd1a-Cre L6b neurons do not project directly to TRN, they do project to L5 (Hoerder-Suabedissen et al 2018; Zolnik et al 2023 in revision) and some L5 subpopulations such as Rbp4-Cre project to segments of TRN (Carroll et al., 2022). Moreover, Drd1a Cre neurons project to higher order thalamic nuclei which project to and receive projections from TRN (Hoerder-Suabedissen et al., 2018).

The power reduction in the sigma range appeared to occur in two hot spots, which could reflect an underlying effect on infraslow oscillations (Lecci et al., 2017). The sigma-frequency reduction did not show specificity to NREM-REM transitions; the way in which L6b might modulate sleep spindles, and whether this modulation is specific to certain types or phases of sleep spindles in different sub-states of NREM sleep remains to be investigated.

Drd1a-Cre is not expressed in the retina and eye (Hoerder-Suabedissen et al., 2018), or SCN, yet a circadian phenotype could still be present. In a circadian screen in a separate cohort of young male L6b silenced animals, the duration of the active phase Alpha was increased in L6b silenced animals during a regular 12:12h light-dark schedule. Moreover, L6b silenced animals showed a reduction in activity counts during a 12:12h light-dark schedule, constant darkness, and constant light. A constant light schedule increased the period in L6b silenced animals to a

larger degree than in wildtype animals. Variations in circadian rhythms have been observed between different mouse strains and between mice of different ages (Banks et al., 2015; Schwartz and Zimmerman, 1990). Circadian rhythm differences have been correlated with genes related to schizophrenia, dopaminergic transmission, arousal and connectivity which are all factors that have been linked to L6b as well (Banks et al., 2015). More research is needed to understand the relationship between the current findings and to examine whether these are the result of biological variation in small group sizes, genetic changes unrelated to L6b, expression of Cre outside of L6b, or an involvement of L6b networks in circadian rhythm.

3.4.3 Limitations

There are several limitations to this experiment. First, the expression of Cre recombinase in the Drd1a Cre line starts from postnatal day 1 (Hoerder-Suabedissen et al., 2018). At that time, cortical development has not been completed in the mouse brain, and therefore, compensatory network changes may develop. This means that the mouse model is not an absolute 'adult' model for the function of L6b, but rather a 'chronic silencing' model in which effects are a combination of changes in postnatal development and non-functional cells in the adult brain.

The strategy of silencing specific neuronal populations through interfering with SNARE proteins has been used for conditional silencing of L5 neurons (Krone et al., 2021) and somatostatin-positive interneurons in L5b (Marques-Smith et al., 2016). This approach that does not require the administration of drugs or light stimulation is an innovative technique to chronically silence a neuronal population of interest. However, it is important to note that SNARE proteins are not exclusively involved in regulated synaptic vesicle release but also in transport of hormones and growth factors, and cellular functions such as cell migration and cell division (Vadisiute et al., 2022). Therefore, expression of manipulated constructs can have effects that range further than single-neuron synaptic silencing and those effects should be considered when interpreting results.

Lastly, Drd1a Cre cells represent only a subset of neurons in L6b (Hoerder-Suabedissen et al reported 25% and Zolnik et al 40%)(Hoerder-Suabedissen et al., 2018; Zolnik et al., 2020). Other neurons in L6b may have different functions or may have similar functions but may be not included when using this Cre line, reducing sensitivity. Moreover, even though the Drd1a Cre line FK164 is relatively specific for L6b, some off-target expression is still observed, including sparse expression in hippocampus and striatum, and more dense expression in some midbrain nuclei and in the cerebellum. No labelled cells have been described in the eye, retina or SCN, which are key to circadian regulation (Hoerder-Suabedissen et al., 2018).

3.5 Conclusion

In this experiment, I observed that selective ablation of regulated synaptic vesicle release from a Drd1a-Cre expressing subpopulation of excitatory neurons in L6b has marked effects on state-specific EEG oscillations, even though the L6b cell population that is targeted is relatively small. Moreover, sleep homeostatic regulation is affected and changes in circadian rhythm are observed. Since these results indicate that L6b cannot be omitted without consequences, L6b may have a unique function in sleep-wake regulation.

4 In vivo effects of orexin in 'layer 6b silenced' mice

4.1 Introduction

Orexin/hypocretin neurons in the hypothalamus project widely, to numerous subcortical nuclei and also to cortex (Peyron et al., 1998) . In Chapter 1 – General Introduction, I reviewed the brain state stabilizing effects of orexin and the in vitro effects of orexin on cortical L6b. In vitro studies showed that excitatory neurons in L6b can be directly activated by orexin (Bayer et al., 2004; Hay et al., 2015; Wenger Combremont et al., 2016a) and inhibitory neurons in L6b indirectly (Wenger Combremont et al., 2016b). Moreover, a projection target of L6b, higher order thalamus, can be directly activated by orexin too (Bayer et al., 2002; Hoerder-Suabedissen et al., 2018). Despite these consistent effects of orexin on L6b in vitro, the in vivo effects of orexin on the function of L6b have not been investigated yet.

In the current chapter, I investigated the in vivo effects of orexin on L6b, by administration of orexin in L6b silenced (Drd1a-Cre::tdTom::Snap25$^{fl/fl}$) and control mice. Orexin activity has been implicated in a variety of homeostatic and emotional regulatory circuits, such as food intake, metabolism, sleep and wakefulness, motivation, anxiety, and addiction (Adamantidis and de Lecea, 2009; Johnson et al., 2010; De Lecea et al., 1998; Sakurai, 2007, 2014; Sakurai et al., 1998; Tsujino and Sakurai, 2013). I focused on sleep-wake behaviour and gathered pilot data on food intake.

I first give an overview of the two orexin isoforms, orexin receptors and orexinergic projections. I then describe the in vivo effects that have been described for orexin on food intake and sleep-wake regulation. I conclude this introduction with stating the hypothesis that I tested with the experiments presented in this chapter.

4.1.1 Nomenclature

Orexin/hypocretin was discovered by two independent groups in the same year. De Lecea *et al.* extracted mRNA from the hypothalamus, demonstrated its brain wide expression pattern and its likely function as a neurotransmitter. Because of similarities to the secretin family of proteins and the exclusive production in the hypothalamus, they named the protein hypocretin (Lecea et al., 1998). Sakurai *et al.* identified the two related peptides orexin A and B as ligands of a previously orphan G-protein coupled receptor (GPCR) and found that injection of the peptide into the intracerebral ventricle (ICV) in rats led to an acute increase in food intake. Because of this effect, they called the peptide orexin, after the Greek word *orexis*, meaning appetite (Sakurai et al., 1998). In literature, the names hypocretin and orexin are used interchangeably; in this thesis, I use the orexin nomenclature for no particular reason. Two iso-proteins of orexin are produced from the mRNA precursor prepro-orexin, the 33-amino acid orexin A (ORXA) and the 28-amino acid orexin B (ORXB) (Sakurai et al., 1998) (Figure 4.1A).

4.1.2 Orexin receptors

Orexin peptides can bind to two GPCRs, the orexin receptor 1 (OX1R) and 2 (OX2R). OX1R has a tenfold higher affinity for ORXA than for ORXB, whereas OX2R has a similar affinity for both peptides (Sakurai et al., 1998). OX1R and OX2R are widely expressed throughout the brain, in partly overlapping but mostly different areas, suggesting complementary functions (Figure 4.1B). In an initial study on orexin receptor mRNA expression in rat brain, the focus was on hypothalamus, but it was also observed that there was weak OX1R expression in cingulate cortex and high density OX2R expression in L6 of the neocortex (Trivedi et al., 1998). In a later study, also in rat brain, low OX1R mRNA expression was reported in L6 and L5 of the neocortex, and moderate OX1R expression in L3 of the cingulate cortex, infralimbic cortex and prefrontal cortex; OX2R was found to be expressed in low levels in infralimbic cortex, and moderate levels in the piriform cortex, and L2 and L6 of the neocortex (Marcus et al., 2001) (Figure 4.1C). In mice, similar patterns of OX1R and OX2R mRNA were observed (Ikeno and Yan, 2018).

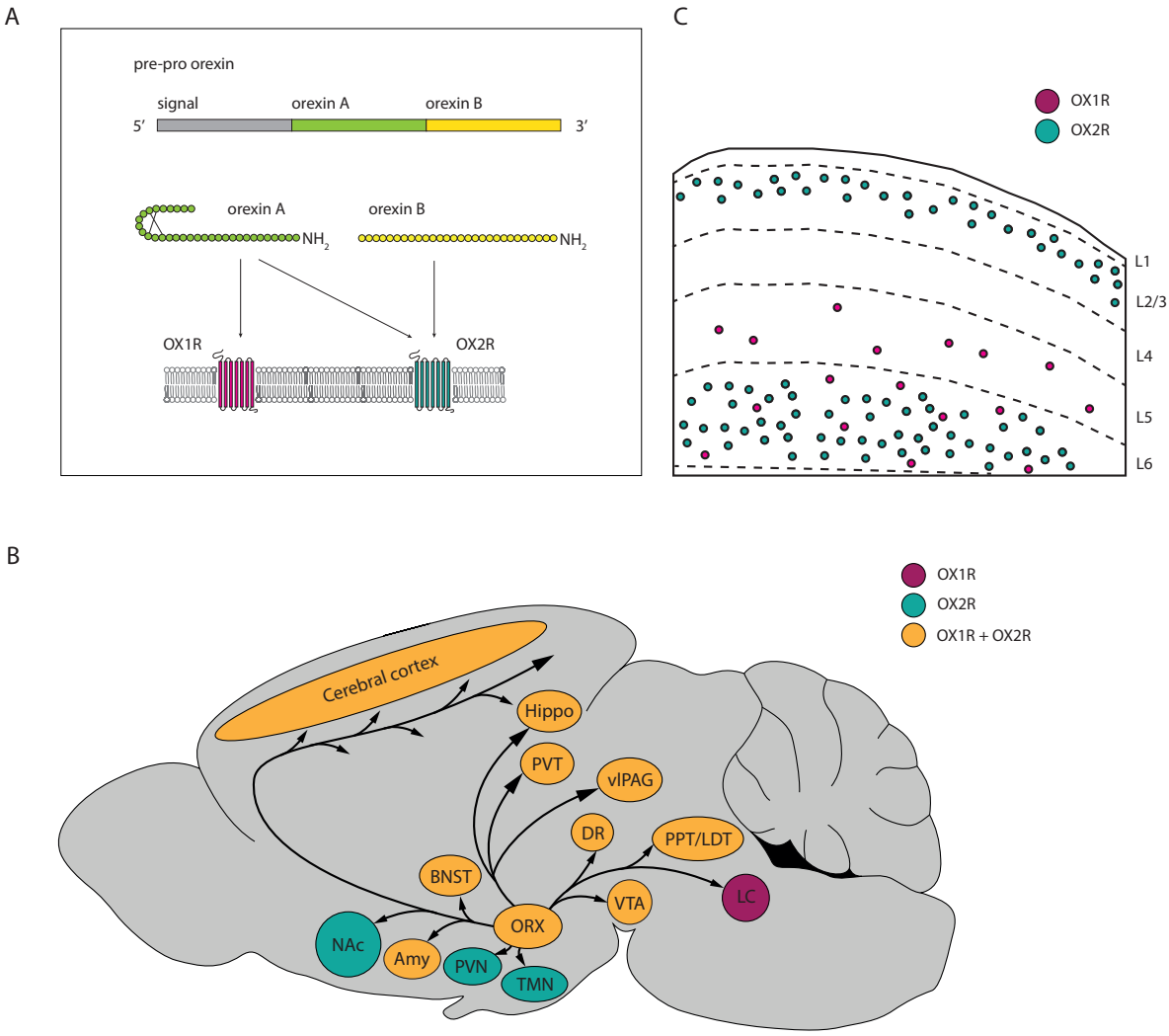

Figure 4.1 Orexin structure, orexin receptor expression and orexinergic projections.
(A) pre-pro-orexin mRNA is translated into 33-amino acid ORXA and 28-amino acid long ORXB. Note two disulphide bonds in the ORXA tertiary structure. OX1R and OX2R are both GPCRs; OX2R binds ORXA and ORXB with equal affinity, but the OX1R has a ten-fold higher affinity for ORXA over ORXB.
(B) Orexinergic efferent projections and orexin receptor expression throughout the brain, based on descriptions in (Peyron *et al*. 1999) and (Marcus *et al*. 2001), both in rats. Distribution of OX1R and OX2R mRNA is comparable in mice (Ikeno & Yan 2018).
(C) Orexin receptor expression pattern in the neocortex, based on the descriptions in (Marcus *et al.* 2001). Expression in prefrontal, piriform and infralimbic cortex were reported separately without laminar specification and are excluded here.
OX1R, orexin 1 receptor; OX2R, orexin 2 receptor; Hippo, hippocampus; PVT, paraventricular nucleus of the thalamus; vlPAG, ventrolateral periaqueductal grey; DR, dorsal Raphe; PPT, pedunculopontine tegmental nucleus; LDT, laterodorsal tegmental nucleus; LC, locus coeruleus; VTA, ventral tegmental area; ORX, orexinergic neurons in the lateral hypothalamus; TMN, tuberomammillary nucleus; PVN, paraventricular nucleus of the hypothalamus; Amy, amygdala; NAc, nucleus accumbens; BNST, bed nucleus of the stria terminalis.

4.1.3 Orexin neuron connectivity

Retro- and anterograde tracing studies have shown that afferents to orexin neurons are found in the lateral hypothalamus, posterior hypothalamus, dorsomedial hypothalamus, the preoptic area, the lateral septum, amygdala, bed nucleus of the stria terminalis, and cortical areas related to emotion and autonomic functions such as infralimbic cortex, claustrum, and medial orbital cortex (Sakurai et al., 2005; Yoshida et al., 2006) (Figure 4.1B). In addition to this wide range of afferents, orexin neurons are sensitive to various humoral factors, including direct regulation by glucose, ghrelin, and leptin (Burdakov et al., 2005; Sakurai, 2007; Yamanaka et al., 2003).

Orexinergic projections are similarly extensive, comprising various brainstem nuclei such as locus coeruleus and the nuclei of the reticular activating system, thalamus, cortex, and spinal cord (Horvath et al., 1999; Peyron et al., 1998; Van Den Pol, 1999)(Figure 4.1B). The diverse input and output connections give orexin neurons the possibility to integrate metabolic, circadian, sleep-wake, emotional and autonomic signals and translate these into widespread arousal.

4.1.4 Food intake

Initially, orexin was identified as a neuropeptide involved in food intake, being produced in the food-regulatory area in the lateral hypothalamus (Edwards et al., 1999; De Lecea et al., 1998; Sakurai et al., 1998). The findings that intracerebroventricular ICV infusion of ORXA in rats leads to an increase in food intake (Sakurai et al., 1998), and administration of an ORXA antagonist decreases food intake in rats (Haynes et al., 2000) and ob/ob mice (Haynes et al., 2002) confirmed this hypothesis. Orexin does not only increase food intake but also metabolic rate, and orexin neuron ablated mice are hypophagic and also have a decreased metabolic rate (Hara et al., 2001).

The cerebral cortex, particularly the orbitofrontal and prefrontal cortex, has also been linked to food intake, and mostly with cognitive aspects of feeding behaviour such as motivation, association, and memory (Petrovich et al., 2007; Rolls, 2023). An orexinergic stimulation of food intake could be (partially) mediated through cortical effects. OX1R is expressed in infralimbic and prefrontal cortex (Marcus et al., 2001), and Drd1a-Cre is also expressed in these areas.

4.1.5 Sleep and wakefulness

Orexin promotes wakefulness, for instance through activation of locus coeruleus, TMN and basal forebrain (Akanmu and Honda, 2005; Hagan et al., 1999; Huang et al., 2001; Piper et al., 2000; Sasaki et al., 2011; Thakkar et al., 2001).

Besides promoting wakefulness, orexin plays a stabilizing role on sleep wake states, as described in Chapter 1. When there is a deficiency of orexin, sleep-wake states become instable with frequent transitions between sleep and wakefulness and direct wake-to-REM transitions which are both symptoms of the disorder narcolepsy (Adamantidis et al., 2020; Bassetti et al., 2019). When there is also sudden loss of postural stability during wakefulness comparable to REM sleep atonia, the condition is referred to as narcolepsy-cataplexy (Adamantidis et al., 2020; Bassetti et al., 2019). A mutation in the OX2R causes narcolepsy in dogs (Lin et al., 1999), and a similar phenotype is observed in mice with a complete orexin knockout (Chemelli et al., 1999) or with a genetic ablation of orexin neurons (Hara et al., 2001; Tabuchi et al., 2014). In human narcolepsy patients, orexin levels in the cerebrospinal fluid (CSF) are abnormal (Nishino et al., 2000), and the number of orexin neurons is reduced (Thannickal et al., 2000). When ORXA is administered to orexin genetically ablated mice, symptoms improve (Mieda et al., 2004), and orexin supplementation as treatment for human narcolepsy patients is under active investigation, for instance in a recent phase II clinical trial that reported improvement of narcolepsy symptoms in narcolepsy patients from an oral OX2R agonist but unfortunately also hepatotoxicity (Dauvilliers et al., 2023).

The effects of orexin on sleep-wake regulation are regulated by both OX1R and OX2R with a predominant role for OX2R: the wake promoting effects of ORXA are somewhat attenuated in OX1R knockout mice, and further attenuated in OX2R knockout mice, demonstrating the predominant role of OX2R. In double receptor knockout mice, ORXA effects are further suppressed, suggesting that there is an additional role of OX1R (Mieda et al., 2011). Moreover, OX2R and double receptor knockout mice show distinct narcolepsy symptoms, also indicating that OX1R plays a complementary role in sleep-wake regulation (Willie et al., 2003).

Orexin neurons in rats fire most actively during wakefulness, fire less actively during NREM sleep and become inactive during REM sleep (Hassani et al., 2009; Lee et al., 2005; Mileykovskiy et al., 2005), in line with the dynamics of cFos expression (Estabrooke et al., 2001) and fluctuation of extracellular ORXA levels across sleep-wake states (Yoshida et al., 2001). Constitutive activation of orexin neurons in CAG/orexin mice promotes wakefulness (Willie et al., 2011), pharmacogenetic activation of orexin neurons increases wakefulness, and pharmacogenetic inhibition reduces wakefulness (Sasaki et al., 2011). Acutely activating orexin neurons through optogenetics promotes the transition from NREM and REM sleep to wakefulness (Adamantidis et al., 2007), although increasing sleep pressure with SD abolishes this effect, due to diminished activation of TMN and LC, downstream targets of orexin neurons (Carter et al., 2009).

Orexin increases the amount of wakefulness but also affects brain oscillatory activities during wakefulness. Orexin is critical for sustaining a substate of wakefulness that is rich in theta and gamma oscillations, and it is this theta-enriched wakefulness that drive sleep pressure (Vassalli and Franken, 2017; Vyazovskiy and Tobler, 2005). Orexinergic signalling also seems to play a role in the establishment of REM sleep oscillations (Bastianini et al., 2016).

4.1.6 Hypothesis

Since orexin is wake promoting and state stabilizing, I expected that administration of orexin would lead to more time spent in wakefulness and potentially less transitions between wakefulness and sleep in control animals. I expected that food intake might be increased, although other studies with orexin in mice usually report outcomes within the first hours after administration. I hypothesized that the effects of orexin could be partially mediated through a network involving cortical L6b, since L6b and one of its targets, higher order thalamic nuclei, can be directly activated by orexin in vitro (Bayer et al., 2002, 2004; Hay et al., 2015; Wenger Combremont et al., 2016b, 2016a). Single cell transcriptomic analysis and single cell patch recordings both demonstrated that the Drd1a-Cre+ neurons are orexin sensitive (Henning et al.,

2023) (Zolnik et al., 2023 in revision and unpublished observations in primary somatosensory cortex; Therpurakal et al., unpublished observation in prefrontal cortex). Therefore, I reasoned that eliminating a subset of L6b, the Drd1a-Cre+ population that is orexin sensitive, from the circuit by chronic silencing might impair the response to orexin in L6b silenced mice. This is the first study investigating in vivo effects of orexin on cortical L6b, so I started this study with an open perspective.

4.2 Methods

4.2.1 Animals and surgeries

Colony breeding, husbandry, and care of the Drd1a-Cre::tdTom::Snap25$^{fl/fl}$ colony, the L6b silenced colony, is described in Chapter 3. For the current experiment, n=8 adult (2-3 months) male L6b silenced animals, and n=5 adult male littermate control animals were used, following conventional group sizes in similar studies (Yamagata et al., 2021).

Pre- and post-surgical care were carried out as described in Chapter 2; the surgeries itself were extended with the unilateral implantation of a cannula in the right lateral cerebral ventricle. The procedure was as described in Chapter 2, with some additional steps from the moment of marking the positions of electrodes, including an extra mark for the position of the prospective canula (Figure 4.2A for EEG and canula coordinates; canula coordinates based on (Suzuki et al., 2005)). Holes were drilled through the skull for the EEG screws and the cannula, with minimal damage to the dura. Next, the guide cannula (C315G/Spc, Plastics1, Protech International Inc., Boerne, Texas, USA) was inserted into the holder in the stereotactic frame and slowly positioned on the dura. The cannula was then lowered to 2.3 mm below the dura. If needed, silicone elastomer (Kwik-Sil, World Precision Instruments Inc., Sarasota, FL, USA) was applied to close the craniotomy. The guide cannula was secured with dental cement (Super bond, Prestige Dental Products Ltd, Bradford, UK), and when the cement had solidified, the holder was removed, and the dummy cannula (C315DC/Spc, Plastics1) was inserted into the guide cannula. After this, the screws of the EEG headstage were secured with additional dental cement. Lastly, the EMG electrodes were placed bilaterally into the nuchal muscles and attached to the headstage with acrylic dental cement (Simplex Rapid, Associated Dental Products Ltd, Swindon, UK). If required, the skin was closed with a suture (Ethicon-W9915, Henry Schein, Gillingham UK). The animal received additional sterile saline (0.1 ml/hour of surgery), was removed from the stereotactic frame, and weighed. It was placed in a recovery chamber until it was able to maintain postural stability, upon which it was moved to a recovery cage and monitored daily for at least 5 days.

4.2.2 Preparation of drug solutions

ORXA (Orexin A (human, mouse, rat) Trifluoroacetate salt, 4028262.0500, lot no 1068668, Bachem AG, Switzerland) was dissolved in sterile saline to a concentration of 0.3 nmol/µl or 0.15 nmol/µl, and ORXB (Orexin B (human) Trifluoroacetate salt, 4028263.0500, lot no 1000056801, Bachem AG) to a concentration of 0.3 nmol/µl, under sterile conditions in a flow cabinet. Solutions were divided in 20 µl aliquots which were immediately frozen at -20°C. Saline aliquots were also frozen for the vehicle condition. On the day of infusion, aliquots were taken from the freezer and administered within one hour. Doses were determined based on previous studies with orexin infusion in mice (Mieda et al., 2011; Mobarakeh et al., 2005; Suzuki et al., 2005) and reported dissolvability of orexin in the product information of the compound.

4.2.3 Experimental procedure

The first day was a baseline recording day, on which animals were only briefly disturbed for inspection and handling at 9AM. Food intake was monitored for several baseline days to obtain an average 24-hour food intake value. On infusions days, the chambers were opened at 9AM, after which the animals were connected to the cannula system. The infusions started within 55 min after light onset and animals were infused with 2 µl of orexin or vehicle, at a rate of 1 µl/min. After the infusion was completed, the infusion system was left in place for an additional 5 minutes to allow diffusion of remaining solution from the internal needle. In the meantime, food measurements were done (see 'Food intake' in methods below), and animals were monitored. When no signs of distress were observed, the chambers were closed, and the mice were undisturbed until the next light onset.

4.2.4 Experimental schedule

After 5-7 days recovery, the dummies were moved in the cannulas every few days, to habituate the animals to the procedure and to keep the cannulas accessible. The animals were moved into tall Plexiglas cages in the recording room and connected to EEG/EMG cables a day later. The signals were inspected for entrainment of the light-dark cycle of the recording room (9AM lights on, 9PM lights off) and when entrainment was deemed sufficient, the experiment was started. ORXA at the higher dose was expected to give the strongest effect, so this infusion and a vehicle infusion were prioritised for the first two infusions in counterbalanced order. As all cannulas remained accessible, additional infusions were administered. For the third and fourth infusion, ORXB was counterbalanced with a half dose of ORXA. For one animal, H2, infusion order was swapped for technical reasons (Table 4.1).

Table 4.1: Order of infusions.

Mouse ID	Infusion	Infusion 2	Infusion 3	Infusion 4
F1	ORXA-high	VEH	ORXB	ORXA-low
F2	VEH	ORXA-high	ORXA-low	ORXB
G1	ORXA-high	VEH	ORXA-low	ORXB
G2	VEH	ORXA-high	ORXA-low	ORXB
G3	VEH	ORXA-high	ORXB	ORXA-low
H1	VEH	ORXA-high	ORXB	ORXA-low
H2	ORXA-high	ORXB	ORXA-low	VEH
H3	ORXA-high	VEH	ORXB	ORXA-low
H4	VEH	ORXA-high	ORXB	ORXA-low
I1	ORXA-high	VEH	ORXA-low	ORXB
I2	VEH	ORXA-high	ORXB	ORXA-low
I3	ORXA-high	VEH	ORXB	ORXA-low
I4	VEH	ORXA-high	ORXA-low	ORXB

ORXA high, orexin A (0.6 nmol).
VEH, vehicle (saline).
ORXB, orexin B (0.6 nmol).
ORXA low, orexin A (0.3 nmol).

4.2.5 Cannula system

Each mouse had a separate tubing system, with an internal needle (C315I/SPC, Plastics1) inserted into the implanted guide canula, connected with transparent tubing (C313CT, C313C, Plastics1), to a Hamilton syringe (SYR 5 µl 75N, Hamilton company, Nevada, USA) in a microinjector pump (Pump 11, Elite, Harvard Apparatus, Massachusetts, USA). The tubing was back-filled with saline and front-filled with 3-4 µl drug solution. In the saline phase, two air bubbles were introduced, to allow monitoring of fluid movements (Figure 4.2B). After infusion, infusion success was verified by the movement of the Hamilton plunger, the bubbles, and the fluid level of the drug solution, with respect to the markings made preceding the infusion procedure.

4.2.6 Data acquisition and offline processing

EEG/EMG signals were recorded continuously in 24-hour blocks as described in Chapter 2, with a sampling rate of 305 Hz with an anti-aliasing filter at 45% of the sampling rate and were stored locally. Signals were resampled offline and further processed in Matlab as described in the General Methods in Chapter 2, section 2.5.5: Signal Processing.

4.2.7 Food intake

To assess 24-hour food intake, food pellets were weighed before introducing them into the cage at 9AM. The next morning, food pellets were weighed again and the difference in weight was taken as a proxy for food consumed in 24 hours. To facilitate quick retrieval of pellets, the number of pellets per cage was limited (3-4) and the bedding was changed from regular brown bedding to white bedding for ease of pellet visualisation.

4.2.8 Histology

At the end of the recordings, animals were culled with an overdose of pentobarbitone and perfused transcardially with 0.1 M PBS followed by 4% paraformaldehyde as described in Chapter 2. After removal of the headstage including the canula, the brains were extracted,

postfixed in 4% paraformaldehyde, cut into 50 μm sections with a vibroslicer, stained with DAPI and inspected for localization of the cannula tract in the lateral cerebral ventricle.

4.2.9 Statistics

All statistical analyses were conducted with GraphPad Prism (version 10.0.2 for Mac, GraphPad Software, Boston, Massachusetts USA). Parameters of sleep architecture were compared with two-way ANOVAs or mixed effects models when there were missing values. The time window for analysis of sleep architecture was from the infusion end for the following 3 hours (2700 epochs of 4 seconds each). Numbers of animals contributing to each outcome measure are reported in the respective figure legends and tables in the Appendix.

For spectral power analyses, offline processing and statistical analysis were performed according to the description in Chapter 2, and for every sub analysis of spectral power, the number of animals that contributed is reported in the respective figure. Time windows for the acute effects of orexin on wakefulness, NREM and REM are described along with the respective results paragraphs. All spectra were inspected for technical quality before selection for inclusion; if less than 140 4-second epochs contributed to the spectrum, it was excluded. Frequency bins <0.5 Hz and >30Hz were excluded from analyses. Comparison of absolute power spectra between orexin vs vehicle was performed with two-way ANOVAs. Absolute spectra were first log-transformed, and only spectra of animals that would contribute to relative spectral comparisons were included. Comparisons of relative spectra were also performed with two-way ANOVAs. The exception was the comparison of relative occipital EEG wake spectra after ORXB, where in two L6b silenced animals, frequency bins <1 Hz and <0.75 Hz were excluded, respectively, after visual inspection because of artefacts, which led to missing values and therefore a Mixed Effects analysis was done. Posthoc differences in frequency bins are only reported if two or more consecutive bins showed a difference (a range of >0.5 Hz), and a range of significantly different frequency bins was only considered interrupted if two or more bins were not significantly different or if one bin showed a large agreement between the spectra that were being compared ($p>0.10$).

4.3 Results

The baseline characteristics were comparable between L6b silenced (n=8) and control (n=5) animals, both concerning animal characteristics and experimental details (Table 4.2). Histology at the end of the experiment confirmed that the cannula was positioned in the right lateral ventricle in all animals (Figure 4.2A), and TdTomato expression confirmed the genotype of the animals labelled as L6b silenced (Drd1a-Cre;TdTom;Snap25fl/fl) based on PCR testing.

On visual inspection, the EEG and EMG traces looked comparable in both genotypes after the respective infusions (Figure 4.2C), allowing unbiased, blinded scoring of the 24-hour files in 4-second epochs, following conventions (Yamagata et al., 2021).

After sleep scoring, for each animal and each vigilance state, 24-hour spectra were calculated, and the shape of the respective spectra confirmed acceptable sleep scoring (Figure 4.2D, see Chapter 3 for a description of spectral patterns across vigilance states).

As a further quality control, EEG slow wave activity (SWA) was plotted aligned with a 24-hour hypnogram for all animals after every treatment condition. The distinct pattern of high SWA during periods scored as NREM sleep, and low SWA during periods scored as REM or Wakefulness indicated the validity of scoring (Figure 4.3).

Table 4.2 Baseline table

	L6b silenced (n=8)	Controls (n=5)	P
Age (days)	95.75 ± 6.364	98.60 ± 6.618	0.4551
Body weight (g)	24.89 ± 1.902	27.04 ± 2.946	0.0840
Implant weight (g)	0.7875 ± 0.1727	0.7800 ± 0.2168	0.9496
Time light onset to start infusion (min)			
Vehicle	22.00 ± 7.946	20.60 ± 9.633	0.7805
Orexin A, low dose	26.13 ± 8.643	26.60 ± 10.36	0.9302
Orexin A, high dose	21.50 ± 7.635	21.20 ± 9.365	0.9506
Orexin B	26.75 ± 9.114	26.00 ± 12.57	0.9026
Time start infusion to closing chambers (min)			
Vehicle	18.50 ± 2.563	18.60 ± 2.702	0.9477
Orexin A, low dose	21.13 ± 5.643	18.80 ± 1.643	0.3952
Orexin A, high dose	19.00 ± 2.726	19.40 ± 2.702	0.8010
Orexin B	18.88 ± 1.642	22.60 ± 7.092	0.1720

All values are expressed as mean ± SD. All characteristics compared with unpaired, two-tailed t-test.

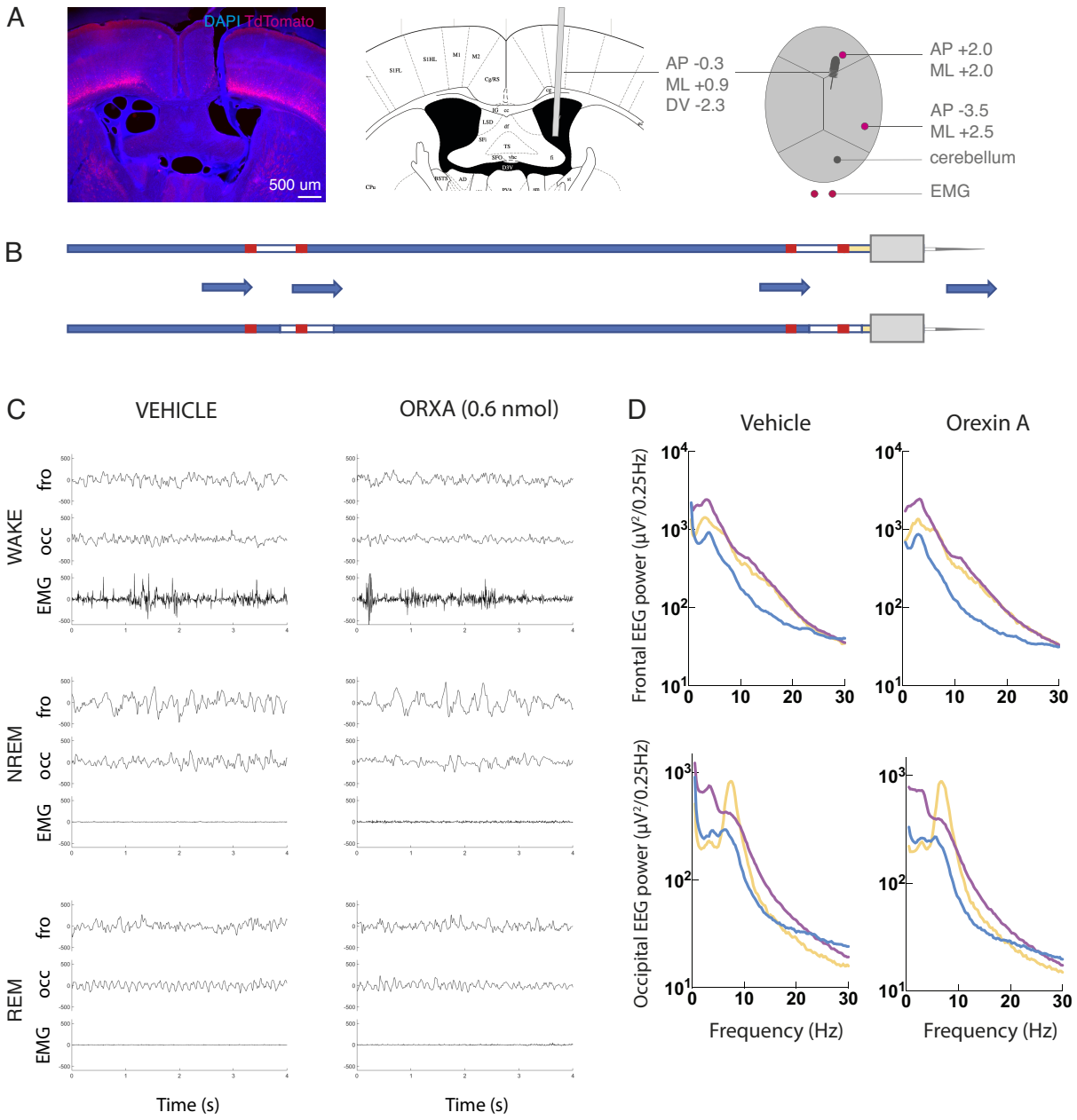

Figure 4.2: In vivo orexin administration with continuous EEG/EMG recording.
(A) The cannula was positioned in the right lateral ventricle, evident from the trace of the headstage that has been removed at the end of the experiment. For this example, a Cre positive animal was chosen, that expresses TdTomato and is L6b silenced. Magenta cells can be seen at the bottom of L6. The stereotactic coordinates of the canula and the EEG/EMG electrodes are indicated by the drawing. The middle drawing is from the Paxinos mouse brain atlas (Paxinos & Franklin, 2001).
(B) Infusion system with air bubbles and marking to verify the success of the infusion.
(C) Example traces from one animal during Wake, NREM and REM, after vehicle and ORXA infusion. After both infusions, the vigilance states are clearly identifiable by the potentials recorded in the frontal EEG (top traces), occipital EEG (middle traces), and EMG (bottom traces).
(D) 24-hour spectra during Wake, NREM and REM after vehicle and ORXA infusion in WT animals showing distinctive patterns in the frontal EEG (top) and occipital EEG (bottom). Frontal EEG, n=7, Occipital EEG n=6.

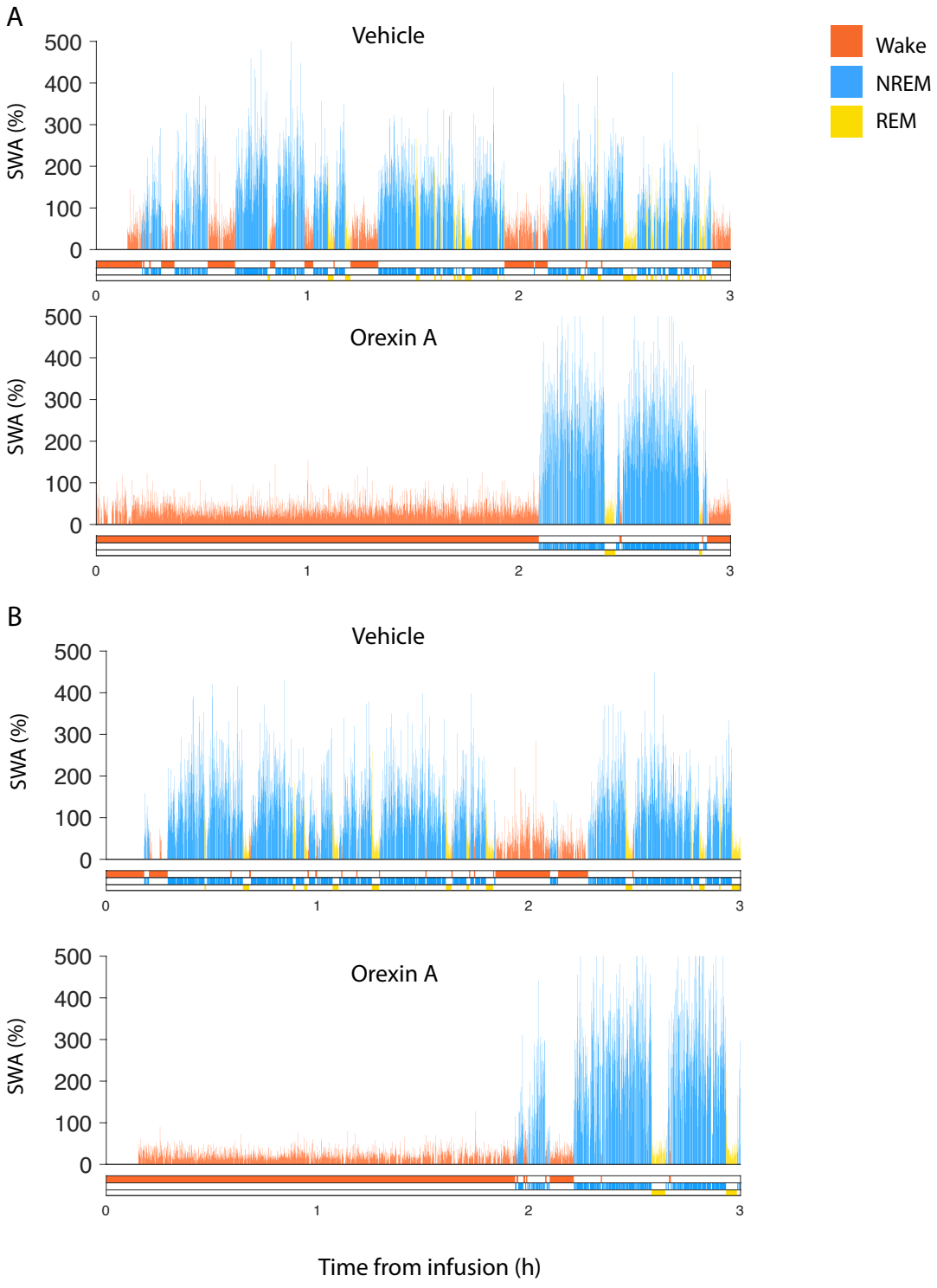

Figure 4.3 Slow wave activity and hypnogram in example animals.
Slow wave activity (SWA, 0.5-4.0 Hz) expressed as a percentage of average slow wave activity on vehicle day. SWA is shown for the first 3 hours after infusion of vehicle and orexin A (0.6 nmol), in an example control animal and an example L6b silenced animal. It is visible that SWA is low during epochs scored as wakefulness and REM sleep and high during epochs scored as NREM sleep.
(A) Example control animal
(B) Example L6b silenced animal

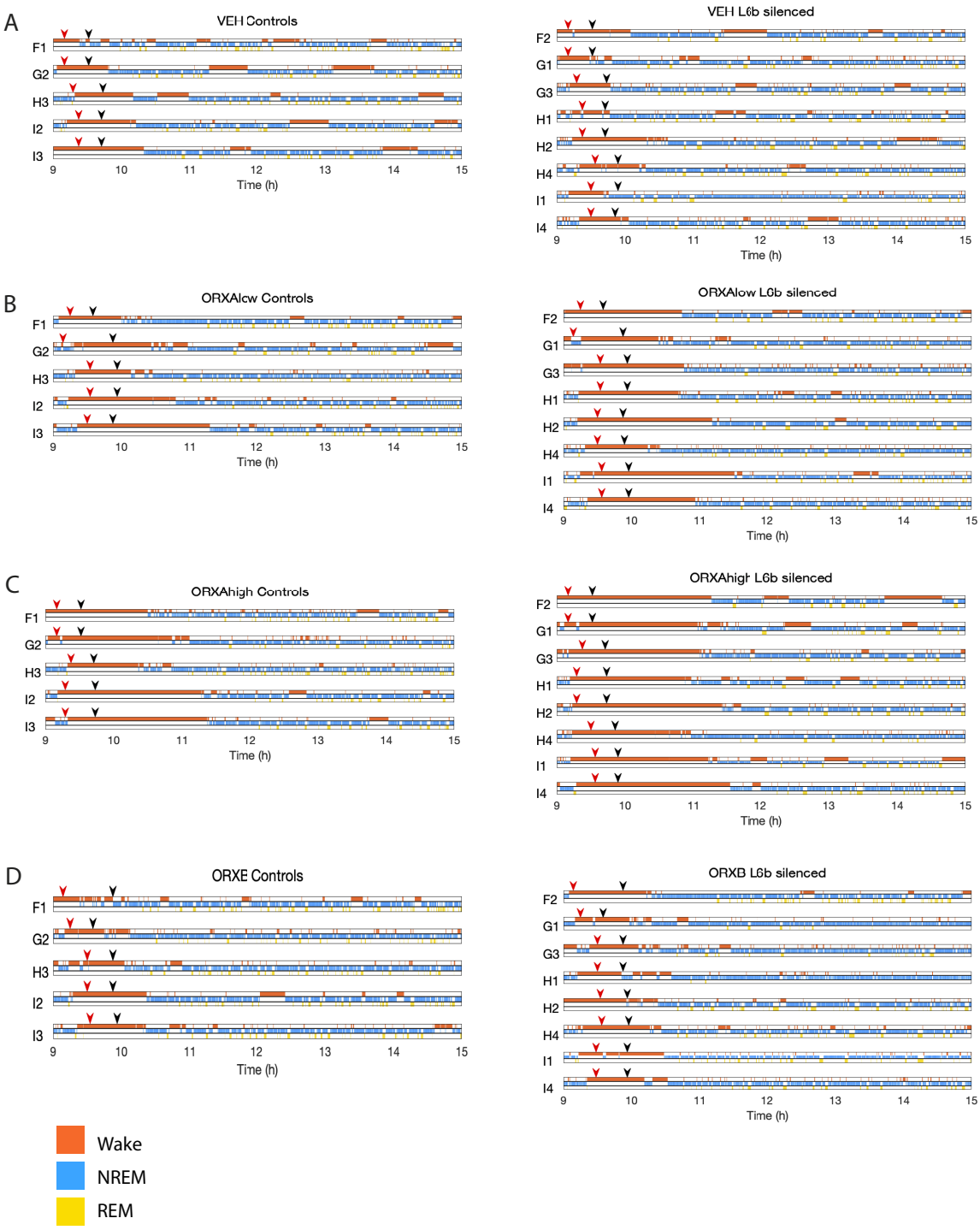

Figure 4.4 Hypnograms of all animals after the different infusions.
Each line with a mouse name in front of it (e.g., 'F1') represents a 6-hour hypnogram from light onset for an individual animal. Red arrowhead: infusion start. Black arrowhead: closure of recording chamber.
(A) Vehicle
(B) ORXA (0.3 nmol)
(C) ORXA (0.6 nmol)
(D) ORXB

4.3.1 Sleep architecture

Orexin was injected at light onset, which is normally the beginning of the inactive phase in mice, with more time spent in NREM sleep and less time spent in wakefulness. However, after ORXA injection, animals of both genotypes stayed awake for a larger proportion of the time, which is apparent in hypnograms of individual animals (Figure 4.4).

When the hourly time courses of vigilance state are plotted, it is visible that effects are most strong in the first three hours after administration (Figure 4.5A). Based on these findings and reports in literature (Huang et al., 2001; Mieda et al., 2011; Piper et al., 2000) on the duration of action of orexin, the time frame for analysis of sleep architecture was defined as the time from the end of the infusion for the duration of three hours.

In the first three hours, ORXA markedly increased the time spent in wakefulness in both L6b silenced and control animals, without a difference in response between the genotypes (Figure 4.5B, left)(ORXA Dose, $F_{(1.316,11.18)}$=27.56; p=0.0001). In line with the increase in time spent in wakefulness, ORXA significantly decreased the time spent in NREM (ORXA Dose, $F_{(1.629,14.66)}$=22.30, p<0.0001) and REM (ORXA Dose, $F_{(1.057,9.516)}$=21.23, p=0.001). Unlike the distinct effects of ORXA, ORXB did not influence the amount of time spent in the respective vigilance states (Figure 4.5, right)(Compared to vehicle; Wake, $F_{(1,9)}$=0.02874, p=0.8691; NREM, $F_{(1,9)}$=0.00898, p=0.9266; REM, $F_{(1,20)}$=1.193, p=0.2878).

The latency to onset of consolidated NREM sleep was significantly increased after infusion of ORXA (ORXA Dose, $F_{(2,22)}$=50.10, p<0.0001)(Figure 4.5C), and consistent with this, the occurrence of the first episode of REM sleep was also delayed (Figure 4.5D)(ORXA Dose, $F_{(1.655,14.89)}$=7.656, p=0.0071)). ORXB did not influence the latency to NREM ($F_{(1,9)}$=0.1050,p=0.7534) or REM sleep ($F_{(1,9)}$=2.339, p=0.1605).

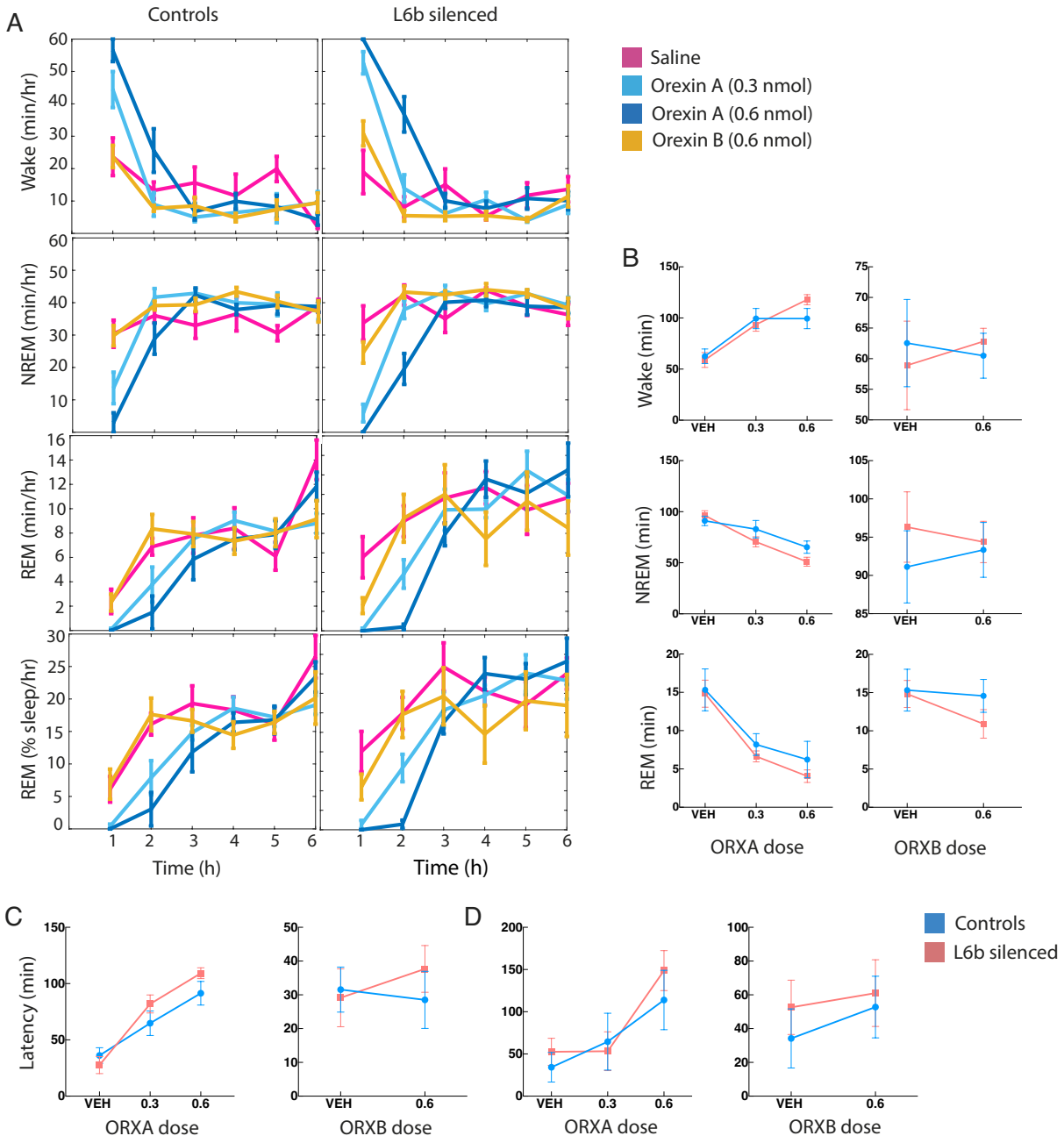

Figure 4.5: Orexin increases wakefulness in the first three hours after infusion.
(A) Time course of wake, NREM, REM, and REM as a percentage of sleep, after injection of vehicle (magenta), 0.3 nmol ORXA (light blue), 0.6 nmol ORXA (navy blue), 0.6 nmol ORXB (yellow) in control animals (left column) and L6b silenced animals (right column).
(B) Time spent in wake, NREM and REM within the first three hours after injection of ORXA (left column) or ORXB (right column) in controls (purple) and L6b silenced animals (orange).
(C) Latency to first consolidated NREM sleep after ORXA or ORXB.
(D) Latency to REM after ORXA or ORXB.
Controls n=7, L6b silenced n=9.

Increased wakefulness after ORXA administration could be the result of an increase in the number of wake episodes, an increase in the duration of wake episodes, or both. Wake episodes were defined as ≥1 min scored as Wake or Wake artefact with ≤16s interruptions. Whereas the number of wake episodes per hour did not change after infusion of ORXA ($F_{(1.399,12.59)}$=0.6447, p=0.4878) or ORXB ($F_{(1,9)}$=0.2753, p=0.6125) in either genotype, the average duration of wake episodes increased significantly after ORXA infusion (ORXA dose, $F_{(2,22)}$=8.995, p=0.0014) (Figure 4.6A). Interestingly, the increase in average wake episode duration was significantly greater in L6b silenced animals (ORXA dose x Genotype interaction, $F_{(2,22)}$=4.376, p=0.0251).

To investigate whether the increased average wake duration was a result of more frequent, relatively longer wake episodes or a single, prolonged wake episode, I plotted the distribution of wake episode duration after vehicle and ORXA (0.6 nmol) administration for both genotypes. It became apparent that after ORXA infusion, extended wake episodes (>1024s or >17 minutes) occurred, that are not observed after vehicle infusion (Figure 4.6B). Indeed, the maximum duration of wake episodes was significantly increased after ORXA infusion (ORXA dose, $F_{(1.730,15.57)}$=46.65, p<0.0001), and this effect was stronger in L6b silenced animals (ORXA dose x Genotype interaction, $F_{(2,18)}$=3.759, p=0.0432)(Figure 4.6C). An exploratory survival analysis of the differential maximal episode duration showed a similar trend (delta (maximal wake episode duration ORXA – maximal wake episode duration vehicle), Genotype groups, log rank test, Chi square 3.410, df 1, p=0.0648)(Figure 4.6D).

Lastly, ORXA increased the number of brief arousals (<16s) from NREM sleep ($F_{(1.460,8.759)}$=7.907, p=0.0149) in both genotypes (Figure 4.6E). ORXB also increased the number of brief arousals in both genotypes ($F_{(1,7)}$=6.431, p=0.0389).

Overall, these results indicate that ORXA promotes prolonged wakefulness and postpones the onset of NREM sleep. Moreover, after administration of ORXA there is an increase in the duration of wakefulness episodes, and this effect is stronger in L6b silenced than in control animals. In addition, both ORXA and ORXB increase the number of brief arousals from NREM sleep, suggesting an increased tendency to transition from sleep to wakefulness.

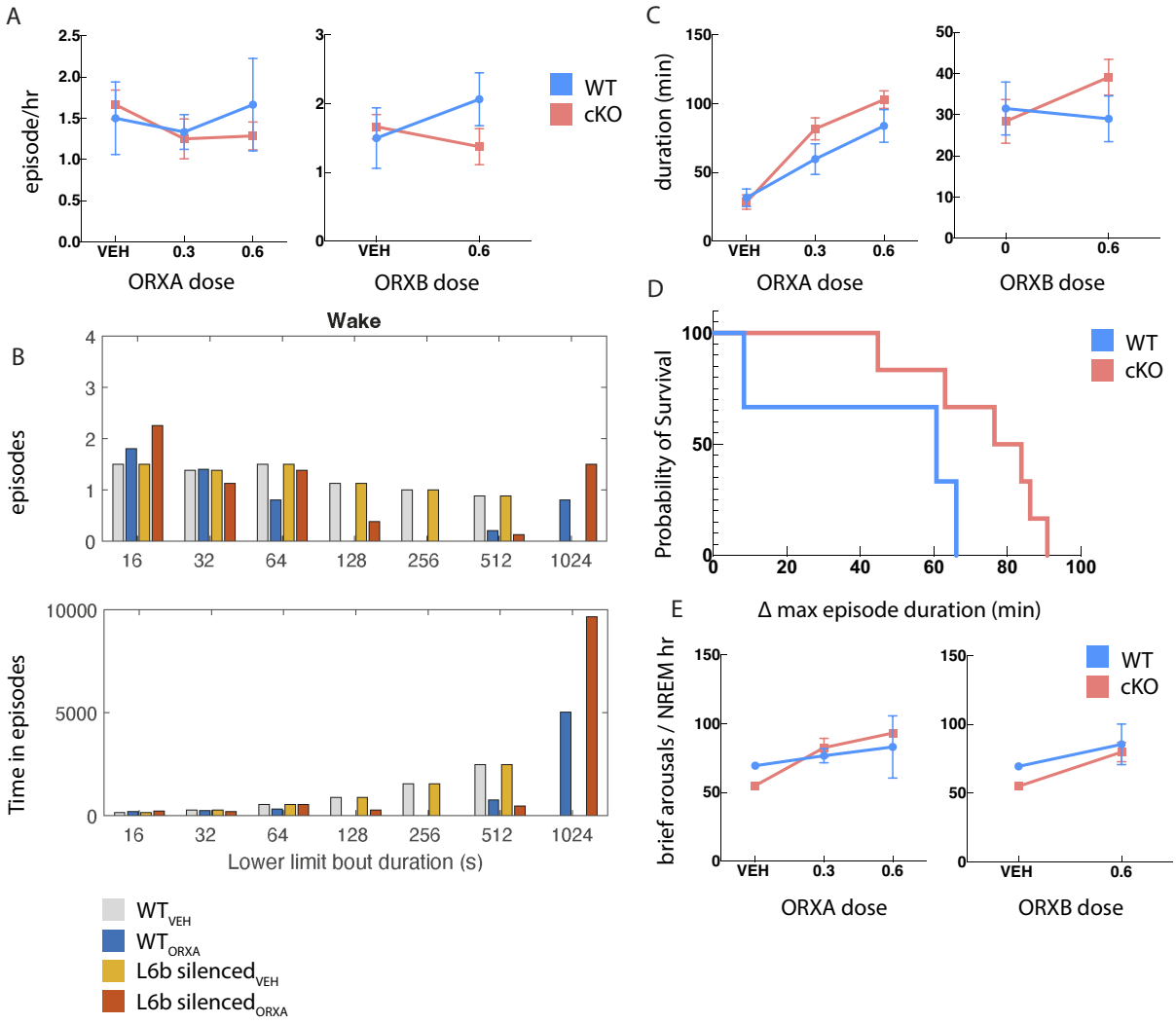

Figure 4.6: Orexin A prolongs wake episodes and increases brief arousals.
(A) Number of wake episodes in the first three hours after infusion after ORXA (left) and ORXB (right). WT n=5, L6b silenced n=8.
(B) Distribution of wake episode duration in control (Ctl) and L6b silenced animals (cKO), over duration categories, with the number on the x axis indicating the lower border of the episode category in seconds. (top) number of episodes in each category and (bottom) how much time is spent in every wake episode duration category. WT n=5, L6b silenced n=8.
(C) Maximal wakefulness episode duration in the first three hours after infusion of ORXA (left) or ORXB (right). WT n=5, L6b silenced n=8.
(D) Survival analysis of differential maximal wake episode duration after ORXA infusion (maximal wake episode duration after ORXA – maximal wake episode duration after vehicle, first calculated as a single value per animal and then averaged across genotype groups in GraphPad Prism).
(E) Number of brief awakenings per hour of NREM in the first three hours after infusion. WT n=4, L6b silenced n=5.

4.3.2 EEG power spectra

Next, I investigated whether ORXA and ORXB affect state-dependent EEG oscillations during sleep and wakefulness. First, the overall quality of the spectra was verified, by visual inspection of 24-hour spectra. Since the effects of orexin are strongest in the first hours after administration as apparent from my own findings and literature, subsequent analysis was performed on earlier time windows (Huang et al., 2001; Mieda et al., 2011; Piper et al., 2000). Time frames were selected in such a way that on the one hand, the acute effects would be visible, and on the other hand, a sufficient number of epochs would contribute to spectral power calculations. I administered two doses of ORXA (0.3 nmol and 0.6 nmol), and often the effects with the low dose of ORXA were consistent with the effects with the high dose of ORXA. For clarity, I will limit my description to the higher dose of ORXA, and ORXB (only administered at higher dose). For readability, I included the results of all statistical tests in a table in the appendix (Appendix, Supplementary Table S4.2-4.4).

Wakefulness

As time frame for wakefulness, the end of the infusion was selected as the lower limit and the onset of the first consolidated NREM sleep (NREM episode of ≥1 min with ≤16s interruptions) as the upper limit. Wakefulness was divided into two sub periods: an early wake frame, when the recording chamber was still open, to investigate the most acute effects of the infusion, and a later frame, after the recording chamber had been closed, to get a signal that is less affected by electrical noise and get a behaviour that may be less affected by external factors in the recording room. Every wakefulness episode within the time with a ≥1 min duration and ≤16s interruptions was included in the analysis. In the wakefulness sub period immediately following infusion ('Wake 1'), most data had to be excluded because animals spent insufficient time in artefact free wakefulness to perform meaningful spectral analysis (Supplementary Table S4.1: number of epochs contributing to spectra). Moreover, some data had to be excluded for technical reasons. Therefore, I will focus on the wakefulness spectra from the EEG recorded after closing the

recording chambers ('Wake 2'); spectra and statistical outcomes of both windows can be found in the appendix (Supplementary Table S4.1,S4.2 and S4.3).

I first investigated the effects of orexin on absolute power spectra during wake in control animals only and here, both ORXA (Figure 4.7A) and ORXB (Figure 4.7B) seemed to enhance theta power in both derivations at visual inspection, but with statistical comparisons, no effects were observed from ORXA or ORXB infusion on wakefulness spectra in control animals (Table S4.2).

In L6b silenced animals, ORXA infusion led to a significant decrease in 2.0-6.0 Hz and 9.75-23.25 Hz frontal EEG power; theta range power seemed increased by initial visual inspection (Figure 4.7A), but the latter effect was not significant (Table S4.3). In the occipital EEG, after ORXA there was a reduction in 3.25-4.0 Hz, 4.5-6.5 Hz and 9.75-16 Hz EEG power and an increase in 7.25-8.0 Hz and 20.75-30 Hz EEG power. After ORXB administration there was a reduction in 3.5-4.0 Hz, 4.75-5.25 Hz, 11.5-19.5 Hz and 20.5-21 Hz and an increase in 7.5-9.0 Hz frontal EEG power. ORXB visually seemed to result in increased theta power in the occipital EEG as well, but this was not significant (Figure 4.7B).

I then compared the responses between the genotypes, by normalising spectra on orexin day to spectra on vehicle day and subsequently comparing genotype-grouped relative spectra (Table S4.3). On vehicle day, several animals fell asleep soon after infusion, which was reassuring in terms of the infusion procedure being stress-inducing but made it impossible to calculate a vehicle wakefulness spectrum to normalise to (see Figure 4.4). Therefore, initial wakefulness orexin spectra (typically across ~1,5 hours after ORXA infusion and across ~35 minutes after ORXB infusion but the duration varied per animal depending on individual NREM latency) were normalised to 24-hour wakefulness vehicle spectra.

For relative wake spectra after ORXA administration in L6b silenced versus control animals, there was a significant Frequency x Genotype interaction in both the frontal and occipital EEG, but not at a specific frequency range. Comparison of occipital EEG power in the theta frequency range did not reveal differences between genotypes (Absolute: $t_{(10.23)}$=1.683, Relative to vehicle: $t_{(5.781)}$=1.215, p=0.2715)(Figure 4.8 A,B).

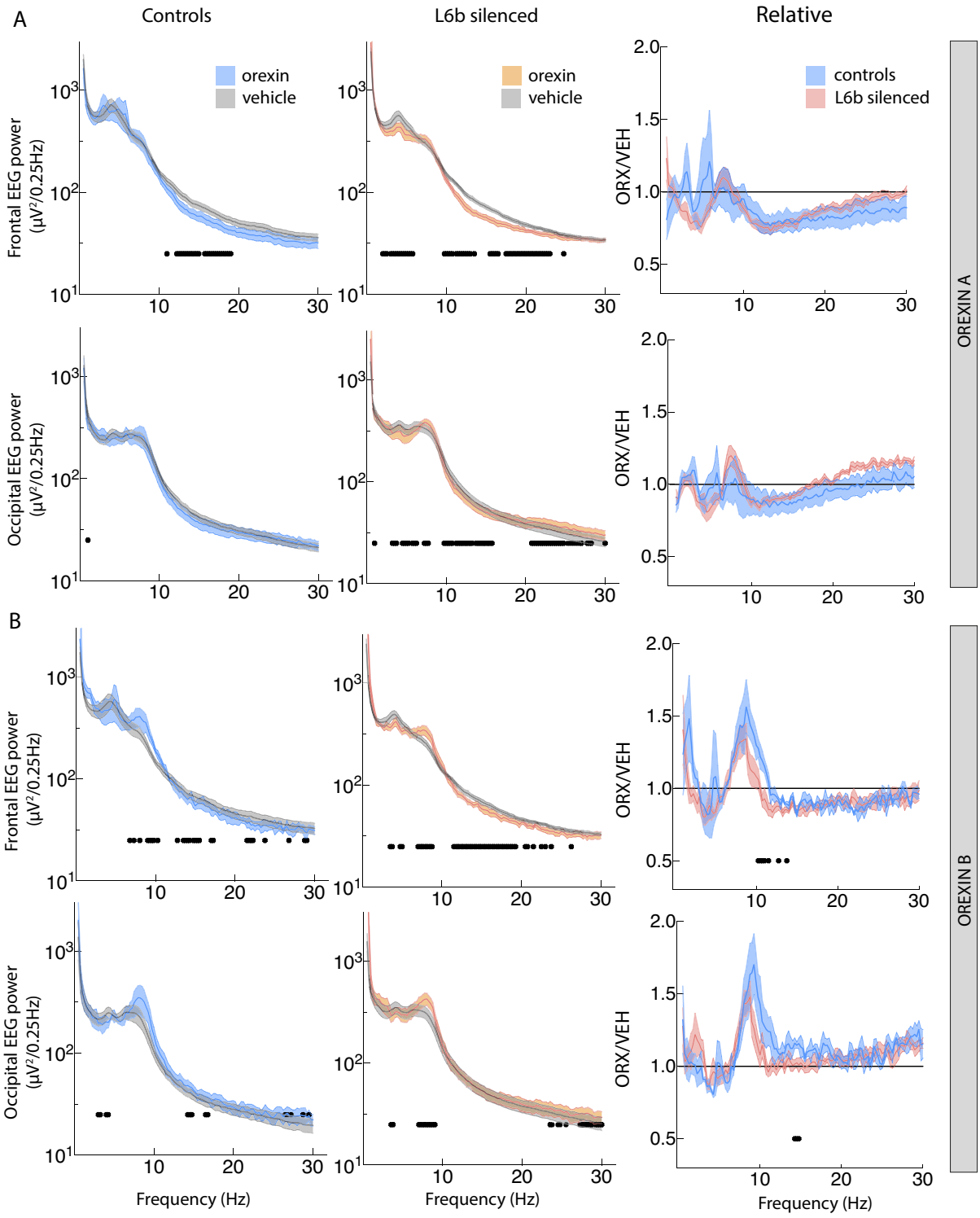

Figure 4.7: EEG spectral power density during wakefulness.
(A) Spectra after ORXA infusion. The left column shows absolute EEG power in WT animals after vehicle (grey) and orexin (blue). The middle column shows absolute EEG power in L6b silenced animals after vehicle (grey) and orexin (red). The right column shows the relative orexin/vehicle EEG power in WT (blue) and L6b silenced animals (red). Number of animals contributing: WT, frontal EEG n=5, occipital EEG n=5; L6b silenced, frontal EEG n=8, occipital EEG n=8.
(B) Spectra after ORXB infusion. The left column shows absolute EEG power in WT animals after vehicle (grey) and orexin (blue). The middle column shows absolute EEG power in L6b silenced animals after vehicle (grey) and orexin (red). The right column shows the relative orexin/vehicle EEG power in WT (blue) and L6b silenced animals (red). Number of animals contributing: WT, frontal EEG n=3, occipital EEG n=3; L6b silenced, frontal EEG n=6, occipital EEG n=6.

The normalised spectra after ORXB infusion showed a significant Frequency x Genotype interaction only in the occipital EEG, with a larger increase in 14.25-15 Hz EEG power in control animals (Figure 4.7B, right column). This could be interpreted as a larger increase in EEG alpha power (8-12 Hz) during wakefulness, but there were no significant differences in occipital EEG power in the alpha frequency range between the genotypes (absolute: $t_{(3.175)}$=0.2845, p=0.7936, relative to wakefulness on vehicle day: $t_{(2.685)}$=1.243, p=0.3115, Welch's t test)(Figure 4.8E,F). There were also no differences between genotypes in EEG theta power (4.5-10 Hz) after ORXB infusion ($t_{(5.037)}$=1.056, p=0.3390)(Figure 4.8C). With theta power after ORXB infusion normalised to theta power after vehicle infusion (as in Figure 4.7 panel B, right column), theta power was lower after ORXB infusion in both genotypes and the reduction was larger in L6b silenced animals ($t_{(4.529)}$=2.833, p=0.0409)(Figure 4.8D). The effect of normalising to 24-hour theta power needs to be considered when looking at this difference in future analysis.

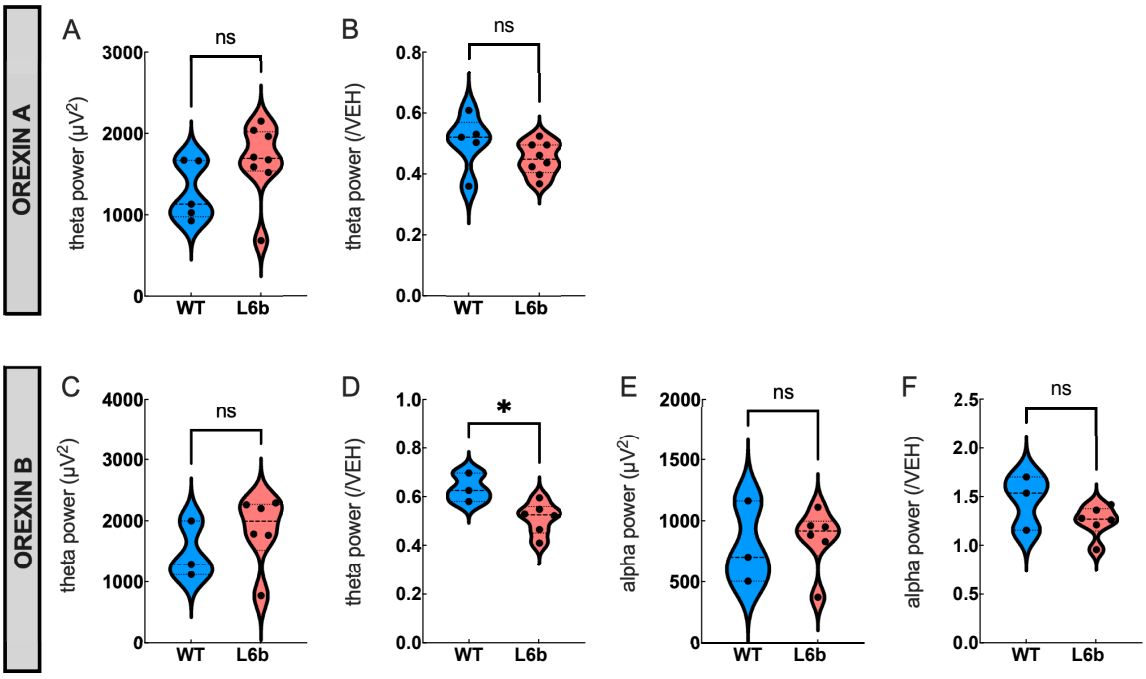

Figure 4.8: EEG power in the theta and alpha frequency range during wakefulness.
All band power calculations shown are for the occipital EEG. Theta power was defined as 4.5-10 Hz and alpha power as 8-12 Hz. The same animals were included as those included for spectra comparisons in Figure 4.7.
(A) theta power, absolute. (B) theta power, relative to VEH infusion (full day 24 hours)
(C) theta power, absolute. (D) theta power, relative to VEH infusion (full day 24 hours)
(E) alpha power absolute. (F) alpha power, relative to VEH infusion (full day 24 hours)

NREM sleep

Next, I assessed whether the administration of orexin affected subsequent NREM sleep spectra. The time frame for NREM sleep spectral analysis was defined to begin at the onset of the first consolidated NREM sleep episode (≥1 min with ≤16s interruptions) and end 3 hours later. Because there were sufficient epochs spent in NREM sleep in the 3-hour time frame after vehicle infusion (see Figure 4.4, Table S4.1), I compared 3-hour NREM spectra after orexin infusion with 3-hour NREM spectra after vehicle infusion.

I first compared orexin to vehicle absolute spectra in control animals (Figure 4.9, left; Table S4.2). After ORXA infusion, the frontal EEG power was increased between 4.0-9.5 Hz, 11-11.5 Hz, 12-12.5 Hz, 14.5-18.75 Hz, 19.25-26 Hz, and 26.75-30 Hz. In the occipital EEG, there was no significant change in the spectrum. After ORXB compared to vehicle, there was a significant overall Treatment effect in the frontal EEG, but the Treatment x Frequency bin interaction was not significant. In the occipital EEG, there was no overall Treatment effect, but there was a significant Treatment x Frequency bin interaction, with ORXB resulting in significantly lower occipital EEG power between 1.25-1.75 Hz and 2.0-2.5 Hz, and higher occipital EEG power between 4.5-5.5 Hz, 9.25-9.75 Hz, 10.25-15.75 Hz, and 17.5-20.5 Hz.

In L6b silenced animals (Figure 4.9, middle; Table S4.3), there was a significant overall increase in both frontal and occipital EEG power after ORXA, without a *Treatment x Frequency bin* interaction. ORXB also resulted in a significant overall increase in frontal EEG power, which appeared to show on the occipital EEG too, but in the occipital EEG the effect was not significant.

Next, I compared relative EEG spectra between the genotypes (Figure 4.9, right; Table S4.4), with orexin spectra normalised to vehicle spectra. After ORXA infusion, there was an increase in frontal EEG power at 3-30 Hz in both genotypes, but only in L6b silenced animals this extended to 0.75-2.75 Hz. There was no difference in frontal EEG power in the delta frequency range between the genotypes (absolute: $t_{(9.422)}$=0.7441, p=0.4750; relative to vehicle spectra, $t_{(10.88)}$=1.320, p=0.2141, Welch's t test)(Figure 4.10A,B).

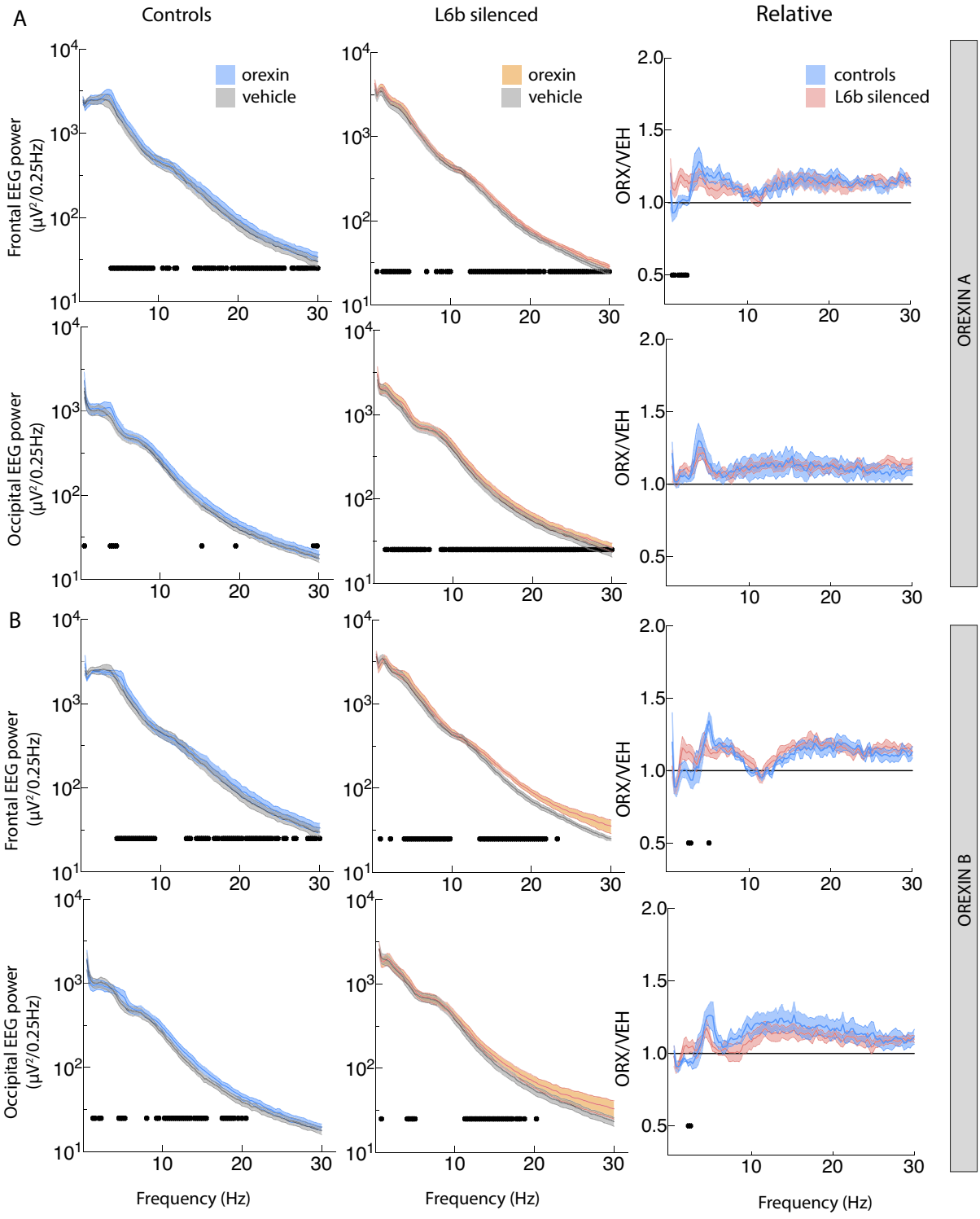

Figure 4.9: EEG spectral power density during NREM sleep.

(A) Spectra after ORXA infusion. The left column shows absolute EEG power in WT animals after vehicle (grey) and orexin (blue). The middle column shows absolute EEG power in L6b silenced animals after vehicle (grey) and orexin (red). The right column shows the relative orexin/vehicle EEG power in WT (blue) and L6b silenced animals (red). Number of animals contributing: WT, frontal EEG n=5, occipital EEG n=5; L6b silenced, frontal EEG n=8, occipital EEG n=8.

(B) Spectra after ORXB infusion. The left column shows absolute EEG power in WT animals after vehicle (grey) and orexin (blue). The middle column shows absolute EEG power in L6b silenced animals after vehicle (grey) and orexin (red). The right column shows the relative orexin/vehicle EEG power in WT (blue) and L6b silenced animals (red). Number of animals contributing: WT, frontal EEG n=5, occipital EEG n=5; L6b silenced, frontal EEG n=7, occipital EEG n=7.

After ORXB infusion, there was also an increase in 3-30 Hz EEG power, this time in both the frontal and occipital EEG; again, the power increase extended to lower frequencies only in L6b silenced animals. Yet, when comparing frontal EEG power in the delta range (1-4 Hz), there was no difference between genotypes (absolute: $t_{(8.875)}$=1.403, p=0.1946, relative to vehicle spectra: $t_{(8.351)}$=1.146, p=0.2837, Welch's t test)(Figure 4.10C,D). In the occipital EEG, delta power was significantly higher in L6b silenced animals ($t_{(9.972)}$=2.639, p=0.0248, Welch's t test)(Figure 4.10E), but when spectra were normalised to vehicle, the difference disappeared ($t_{(8.871)}$=1.412, p=0.1921, Welch's t test)(Figure 4.10F). There were also no significant genotype differences in theta frequency range power, neither in the frontal EEG (absolute: $t_{(8.020)}$=0.3154, p=0.7605, relative to vehicle $t_{(10.46)}$=0.8036, p=0.4395)(Figure 4.10G,H) nor the occipital EEG (absolute $t_{(10.90)}$=1.837, p=0.0936, relative to vehicle $t_{(9.365)}$=1.292, p=0.2275, Welch's t test)(Figure 4.10H,I).

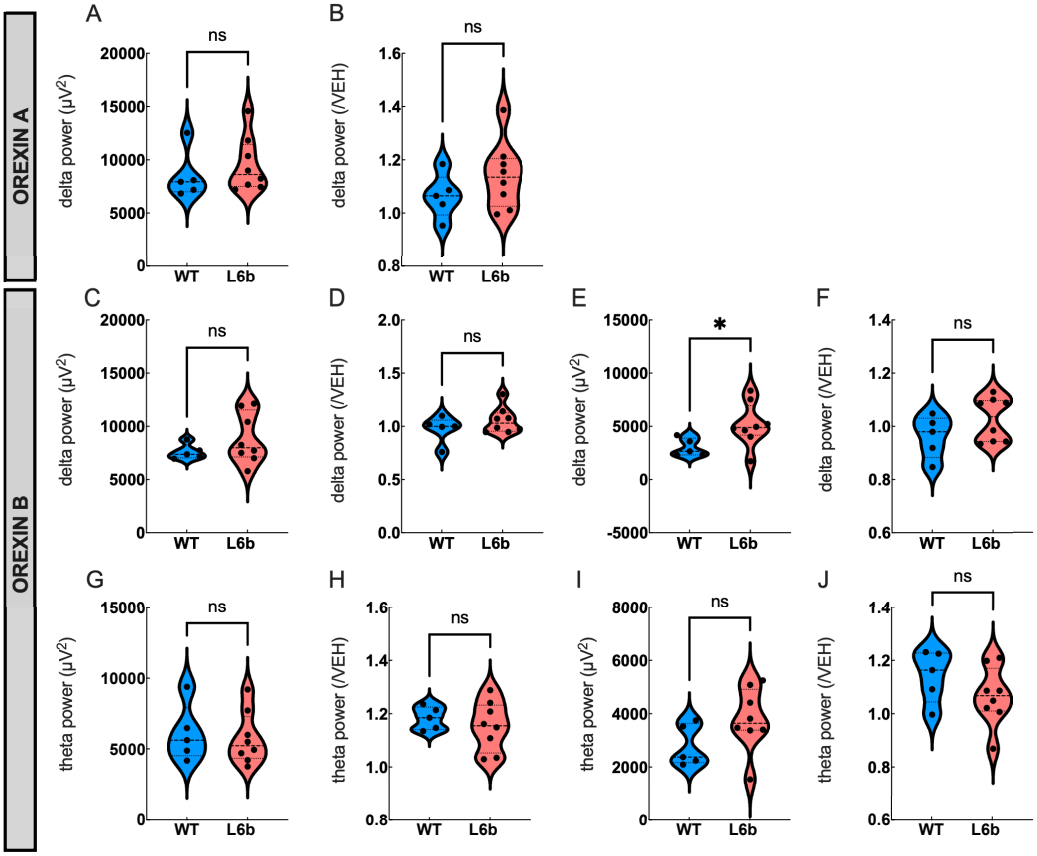

Figure 4.10: EEG power in the delta and theta frequency range during NREM sleep. The delta frequency range was defined as 104 Hz, theta frequency as 4.5-10 Hz. Abs=absolute, Rel=relative to 3-hour vehicle spectra. Animals contributing: WT n=5, L6b silenced n=9. (A) ORXA high, EEG1 delta abs. (B) orxa high eeg1 delta rel. (C) ORXB eeg1 delta abs. (D) orxb eeg1 delta rel. (E) orxb eeg2 delta abs. (F) orxb eeg2 delta rel. (G) orxb eeg1 theta abs. (H) orxb eeg1 theta rel. (I) orxb eeg2 theta abs. (J) orxb eeg2 theta rel

REM sleep

For REM sleep, the same time frame was used as for NREM sleep, from the first epoch of consolidated NREM sleep for the consecutive 3 hours, and REM sleep episodes of ≥16 seconds with ≤8s interruptions were included in the analysis. Nearly all animals spent a sufficient number of epochs in REM sleep across treatment conditions to calculate reliable spectra (Table S4.1), so comparisons are made for spectra calculated from comparable time windows between vehicle and the respective orexin treatments, similarly to the comparisons made for NREM spectra.

In control animals, comparison between orexin and vehicle spectra showed that ORXA did not have any effects on EEG spectra in REM sleep, neither in the frontal nor the occipital EEG (Figure 4.11, left column; Table S4.2). There was also no change in occipital EEG theta peak value ($t_{(7.225)}$=0.5341, p=0.6093) or theta peak frequency ($t_{(6.702)}$=0.5657, p=0.5900)(Figure 4.12A,B). After ORXB infusion, there was a significant change in spectra in both EEG derivations, but the posthoc analyses did not reveal specific frequency ranges at which differences occurred (Table S4.2); by visual inspection, it appeared like ORXB shifted the theta peak frequency to a higher frequency (Figure 4.11, left). However, analysis of the theta peak did not reveal changes after ORXB infusion compared to vehicle in control animals (peak value: $t_{(7.815)}$=0.1891, p=0.8548; peak frequency: $t_{(5.882)}$=0.7171, p=0.5008)(Figure 4.12E,F).

Comparison between orexin and vehicle spectra in L6b silenced animals (Figure 4.11, middle column; Table S4.3) gave similar results to control animals. The *Treatment x Frequency bin* effect was only significant in the occipital EEG in L6b silenced animals. In L6b silenced animals, occipital EEG theta peak characteristics were not significantly affected by orexin A compared to vehicle (peak value: $t_{(11.29)}$=0.6734), p=0.5134, peak frequency: $t_{(12.41)}$=2.152, p=0.0517)(Figure 4.12C,D), although there was a trend towards a slowing of the theta rhythm. ORXB infusion did not result in a significant change in occipital EEG theta peaks in L6b silenced animals compared to vehicle infusion (peak value: $t_{(7.675)}$=0.01774, p=0.9863, peak frequency: $t_{(6.669)}$=1.397, p=0.2072)(Figure 4.12G,H).

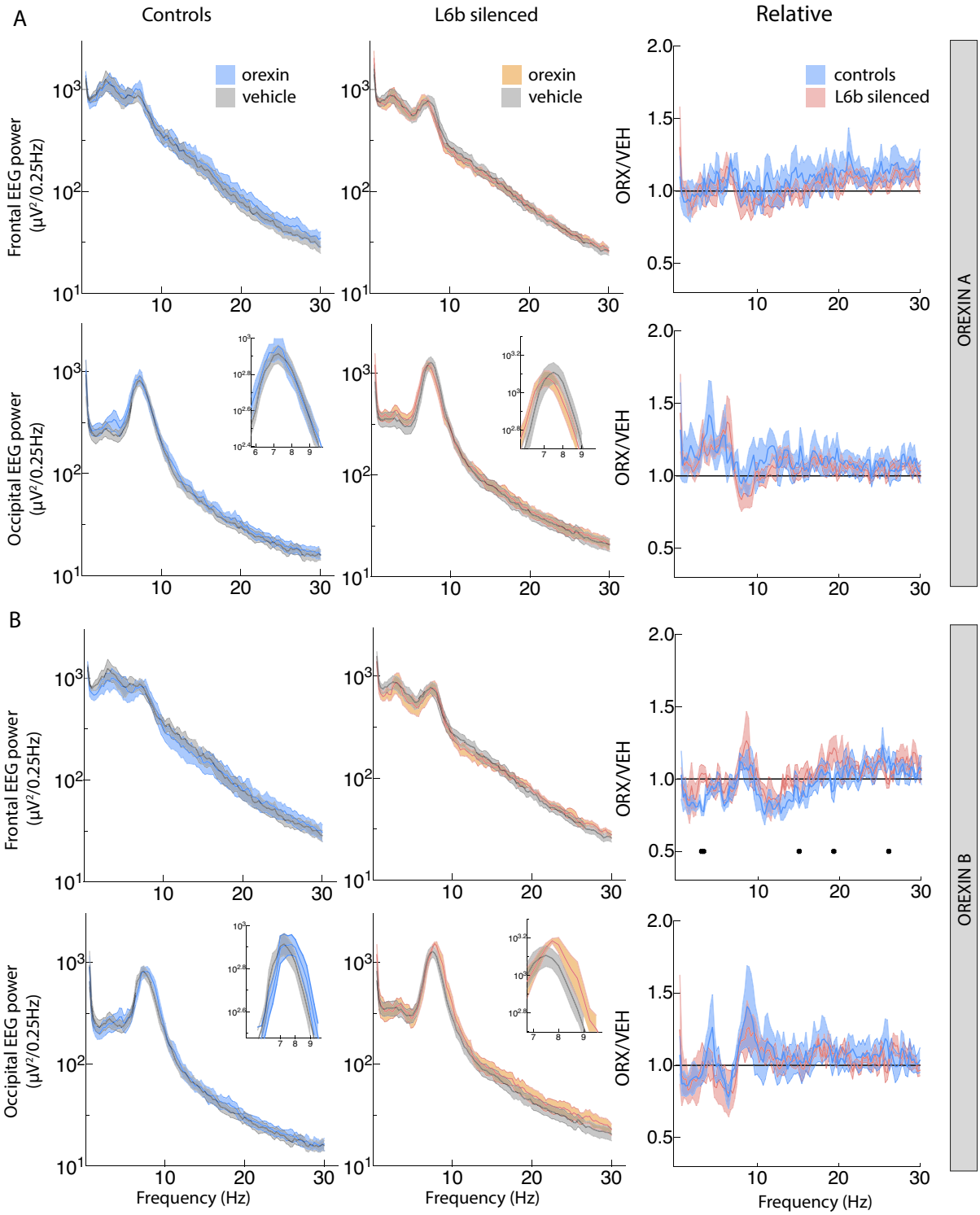

Figure 4.11: EEG spectral power density during REM sleep.
(A) Spectra after ORXA infusion. The left column shows absolute EEG power in WT animals after vehicle (grey) and orexin (blue). The middle column shows absolute EEG power in L6b silenced animals after vehicle (grey) and orexin (red). The right column shows the relative orexin/vehicle EEG power in WT (blue) and L6b silenced animals (red). Number of animals contributing: WT, frontal EEG n=5, occipital EEG n=5; Insets show theta frequency range in more detail. L6b silenced, frontal EEG n=7, occipital EEG n=7.
(B) Spectra after ORXB infusion. The left column shows absolute EEG power in WT animals after vehicle (grey) and orexin (blue). The middle column shows absolute EEG power in L6b silenced animals after vehicle (grey) and orexin (red). The right column shows the relative orexin/vehicle EEG power in WT (blue) and L6b silenced animals (red). Number of animals contributing: WT, frontal EEG n=5, occipital EEG n=5; Inset show theta frequency range in more detail. L6b silenced, frontal EEG n=4, occipital EEG n=4.

Interestingly, the absolute theta peak value after ORXB infusion was higher in L6b silenced compared to control animals ($t_{(6.949)}$=6.881, p=0.0002)(Figure 4.12I), although in baseline condition, no difference was observed in theta peak value between L6b silenced and control animals (Figure 3.8G).

Lastly, REM spectra after the orexin infusions were normalised to those after vehicle infusion and the resultant relative spectra were compared between the genotype groups (Figure 4.11, right column; Table S4.4). No significant differences were detected between L6b silenced and control animals.

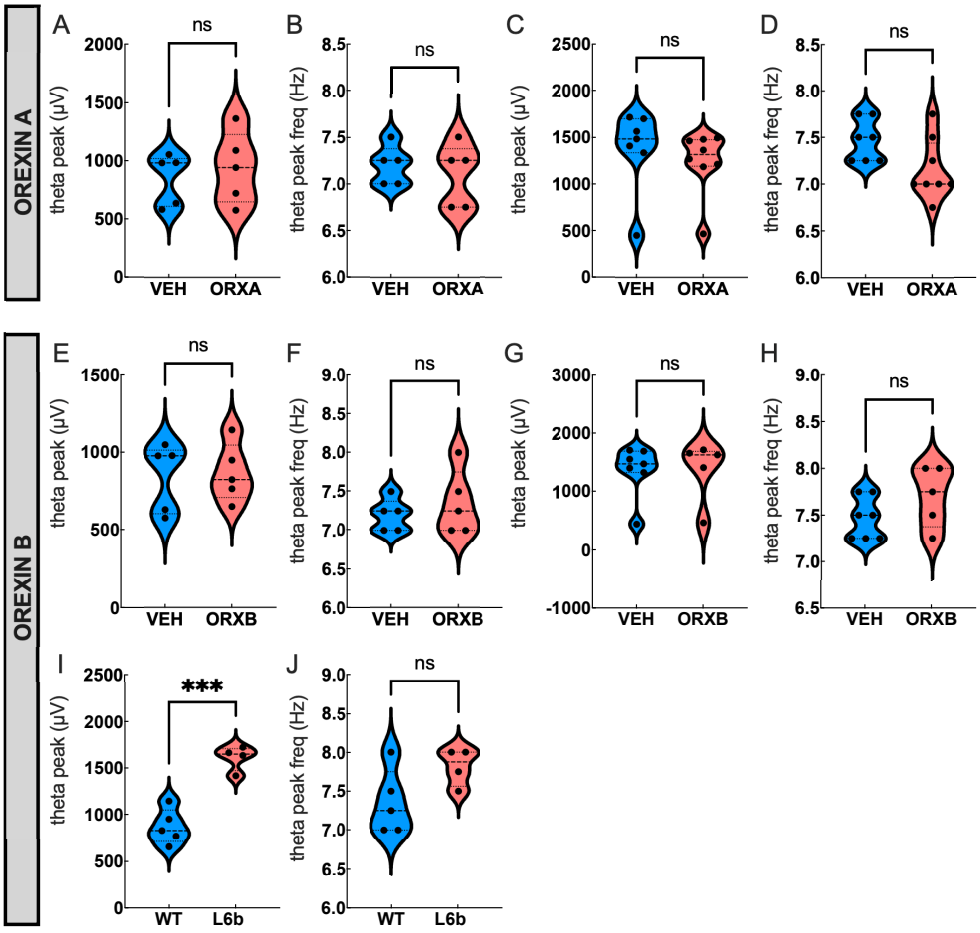

Figure 4.12: Theta peak characteristics during REM sleep after ORX infusion.
Theta was defined as 4.5-10 Hz, all calculations performed on occipital EEG spectra.
(A) VEH vs ORXA ctl, peak value n=5 (B) VEH vs ORXA, CTL, peak frequency n=5. (C) VEH vs ORXA L6b silenced, peak value, n=8. (D) VEH vs ORXA L6b silenced, peak frequency, n=8. (E) VEH vs ORXB CTL, peak value n=5 vs n=5. (F) VEH vs ORXB CTL peak frequency, n=5 vs n=5. (G) VEH vs ORXB L6b silenced, peak value n=7 vs n=4. (H) VEH vs ORXB L6b silenced, peak frequency n=7 vs n=4. (I) Absolute ORXB CTL vs L6b silenced, peak value n=5 vs n=4. (J) Absolute ORXB CTL vs L6b silenced, peak frequency n=5 vs n=4.

4.3.3 Homeostatic regulation of sleep

Since orexin promotes wakefulness, its administration at light onset in light phase-inactive mice can be regarded as pharmacological induction of sleep deprivation. Whereas ORXA caused a significant increase in the time spent in wakefulness in the first 3 hours, wakefulness was back to normal levels from the third hour onwards, and 24-hour percentages in the respective vigilance states were comparable after ORXA and vehicle infusions in both genotypes (Wake, $F_{(2,22)}$=0.7016, p=0.9556; NREM, $F_{(1.674, 18.41)}$=1.715, p=0.2092; REM, $F_{(1.686,18.55)}$=2.235, p=0.1409) (Figure 4.13). The total 24-hour time spent in REM sleep was reduced in L6b silenced compared to controls (Genotype effect, $F_{(1,11)}$=13.99, p=0.0033). This was unexpected, because in the baseline sleep phenotyping of L6b silenced animals, no change in total REM time was observed (Chapter 3).

After infusion of ORXA, the dissipation of SWA in the first 3 hours (in 30 min bins) after the onset of consolidated NREM sleep was not different between L6b silenced and control animals (Frontal, Time x Genotype $F_{(5,55)}$=0.4621, p=0.8027, Occipital, Time x Genotype, $F_{(5,55)}$=1.373, p=0.2485)(Figure 4.13C). However, SWA in the occipital EEG during the first 3 hours of NREM after ORXA was decreased in L6b silenced animals (Genotype, $F_{(1,11)}$=6.818, p=0.0242). ORXB did not increase the duration of wakefulness, and consequently, the accumulation and subsequent release of SWA was less evident.

Slow wave energy (SWE) is the cumulative sum of EEG delta power across all artefact-free epochs scored as NREM sleep (Figure 4.13D,E). After administration of vehicle, SWE was not significantly different between genotypes (Mixed effects $F_{(23,230)}$=0.2968, p=0.9994). When frontal EEG SWE after orexin infusion was normalised to SWE after vehicle infusion, it looked like ORXB did not change SWE (Figure 4.13E) but ORXA increased SWE in control but not L6b silenced animals (Figure 4.8D). However, there was no difference between the genotypes in normalised SWE after ORXA (Genotype, $F_{(1,9)}$=1.168, p=0.3080), neither was the time course of normalised SWE (Genotype x Time, $F_{(23,207)}$=0.3333, p=0.9985).

These results indicate that, although the homeostatic rebound sleep is delayed in L6b silenced mice, homeostatic regulation of sleep after ORXA-induced wakefulness is not changed.

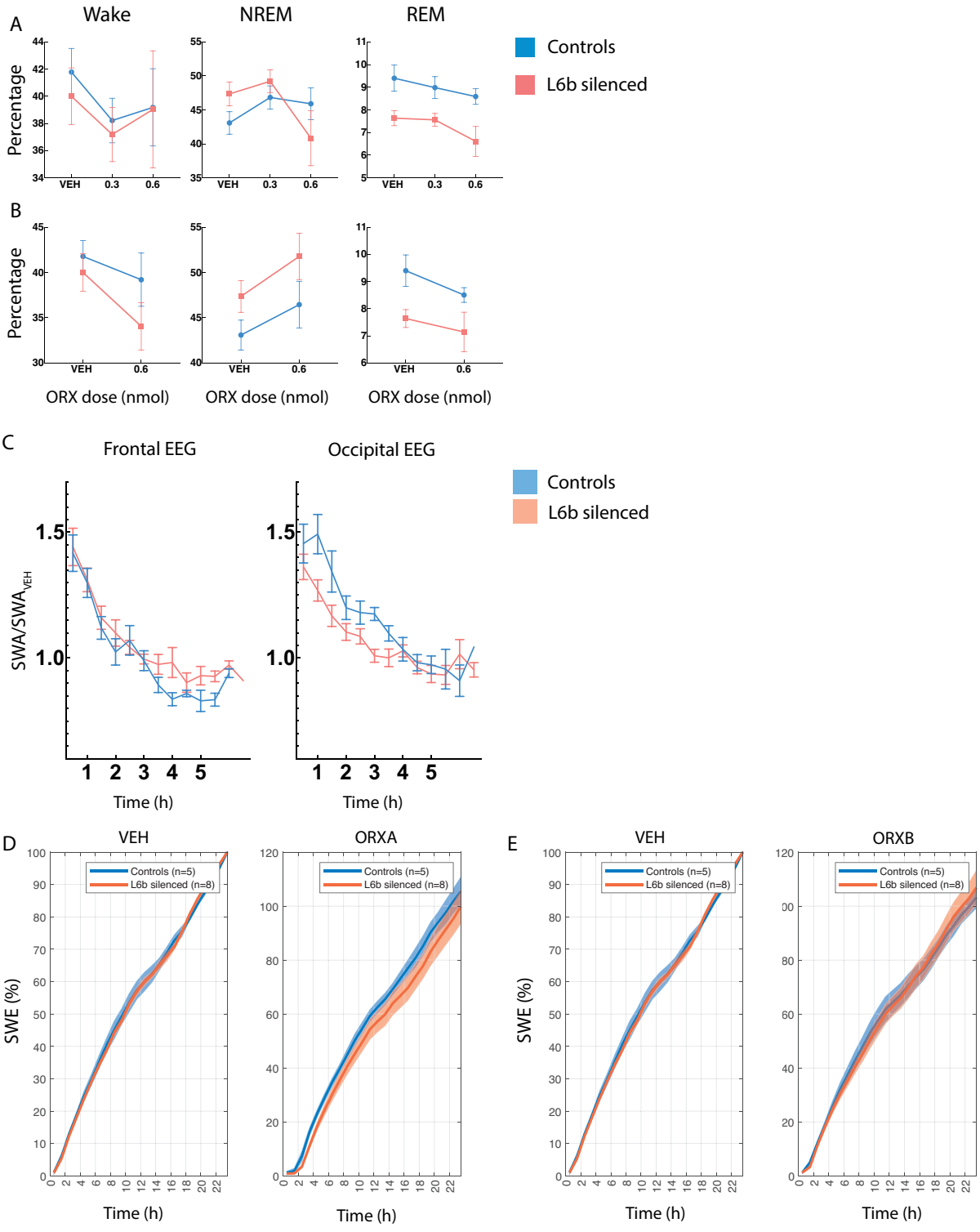

Figure 4.13: Homeostatic regulation of sleep after orexin infusion.
(A) Time spent in wake, NREM and REM after ORXA infusion (dose 0.3 nmol and 0.6 nmol respectively) and vehicle infusion.
(B) Time spent in wake, NREM and REM after ORXB (dose 0.6 nmol) and vehicle infusion.
(C) Slow wave activity rebound during NREM after infusion of ORXA (0.6 nmol) in the frontal EEG and occipital EEG.
(D) Slow wave energy (SWE) after vehicle (left) and ORXA (0.6 nmol) infusion, with SWE on ORXA day normalised to SWE on vehicle day.
(E) SWE after vehicle (left) and ORXB infusion, with SWE on ORXB day normalised to vehicle day.
Controls n=5, L6b silenced n=8.

On inspection of the plots of time course of SWA aligned with hypnograms (Figure 4.3), it appeared like there might be a change in the duration and SWA during the initial NREM episode after prolonged wakefulness following ORX infusion. However, closer analysis of the first NREM episode following ORXA infusion revealed that duration ($t_{(10.82)}$=0.5481, p=0.5947) and SWA (absolute: $t_{(8.673)}$=1.080, p=0.3093), relative to vehicle ($t_{(10.51)}$=0.3370, p=0.7427) were similar between genotypes (Figure 4.14A-C). There were also no genotype differences in duration ($t_{(9.626)}$=1.020, p=0.3327) or SWA (absolute: $t_{(6.682)}$=1.226, p=0.2616, relative to vehicle: $t_{(5.235)}$=1.594, p=0.1693) of the first NREM episode after ORXB infusion (Figure 4.14D-F).

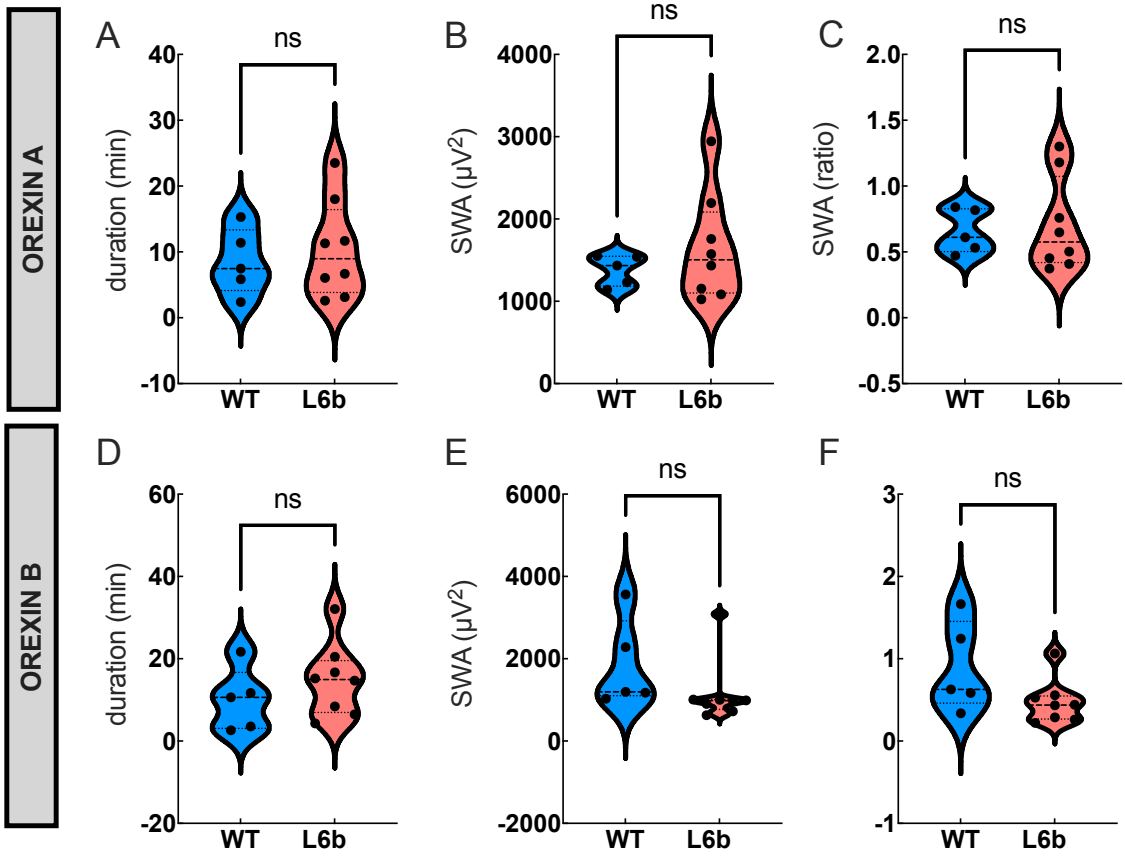

Figure 4.14: Characteristics of the first NREM episode after orexin infusion.
Slow wave activity (SWA) was defined as 0.5-4.0 Hz and calculated for the frontal EEG. Number of animals included: controls n=5 vs L6b silenced n=8.
(A) Duration of the first NREM episode after ORXA infusion. (B) SWA during the first NREM episode after ORX infusion. (C) SWA during the first NREM episode after ORXA infusion relative to SWA in the first NREM episode after VEH infusion. (D) Duration of the first NREM episode after ORXB infusion. (E) SWA during the first NREM episode after ORXB infusion. (F) SWA during the first NREM episode after ORXB infusion relative to SWA during the first NREM episode after VEH infusion.

4.3.4 Food intake

Orexin was initially identified as a promoter of food intake (Sakurai et al., 1998). If the food intake stimulating effect of orexin would be at least partially mediated through cortical L6b, one would expect that silencing L6b would reduce the food intake promoting effect of orexin.

In this exploratory analysis I assessed 24-hour food intake after the infusion of vehicle, ORXA and ORXB, together with Marissa Mueller, a rotation student from the MRC program in Neuroscience. We found that ORXA did not change 24-hour food intake (Treatment, $F_{(1.612,11.29)}$=2.071, p=0.1751) and that there was no genotype difference in the response to ORXA (Treatment x Genotype, $F_{(1.589,3.178)}$=1.769, p=0.7946) (Figure 4.15). Similarly, ORXB did not affect 24-hour food intake (Treatment, $F_{(1,20)}$=1.800, p=0.1948) nor did it elicit a genotype-dependent response (Treatment x Genotype, $F_{(1,20)}$=0.2495, p=0.6229).

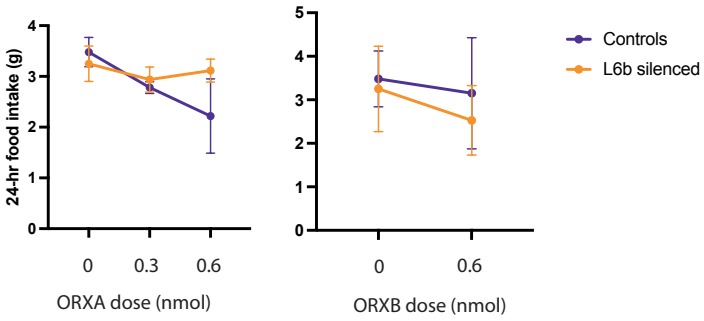

Figure 4.15: Food intake after orexin infusion.
Food intake was tracked by weighing the food pellets on the floor of the cage at the time of infusion and 24 hours later. Food intake was then compared to food intake across baseline days (ORXA/ORXB dose=0 nmol) and no differences were observed.
(left) 24-hour food intake after ORXA infusion.
(right) 24-hour food intake after ORXB infusion.
Controls n=5, L6b silenced n=8.

4.4 Discussion

4.4.1 Summary of findings

In this experiment, I administered ORXA, ORXB, and vehicle ICV to L6b silenced and control mice and recorded EEG/EMG for 24 hours continuously. I found that after ORXA but not ORXB there was an increase in the amount of wakefulness and a decrease of NREM and REM in the first three hours after infusion. The increase in the amount of wakefulness was the result of the occurrence of prolonged wake episodes. Along with the promotion of wake maintenance, the incidence of brief awakenings during subsequent NREM increased and the latter occurred both after ORXA and ORXB infusion. The wakefulness promoting effects were seen in both genotypes, but the wake episode prolonging effect was stronger in L6b silenced compared to control animals.

Normalised spectra for wakefulness immediately following ORXA and ORXB administration were significantly different between genotypes but not at a specific frequency range. ORXB visually had a greater effect on EEG oscillations. After ORXB infusion, both genotypes showed a decrease in theta range (4.5-10 Hz) EEG power and an increase in alpha range (8-12 Hz) EEG power in both derivations. The decrease in theta power was larger in L6b silenced animals; the alpha frequency increase was comparable between genotypes.

In the first three hours of NREM sleep following ORXA and ORXB infusion, there was an increase in frontal EEG power in the 3-30 Hz range in both genotypes, which extended to lower frequencies only in L6b silenced animals. Since low frequency oscillations visually appeared most clearly affected, I compared EEG band power in the delta (1-4 Hz) and theta (4.5-10 Hz) frequency ranges and found no differences between genotypes in either EEG.

REM sleep spectra were not clearly affected by ORXA or ORXB infusion and there were also no differences between genotypes in normalised REM spectra. The only statistically significant difference was a higher theta peak value in L6b silenced animals compared to control animals after ORXB infusion.

SWA dynamics in NREM sleep after ORXA-prolonged wakefulness were comparable between L6b silenced and control animals, with the exception of a lower maximal SWA in L6b silenced animals in the occipital EEG.

Lastly, 24-hour food intake after orexin and vehicle treatment were not significantly different and there was no effect on genotype on this measurement.

4.4.2 Comparison of findings to literature

The finding that ICV administration of ORXA increases the time spent in wakefulness is well-described, and the duration of wakefulness promotion is also in line with previous reports in mice and rats (Mieda et al., 2011; Piper et al., 2000).

The increase in brief arousals after ORXA and ORXB administration suggests a potentiation of sleep-wake transitions. Photostimulation of orexin neurons has been shown to reduce the latency from NREM to wakefulness, which agrees with this sleep-wake transition promoting effect (Adamantidis et al., 2007). Moreover, CAG/orexin mice, in which orexin is constitutively expressed, show fragmentation of NREM sleep, which indicates that the presence of a high orexin tone during NREM sleep disrupts NREM sleep stability (Willie et al., 2011).

Besides this effect on sleep-wake promotion, I found a substantial prolongation of wakefulness episodes, reflecting stimulation of wakefulness maintenance. This is a key effect of orexin that has been demonstrated in several other studies.

First, when the BNST is stimulated chemogenetically, there is prolongation of wakefulness and this effect is blocked by the dual orexin receptor antagonist DORA-22, indicating that orexin is required for sustained wakefulness. In the same study it was demonstrated that optogenetic stimulation of BNST in mice leads to direct sleep-wake transitions and that this effect is not inhibited by DORA-22, which made the authors conclude that orexin is more important in wakefulness maintenance than in sleep-wake transitions (Kodani et al., 2017).

Second, orexin knockout mice and human narcolepsy patients are not able to maintain wakefulness and repeatedly fall asleep, but they can be aroused from external stimuli such as the

sound of an alarm, again supporting a predominant role of orexin in wakefulness maintenance (Sakurai, 2014).

Exogenous ORXA or ORXB infusion caused a decrease in low theta power and an increase in high theta power during wakefulness in L6b silenced animals. This is in line with the finding in orexin knockout mice that orexin promotes a substate of wakefulness that is enriched in theta power (Vassalli and Franken, 2017). However, these findings are not identical, as I did not assess what percentage of time the animals were in a 'theta enriched' state, a state that was defined by specific criteria in the orexin knockout study (Vassalli and Franken, 2017). It is unexpected that ORXA and ORXB caused less spectral changes during wakefulness in control animals than in L6b silenced animals, but this could be due to a statistical power issue rather than a biological effect. There were few genotype differences in the comparison of relative EEG spectra.

Along with the increase in 7-9 Hz in the occipital EEG, L6b silenced animals also showed a decrease in 3-6.5 Hz EEG power in the occipital EEG following ORXA infusion. This is unexpected, since ORXA infusion can be regarded as 'pharmacological sleep deprivation' and elevations in delta and low theta power that are most prominent in the occipital EEG are linked to an increase in sleep pressure during wakefulness and have also been observed during acute and chronic sleep deprivation (Leemburg et al., 2010; Vyazovskiy and Tobler, 2005). Whether there is deficit in the build-up of sleep pressure in this experiment, should be explored in future analysis.

To my knowledge, only one study has reported on the effects of ORXB on sleep-wake regulations. In that study, in rats, it was shown that ORXB increases wakefulness, but besides the species difference, experimental conditions were also different to mine, with a continuous infusion and considerately higher doses for ORXB than for ORXA (Akanmu and Honda, 2005). A variant of ORXB was also examined with a higher affinity for the OX2R and the authors found that this compound increased wakefulness to a similar level as (lower doses of) ORXA (Akanmu and Honda, 2005).

With OX1R, OX2R and dual receptor knockout mice, it has been demonstrated that the sleep-wake regulating effects of orexin are probably mediated by a synergy of the two receptors, with a dominant role for the OX2R (Mieda et al., 2011; Willie et al., 2003). This suggests that ORXA, which can activate both receptors, has the strongest effects on sleep-wake states and this is in line with my findings. In vitro, it has been shown that ORXA or ORXB can both directly activate L6b in multiple cortical areas and because the effects of ORXA and ORXB were comparable in vitro, it was concluded that orexinergic activation of L6b is probably OX2R-mediated (Bayer et al., 2004). I also administered ORXA and ORXB on separate days, and I found that ORXA had stronger wake-promoting effects than ORXB, which is probably mostly mediated through stronger activation of the reticular ascending arousal system by the former (Figure 4.1).

The effects of orexin on sleep homeostasis have been investigated in orexin knockout animals, where it was shown that the absence of orexin reduces the time spent in spontaneous theta-enriched wakefulness and that this is correlated with a reduction in EEG SWA in subsequent NREM sleep (Vassalli and Franken, 2017). Consistent with these findings, I found an increase in high theta power after ORXA during wake, and an increase in delta power during subsequent NREM in L6b silenced but not control animals. However, when I plotted the time course of SWA during NREM sleep (normalised against 24-hour vehicle NREM SWA), I found that NREM SWA in the occipital EEG was higher in control animals. This could be related to the different methods of normalisation.

The absence of an effect of orexin infusion on food intake could be explained by the low time resolution of the current measurement or by a genuine absence of a direct effect of orexin on food intake. With the development of new methods of assessing food intake with a higher temporal accuracy, such questions can be addressed in the future.

4.4.3 Implications for understanding of neuronal circuits

Based on my findings, it seems like ORXA and ORXB both increase the number of brief arousals, which could be regarded as sleep-wake transition attempts, but only ORXA promotes

wakefulness maintenance. Although in physiological situations, these peptides might be released at the same time, making this finding less applicable, it is a novel finding that has not been reported before and could be interesting from a mechanistic point of view.

The main implication of my study is that some of the effects of orexin may be mediated through cortical L6b since there were significant differences in sleep-wake architecture parameters and in spectral power distribution between the two genotype groups, implying that the expression of orexin receptors in L6b is not just a remnant feature of development or evolution but functionally relevant. The finding that cortical L6b silenced animals stay awake longer than control animals is unexpected. Beforehand, I had reasoned that L6b may play a role in orexin-induced wakefulness and that silencing L6b may reduce the wakefulness inducing effects of orexin. However, I observed the opposite effect, which could suggest that there may be a di-synaptic mechanism in play, in which cortical L6b is part of a circuit involving inhibitory interneurons that results in the inhibition of cortical arousal; in this hypothetical model, silencing L6b would lift this inhibitory loop, resulting in stronger or longer cortical arousal.

It is important to consider that silencing through the conditional KO of Snap25 from a selected group of cortical neurons is a chronic process that starts from the time of Cre recombination, that is estimated to start from birth (Hoerder-Suabedissen et al., 2018). The subsequent development of intracortical and cortico-thalamic circuits is altered in these chronically silenced animals (see Vadisiute, Meijer et al., 2023). There are changes in synaptic and myelin maintenance, distribution if microglia, astrocytes, and even GABAergic interneurons. The responsiveness of such altered circuits could change, and they should not simply be considered as an acutely silenced system that otherwise indistinguishable from WT animals.

4.4.4 Clinical implications

Modulation of the orexin system has been an area of interest for clinical application from the moment the neuropeptide was identified, illustrated by the author list of one of the two foundational papers – the second half of the list is affiliated with a pharmaceutical company

(Sakurai et al., 1998). The major clinical targets for intervening with the orexin system are narcolepsy, by orexin agonism, and insomnia, by orexin antagonism. The administration of orexin agonists has proved challenging, with only one trial with an OX2R agonist, TAK-925, showing efficacy in human narcolepsy patients (Evans et al., 2023), and a recent phase II clinical trial that reported improvement of narcolepsy symptoms but also hepatotoxicity (Dauvilliers et al., 2023). More advances have been made in the development of orexin antagonists for insomnia, and three dual orexin receptor antagonists (DORAs) have been approved by the FDA, suvorexant, Lemborexant and daridorexant (Herring et al., 2019; Park et al., 2023).

Other clinical focuses for intervention in the orexin system are neuropsychiatric disorders, such as schizophrenia, depression, anxiety, addiction, eating disorders and neurodegenerative disorders (Ten-Blanco et al., 2023). For multiple psychiatric disorders, one of the symptoms is sleep-wake disruption, and other symptoms can be evoked or exacerbated by certain sleep-wake behaviours. In this respect, the link between L6b and orexin is potentially interesting, since for multiple neuropsychiatric disorders, abnormalities in interstitial white matter cells in human (the equivalent cells of L6b in mouse) have been described, such as in autism (Bailey et al., 1998) and schizophrenia (Akbarian et al., 1996; Eastwood and Harrison, 2003; Kirkpatrick et al., 2003).

The finding that high orexin levels have a particularly strong wake-promoting effect in L6b silenced animals could indicate that abnormalities in L6b might make individuals especially sensitive to orexin tone. In this speculative model, when a threat has disappeared, but orexin is still present, L6b might counteract this and signal that no vigilance is needed anymore. Patients with sleeping problems such as insomnia and L6b abnormalities would in this speculation especially benefit from orexin-targeting treatments.

4.4.5 Limitations

The difference in orexin responsivity between L6b silenced and control animals could be explained by the difference in genotypes, but there are potential confounders. First, the control

group was smaller, due to breeding issues, which limits statistical power of this study (n=5, and in some analysis animals had to excluded vs n=8 L6b silenced animals). Second, I do not have pre-infusion EEG spectra for all animals, which makes it impossible to validate whether sleep-wake history is comparable between the groups in all conditions. The mostly consistent findings with the two doses of ORXA, which were administered at different treatment days, are reassuring.

I found fewer wake-promoting effects of ORXB than of ORXA. This is probably physiological but there are other possible explanations. First, ORXA has two intramolecular stabilizing disulphide bonds which ORXB does not have, making ORXB less stable (Sakurai 1998), so theoretically, ORXB could have been denatured in my experiment. A positive control was the use of the same preparation for in vitro experiments by Dr Rajeev Therpurakal (Molnár and Mann Laboratories) who found clear effects of orexin B bath application. Albeit this indicates that the solution contained orexin B, it does not include denaturing of the protein within the infusion system that I used. Moreover, I used a solution of 0.3 nmol/µl for both ORXA and ORXB, based on the solubility limits, infusion volume limits and previous studies. This was an effective dosage for ORXA but might have been insufficient for ORXB, especially since the only study that reported ORXB effects on wakefulness used higher doses for ORXB (Akanmu and Honda, 2005). Moreover, the time frame was selected based on visible ORXA effects on the distribution of time spent in different vigilance states, which might not be optimal for ORXB effects.

In general, the doses, localization and timing of orexin administration used in this study are not physiological and therefore, the neuropharmacology might be different from endogenous orexin effects. In my study, orexin levels were high during the light phase, whereas normally, orexin neurons are active during wake, especially active wake, less active during NREM and inactive during tonic REM (Lee et al., 2005; Mileykovskiy et al., 2005). High orexin levels that peak at the beginning of the inactive phase are therefore an unnatural situation.

Another strategy to investigate orexin effects on L6b could be to administer an orexin receptor antagonist. Based on the higher expression of OX2R in L6, administration of an OX2R selective antagonist would be logical, and could shed light on the role of OX2R signalling in L6b

for mediating the effects of endogenous orexin. This was my initial plan for this experiment, but due to the low pH of the solution of the compound than I had selected, YNT-185, I was not able to use this substance in vivo (Irukayama-Tomobe et al., 2017).

Patch-clamp recordings by Dr Rajeev Therpurakal confirmed that Drd1a cells in L6b are activated by orexin. Ideally, experiments would be repeated in the presence of tetrodotoxin (TTX) to confirm monosynaptic activation of Drd1a-Cre L6b neurons by orexin. Moreover, in Dr Therpurakal's experiments, fluorescent (tdTom+) L6b cells have been compared to non-fluorescent L6b cells in prefrontal cortex and eventually, it would be important to also record neurons in other cortical layers, especially those that express orexin receptors, and repeat recordings in other brain areas, as effects may strongly vary with specific cell types and with area.

Lastly, the analysis of food intake was preliminary, and other studies that measure food intake after orexin infusion use a higher temporal resolution. In this study, this was however not possible since animals needed to be undisturbed for 24-hour EEG/EMG recordings. While recording 24-hour food intake, Marissa Mueller started working on a device to track food intake automatically at high temporal resolution. This novel method is under development and a promising tool for future studies (Mueller et al., 2022).

4.5 Conclusion

In this experiment, I investigated the in vivo effects of orexin on L6b, by administering ORXA and ORXB to L6b silenced and control animals. I found that the wake episode prolonging effects of ORXA are stronger in L6b silenced than in control animals. Moreover, ORXA and ORXB had different effects on spectral EEG power density in the two genotypes. The differential effects in L6b silenced and control animals suggest that chronic silencing of L6b affects orexin responsivity.

5 Auditory perception in 'layer 6b silenced' mice

5.1 Introduction

Transitions between brain states mark alterations in perceptiveness to internal and external stimuli (McGinley et al., 2015). At the same time, internal and external stimuli can cause transitions from one brain state to another. Stimuli that cause brain state transitions tend to be those that indicate change, since changes in the environment can signify danger. The perception of change is governed by an interplay between sensory cortical areas of the modality in play and the prefrontal cortex, which is a key change detector (Bastos et al., 2012; Casado-Román et al., 2020; Keller and Mrsic-Flogel, 2018). In section 1.3.7, I outlined the thalamocortical networks that may play a role in deviance detection. In the current chapter, I describe my investigation of deviance detection in "L6b silenced" mice (Drd1a-Cre:Snap25$^{fl/fl}$) with an auditory oddball paradigm. I will first give an overview of how auditory perception is measured, what the key concepts of auditory oddball paradigms are, and how change is thought to be detected by the brain. I conclude this introduction with the hypothesis that I tested with this experiment.

5.1.1 Auditory evoked potential

An evoked response or event-related potential (ERP) is a potential recorded from a specific part of the brain following and time-locked with the presentation of a stimulus. When the stimulus is a sound, the potential is also called an auditory evoked potential (AEP).

The shape of the AEP can be described based on activity in neural populations along the auditory pathway. The auditory pathway starts at the cochlea and via the cochlear nerve, cochlear nucleus, superior olivary nucleus, lateral lemniscus, inferior colliculus, and medial geniculate

body, reaches the auditory cortex (Figure 5.1A). The functioning of the first components of the pathway can be measured as a potential recorded with electrodes behind the ear, the auditory brainstem response (ABR) ≤10ms after stimulus presentation (Figure 5.1B). Processing ≥10 ms, which represents signalling from the level of the auditory thalamus onwards, is assessed by extracting AEPs from EEG or LFP signals. Both techniques are used clinically to assess hearing function, and in research settings to investigate network connectivity (Modi and Sahin, 2017).

The shape of the AEP is dependent on subject characteristics such as genetic background and network variations, and experiment characteristics, such as recording electrode configuration, but some general components can be identified and used for quantifying responses (Bickel et al., 2008; Ehlers and Somes, 2002; Siegel et al., 2003). I describe peaks and time ranges in rodents; in humans, latencies are longer because of the larger size of the brain and amplitudes are usually smaller because of the use of scalp electrodes.

When recording EEG with an electrode placed above the fronto-temporal cortex, a first peak occurs 20-30 ms after stimulus onset in rodents. It arises from activity in the auditory thalamus and temporal cortex, and because it is usually a positive deflection, it is referred to as P1. The next peak follows between 30-50ms and is negative in common recording configurations and therefore indicated as N1. The N1 reflects activity in primary and secondary auditory cortex. The following peak, P2, is thought to originate from activity in association cortices, and occurs between 50-125 ms. A fourth peak has been identified around 125-225ms in rodents and around 300ms in humans; in humans it is commonly referred to as P300 or P3, in rodents as P3. This last peak is associated with processing in the frontal and parietal cortex and has been linked with higher order cognitive functions and is consistent across different modalities (Bickel et al., 2008; Modi and Sahin, 2017; Siegel et al., 2003; Umbricht et al., 2004).

AEPs can be recorded from primary auditory cortex during wakefulness, but also during sleep, anaesthesia, and comatose states, indicating that sound still reaches the primary auditory cortex despite the sensory disconnection that occurs during these states (Nir et al., 2015). Single-unit responses recorded from primary auditory cortex are similar in magnitude across vigilance

state, but the magnitude of AEPs varies with vigilance state, with larger amplitude AEPs elicited during NREM sleep compared to those elicited during wakefulness or REM sleep (Colrain and Campbell, 2007; Hall and Borbely, 1970; Nir et al., 2015; Velluti, 1997). The difference between single unit responses and evoked potentials has been suggested to arise from the difference in recording techniques, and the evoked potentials reflecting the recruitment of a larger population of neurons to respond to the stimulus during sleep (Nir et al., 2015).

A

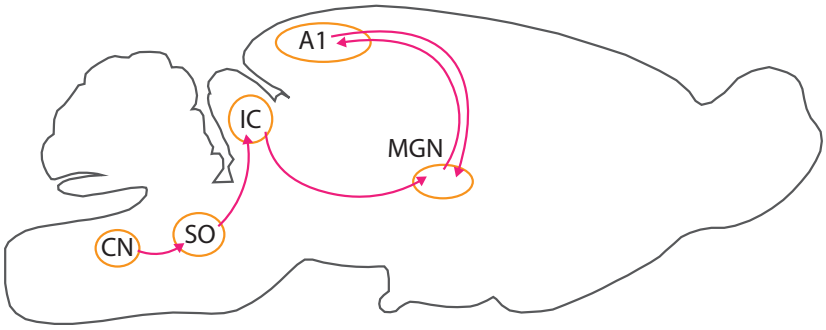

B

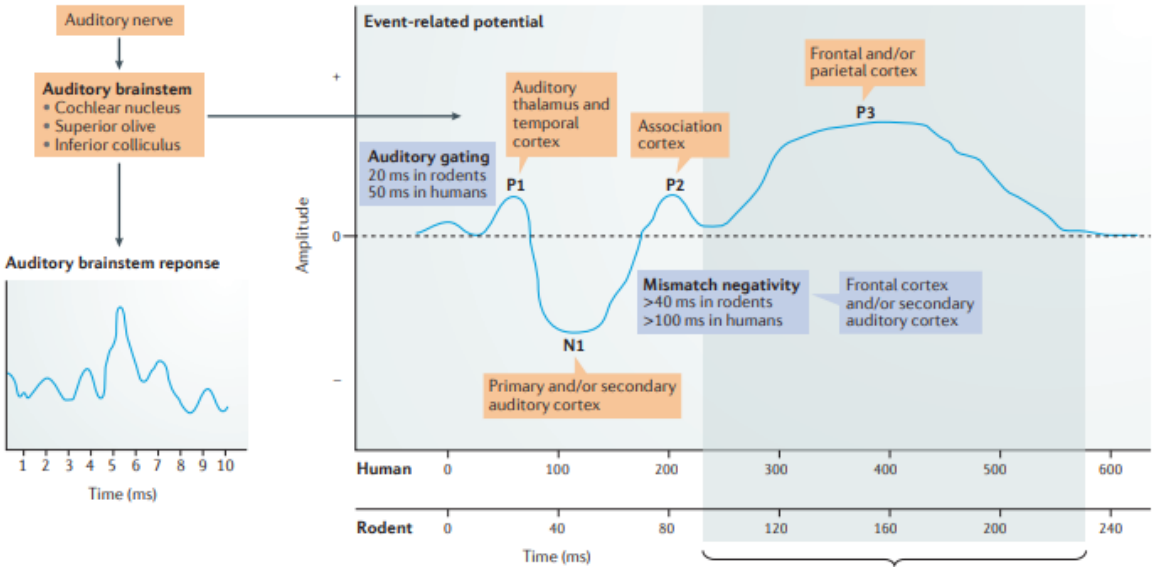

Figure 5.1 Auditory perception in the mouse.
(A) Ascending auditory system in the moue, schematically. Sound arrives at the cochlea and is converted into an electrical signal by hair cells, from where it is transmitted via spiral ganglion neurons in the cochlear nucleus (CN), to the superior olivary nucleus (SO) and inferior colliculus (IC). From there, the signal reaches the medial geniculate nucleus (MGN) and is transmitted to the primary auditor cortex (A1).
(B) Auditory evoked potential. After presentation of an auditory stimulus, a peak appears that can be recorded from the auditory brainstem as the auditory brainstem response in first 10ms after stimulus presentation. On a more prolonged time scale, signal progression through the auditory pathway can be recorded as field potentials, the event-related potential that is similarly time locked with the stimulus. Characteristic peaks correspond with activity in distinct brain area. The P1 and N1 peaks are related to auditory gating. Note the different time scales in humans and rodents indicated as different latencies below the x axis. The y axis is not quantitative since peak amplitudes vary with recording area and technique. Usually, human studies are performed with scalp electrodes and mice studies with implanted epidural electrodes, and therefore, amplitudes in mouse studies tend to be larger. From Modi & Sahin 2017.

5.1.2 The auditory mismatch response

Several mechanisms in the auditory pathway provide context to novel sounds and are responsible for setting the auditory scene. These processes can be investigated with an oddball paradigm, in which a sequence of frequently occurring standard tones is interrupted by an infrequently occurring deviant tone (Näätänen et al., 1978). This results in the generation of a mismatch response upon hearing the deviant tone, that can be observed as changes in amplitude in the AEP and changes in neuronal spiking rates (Näätänen et al., 1978, 2007).

When field potential responses to standards are subtracted from responses to deviants, the resultant difference wave shows a negative deflection starting around 50ms and reaching a peak between 100-300ms or even longer in mice, the mismatch negativity (MMN) (Fitzgerald and Todd, 2020; Garrido et al., 2009a; Näätänen et al., 1978, 2007). The terms mismatch response and MMN are often used interchangeably but some have reserved mismatch response for animal experiments, where polarities and latencies are different, and which can show different dynamics (Harms et al., 2016; O'Reilly and Conway, 2021).

A mismatch responses can be elicited by a deviant of a different frequency, duration, intensity, or direction but also by deviants that show changes in more complex features of sounds, such as variations in speech (Dehaene-Lambertz, 1997; Näätänen et al., 1978) and abstract rules like grammar and tonal order (Tervaniemi et al., 1994).

The size of the mismatch response depends on stimulus characteristics such as the probability of standards and deviants in the sequence, the interstimulus interval, and the degree of difference between standards and deviants but also on subject characteristics such as hearing function, directed attention, and neural network connectivity (Kurkela et al., 2018; Näätänen et al., 2007). The latter is employed in preclinical and clinical research, where changes in MMN are used as a biomarker for network connectivity (Featherstone et al., 2018).

Oddball experiments are often performed during wakefulness, but an MMN can be recorded during sleep (Nashida et al., 2000), anaesthesia (Koelsch et al., 2006), and comatose states (Fischer et al., 1999; Morlet and Fischer, 2014; Rodriguez et al., 2014). Although the later

components of the MMN are changed during sleep (Strauss et al., 2015), the early components are preserved and comparable across vigilance states (Nir et al., 2015; Strauss et al., 2015).

5.1.3 Neurobiology of the mismatch response

The detection of change in a mismatch response is the result of suppression of repeated standard stimuli on the one hand, and model adjustment on the other hand. The latter is also referred to as 'genuine deviance detection' (Casado-Román et al., 2020).

At the level of single neurons, the high probability of standard tones leads to adaptation specific to the standard tones, stimulus-specific adaptation (SSA) (Jääskeläinen et al., 2004; May and Tiitinen, 2010; Ulanovsky et al., 2003). SSA has been recorded at different levels along the auditory pathway, starting from the level of inferior colliculus ranging to the auditory cortex, and the higher up in the hierarchy the more complex the patterns of adaptation (Duque and Malmierca, 2015; Pérez-González and Malmierca, 2014).

At a more global level, the responses to standard tones are also diminished in the process of repetition suppression (RS), which differs from SSA in that it is less specific to the exact properties of the stimulus and instead more general to the associated meaning of sounds. RS is a component of the predictive processing framework, which is a model that explains how the brain matches incoming perceptual information with existing models in the brain (Auksztulewicz and Friston, 2016; Garrido et al., 2009a). As described in Chapter 1, section 1.3.8, predictive processing is a hierarchical process in which ascending incoming sensory information is tested against descending prediction models to allow efficient change detection in the sensory environment. When the descending predicted signal is similar to incoming information, the response is suppressed, in the process of RS. When the two information streams are different, however, an ascending prediction error signal is generated (Auksztulewicz and Friston, 2016; Garrido et al., 2009a).

The MMN can be localized to two generators: one bilaterally in the posterior auditory field (Parras et al., 2021) linked to pre-attentive processing, and one in the frontal and prefrontal

cortex, predominantly in the right hemisphere, linked to attention switching (Casado-Román et al., 2020; Näätänen and Michie, 1979; Näätänen et al., 1978, 2007). According to the adaptation hypothesis of MMN, MMN is exclusively explained by SSA (Jääskeläinen et al., 2004; May and Tiitinen, 2010; Ulanovsky et al., 2003), and according to the memory hypothesis, the MMN is formed entirely from model adjustment (Näätänen et al., 1978, 2007). Predictive coding frameworks suggest that both mechanisms co-exist (Fitzgerald and Todd, 2020).

5.1.4 Practical considerations for auditory oddball paradigms

The auditory system responds differently to tones with different properties, e.g., loud tones, long tones and tones in a species-specific relevant frequency range are more strongly perceived. Therefore, when standards and deviants with different physical properties are presented to elicit a deviance response, part of the MMN will result from differences in physical properties of the stimuli rather than adaptation or model adjustment (Näätänen et al., 2007; O'Reilly and Conway, 2021). Although some have suggested that physical properties of the sound account for the entire mismatch response in mice (O'Reilly and Conway, 2021), many others report similarities between the murine mismatch response and the human MMN, and that with adequate controls the mismatch response can be regarded as the murine analogue of the human MMN (Casado-Román et al., 2020; Kurkela et al., 2018; Parras et al., 2021). Moreover, both physical responsiveness and SSA mostly affect the N1 time range which suggests that differences detected in later time ranges could be a good indicator of the mismatch response (Kurkela et al., 2018; Näätänen et al., 2007).

A common control paradigm is the use of two stimulation blocks, where the standard and deviant condition are reversed, the 'flip-flop model'. When an effect occurs in both conditions, it is likely to be caused by MMN, but when it is only seen in one direction, it is more plausible that physical properties of the stimuli cause changes in responses (Harms et al., 2014) (Figure 5.2B,D).

Whereas the flip-flop control is effective to verify the validity of the mismatch response, it does not give information on the contribution of component mechanisms. A non-repetition

control was introduced, the 'many standards' control paradigm, in which different standard tones are played, each with the same probability as the deviant tone in the oddball paradigm (Figure 5.2). One of the standard tones in the control paradigm has the same properties of the deviant tone in the oddball paradigm and therefore, the deviant in the oddball paradigm can be compared with a physically identical tone with the same probability, with the only difference that it is not a deviant (Schröger and Wolff, 1996).

A further refinement was presented, the 'cascade' control paradigm. This is also a non-repetitive sequence of control tones with the same probability as the deviant tone, but instead of in a random order it is played in an ascending or descending cascade (Figure 5.2). Thus, the context immediately preceding the tone is comparable in the oddball and the control paradigm, with the only difference between the cascade control paradigm and the oddball paradigm that the tone in the oddball paradigm is deviant and in the cascade control paradigm is part of a regular sequence (Ruhnau et al., 2012).

5.1.5 Hypothesis

In this experiment, I performed an auditory oddball paradigm in L6b silenced and control animals (Drd1a-Cre$^{+/?}$;Snap25$^{fl/fl}$ and Drd1a-Cre$^{-/-}$:Snap25$^{fl/fl}$). Since L6b is one of the infragranular layers and is well connected both to supragranular layers and to thalamus (Hoerder-Suabedissen et al., 2018), L6b could be involved in the generation of a deviance response (Chapter 1). Only sparse Drd1a-Cre positive cells in L6b of the auditory cortex are part of the primary ascending pathway, so it may be more likely that L6b is involved in prediction error signalling and repetition suppression than in SSA. Within the framework of prediction coding, the excitatory Drd1a-Cre neurons that lack the ability to communicate with other neurons through regulated synaptic vesicle release in the L6b silenced mouse are more likely to code predictions than prediction errors. If L6b is involved in the generation of a mismatch response, I would expect that L6b silenced animals show a reduced mismatch response to deviant tones.

5.2 Methods

5.2.1 Animals and surgeries

For this experiment, the same 15 male animals were recorded as for general sleep phenotyping (wildtype (n=7), age 11±0.48 weeks, body weight 23±0.67 g; L6b silenced (n=9), age 11±0.39 weeks, body weight 21±0.47 g); at this age, the early age related hearing loss that is seen in C57BL6 animals has begun but is still limited (Ison and Allen, 2003). After sleep phenotyping, animals were given at least 2 days recovery prior to starting the auditory stimulation experiment. EEG/EMG derivations were the same as for baseline sleep phenotyping, with frontal and occipital EEGs referenced to the cerebellum, and EMGs in the neck muscles.

5.2.2 Electrophysiological recording setup

Electrophysiological recording took place as described in Chapter 2, with the exception that signals were recorded at a sampling rate of 1017.3 Hz to allow higher resolution of evoked potentials. Signals were filtered online with an anti-aliasing filter at 45% of the sampling rate.

5.2.3 Free-field auditory stimulation setup

Auditory sequences were programmed in the Ultrasonic stimulation gizmo in the Synapse software and produced with the RZ2 processor also used for electrophysiological recording (Tucker-Davis Technologies Inc, Alachua, FL, USA (Figure 5.2). The digital-to-analogue converter port from the RZ2 was connected via an amplifier (LP-2024A+, Lepai, China) with rodent-optimized speakers (MF1, Tucker-Davis Technologies) attached to the ceiling of each recording chamber. The setup was calibrated between 75-90 dB with a microphone (Nor140, Norsonic, Tranby, Norway) and to further ensure comparable acoustic conditions for both genotype, genotypes were counterbalanced per recording chamber, with the exception of one obligatory L6b silenced-only chamber due to the imbalance between the groups (Chapter 3). Animals could move freely during the experiment.

5.2.4 Auditory stimulation paradigm

The oddball paradigm consisted of 1000 tones in total, containing 900 standards (p=0.9) and 100 deviants (p=0.1). The sequence was pseudorandom, modified such that there were at least 3 standard tones between consecutive deviant tones. There was an ascending oddball paradigm (f_{STD}=7.99 kHz, f_{DEV}=11.3 kHz), and a descending oddball paradigm (f_{STD}=11.3 kHz, f_{DEV}=7.99 kHz)(Figure 5.2B,D). All tones were 75ms duration pure tones, with an on/off ramp of 5ms. The interval between consecutive onsets was 1000ms. The amplitude of the generated waveform was kept constant throughout the experiment. Each stimulation block lasted about 13 minutes (1000 seconds). To investigate the attribution of deviance detection and stimulus specific adaptation, respectively, a nonrepetitive control block was added after each oddball paradigm (Figure 5.2C,E). A control block consisted of a sequence of 10 logarithmically spaced tones (1.00-22.59 kHz) in either ascending or descending order, including the frequency pair of the oddball paradigm. Each tone in the control block was played 100 times (p=0.10). In this way, responses to the deviant tone in the oddball paradigm and the tone of the same frequency in the cascade control paradigm can be compared, as a proxy of deviance detection through prediction error signalling (Ruhnau et al., 2012).

5.2.5 Experimental procedure

The chambers were briefly opened just before lights off (9PM) for a quick health and cable check. Next, the chambers were closed, and the animals were left undisturbed during stimulation. Just after 9PM, the first stimulation block was started. Each block lasted 13 minutes and was followed by 10 minutes rest before the next stimulation block. There were 4 stimulation blocks per session (oddball ascending, cascade ascending, oddball descending, cascade descending) and each animal experienced one session. The aim was for the animals to be awake during stimulation, to reduce the influence of vigilance state on AEP amplitudes (Hall and Borbely, 1970; Nir et al., 2015). This was more successful in the second cohort of animals, as nests were removed, and a novel object was introduced to the cage (a piece of tissue paper) to keep the animals awake (Figure 5.4).

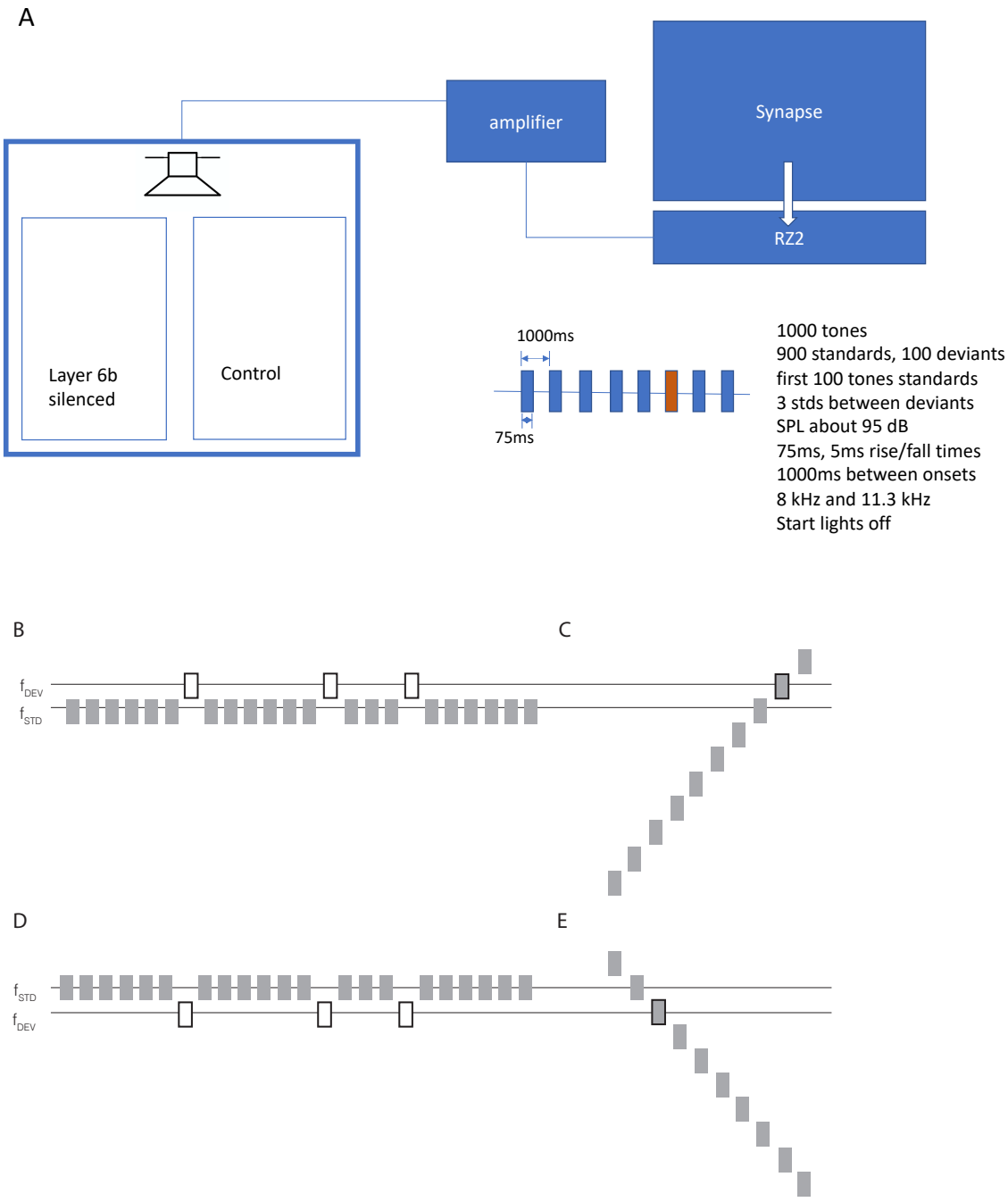

Figure 5.2 Free-field auditory stimulation setup.
(A) Stimulation setup. Tones were programmed in Synapse (TDT) and produced by the RZ2 processor, sent to an amplifier, and played through speakers attached to the ceiling of each recording chamber. Each recording chamber housed a wildtype and a L6b silenced animal. Tone characteristics are shown in the figure.
(B) In the ascending oddball paradigm, the deviant tone had a higher frequency (f=11.3 kHz) than the standard tone (f=7.99 kHz).
(C) In the ascending cascade control paradigm, 10 tones formed a regular sequence, including the oddball pair.
(D) In the descending oddball paradigm, the deviant tone had a lower frequency (f=7.99 kHz) than the standard tone (f=11.3 kHz).
(E). In the descending cascade control paradigm, 10 tones formed a regular sequence, including the oddball pair.

5.2.6 Data analysis

Locally stored data tanks from Synapse were loaded into Matlab (The MathWorks Inc, Natick, MA, USA, v R2021a) and the stimulation timepoints were extracted from the stimulation channel, as well as continuous EEG and EMG data from the signal channels. EEG and EMG event epoch analyses are described separately below. In parallel, EDFs were generated, and vigilance states were manually blinded annotated in 4s-epochs in SleepSign (Kissei Comtec Co., Ltd., Nagano, Japan) as described in Chapter 2.

For EEG analysis, event epochs of raw signals were extracted from 0.2 second before tone onset until 0.5 second after tone onset, and 0.2 second pre-stimulus baseline subtraction was applied. Then, grand average responses to all tones across all vigilance states were calculated and plotted for individual animals. Based on this plot, peak windows were determined. I focused on the frontal EEG derivation because the mismatch response is thought to be mostly frontally located (Casado-Román et al., 2020; Näätänen et al., 2007) and because the peaks of the evoked potentials were more consistently identifiable in the frontal EEG in my recordings.

Next, event epochs of tones that were not played during artefact-free wakefulness were excluded, to avoid vigilance state specific changes in ERP amplitudes (Nir et al., 2015). Event epochs were then categorised as standards or deviants for the oddball paradigm, or subsets of standards for the adaptation analyses. A grand average waveform per condition within each paradigm was calculated and plotted for individual animals. Peak amplitudes and latencies were identified within this waveform by finding the minimum and maximum values in the pre-determined peak windows with the predetermined polarities. The waveform was plotted for individual animals including the automatically identified peaks and the quality of signals and peak detection was assessed by visual inspection and when either was deemed insufficient for either of the conditions compared, the animal was excluded from the analysis (Figure 5.3). Excluded animals are listed in Table 5.1 and the number of animals contributing to each analysis is reported with the respective results.

For analysis of adaptation, only 20 tones were included per condition, and some of these had to be excluded because they were not played during wakefulness, and therefore averaged AEPs were less obvious for individual animals and peak detection did not seem reliable for most animals, which made statistical testing not possible. Therefore, after excluding one wildtype animal because of strong electrical noise and one L6b silenced animal because of a large drift, group averages were plotted, and some patterns occurred.

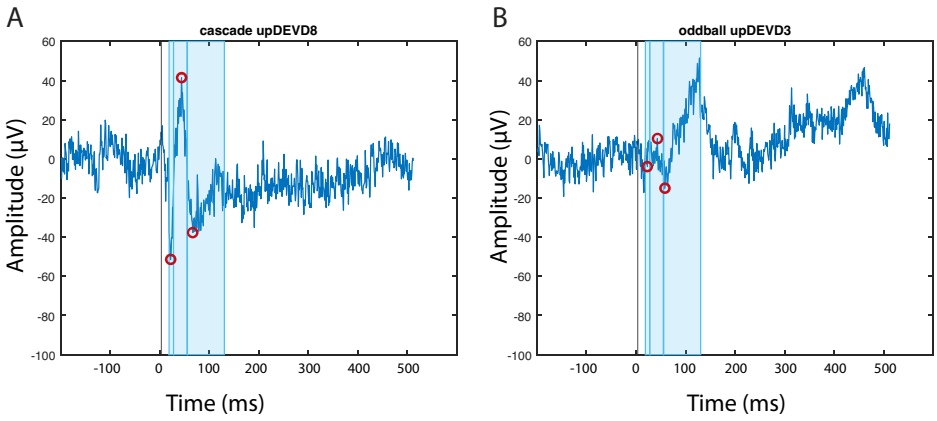

Figure 5.3 Example EEG traces with peak detection. (A) and (B) are examples of frontal EEG responses with detection of P1, N1 and P2 peaks marked with red open circles. Peak detection windows are shown in light blue. (A) An example of a grand average waveform and peak detection that was assessed as good quality and (B) an example of a waveform that was judged as insufficient quality because there were no obvious peaks visible. The animal in (B) was therefore excluded from analysis.

Table 5.1: Excluded animals

	Excluded WT	Excluded L6b silenced	WT included	L6b silenced included
Ascending paradigms				
Frontal EEG	D4	D3	n=6	n=8
Descending paradigm				
Frontal EEG	C2	C5, D3	n=6	n=7

The names of the animals that were excluded are shown per animal, and the number of animals that was included per genotype is also shown. Ascending refers to both the ascending oddball paradigm (**$f_{deviant} > f_{standard}$**), and the ascending control sequence and descending to both the descending oddball paradigm $f_{deviant} < f_{standard}$) and the descending cascade. For the ascending paradigms, only n=2 L6b silenced animals could be included for EMG analysis.

For comparison of EEG peak amplitudes, peak-to-peak amplitudes were calculated, i.e., P1-N1 and N1-P2, to limit the effects of deviations from the baseline. For the oddball paradigm, a (deviant – standard) difference wave was calculated.

In the EMG signal, the acoustic startle reflex was examined. This reflex can be observed in response to suprathreshold stimuli within 5-12 milliseconds after stimulus onset, and its magnitude varies with stimulus properties and subject characteristics(Fendt and Koch, 2013; Pantoni et al., 2020). In mouse models of neuropsychiatric diseases, the acoustic startle response is often altered, and therefore it is frequently used in preclinical research and drug development settings (Fendt and Koch, 2013).

For EMG analysis, the raw data from the EMG channel was resampled to 256 Hz and filtered between 3-100 Hz. Next, event epochs were extracted 0.2 seconds before tone onset until 0.5 seconds after tone onset. Event epochs were categorized into standards and deviants for the oddball paradigm, or subcategories of standards for the adaptation analyses, and event epochs around tones that were not played during artefact-free wakefulness were excluded. The root mean square (RMS) was calculated across all event epochs for a condition (standard, deviant, control) for individual animals, and normalised to the average signal in the 0.5 seconds before stimulus onset, to facilitate the distinction between background muscle activity and responses to tones. For the acoustic startle reflex, a time window of 0-12 ms after tone onset was examined, which was based on literature on the acoustic startle reflex (Pantoni et al., 2020). The resulting normalised acoustic startle reflexes of individual animals were evaluated by visual inspection but of insufficient quality for quantification. Therefore, they were compared visually.

5.2.7 Statistics

Responses to deviant tones were compared to responses to standard or control tones. If the response to either condition was excluded for an individual animal, the animal was excluded from both conditions of the analysis. Peak-to-peak amplitudes and peak latencies were compared with a two-way ANOVA with genotype (wildtype vs L6b silenced) and condition (standard or control

vs deviant) as independent variables. For posthoc comparisons, comparisons within each factor were tested separately and no correction was applied. For significance testing of the difference wave calculated in the oddball paradigm, multiple two-tailed t tests were performed for all time points for the difference wave at the original sampling rate (1017.3 Hz) for comparison to zero. All statistical analyses were conducted in GraphPad Prism (version 10.0. 2 for MacOS; GraphPad Software, San Diego, CA, USA) except for statistical testing of the difference waves which was done in Matlab.

5.3 Results

The experiment started at lights off, with the aim of performing the experiment when animals were awake. When I started the experiment with the first cohort of animals, I verified whether animals were still awake at the end of the first stimulation block and noticed that some animals had fallen asleep, which I had not expected because of the intensity of the sounds. To ensure that the animals were all awake during the rest of the experiment, I removed the bedding and introduced a novel object (a piece of tissue paper) during the 10-minute break at the end of the first stimulation block in this first cohort of animals. In the second cohort of animals, I followed this 'sleep deprivation' procedure from the start, which successfully kept the animals awake as can be seen from the hypnograms plotted for the hours during which the auditory stimulation experiment was performed (Figure 5.4).

After sleep scoring, I aligned the tones with the vigilance state assignment, and excluded the event epochs corresponding to tones that were not played during artefact-free wakefulness. The number of tones played during wakefulness is summarized for each paradigm in each animal in Table 5.2. For excluded animals, the number of event epochs during wake around standard and deviant tones is reported in Table 5.1.

	Oddball up	Casc up	Oddball down	Cascade down		Oddball up	Casc up	Oddball down	Cascade down
C1	572	60	0	0	D1	48	12	28	72
C2	68	412	312	156	D2	136	156	44	192
C3	916	56	156	0	D3	88	8	0	24
C4	4	12	8	4	D4	0	0	60	4
C5	8	8	0	0	D5	40	8	0	0
C6	4	0	0	0	D6	0	56	20	4
C7	108	180	88	0	D7	0	0	0	336
C8	612	0	36	0	D8	4	48	0	4

Table 5.2: Excluded tones. For each animal (C1-C8 for first cohort and D1-D8 for second cohort), the number of tones that is not played during an epoch of artefact-free wakefulness is indicated. Note that during the first stimulation block ('Oddball up'), many tones had to be excluded (see also top panel in Figure 5.1) for the C cohort. In the D cohort, animals were kept awake from the start, which successfully reduced the number of tones that had to be excluded.

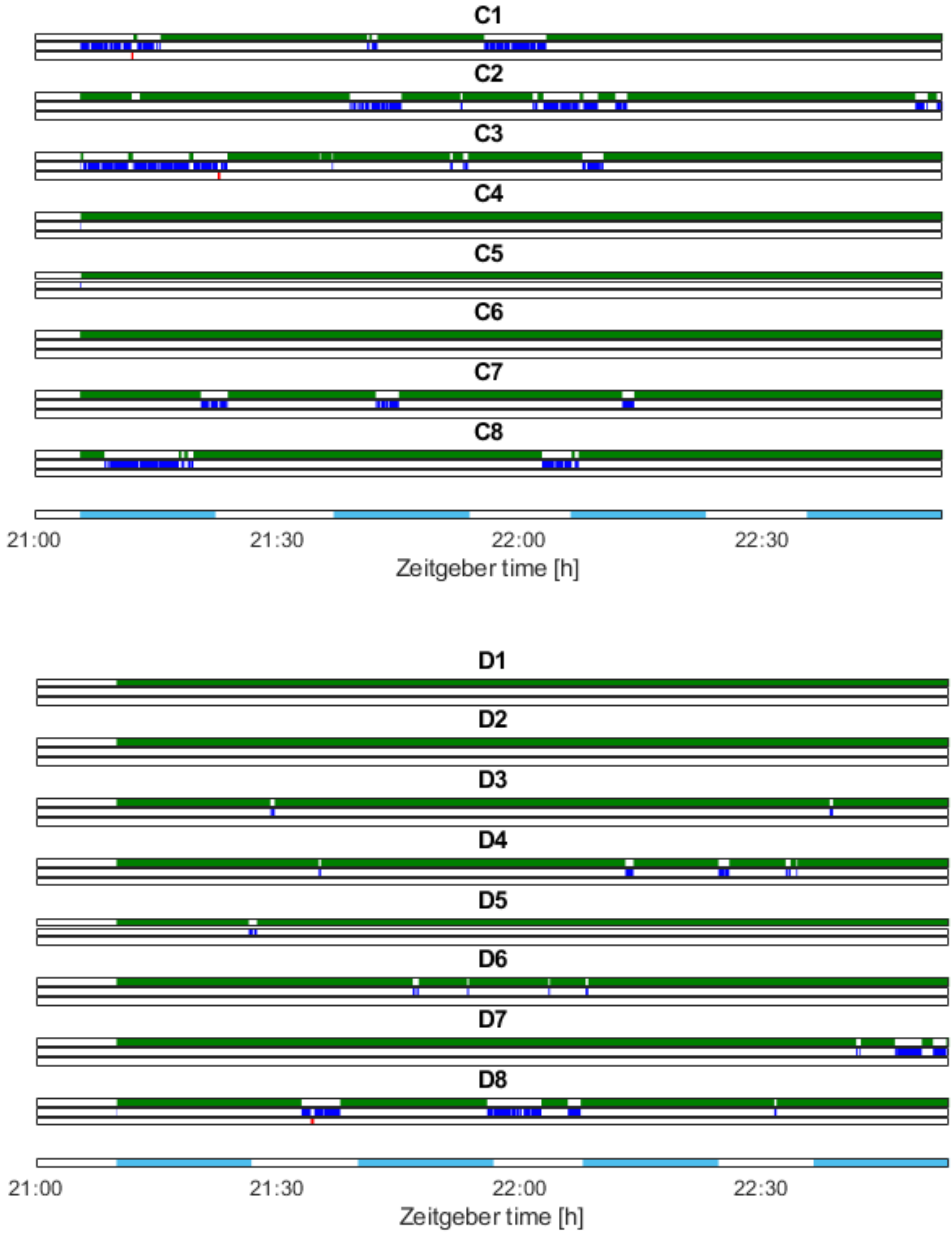

Figure 5.4: Hypnograms of all animals aligned with stimulation blocks. Each row is a hypnogram from an individual animal. Hypnograms show distribution of time spent in vigilance states: wake (green), NREM (blue), REM (red). Bar below shows stimulation sequence, starting from 9PM (lights off). Shaded light blue represent the stimulation blocks: ascending oddball paradigm, ascending cascade control sequence, descending oddball paradigm, descending cascade control sequence. In between stimulation blocks, there was a ~10 min break.

5.3.1 Peak windows evoked potential

The responses to all tones across all vigilance states were averaged per animal, to define time windows to extract peak amplitudes and latencies from. The evoked response in my experiment showed a negative deflection in the P1 time range (20-30 ms), a positive deflection in the N1 time range (40-50 ms) and a negative deflection in the P2 time range (75-125 ms). This is a reversed polarity to what is reported in most studies in literature, which could be related to the positions of the electrodes in my experiment: the frontal electrode was referenced to a cerebellar electrode, whereas in classic experiments, frontocentral electrodes are referenced to a nose or mastoid electrode (Näätänen and Michie, 1979; Näätänen et al., 1978, 2007).

I refer to the deflection in the P1 time range as P1 (despite its negative polarity) with P1 time window 16-24 ms after tone onset, the deflection in the N1 time range as N1 (despite positive polarity), with N1 window as 24-51 ms and the deflection in the P2 time range as P2 (despite negative polarity), with P2 window 51-125 ms after tone onset. There was no evident peak in the P3 time range (125-300ms), so no time window was set for this peak.

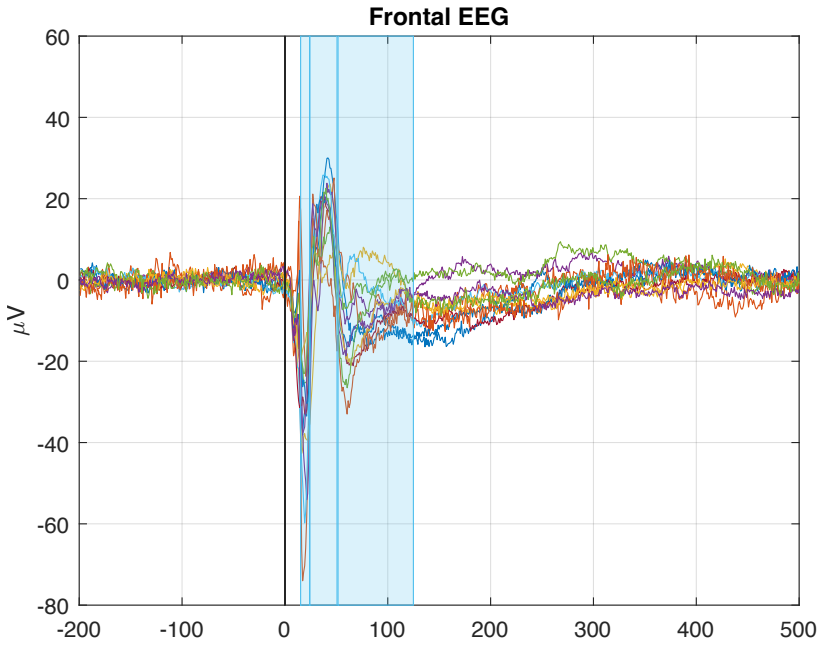

Figure 5.5: Auditory evoked response averaged across all tones. Traces are shown for individual animals, averaged across all 4000 tones that were played (4 stimulation blocks of 1000 tones each). The black line at t=0 represents tone onset. The shaded areas indicate the time windows that were defined for peak extraction, in chronological order, P1: 16-24 ms, N1 24-51 ms and P2 51-125 ms. P3 is expected to occur around 200-300ms but since this deflection was not clear, this peak was not further analysed. n=16 animals, L6b silenced (n=9), Controls (n=7).

5.3.2 Mismatch response

For investigating the mismatch response, AEP peak-to-peak amplitudes after standard tones were compared to deviant tones.

Ascending oddball paradigm

In the ascending oddball paradigm ($f_{deviant} > f_{standard}$), the P1-N1 amplitude was larger after deviant tones than after standard tones (STD vs DEV, $F_{(1,12)}=7.857$, $p=0.0160$), but this difference between responses to standards and deviants was only present in L6b silenced animals (posthoc comparison, L6b silenced, STD vs DEV, $p=0.0028$) and not control animals (WT, STD vs DEV, $p=0.6496$)(Figure 5.6A), which resulted in a statistical trend of a different STD vs DEV response between the genotypes (Genotype x (STD vs DEV), $F_{(1,12)}=4.716$, $p=0.0577$). This seemed to be based on a smaller response of L6b silenced animals to standards (posthoc comparison, STD, WT vs L6b silenced, $p=0.0078$) rather than a larger response of L6b silenced animal to deviants, since responses to deviants were not different between the genotypes (posthoc comparison, DEV, WT vs L6b silenced, $p=0.6678$).

The N1-P2 amplitude was also significantly larger after deviant tones than after standard tones (STD vs DEV, $F_{(1,12)}=21.35$, $p=0.0006$)(Figure 5.6B). The larger N1-P2 after deviant tones was strongly significant in L6b silenced animals (posthoc comparison, L6b silenced, STD vs DEV, $p<0.0001$) but not significant in control animals (posthoc comparison, WT, STD vs DEV, $p=0.3132$), resulting in a significantly different STD vs DEV response between the genotypes (Genotype x (STD vs DEV), $F(1,12)=9.174$, $p=0.0105$). The difference between genotypes in STD vs DEV response was the result of a stronger response of L6b silenced animals to deviant tones (posthoc, DEV, WT vs L6b silenced, $p=0.0196$) with comparable response amplitudes to standard tones between genotypes (posthoc, STD, WT vs L6b silenced, $p=0.3145$). Peak latencies were not affected (Figure 5.6C).

In the EMG, a stronger response to deviants than to standards was observed, as expected. This was seen both in L6b silenced and wildtype animals (Supplementary Figure S5.2).

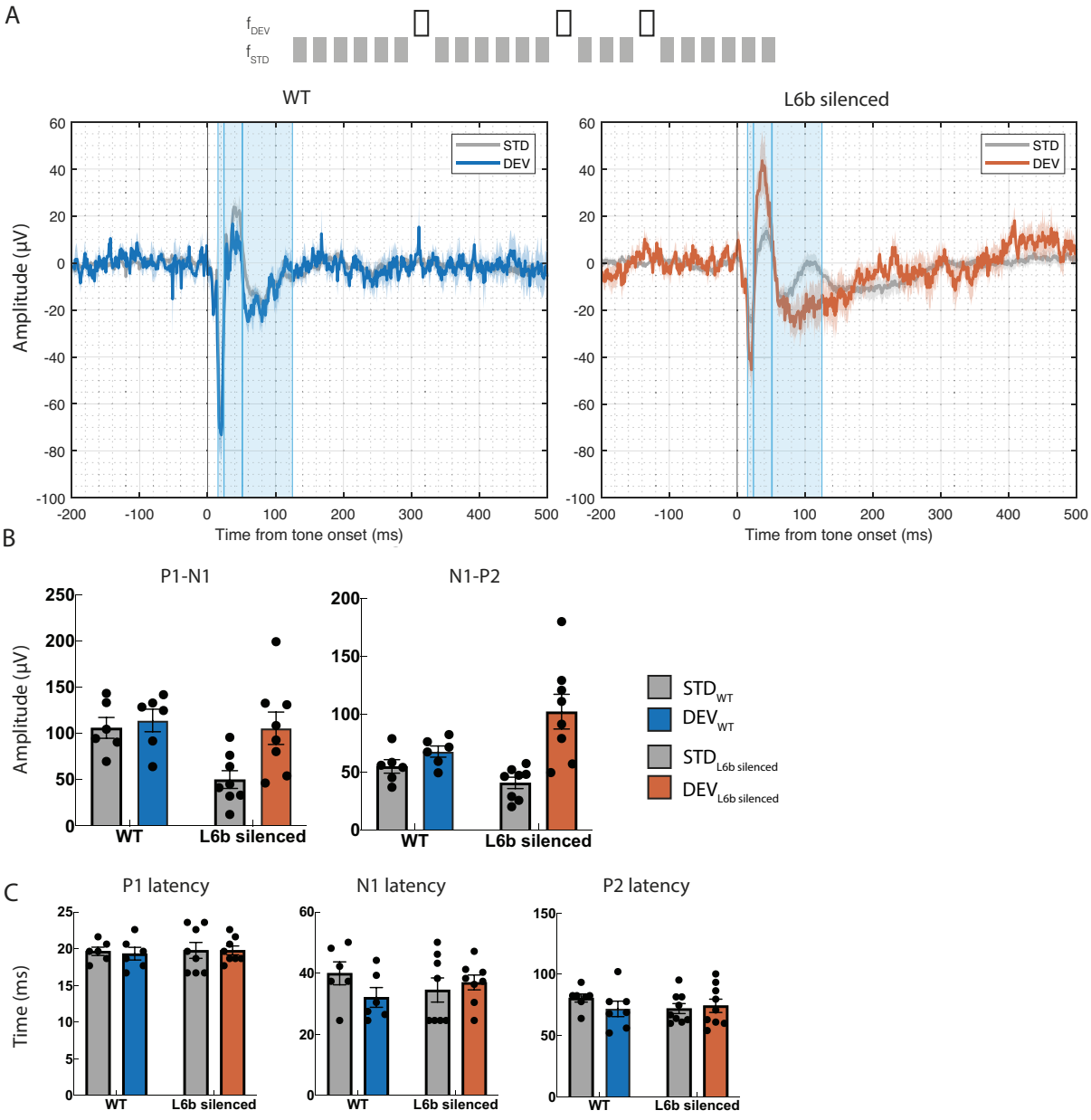

Figure 5.6: Ascending oddball paradigm.
(A) Frontal EEG responses to deviant tones and standard tones in wildtype (left, n=6) and L6b silenced (right, n=8) animals.
(B) Comparison between standard and deviant peak-to-peak amplitudes. Time windows from which P1, N1, and P2 peaks are extracted are indicated with shaded areas in (A).
(C) Comparison between standard and deviant peak latencies.

Descending oddball paradigm

In the descending oddball paradigm ($f_{deviant} < f_{standard}$), the P1-N1 amplitude did not increase after deviant tones (STD vs DEV, $F_{(1,11)}$=0.2333, p=0.6386) but the N1-P2 amplitude did (STD vs DEV, $F_{(1,11)}$=8.127, p=0.0158) (Figure 5.7B). The increase in N1-P2 amplitude in response to deviant tones was significant in control animals (WT, STD vs DEV, p=0.0189) but not in L6b silenced animals (L6b, STD vs DEV, p=0.2462). Peak latencies were not affected (Figure 5.7C).

Besides comparing peak amplitudes and latencies, AEPs after standard and deviant tones can be compared by calculating differences waves, which are especially useful for demonstrating later MMN responses. Differences were significant at time ranges consistent with, and most likely reflecting, the changes in P1 and N1 peak amplitudes, but no differences were observed at later time ranges, consistent with the initial AEP evaluation (Figure 5.5) (Supplementary Figure S5.1).

In addition to the STD vs DEV changes that were observed in the oddball paradigms, there was also a statistical trend towards smaller P1-N1 amplitudes in L6b silenced animals than in control animals (Ascending oddball paradigm, Genotype P1-N1, $F_{(1,12)}$=4.257, p=0.0614; Descending oddball paradigm, Genotype P1-N1, $F_{(1,11)}$=4.643, p=0.0542).

Summarizing, in the frontal EEG deviant tones elicit a larger N1-P2 peak amplitude in both paradigms, but this effect was only significant in the ascending oddball paradigm for L6b silenced animals and only in the descending oddball paradigm for control animals. In the ascending paradigm, L6b silenced animals showed a smaller response to standards. Across both standards and deviants and both the ascending and descending oddball paradigm paradigms, there was a trend towards smaller P1-N1 amplitudes in L6b silenced animals compared to controls.

In the EMG signal, the response to deviants appeared again larger than the response to standards in both genotypes. Whether there were genotype-specific effects is not possible to tell based on these results (Supplementary Figure S5.2).

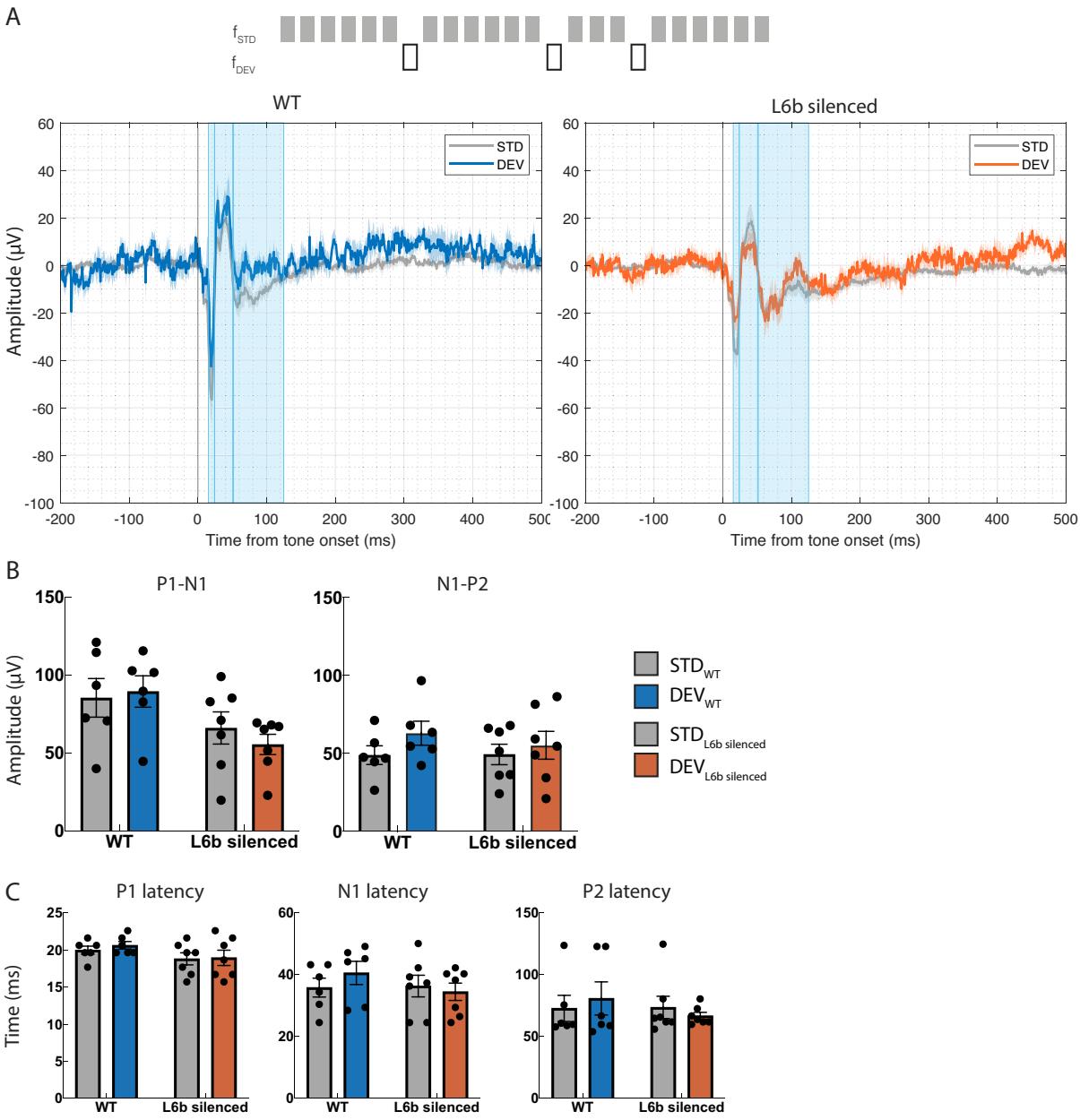

Figure 5.7: Descending oddball paradigm.
(A) Frontal EEG responses to deviant tones and standard tones in wildtype (left, n=6) and L6b silenced (right, n=7) animals.
(B) Comparison between standard and deviant peak-to-peak amplitudes. Time windows from which P1, N1, and P2 peaks are extracted are indicated with shaded areas in (A).
(C) Comparison between standard and deviant peak latencies.

5.3.3 Adaptation

Because of the smaller N1-P1 amplitude in L6b silenced animals in the first paradigm, and the reported effect of adaptation on the N1 time range (Näätänen et al., 2007), I wondered whether there was an increase in adaptation in L6b silenced animals.

To assess fast, within-paradigm adaptation, I compared the responses to the first 20 standard tones with the responses to the last 20 standard tones within the ascending oddball paradigm (Figure 5.8). Peak characteristics could not be determined in individual animals, and therefore only patterns are described based on inspection of the genotype-grouped graphs (see Methods - Statistics for description of excluded animals).

In wildtype animals, repeated stimulation seems to reduce N1 latency and to a lesser degree N1 amplitude. In L6b silenced animals, a strong reduction of the N1 amplitude at the end of the paradigm is visible for both the ascending and the descending oddball paradigm.

For assessing the degree of adaptation between paradigms, I compared the response to the first 20 standard tones in the ascending oddball paradigm to the first 20 standard tones in the descending oddball paradigm. Visual inspection suggested that wildtype mice showed adaptation between paradigms, with a smaller response at the start of the later paradigm, whereas adaptation in L6b silenced animals was less pronounced.

When comparing EMG responses visually across the ascending oddball paradigm with those across the entire descending oddball paradigm (Supplementary Figure S5.2), in wildtypes, peak EMG amplitudes seemed to reduce from the first oddball paradigm (ascending paradigm) to the later oddball paradigm (descending paradigm). In L6b silenced animals, it is difficult to interpret findings because of the technical issues, but the response to standards seemed to reduce within the first oddball paradigm and not reduce further in the late paradigm.

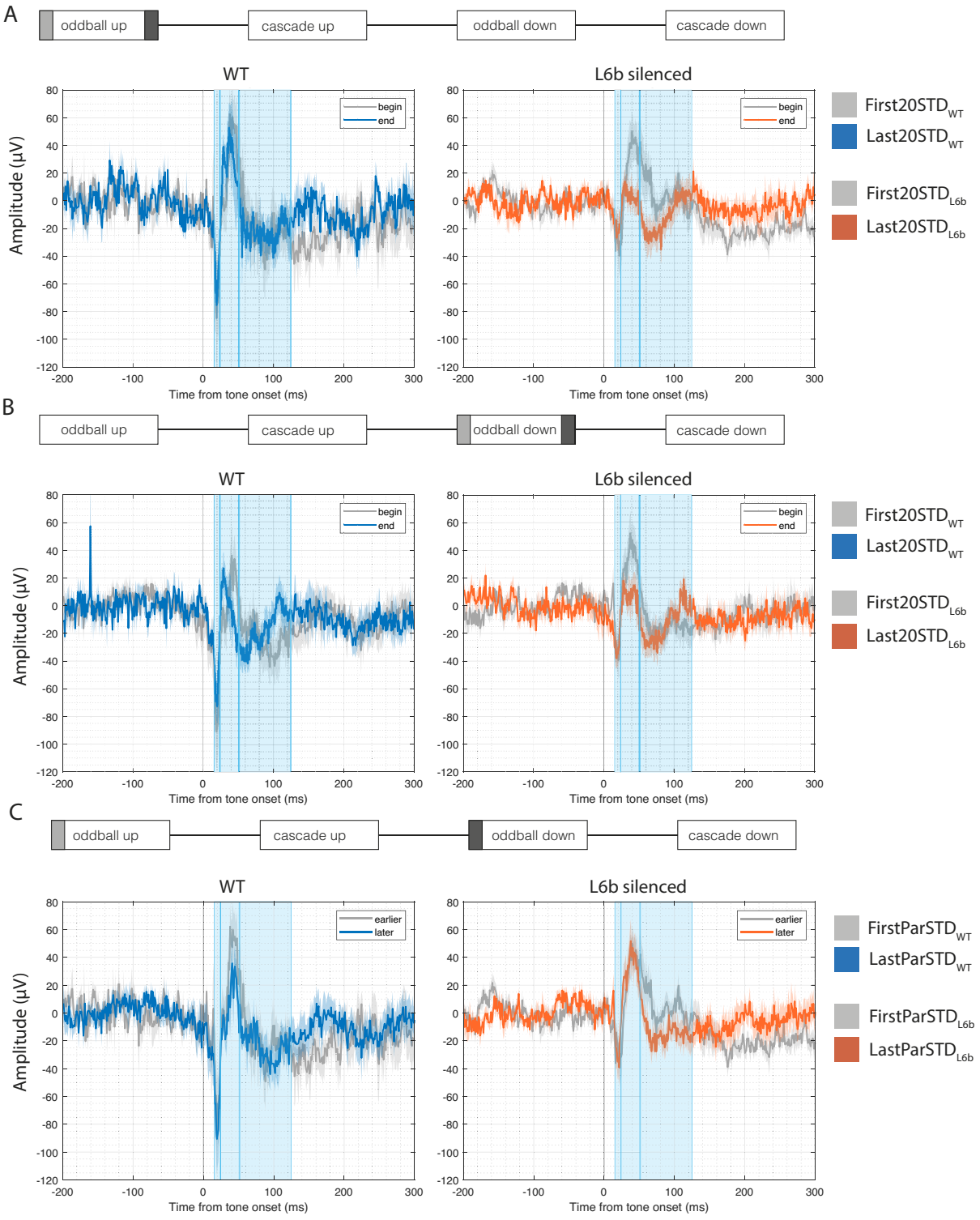

Figure 5.8: Adaptation within and between paradigms.
(A) Frontal EEG responses of the last 20 standards of the first paradigm compared with the first 20 standards of the same paradigm (WT, n=6; L6b silenced, n=8).
(B) Frontal EEG responses of the last 20 standards of the second oddball paradigm compared with the first 20 standards of the same paradigm (WT, n=6; L6b silenced, n=8).
(C) Frontal EEG responses of the first 20 standards of the descending oddball paradigm compared with the first 20 standards of the ascending oddball paradigm (WT, n=6; L6b silenced, n=8).

5.3.4 Prediction error signalling

To dissect the mismatch response into adaptation and prediction error signalling, I included cascade control sequences for both oddball paradigms. The response to the deviant tone in the oddball paradigm was compared with the response to the tone with the same frequency in the respective cascade control sequence, the 'control' tone. In this way, tones with the same probability and frequency were compared, between a condition where it was 'odd' and a condition where it was not. An increase in response amplitude between deviants and control tones can then be regarded as a result of prediction error signalling (Figure 5.9).

The same animals were included for the two control sequences as for the respective oddball paradigms. In the ascending paradigm, wildtype animals showed a larger P1-N1 amplitude to control tones than to deviant tones (STD vs DEV, $F(1,12)=14.66$, $p=0.0024$), which is opposite from what would be expected if a mismatch response was elicited, which would enlarge the amplitude to deviant tones compared to control tones. In L6b silenced animals, there was no significant difference between responses to control and deviant tones. The N1-P2 amplitude was larger for deviants than control tones in L6b silenced animals, which is in line with expectations, but again larger for control tones than for deviant tones in wildtypes animals. These are unexpected and unexplained results and are likely to be artefactual, in line with the major inter-subject variability for both the N1-P1 (Subject, $F(12,12)=14.98$, $p<0.0001$) and P1-N2 (Subject, $F(12,12)=8.696$, $p=0.0004$) amplitudes.

In the descending paradigm, there were also large and significant inter-subject variabilities; besides that, no differences between peak-to-peak amplitudes for deviant and control tones were detected. No differences in peak latencies were observed in either paradigm.

Altogether, the control paradigm was added to the experiment with the aim of dissecting deviance detection into adaptation versus prediction error signalling effects, but the responses did not show a logical or explainable effect direction and did show a large inter-subject variability, so no conclusions can be drawn from this experiment.

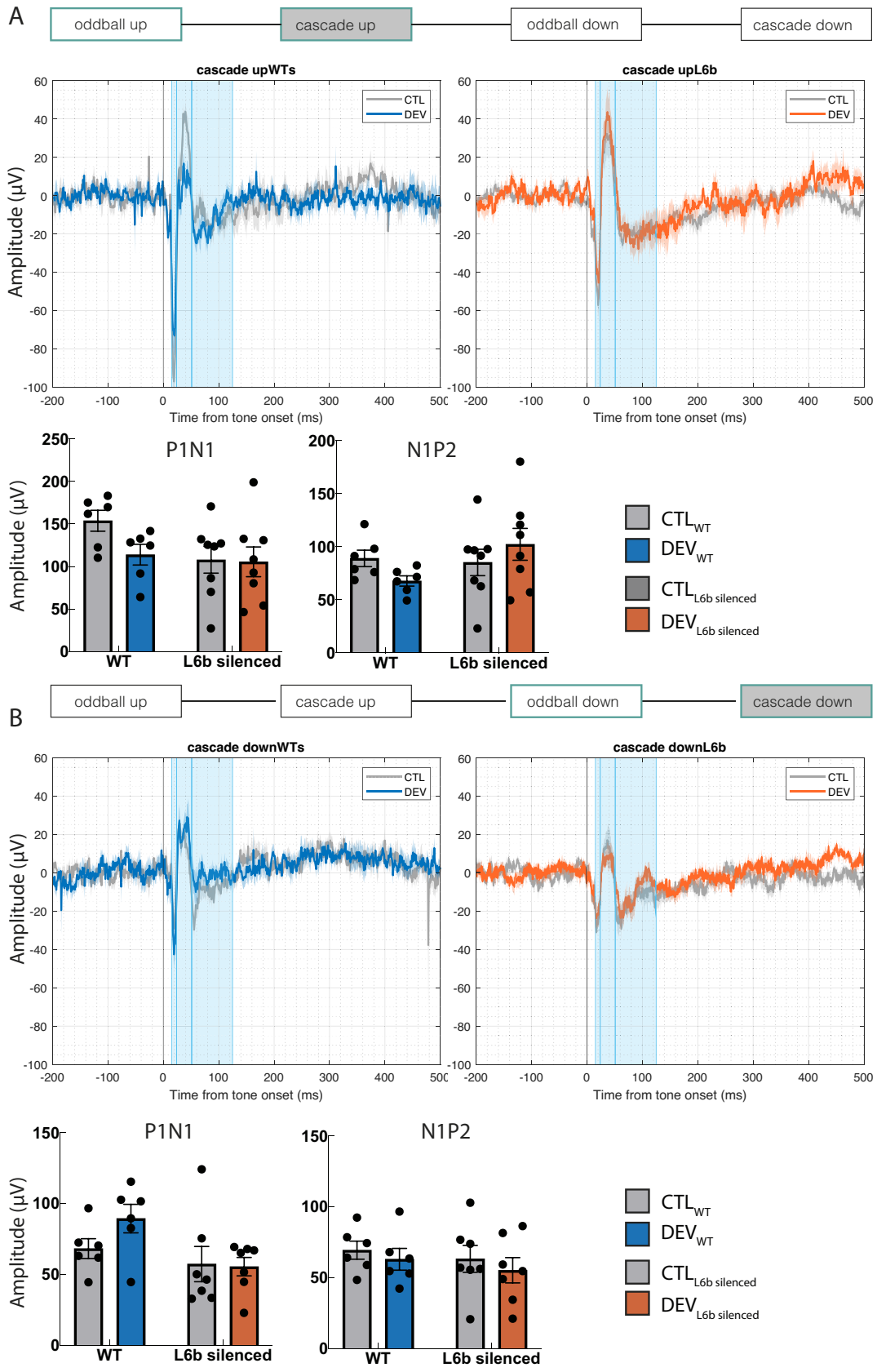

Figure 5.9: Investigation of the role of prediction error signalling. P1-N1 and N1-P2 peak-to-peak amplitudes are compared for peaks extracted in the blue shaded areas.
(A) Comparison of frontal EEG responses to deviant tones (f=11.3 kHz) in the ascending oddball paradigm with f=11.3 kHz tones in the ascending control paradigm. WT (n=6), L6b silenced (n=8).
(B) Comparison of frontal EEG responses to deviant tones (f=7.99 kHz) in the descending oddball paradigm with f=7.99 kHz tones in the descending control paradigm. WT(n=6), L6b silenced (n=7).

5.4 Discussion

5.4.1 Summary of findings

In this experiment, I performed an auditory oddball paradigm in L6b silenced and wildtype animals, to investigate whether chronically silencing L6b affects the generation of a mismatch response to changing stimuli as a result of adaptation and prediction error signalling.

I found an increase in the N1-P2 peak-to-peak amplitude after deviant tones compared to standard tones in both an ascending and a descending oddball paradigm. The increase in deviant N1-P2 amplitude was only observed in the ascending paradigm for L6b silenced animals and only in the descending paradigm for control animals. In the EMG, the acoustic startle response showed a higher amplitude to deviants than to standards in both paradigms.

In general, the P1-N1 amplitude tended to be smaller in L6b silenced than in control animals. Moreover, in L6b silenced animals, P1-N1 amplitudes were larger for deviant tones than for standard tones, and this effect seemed to depend on an increased adaptation to standard tones rather than an increased change detection to deviant tones. Consistent with this, when the responses to the first 20 and last 20 standards within the first paradigms were plotted, L6b silenced animals showed a more pronounced adaptation than control animals, suggesting faster or stronger adaptation. On the other hand, slower, between-paradigm adaptation appeared more prominent in control animals. Acoustic startle reflexes showed adaptation as well, with smaller amplitudes in tones later within the same paradigm and in a later paradigm.

Finally, an attempt was made to detect prediction error signalling as a contributor of the mismatch response, but the results were not consistent between paradigms nor with the underlying assumptions of the control sequence that was used; the inconsistent results can be explained by the large and significant variation between animals.

5.4.2 Comparison of findings to literature

Despite the increases in P1-N1 and N1-P2 peak-to-peak amplitude after deviant tones, I found no consistent increase in amplitude in the later time ranges. This is not in line with studies in rodents that report that the MMN gradually increases from 50-100ms onwards to reach a peak around 300 ms or even later (Casado-Román et al., 2020; O'Reilly and Angsuwatanakul, 2021; Ruusuvirta et al., 1998; Shinba, 1997; Yamaguchi et al., 1993). Other reports on free-field auditory stimulation in rodents, however, do not find late effects (Nir et al., 2015; Umbricht et al., 2005). It has been suggested that the absence of P3-like effects in the latter studies may be the result of stimulation parameters such as probability of deviant tones and duration of interstimulus intervals, or the use of a passive rather than active paradigm (Nir et al., 2015). The use of an active paradigm, in which is the deviant tone is associated with a reward or aversive paradigm, is associated with an increase in the P3 amplitude (Sambeth et al., 2003; Shinba, 1997). However, P3 potentials have also been detected with passive paradigms including during anaesthesia, suggesting that association with a rewarding or aversive outcome is not a necessity for eliciting a P3 response (Casado-Román et al., 2020; O'Reilly and Angsuwatanakul, 2021; Ruusuvirta et al., 1998; Shinba, 1997; Yamaguchi et al., 1993).

P3 components in passive paradigms have been reported to have a larger amplitude in parietal EEG than in frontal and temporal EEG and have a shorter latency than in active paradigms (Shinba, 1997). In more local recordings of LFP during passive paradigms, it was shown that the MMN in auditory cortex starts to rise by 40ms and has decayed by 160 ms after stimulus onset, whereas the MMN in mPFC only rises around 140 ms and decays after more than 600 ms (Casado-Román et al., 2020; Parras et al., 2021). Processing in the prefrontal cortex in the later time frame has been most strongly linked to deviance detection through prediction error signalling (Casado-Román et al., 2020), but modelling approaches show that predictive processing may also contribute to effects in the N1 time range, along with SSA (Garrido et al., 2009b). Concluding, the absence of a P3 like response in my experiment is in line with several previous reports and does not invalidate the other differences that were found.

It is surprising that in control animals, the descending oddball paradigm elicited a change in N1-P2 amplitude whereas the ascending oddball paradigm did not. The animals, which had a C57BL6 background, are assumed to have a similar sensitivity to both tones of the oddball pair (7.99 Hz and 11.3 Hz) or a slightly higher sensitivity to the tone with the higher frequency (Ison and Allen, 2003). The slightly higher sensitivity to the 11.3 kHz tone could skew the responses to a stronger response to the deviant tone in the ascending paradigm and a stronger response to the standard tone in the descending paradigm in the first 100 ms after tone onset in the AEP (O'Reilly and Conway, 2021). Therefore, it is less logical that the descending but not the ascending paradigm elicits a stronger mismatch between deviants and standards, albeit the MMN that is generated in the descending paradigm might be closer related to 'genuine deviance detection', less distorted by differences in physical properties between the tones. Onset of hearing loss is not an explanation for this effect since the advanced age-related hearing loss in C57Bl6 animals affects the frequencies in the sensitivity range initially to a lesser extent (Ison and Allen, 2003).

5.4.3 Implications

The absence of an effect in the time range later than P2 and the inconsistency in results between the ascending and descending paradigms raise questions about whether the oddball paradigms succeeded at eliciting a 'genuine deviance response' in wildtype animals in this experiment which makes genotypes comparisons difficult. On the other hand, changes in adaptation processes were visible, with an apparent enhancement of within-paradigm adaptation and an apparent reduction of between-paradigm adaptation in L6b silenced animals.

Adaptation is the result of both SSA at the single neuron level, and repetition suppression at a global level. SSA has been reported to occur in single neuron recordings from inferior colliculus (Ayala and Malmierca, 2012), medical geniculate body of the thalamus (Antunes et al., 2010) and auditory cortex (Ulanovsky et al., 2003). Drd1a-Cre is expressed in L6b of the auditory cortex in the FK164 mouse line that was used in the current study, albeit relatively sparsely

(Http://www.gensat.org, 2023), so there could be a contribution of SSA in L6b neurons in auditory cortex to the process of adaptation.

An alternative explanation for changed adaptation dynamics is that L6b would be involved in repetition suppression. L6b is one of the infragranular layers and is well connected with other cortical layers and higher order thalamic nuclei which could make it a suitable candidate for being involved in predictive processing (Auksztulewicz and Friston, 2016; Hoerder-Suabedissen et al., 2018; Zolnik et al., 2020).

A study investigating changes in P3 amplitude in an auditory oddball task in humans found within-session adaptation to the standard tone, and between-sessions adaptation to the deviant tone. They explained these differences in adaptation by automatic bottom-up habituation occurring within-session, and higher order top-down attention switching occurring between sessions (Debener et al., 2002). I was not able to look at P3 effects in my study, but if similar mechanisms are involved in adaptation within the P1-N1-P2 time range, the differences in within- and between- paradigm adaptation that I found could indicate that automatic adaptation is enhanced in L6b silenced animals and top-down higher order adaptation is reduced.

The overall decrease in P1-N1 amplitudes in L6b silenced animals was found not only in the standards but also in deviants and led to an overall genotype effect on P1-N1 amplitude. The reduced P1-N1 amplitude could be a result of a general hearing impairment. In the mouse line used in this study, dense Drd1a-Cre expression has been reported in the dorsal cochlear nucleus(Hoerder-Suabedissen et al., 2018). Since Snap25 is involved in synaptic transmission in ribbon synapses between hair cells and spiral ganglion neurons (Johnson et al., 2019) and ribbon synapse formation is not completed at P1, when Drd1a-Cre is starting to be expressed (Hoerder-Suabedissen et al., 2018; Michanski et al., 2019), hearing could be impaired. However, the findings that the N1-P2 was not reduced in L6b silenced animals and that the acoustic startle reflexes appeared broadly comparable between L6b silenced and control animals, suggest that the significant P1-N1 amplitude reduction is a result of effects specific to P1, N1 or both rather than a general hearing impairment.

The alternative explanation for the reduced P1 and N1 amplitudes in L6b silenced animals is that there are changes in auditory gating mechanisms, which affect P1 and N1 (Bickel et al., 2008). Importantly, abnormalities in auditory gating and adaptation have been described in patients with neuropsychiatric disorders such as schizophrenia and their first-degree relative and are thought to reflect impairments in NMDA receptor signalling and changes in network connectivity (Adler et al., 1982; Boutros et al., 2004; Shelley et al., 1999; Siegel et al., 1984). Histopathological abnormalities have been found in the human subplate derived neuronal population, interstitial white matter neurons, in patients with schizophrenia and ASD (Bailey et al., 1998; Casanova, 2015; Duchatel et al., 2019). Therefore, the abnormalities in gating in L6b silenced mice could suggest a potential functional link between L6b or interstitial white matter neurons and network development in neuropsychiatric disease.

5.4.4 Limitations

Ideally, Drd1a-Cre expression would be documented along the auditory pathway, including in the cochlea. In general, it would have been desirable to start this experiment with a baseline assessment of hearing function in L6b silenced animals, by measuring ABR for the general auditory threshold and distortion product otoacoustic emission (DPOAE) for frequency discrimination, since both are crucial in a frequency-based oddball paradigm. Most studies do not report these baseline characteristics.

The setup of the experiment could be improved by using dedicated auditory stimulation equipment. The RZ2 processor that was used to generate tones is a potent processor for recording continuous electrophysiological signals from multiple animals in vivo but the sampling rate cannot exceed 50 kHz which reduces the frequency range across which tones can be played and leads to the generation of 'tinny' sounds. This could affect frequency discrimination between the tones. The recording chambers were soundproof but not as sound isolated as those used in auditory research settings, for instance they had a hole in the ceiling to allow connection of EEG/EMG cables. The speakers attached to the ceiling of each chamber were calibrated, but sound

levels will have varied slightly per chamber, and variation in sound intensity can in itself cause a mismatch response (Lindín et al., 2005), which can obscure findings. I attempted to correct for the latter effect by balancing wildtype and L6b silenced animals over the chambers.

In addition, animal movement will have caused slight changes in sound intensity. I tried to limit movement by offering the novel object in the same corner of the cages for all animals, but, unsurprisingly, the animals moved the objects. Ensuring equal sound intensity is difficult to achieve with speakers. For rats, miniature headphones have been developed, 'ratphones' (Valente et al., 2023), but for mice these do not exist, and the combination with EEG/EMG head stages would be difficult. Importantly, free-field auditory oddball experiments with speakers have been successfully carried out in rodents before (Harms et al., 2014; Jodo et al., 2019).

With regards to the paradigm, this could be further optimised, which I did not currently do as I wanted to limit habituation. Examples of modifications I would try are reducing sound intensity, varying numbers of standards and deviants, testing different frequency pairs, and introducing jitter in interstimulus intervals to enhance temporal irregularity (Costa-Faidella et al., 2011; Näätänen et al., 2007). I could also try running the experiment during sleep instead of during wakefulness, which would reduce the location variability within a paradigm. However, the amplitude of the AEP can vary with slow wave phase, which may complicate comparison of peak amplitudes. Moreover, animals may wake up in the course of the paradigm.

5.5 Conclusion

Altogether, in the oddball paradigms, stronger responses to deviants than to standards were observed, but findings were not consistent between genotypes or paradigms, so results should be interpreted with caution. Two differences were observed between genotypes: (I) the P1-N1 amplitude was decreased in L6b silenced animals and (II) the timescale of adaptation seemed altered, with stronger within-paradigm adaptation and less between-paradigm adaptation in L6b silenced animals. These differences suggest that there are changes in network connectivity in L6b silenced animals that may have parallels with neuropsychiatric disorders.

6 General discussion

In this final chapter, I summarize the key findings of my study and describe the implications these may have for the understanding of sleep-wake regulation, sleep homeostasis, and sensory processing. I then outline in which ways my findings may contribute to the understanding of neurological and neuropsychiatric disorders and I conclude with outlook for future research.

6.1 Implications for the understanding of sleep-wake regulation

In Chapter 3, I assessed the sleep phenotype of mice in which the synaptic protein Snap25 is ablated in the Drd1a expressing subpopulation of L6b (Drd1a-Cre; Snap25$^{fl/fl}$;TdTom), the 'L6b silenced mouse'. I found that the daily sleep architecture in L6b silenced mice was not different from wildtype animals, including the distribution of vigilance states, measures of sleep consolidation and sleep fragmentation. However, the EEG oscillatory activities were altered. Specifically, during wakefulness EEG theta-frequency power, which is the signature of active, exploratory wakefulness (Vassalli and Franken, 2017), was suppressed in L6b-silenced animals. In REM sleep, also called paradoxical sleep since it is like wakefulness characterized by cortical activation while the animal is behaviourally asleep, there was also a reduction in theta-frequency power, along with a reduction in gamma-frequency power. In both wake and REM, there was a slowing of theta oscillations with a smaller peak amplitude and EEG power in the high theta frequency range was reduced. Moreover, the increase in high theta power observed during sleep deprivation was blunted in L6b silenced animals. We posit that silencing L6b leads to a decrease in alertness, exploratory wakefulness or more generally activated brain state, which suggests that L6b may have a role in promoting or allowing wakefulness, vigilance, and alertness. This

conclusion is in line with *in vitro* studies that have shown that L6b neurons can be activated by orexin, neurotensin, noradrenaline, histamine and dopamine, all powerful promoters of arousal (Bayer et al., 2004; Wenger Combremont et al., 2016b, 2016a).

Anatomically, L6b is in an ideal position to contribute to wakefulness promoting functions. It receives input predominantly from long-range intracortical projections and projects selectively to higher order nuclei of the thalamus (Hoerder-Suabedissen et al., 2018; Zolnik et al., 2020). This means that L6b can integrate inputs from wake-promoting subcortical neuromodulatory areas as well as information from distant cortical areas and convert this information into wide-spread cortical activation through activation of higher-order thalamic nuclei. Higher order thalamic nuclei can themselves also be directly activated by orexin (Bayer et al., 2002), and orexinergic activation of L6b can enhance the integration of higher order thalamic inputs in L6a (Hay et al., 2015), further enhancing the wake promoting potency of this proposed transthalamic corticocortical network.

Notably, new data from Zolnik *et al.* show that optogenetic activation of the same Drd1a subpopulation of L6b in head-restrained awake mice can promote the conversion from delta oscillations to gamma oscillations, thus promoting a state of cortical activation as seen in wakefulness and REM sleep (Zolnik et al., 2023). The conclusion that acute activation of L6b causes an activated brain state is consistent with my results that chronic silencing of L6b results in a reduction in active substates of wakefulness.

What would be the circuit substrate of modulation of fast rhythms by L6b? This cannot be derived from my results since I only performed EEG recordings after brain-wide manipulation of L6b. One could speculate that projections from L6b pyramidal neurons to L6b and L6a interneurons (Tantirigama et al., 2020; Zolnik et al., 2023) could result in the generation of fast rhythms, such as the stimulation of PV interneurons that have been associated with gamma rhythms (Wenger Combremont et al., 2016b).

6.2 Implications for understanding the effects of orexin on neocortex

With the finding that a subpopulation of cortical L6b neurons plays a role in regulating state-dependent brain oscillatory activities, specifically altering EEG patterns characteristic of active wakefulness, I next asked how the L6b silenced animals respond to the administration of exogenous orexin.

To this end, in Chapter 4, I investigated the effect of in vivo orexin administration on sleep and wakefulness in L6b silenced (Drd1a-Cre:Snap25$^{fl/fl}$) and wildtype animals. I found that ORXA significantly increased wakefulness in the first three hours in both genotypes and did this through promoting sustained wakefulness. The wake maintenance enhancing effect was stronger in L6b silenced animals, with a longer maximal duration of wakefulness episodes. In subsequent NREM sleep, both ORXA and ORXB destabilized sleep, as reflected in more frequent brief awakenings in both genotypes. ORXA and ORXB did not significantly change brain oscillations during wakefulness in wildtype animals but caused a significant decrease in delta power and increase in high theta power in L6b silenced animals. After ORXB there was reduction in theta power during REM sleep and this reduction was greater in L6b silenced than control animals.

These findings are the opposite from what I had expected initially, since I had hypothesized that orexin would activate L6b and that this would promote cortical arousal; therefore, silencing L6b would reduce the arousal-promoting effects of orexin in L6b silenced animals. The stronger effects of orexin in L6b silenced animals can be explained in three ways.

First, the difference between genotypes can be purely accidental, caused, in part by a difference in group sizes as a consequence of colony breeding difficulties (L6b silenced, n=8 and wildtype, n=5), which reduced statistical power making the comparison not reliable. While this possibility is unlikely, future experiments are needed on a larger cohort to reproduce the results.

Second, as the L6b silenced mouse is a model of chronic silencing of L6b, compensatory remodelling could have taken place, potentially reversing some effects. This possibility is also unlikely, given that the results of baseline sleep phenotyping was exactly in line with the idea that L6b has a wake promoting effect.

A third explanation, which in our opinion is most likely, is that the heterogeneity of L6b causes different subpopulations to have distinct contributions to specific aspects of state control and regulation of different oscillatory activities or that L6b subpopulations have different roles in different vigilance states. It is conceivable that orexin promotes wakefulness by activation of some populations of L6b but that other populations of L6b counteract the effects of orexin when wakefulness or vigilance is no longer needed. This would add a higher temporal precision to the wakefulness promotion by orexin, by quickly balancing wake promotion when the neuromodulatory tone is still high.

6.3 A role of cortical L6b in NREM sleep oscillations

Silencing a subpopulation of L6b not only changed oscillations during wakefulness and REM sleep, but also during NREM sleep, as reflected in a reduction in EEG spectral power density across a broad frequency range, including delta (0.5-4 Hz), theta (5-10 Hz), sigma (10-15 Hz), and gamma (30-100 Hz) frequencies, although when analysing absolute band power differences, only the EEG power in the sigma frequency range appeared significantly different between genotypes.

Activity in the delta frequency range is an expression of the synchronization of neuronal populations in slow waves (Steriade et al., 1993c, 2001; Vyazovskiy et al., 2009), so the reduction in delta frequency range in L6b silenced animals suggests that there may be a reduction in network synchrony. Slow wave activity (SWA, 0.5-4 Hz) is a marker of sleep intensity and reflects the levels of sleep pressure, which builds up as a function of preceding wakefulness duration (Achermann and Borbély, 2003; Borbély, 1982). A reduction of delta power during NREM sleep in L6b silenced animals agrees with a reduction of theta power during wakefulness, since it is the theta substate of wakefulness that drives the build-up of sleep pressure (Vassalli and Franken, 2017; Vyazovskiy and Tobler, 2005; Yamagata et al., 2021).

The reduction in sigma power (10-15 Hz) was prominent both in overall spectral comparisons and in band power analysis and is particularly interesting, because this is the frequency range of sleep spindles. Sleep spindles are waxing and waning bursts of activity that

are thought to originate from interactions between cortex, thalamus, and the thalamic reticular nucleus (TRN) (Crunelli et al., 2006; Steriade et al., 1993b). Sleep spindles have been linked to a memory consolidation functions of sleep, facilitating information transformation for long-term storage (Hahn et al., 2019; Helfrich et al., 2018). L6b has no direct projections to the TRN, but there are projections from L6b to L5, and subpopulations of L5 innervate segments of the TRN in an area-specific pattern (Carroll et al., 2022; Hádinger et al., 2023; Hoerder-Suabedissen et al., 2018). This suggests that the thalamocortical network involved in the generation of sleep spindles might have an extra layer of complexity, involving an additional influence of a subpopulation of L6b on the cortical, thalamic or both populations involved in the generation of spindles.

6.4 An active role for the neocortex in sleep regulation

The findings in the current study not only shed light on the role of L6b in sleep-wake regulation but also provide further insights into the contribution of the neocortex to global sleep-wake regulation. The control of sleep-wake state transitions has been described with several models.

The 'sleep-wake switch' model regards brain state transitions as a more or less dichotomous choice that is made when state-specific subcortical nuclei become activated and through the release of neuromodulators causes the entire brain to convert to a different brain state, i.e., a transition is made directly at the 'global' level (Saper et al., 2001). State transitions have been found to occur less frequently when network excitability is reduced in mice with a mutation in the synaptic vesicle protein VAMP2 (Banks et al., 2020). In L6b silenced mice, synaptic function is selectively suppressed from a subpopulation of L6b neurons.

The thalamocortical model states that brain state transitions are prompted by activity in thalamocortical networks, begin at a 'local' level and then, depending on the requirements of the situation, converge to a 'global' brain state transition (Krueger et al., 2008).

How do my findings align with these models? I found that chronic silencing of a subpopulation of excitatory L6b neurons causes changes in oscillatory activity during sleep and

wakefulness, suggesting that L6b is involved in the recruitment of brain networks that generate these activity pattern. Mice with a chronically silenced cortical L5, however, show a substantial reduction in time spent asleep without clearly affecting global EEG oscillations (Krone et al., 2021). Where does this position L6b in relation to L5 in the regulation of sleep-wake states? Based on connectivity, L6b receives its strongest input from L5 and in return it also projects to L5 (Hoerder-Suabedissen et al., 2018; Zolnik et al., 2020). Whereas L6b can be activated by various arousal-promoting neurotransmitters, L5 can be hyperpolarised by adenosine, a substance that signals sleep debt, which suggests that the interplay between these two lamina is a balanced system for the control of sleep and wakefulness (Aerde et al., 2015; Radnikow and Feldmeyer, 2018).

The findings that chronic silencing of L5 and chronic silencing of L6b both markedly affect sleep-wake regulation, one in terms of the time spent in different vigilance states, the other in terms of state-specific oscillations, strongly suggests that sleep is not only regulated via subcortical systems forming a 'sleep wake switch' but that the neocortex is also actively involved. This supports the concept that sleep is regulated in thalamocortical networks in a distributed pattern (Krueger et al., 2008). Recent work has shown that activity in the PFC contributes to sleep-preparatory behaviour and regulation of REM sleep (Hong et al., 2023; Tossell et al., 2023), and it is possible that a prefrontal population of L6b neurons is involved in brain state regulation through thalamocortical networks. However, my findings also suggest an important role of subcortical nuclei, since orexin released from the lateral hypothalamus is likely to directly affect the activity in L6b, as are other neuromodulators released from subcortical nuclei including at least noradrenaline, dopamine, neurotensin and histamine (Wenger Combremont et al., 2016b, 2016a).

6.5 Implications for the study of sleep homeostasis

After sleep deprivation, EEG SWA during NREM sleep dissipated at a lower rate in L6b silenced than in wildtype animals. This may be related to the overall lower absolute low frequency EEG

power during NREM sleep, suggesting a less intense sleep or a deficit in network synchronisation, which might affect restorative properties of sleep.

After chronic silencing of a subpopulation of cortical L5, sleep homeostasis was more drastically affected, with a reduced sensitivity of L5 silenced mice (Rbp4-Cre:Snap25$^{fl/fl}$) to the effects of sleep deprivation (Krone et al., 2021). Based on the synaptic homeostasis hypothesis, this effect could be purely explained by the reduced number of synapses that are present (Cirelli and Tononi, 2008). In this reasoning, silencing a subpopulation of L6b would also cause a reduction in NREM sleep, albeit to a lesser degree because of the size differences between L5 and L6b subpopulations.

The current findings, however, argue against this possibility since silencing a subpopulation of L6b had very different effects from silencing a subpopulation of L5 and therefore support the conclusion from the L5 study, that the specific silencing of a subpopulation of L5 caused the reduction in time spent asleep (Krone et al., 2021).

Currently ongoing experiments are testing whether the long range or the short-range cortical L5 projections are responsible for the wake promoting effects, since the Rbp4-Cre population that was used in the previous study contained both populations. In L6b, Ctgf-Cre and Drd1a-Cre L6b populations are different in their connectivity, and it would be interesting to explore the Ctgf-Cre:Snap25$^{fl/fl}$ model in the future (Henning et al., 2023).

6.6 Implications for the understanding of sensory processing

In Chapter 5, I tested auditory processing in L6b silenced (Drd1a-Cre:Snap25$^{fl/fl}$) animals with an auditory oddball paradigm with pure tones that differed in frequency. Mismatch responses were elicited in both genotypes but in an inconsistent manner, with a mismatch response in the ascending paradigm in L6b silenced but not in wildtype animals, and a mismatch response in the descending paradigm in wildtype but not L6b silenced animals. More importantly, changes in adaptation became apparent, with an increase in within paradigm adaptation in L6b silenced animals, but a decrease in between-paradigms adaptation in L6b silenced animals.

Changed adaptation dynamics may reflect changes in the networks that are recruited during adaptation processes. Adaptation is the result of both single stimulus adaptation and repetition suppression, and although these processes have been suggested to co-occur at the same time range after tone onset at the single stimulus level, their influence may vary with different dynamics during a longer time range (Fitzgerald and Todd, 2020). It is conceivable that SSA, regarded as a lower order process, is prominent in the early time scale, and causes a reduced responsiveness to standard tones within the same paradigm in an automatic manner. Repetition suppression, which is a component of the predictive coding framework, and regarded as a higher order process, may on the other hand work at a later time range, and be involved in between paradigm adaptation. A reduction in higher order, between paradigm adaptation in L6b silenced animals might be partially compensated for with an enhanced SSA in lower order neurons in the early time range. In line with this hypothesis, L6b projects to L1, which plays a key role in predictive processing frameworks (Clancy and Cauller, 1999; Ledderose et al., 2023).

An alternative explanation for the changes in adaptation in L6b silenced animals could be that L6b in auditory cortex plays a role in SSA and that this causes compensatory or at least concomitant changes in repetition suppression. Although the underlying mechanisms remain speculative at this point, the current findings do establish a role for L6b in sensory processing and that in itself is a novel finding.

A potential function of L6b in adaptation would align well with a role in wakefulness promotion, since adaptation serves to reduce responsiveness to repeated stimuli to allow enhanced responsiveness to novel stimuli, allowing to detect salient information in the environment.

Apart from the strong connectivity of L6b neurons in motor, somatosensory and visual cortex to near and distant cortical areas (Hoerder-Suabedissen et al., 2018), L6b neurons in entorhinal cortex have been reported to project to hippocampus (Ben-Simon et al., 2022). Silencing these L6b-hippocampus connections results in behavioural impairments, suggesting functional importance (Ben-Simon et al., 2022).

The integrative connectivity of L6b allows it to combine information on context, past experience, and from other modalities and in this way set the scene for the perception of new information. Disruptions in this network could lead to dysfunctional integration relevant to neuropsychiatric diseases.

6.7 Clinical implications

The L6b silenced mouse (Drd1a-Cre:Snap25$^{fl/fl}$) is a model of chronic silencing of a subpopulation of L6b from shortly after birth (Hoerder-Suabedissen et al., 2018), and not an acute functional disruption of L6b, which limits the degree to which conclusions can be drawn on the function of L6b. On the other hand, chronic silencing of L6b could potentially be a suitable way to model neuropsychiatric disease, which are often a result of subtle changes in neurodevelopment resultant rewiring of circuits that have chronic effects on the activity of the brain.

Naturally, since this study involved orexin, its results could open up new possibilities for investigation of narcolepsy. Narcolepsy is the result of insufficient orexin signalling, probably from an autoimmune process targeting orexin neurons, and narcolepsy patients suffer from pathological intrusions of REM sleep and/or NREM sleep into wakefulness, and fragmentation of sleep and wakefulness (Sakurai, 2007). Importantly, many narcolepsy patients suffer from daytime sleepiness, hypersomnolence and inability to focus, which could be explained as a result of a lack of consolidated sleep during the night but could also be a direct result of impaired executive network function because of impaired orexin signalling in the cortex (Lambe and Aghajanian, 2003; Lambe et al., 2005; Naumann et al., 2001; Rieger et al., 2003).

The finding that mice with chronic silencing of L6b have a change in theta-frequency oscillations, the hallmark of exploratory wakefulness, suggests that orexin may have a direct effect on cortex. This could be an explanation for the problems with focused attention that narcolepsy patients suffer from, alternative than linking this straight to a lack of sleep. However, such an effect of orexin on cortex may not exclusively be mediated through L6b since it has been shown in prefrontal cortex that also L2/3 and L5 neurons can be activated by orexin (Lambe and

Aghajanian, 2003; Li et al., 2010; Song et al., 2006; Xia et al., 2005; Yan et al., 2012b). More research is needed to investigate how these effects combine and whether there are differential roles of OX1R signalling, which is mostly expressed in prefrontal cortex, and orexin 2 receptor OX2R signalling, which seems more important in other cortical areas studied so far (Bayer et al., 2004; Marcus et al., 2001).

In L6b silenced animals, orexin caused a more robust prolongation of wakefulness, which can be explained as a statistical artefact, a differential role of different cell types, or a change in network connectivity by compensatory modelling in the chronic absence of a functional Drd1a subpopulation of L6b neurons. Changes in network wiring could underpin neurodevelopmental disorders, such as autism spectrum disorder (ASD) and schizophrenia. Notably, in both ASD and schizophrenia, subtle histopathological abnormalities have been found in the human homologue of L6b, interstitial white matter neurons, and sleep-wake symptoms such as insomnia are also common (Bailey et al., 1998; Casanova, 2015; Duchatel et al., 2019; Miano and Ferri, 2010; Waite et al., 2016). These histopathological studies should be continued with more specific markers of subpopulations of interstitial white matter cell populations and also explore possible areal differences. In vitro recording experiments from human interstitial white matter cells confirmed orexin responsiveness (Zolnik et al., unpublished observations). The increased wake promotion by orexin in L6b silenced mice might reflect neurobiological mechanisms leading to insomnia in such disorders, and perhaps also in other neuropsychiatric disorders such as anxiety and mood disorders, i.e., chronic L6b silencing might result in network changes that infer an increased sensitivity to an elevated orexin tone disrupting the onset of sleep.

There was also an overall reduction in P1-N1 amplitude and adaptation between paradigms seemed impaired in L6b silenced animals, which could reflect changes in auditory gating. Auditory gating abnormalities have been described for multiple neuropsychiatric disorders (Adler et al., 1982; Boutros et al., 2004; Shelley et al., 1999; Siegel et al., 1984). Gating deficits in schizophrenia have been correlated with NMDA receptor signalling and the auditory mismatch response is dependent on NMDA receptor signalling too (Shelley et al., 1999). Recent

in vitro electrophysiology findings showed that L6b triggers spikes in the apical tuft dendrites of L5 neuron in L1, and that this effect is NMDA receptor dependent (Zolnik et al., 2023, in review). This makes the link between L6b and perceptual inference even more interesting. Although in my oddball experiment, a mismatch response was not obviously elicited in either genotype, this would be an interesting starting question for future research.

Could knowledge on L6b have any therapeutical consequences? If orexin signalling in the cortex is a component of any disease, this needs to be further identified, to obtain the desired therapeutical effects more effectively, or to reduce the occurrence of undesired side effects. For instance, if the cortical effects of orexin are involved in insomnia and anxiety/panic disorders (Flores et al., 2015), selective inhibition of orexin signalling in L6b could potentially reduce these symptoms without disrupting the other effects of orexin, which are crucial for homeostasis, such as sleep-wake regulation and appetite regulation. The other way around, if cortical effects of orexin are the basis of attention problems in narcolepsy patients, more targeted stimulation orexin receptors in the cortex may contribute to more focused attention during the daytime, reducing the burden of disease not only in the realm of psychosocial wellbeing but also in socioeconomic participation.

6.8 Future directions

The findings in this study open many new questions and potential routes of future research. In this last section, I offer some suggestions that would be interesting to further explore.

In my experiments, oscillatory changes in L6b silenced mice became apparent, and it would be interesting to investigate the functional consequences of these changes. I proposed that the reduction in theta power in wakefulness is correlated with a reduction in active, exploratory wakefulness, but based on observation I cannot confirm that the L6b silenced mice are behaviourally different from their wildtype littermates. Would they perform differently in attention tests? In pre pulse inhibition tests? Previous efforts have indicated that L6b silencing causes a reduction in anxiety-like behaviour, and this would be consistent with a vigilance-

promoting role of L6b (Guidi et al., 2016). Further behavioural examination is important to assess if chronic silencing of L6b can be an endophenotype of certain neurodevelopmental disorders or is rather a general altered network development not related to any disease or symptom in particular.

It would also be important to further characterise the functional role of different cell types in L6b, historically known as a heterogenous cortical layer. It has been shown that orexin can activate both pyramidal neurons and interneurons in L6b (Bayer et al., 2004; Wenger Combremont et al., 2016b, 2016a) but it needs to be established what the functional consequences are of activation of these different cell types. Moreover, it would be interesting to investigate the dynamics between L6b activity and glia cells. In chronically L5 silenced models (Rbp4-Cre:Snap25fl/fl), changes in astrocytes, microglia and PV+ Gabaergic neurons were observed and changes may occur after L6b silencing as well (Vadisiute et al., 2022).

Not only is it plausible that different cell types in L6b have different functional roles, also could L6b have different effects in different cortical areas and the contribution of L6b might show regional differences, based on differences in connectivity and in how many L6b neurons are present. This is a question that warrants further investigation.

A way to start an investigation of local differences in the role of L6b could be to acutely or sub acutely stimulate or inhibit L6b in specific cortical areas by optogenetics or chemogenetics. Not only could this shed light on the role of specific areas but also on the effects of acute manipulation of L6b, rather than chronic changes in network connectivity that may have led to adaptive remodelling in the chronically L6b silenced mice.

A general side note to the interpretation of findings in the L6b silenced mouse model is that the Cre-dependent functional ablation of Snap25 leads to deficits in synaptic transmission but could also have other cellular effects. Snap25 is also involved in processes like endocytosis, so these processes could be affected too, and result in changes in local network function (Vadisiute et al., 2022). Comparing results between chronic silencing through selective Snap25 ablation and silencing L6b neurons through optogenetics or chemogenetics could give insights

into the relative contribution of other cellular processes to the phenotype observed. Chemogenetic manipulation of the L5-Rbp4 subpopulation in mice results in considerable changes in microglia, astrocytes, and interneurons 90 minutes after CNO administration and it would be interesting to investigate whether similar changes occur when L6b subpopulations are manipulated (Vadisiute et al, submitted).

Silencing or activating L6b, chronically or acutely can all be applied to investigate the function of L6b but arguably it will be unphysiological, and caution is warranted with interpreting the results. Ideally, L6b activity would be explored in a more naturalistic environment, where manipulation is as limited as possible. In general, this is difficult to achieve for the investigation of cortical subpopulations and specifically for L6b it is challenging because of its anatomical location at the bottom of the cortex. With the development of newer models of recording probes and analytical software, this might be a possibility in future research.

It would be important to address a major drawback in this study in future research, the exclusive use of male animals. L6b activity may vary considerably across sexes, especially because it can be activated by various neuromodulatory influences that can vary between sexes, and because there are differences in sex-dependent incidence and presentation of neuropsychiatric disorders that may relate to L6b function (Li et al., 2022; Werling and Geschwind, 2013).

Since L6b or its human counterpart me be involved particularly in higher order cognition, it would be beneficial to also explore the role of these cells in humans. Psychological research allows more controlled levels of attention and can further explore executive and emotional effects that are not straightforward to model in mice. To correlate such outcome measures with L6b activity, options should be explored to identify proxies of L6b activity, such as quantification of L6b thickness in imaging modalities like MRI and extraction of L6b multi-unit activity from local probe recordings in patients who have a probe implanted for a medical indication such as finding the foci of medication-resistant epileptic seizures.

Once more experimental evidence is obtained on the local and global network connectivity of L6b, and functional roles of different cell types in L6b, in silico approaches could

be employed to combine the information obtained from experimental studies and model the effects of experimental findings into a putative framework of L6b actions.

6.9 Conclusion

Layer 6b is a cortical layer at the bottom of the cortex that is found in many species yet is ignored in many aspects of cortical processing since its functional role is not clearly established. The findings in this study suggest that L6b has a role in sleep-wake regulation and in adaptation mechanisms in sensory processing and that there is a functional link between orexin signalling and L6b. L6b may have multiple functions, dependent on cellular subtype, cortical area, sex, and context and some of these functions may be disrupted in neuropsychiatric diseases. The current findings open up many new questions and with further research, the role, or roles, of L6b in brain state regulation can be further understood and help to ultimately establish the position of L6b in schemes of cortical processing.

Appendix

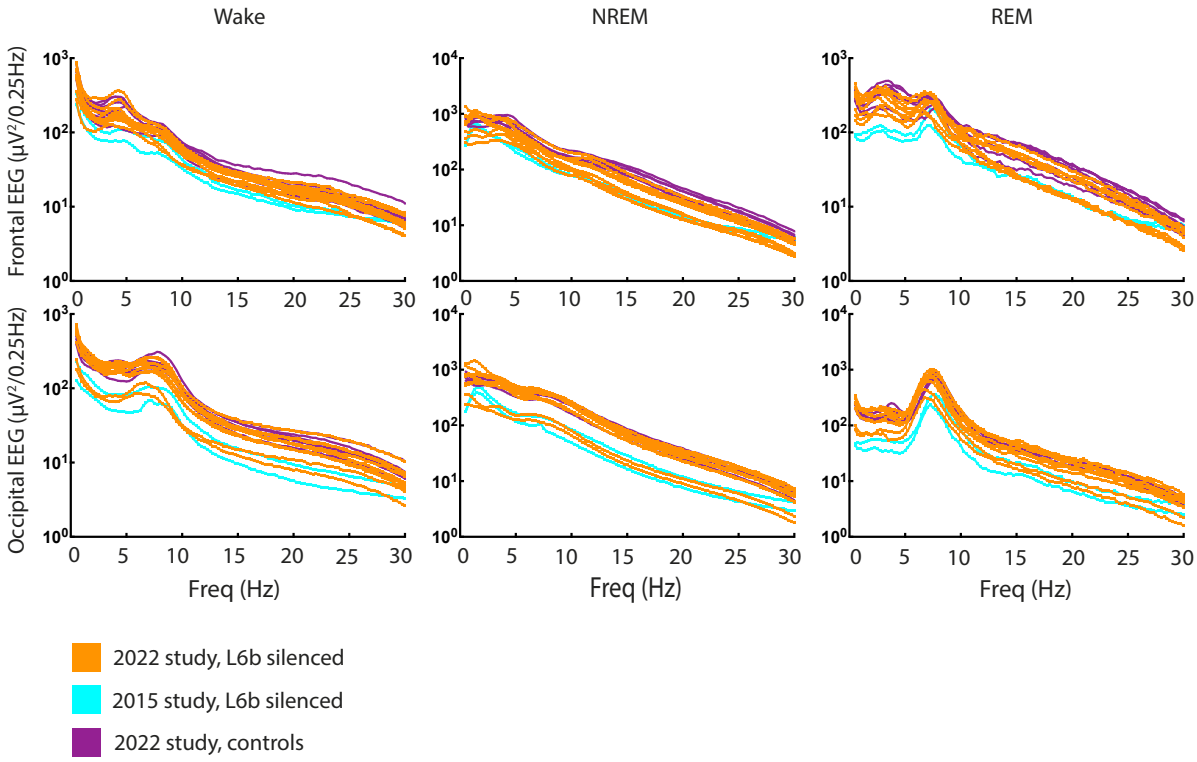

Supplementary Figure S3.1: Comparison of current data with pilot data. Fast Fourier transforms were exported for the frontal and occipital EEG from SleepSign and averaged across epochs scored as artefact free wakefulness, NREM sleep or REM sleep. For the pilot study (2015), only data from L6b silenced animals (n=2) was available. For the current study (2022), the group consistent of L6b silenced animals (n=9) and control animals (n=7).
The 2015 pilot study was performed by Associate Professor Tomoko Yamagata.

Supplementary Table S3.1 Comparison of current data with pilot data

	Cohort		Frequency x Cohort	
	F(DFn,DFd)	p	F(DFn,DFd)	p
Frontal EEG				
Wake	F(1,9)=9.122	0.0145	F(118,1062)=2.459	<0.0001
NREM	F(1,9)=1.873	0.2043	F(118,1062)=5.575	<0.0001
REM	F(1,9)=3.723	0.0857	F(118,1062)=9.843	<0.0001
Occipital EEG				
Wake	F(1,9)=5.604	0.0421	F(118,1062)=3.474	<0.0001
NREM	F(1,9)=4.423	0.0648	F(118,1062)=11.02	<0.0001
REM	F(1,9)=6.761	0.0287	F(118,1062)=11.74	<0.0001

All comparisons are made between L6b silenced animals from pilot study (n=2) and L6b silenced animals from current study (n=9). Statistical testing was performed on log transformed spectra in GraphPad Prism v10. Comparisons were tested with 2-way ANOVA, with Geisser-Greenhouse correction applied.

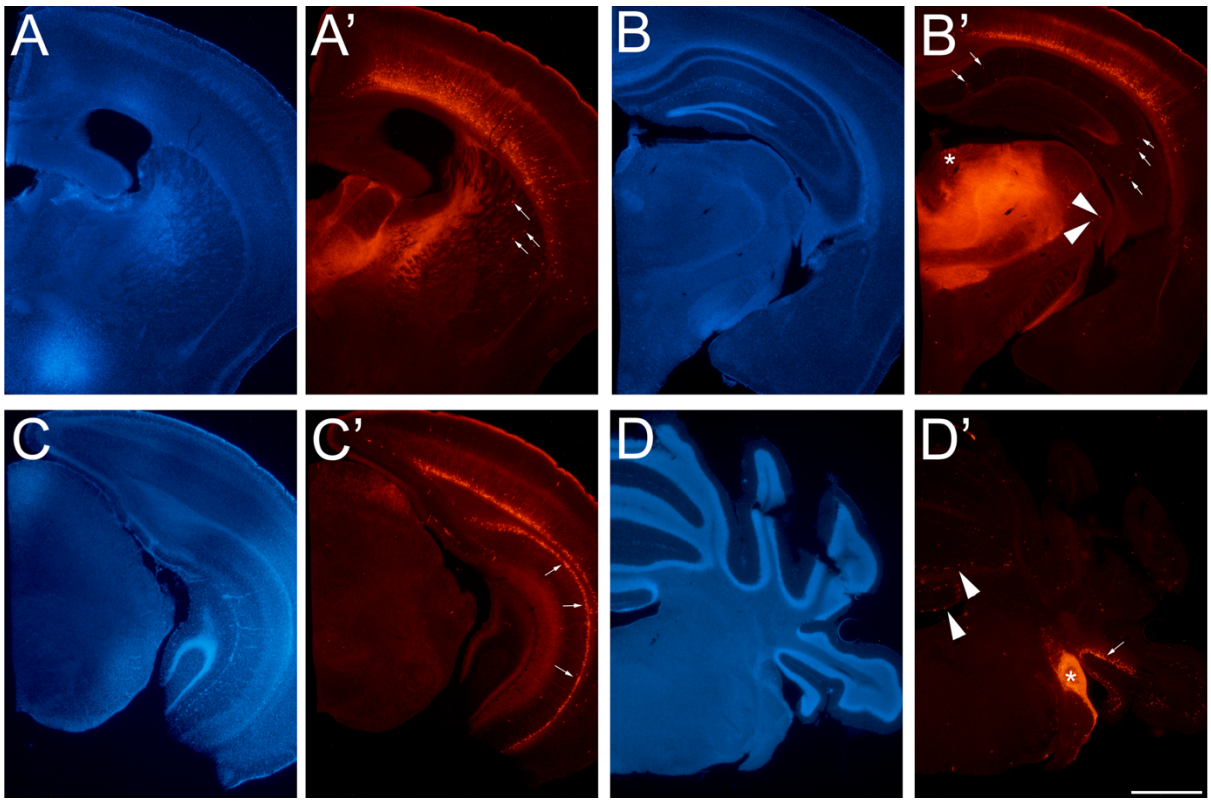

Supplementary Figure S3.2: Subcortical Cre expression in the Drd1a-Cre driver line.
Cre expression in adult Drd1a-Cre;Ai14+ mice, the same Drd1a-Cre line that was used in my study. Cre expressing cells are visualised by expression of TdTom+.
(A,A') Scattered TdTom+ cells in striatum.
(B,B') Scattered TdTom+ cells in hippocampus (arrows), ventral lateral geniculate nucleus (arrowheads). Denser TdTom+ cells in medial pretectal area (asterisk).
(C,C') More caudally, TdTom+ cells are more numerous in subicular pyramidal layer and pyramidal layer of the hippocampus (arrows).
(D,D') Dense TdTom+ cells in dorsal cochlear nucleus (asterisk), scattered cells in flocculus (arrows) and granular layer (arrowheads).
Scale bar = 1 mm.

Reproduced from Hoerder-Suabedissen et al. 2018

VEHICLE				
	Wake1	Wake2	NREM	REM
F1	64	0	1400	338
F2	181	0	1145	86
G1	199	0	1793	247
G2	172	207	1683	237
G3	61	127	1622	272
H1	10	0	1713	304
H2	194	671	2097	354
H3	0	271	1652	281
H4	147	290	1867	327
I1	55	0	2262	175
I2	108	131	1647	267
I3	30	428	1941	287
I4	62	16	1634	317

Control
L6b silenced

ORXA low				
	Wake1	Wake2	NREM	REM
F1	53	485	1922	223
F2	315	861	1801	245
G1	182	553	1908	198
G2	169	574	1767	202
G3	43	879	1869	154
H1	19	813	1689	242
H2	152	1226	2056	281
H3	195	312*	1880	215
H4	202	446	1981	219
I1	242	1413	1845	244
I2	0	739	1911	277
I3	128	581	1874	292
I4	182	676	1961	241

Included
Included, despite epochs <150
Excluded, epochs <150
Excluded, technical issue

*Third control animal (H3): has a very clear delta peak – maybe some NREM accidentally scored as wakefulness. Excluded this animal for this reason.

ORXA high				
	Wake1	Wake2	NREM	REM
F1	77	896	1683	208
F2	171	1650	1512	251
G1	193	1333	1607	223
G2	214	1071	1853	169
G3	9	445	1983	217
H1	116	797	1558	194
H2	69	1359	1927	349
H3	176	615	1769	337
H4	232	986	2190	164
I1	184	607	1681	192
I2	135	1323	1835	239
I3	172	959	1913	225
I4	7	809	1851	276

ORXB				
	Wake1	Wake2	NREM	REM
F1	280	0	1714	318
F2	57	701	1916	300
G1	185	0	1627	96
G2	203	38	1761	155
G3	8	225	1750	143
H1	51	67	1744	29
H2	68	304	1780	390
H3	200	260	1685	388
H4	89	251	1719	317
I1	158	440	1946	321
I2	200	412	1798	322
I3	102	212	1863	332
I4	146	227	1809	249

Control
L6b silenced

Included
Included, despite epochs <150
Excluded, epochs <150
Excluded, technical issue

Table S4.1: epochs contributing to spectral power calculations within the defined time frames.
F1-I4 are animal names. Epochs are shown for individual animals. The colour of the first column reflects the genotype of the animal. The numbers in the columns 'Wake 1', 'Wake 2', 'NREM', and 'REM' indicate how many 4s-epochs occur within that state in the defined time frame and contribute to the spectral power. The colour reflects the reason for exclusion, with none: included, red: excluded because there are too few epochs, orange: just below the 150-epoch cut-off, included after careful examination of spectrum and recording notes, blue: excluded for technical reasons.

(A) After vehicle infusion (saline).
(B) After the lower dose of ORXA (0.3 nmol).
(C) After the higher dose of ORXA (0.6 nmol).
(D) After ORXB (0.6 nmol).

Note, for wakefulness, for the vehicle spectra within the time frames 'Wake 1' and 'Wake 2', many animals needed to be excluded. Therefore, these are not used, and comparisons and normalisation were performed with 24-hour vehicle spectra instead. The vehicle spectra for the time frames 'NREM' and 'REM' are used, which leads to exclusion of L6b silenced animal 'F2' from REM spectral power comparisons and normalisations.

	Treatment effect		Frequency x Treatment		Post-hoc significant bins (Hz)
	F(DFn,DFd)	p	F(DFn,DFd)	p	
Wake 1					
Frontal					
ORXA 0.3 (n=3)	F (1.000, 2.000) = 26.30	P=0.0360	F (1.620, 3.240) = 1.827	P=0.2862	0.75-1.25, 11-11.5,11.75-16.25, 17.5-18.75,20.25-20.75,22.5-23.75
ORXA 0.6 (n=3)	F (1.000, 2.000) = 1964	P=0.0005	F (1.471, 2.942) = 0.7796	P=0.4964	10.5-15.5,16-16.5,17-17.75, 18.75-20.25,20.75-21.5
ORXB (n=3)	F (1.000, 2.000) = 0.2982	P=0.6398	F (1.602, 3.205) = 1.507	P=0.3332	12.5-13,23.25-23.75
Occipital					
ORXA 0.3 (n=3)	F (1.000, 2.000) = 2.007	P=0.2923	F (1.738, 3.475) = 1.549	P=0.3234	29-29.5
ORXA 0.6 (n=3)	F (1.000, 2.000) = 1.835	P=0.3083	F (1.601, 3.201) = 2.494	P=0.2185	27.5-28.25
ORXB (n=3)	F (1.000, 2.000) = 4.420	P=0.1702	F (1.493, 2.985) = 2.589	P=0.2171	25.75-26.5,29.75-30
Wake 2					
Frontal					
ORXA 0.3 (n=5)	F (1.000, 4.000) = 0.7671	P=0.4306	F (1.993, 7.971) = 2.216	P=0.1717	15-15.5
ORXA 0.6 (n=5)	F (1.000, 4.000) = 3.556	P=0.1324	F (2.520, 10.08) = 1.118	P=0.3778	12.75-14.25,16-16.75,18-18.75
ORXB (n=3)	F (1.000, 2.000) = 0.3953	P=0.5938	F (1.353, 2.707) = 3.335	P=0.1809	9-10.5,13.5-14.5,14.75-15.75,17-17.5,21.5-22.5,28.75-29.25
Occipital					
ORXA 0.3 (n=5)	F (1.000, 4.000) = 3.466	P=0.1361	F (1.966, 7.864) = 1.137	P=0.3674	2.0-2.5,2.75-3.25, 25.5-26.25,26.75-27.5,27.75-28.75,29-30
ORXA 0.6 (n=5)	F (1.000, 4.000) = 0.7879	P=0.4249	F (2.049, 8.195) = 1.421	P=0.2959	-
ORXB (n=3)	F (1.000, 2.000) = 4.128	P=0.1792	F (1.655, 3.309) = 5.322	P=0.0937	3.0-3.5,4.0-4.5,14.25-15,16.5-17,26.5-27
NREM					
Frontal					
ORXA 0.3 (n=5)	F (1.000, 4.000) = 5.561	P=0.0778	F (2.024, 8.095) = 1.563	P=0.2670	4.75-8.75,28.5-29.5
ORXA 0.6 (n=5)	F (1.000, 4.000) = 15.52	P=0.0170	F (3.317, 13.27) = 3.385	P=0.0469	4.0-9.5,10.5-11.5,12-12.5,14.5-15.5,15.75-18.75,19.25-26,26.75-30

ORXB (n=5)	F (1.000, 4.000) = 32.69	P=0.0046	F (2.275, 9.098) = 3.525	P=0.0696	4.5-9.5,13.25-14,14.5-16.25,16.75-25.0,25.5-26,26.75-27.25,28.5-30
Occipital					
ORXA 0.3 (n=5)	F (1.000, 4.000) = 6.394	P=0.0648	F (3.525, 14.10) = 3.490	P=0.0390	11-11.5,12.25-13.25,15-15.5,18.5-19.75,20-20.5,23.5-30
ORXA 0.6 (n=5)	F (1.000, 4.000) = 3.882	P=0.1201	F (2.955, 11.82) = 1.529	P=0.2583	3.75-4.75,29.25-29.75
ORXB (n=5)	F (1.000, 4.000) = 6.142	P=0.0683	F (2.767, 11.07) = 5.652	P=0.0147	1.25-1.75,2.0-2.5,4.5-5.5,9.25-9.75,10.25-15.75,17.5-20.75
REM					
Frontal					
ORXA 0.3 (n=5)	F (1, 8) = 0.01113	P=0.9186	F (118, 944) = 0.6648	P=0.9972	-
ORXA 0.6 (n=5)	F (1, 8) = 0.06660	P=0.8029	F (118, 944) = 0.6684	P=0.9968	-
ORXB (n=5)	F (1, 8) = 0.04837	P=0.8314	F (118, 944) = 1.698	P<0.0001	-
Occipital					
ORXA 0.3 (n=5)	F (1, 8) = 0.1742	P=0.6874	F (118, 944) = 0.3552	P>0.9999	-
ORXA 0.6 (n=5)	F (1, 8) = 0.2899	P=0.6049	F (118, 944) = 0.7769	P=0.9584	-
ORXB (n=5)	F (1, 8) = 0.03042	P=0.8659	F (118, 944) = 1.571	P=0.0002	-

Table S4.2: Comparison of absolute log-transformed EEG spectral power in Control animals. Orexin A or orexin B vs vehicle (24h for wakefulness, 3h for NREM and REM).
All spectra were compared with 2-way ANOVA, with Geisser-Greenhouse correction applied, not corrected for multiple comparisons.

	Treatment effect		Frequency x Treatment		Post-hoc significant bins (Hz)
	F(DFn,DFd)	p	F(DFn,DFd)	p	
Wake 1					
Frontal					
ORXA 0.3 (n=4)	F (1.000, 3.000) = 3.104	P=0.1763	F (2.713, 8.139) = 1.340	P=0.3244	4.0-5.0, 19.75-20.5
ORXA 0.6 (n=4)	F (1.000, 3.000) = 15.52	P=0.0291	F (2.263, 6.788) = 2.374	P=0.1635	4.0-4.75,10-10.5,11-18.75,19.25-20.5,23.25-23.75
ORXB (n=3)	F (1.000, 2.000) = 0.9014	P=0.4426	F (1.839, 3.678) = 0.9149	P=0.4671	-
Occipital					
ORXA 0.3 (n=4)	F (1.000, 3.000) = 12.36	P=0.0390	F (2.589, 7.768) = 3.224	P=0.0884	6.5-7.75,19.25-20.25,20.75-23,23.75-30
ORXA 0.6 (n=4)	F (1.000, 3.000) = 65.71	P=0.0039	F (2.026, 6.077) = 3.836	P=0.0834	1-1.75,6.5-8.0,16.5-21.5,21.75-30
ORXB (n=3)	F (1.000, 2.000) = 6.518	P=0.1252	F (1.694, 3.388) = 0.6347	P=0.5594	6.5-7.5,21-21.5,25.5-26
Wake 2					
Frontal					
ORXA 0.3 (n=8)	F (1.000, 7.000) = 23.73	P=0.0018	F (2.847, 19.93) = 9.498	P=0.0005	3.75-5.75,7.75-8.75,10-26
ORXA 0.6 (n=8)	F (1.000, 7.000) = 23.53	P=0.0019	F (3.845, 26.91) = 8.552	P=0.0002	2-6,9.75-23.25
ORXB (n=6)	F (1.000, 5.000) = 2.476	P=0.1764	F (2.270, 11.35) = 4.037	P=0.0435	3.5-4.0,4.75-5.25,7.0-9.0,11.5-19.5,20.5-21
Occipital					
ORXA 0.3 (n=8)	F (1.000, 7.000) = 0.9950	P=0.3518	F (3.503, 24.52) = 8.247	P=0.0004	4.0-6.0,7.25-8.75,10.75-13.25,21.25-22,22.5-30
ORXA 0.6 (n=8)	F (1.000, 7.000) = 0.4765	P=0.5122	F (3.447, 24.13) = 7.666	P=0.0006	3.25-4.0,4.5-6.5,7.25-8.0,9.75-16,20.75-30
ORXB (n=6)	F (1.000, 5.000) = 5.286	P=0.0698	F (1.921, 9.605) = 3.054	P=0.0953	3.5-4.0,7-9.25,23.5-24,24.5-25,27.25-30
NREM					
Frontal					
ORXA 0.3 (n=8)	F (1.000, 7.000) = 14.91	P=0.0062	F (4.227, 29.59) = 1.200	P=0.3322	1.75-2.25,4.0-4.5,7.75-10.5,12-30
ORXA 0.6 (n=8)	F (1.000, 7.000) = 13.08	P=0.0085	F (5.023, 35.16) = 1.928	P=0.1141	1.5-5.0,8.25-10.25,12.5-30

ORXB (n=8)	F (1.000, 7.000) = 7.761	P=0.0271	F (1.396, 9.775) = 2.945	P=0.1103	4.0-10,13.50-21.75
Occipital					
ORXA 0.3 (n=8)	F (1.000, 7.000) = 15.20	P=0.0059	F (3.768, 26.37) = 2.259	P=0.0929	4.0-6.25,8.5-23.5,25-30
ORXA 0.6 (n=8)	F (1.000, 7.000) = 27.61	P=0.0012	F (4.066, 28.46) = 1.461	P=0.2396	1.5-7.25,8.5-30
ORXB (n=8)	F (1.000, 7.000) = 4.313	P=0.0765	F (1.484, 10.39) = 2.236	P=0.1615	4.0-5.25,11.25-19
REM					
Frontal					
ORXA 0.3 (n=7)	F (1, 13) = 0.009503	P=0.9238	F (118, 1534) = 0.6515	P=0.9984	-
ORXA 0.6 (n=7)	F (1, 13) = 0.003023	P=0.9570	F (118, 1534) = 1.148	P=0.1403	-
ORXB (n=4)	F (1, 9) = 0.003456	P=0.9544	F (118, 1062) = 1.833	P<0.0001	-
Occipital					
ORXA 0.3 (n=7)	F (1, 13) = 0.2237	P=0.6441	F (118, 1534) = 0.7817	P=0.9573	-
ORXA 0.6 (n=7)	F (1, 13) = 0.07275	P=0.7916	F (118, 1534) = 2.532	P<0.0001	-
ORXB (n=4)	F (1, 9) = 0.4433	P=0.9758	F (118, 1062) = 1.586	P=0.0002	-

Table S4.3: Comparison of absolute EEG spectral power in L6b silenced animals
Orexin A or orexin B vs vehicle (24h for wakefulness, 3h for NREM and REM).
All spectra were compared with 2-way ANOVA, with Geisser-Greenhouse correction applied, not corrected for multiple comparisons.

	CTL n=	L6b n=	Genotype effect		Frequency x Genotype		Post-hoc significant bins (Hz)
Wake 1			F(DFn, DFd)	p	F(DFn, DFd)	p	
Frontal							
ORXA 0.3	2	4	F (1, 4) = 2.137	0.2176	F (118, 472) = 2.113	<0.0001	2.0-2.5 29.25-29.75
ORXA 0.6	3	4	F (1, 5) = 3.417	0.1238	F (118, 590) = 0.8091	0.9218	17-17.5
ORXB	3	2	F (1, 3) = 0.003232	0.9582	F (118, 354) = 0.9174	0.7066	14.5-15, 29-29.5
Occipital							
ORXA 0.3	2	4	F (1, 4) = 0.2218	0.6622	F (118, 472) = 1.364	0.0130	-
ORXA 0.6	3	4	F (1, 5) = 0.06636	0.8070	F (118, 590) = 1.252	0.0501	-
ORXB	3	2	F (1, 3) = 0.6076	0.4925	F (118, 354) = 0.5647	0.9998	-
Wake 2							
Frontal							
ORXA 0.3	4	8	F (1, 10) = 2.170	0.1715	F (118, 1180) = 0.9953	0.4990	2.00-2.75
ORXA 0.6	5	8	F (1, 11) = 0.02616	0.8744	F (118, 1298) = 1.812	<0.0001	-
ORXB	3	6	F (1, 7) = 1.324	0.2877	F (116, 812) = 1.192	0.0949	10.75-11.75
Occipital							
ORXA 0.3	4	8	F (1, 10) = 3.567	0.0882	F (118, 1180) = 0.9064	0.7495	2.0-2.5
ORXA 0.6	5	8	F (1, 11) = 1.338	0.2718	F (117, 1287) = 1.462	0.0015	-
ORXB*	3	6	F (1, 7) = 0.4591	0.5198	F (118, 822) = 1.841	<0.0001	14.25-15.0
NREM							
Frontal							
ORXA 0.3	5	8	F (1, 11) = 0.2868	0.6029	F (118, 1298) = 1.086	0.2572	-
ORXA 0.6	5	8	F (1, 11) = 0.002342	0.9623	F (118, 1298) = 2.017	<0.0001	0.75-1.25, 1.5-2.75
ORXB	5	7	F (1, 10) = 0.3541	0.5650	F (118, 1180) = 1.320	0.0158	2.5-3.0
Occipital							
ORXA 0.3	5	8	F (1, 11) = 0.1066	0.7502	F (118, 1298) = 0.6286	0.9992	-
ORXA 0.6	5	8	F (1, 11) = 0.02265	0.8831	F (118, 1298) = 0.6505	0.9984	-
ORXB	5	7	F (1, 10) = 0.5589	0.4719	F (118, 1180) = 1.397	0.0047	2.25-2.75
REM							
Frontal							
ORXA 0.3	5	7	F (1, 10) = 0.009936	0.9226	F (118, 1180) = 0.8085	0.9298	-

ORXA 0.6	5	7	F (1, 10) = 0.5156	0.4892	F (118, 1180) = 0.6911	0.9944	-
ORXB	5	4	F (1, 7) = 0.9620	0.3594	F (118, 826) = 0.8623	0.8436	3.0-3.5
Occipital							
ORXA 0.3	5	7	F (1, 10) = 0.08122	0.7815	F (118, 1180) = 0.6987	0.9931	-
ORXA 0.6	5	7	F (1, 10) = 0.3620	0.5608	F (118, 1180) = 0.6782	0.9961	-
ORXB	5	4	F (1, 7) = 0.05951	0.8143	F (118, 826) = 0.4978	>0.9999	-

Table S4.4: Comparison of relative EEG spectral power between L6b silenced and control animals.

All spectra were compared with 2-way ANOVA except for ORXB Wake 2 occipital (*), which was compared with a Mixed Analysis because for some animals, artefacts in the lower frequencies extended to 0.75 Hz or 1.0 Hz – exclusion of those bins in selected animals resulted to 'missing data'.

For all comparisons, Geisser-Greenhouse correction was applied, no correction for multiple comparisons was applied for posthoc analyses.

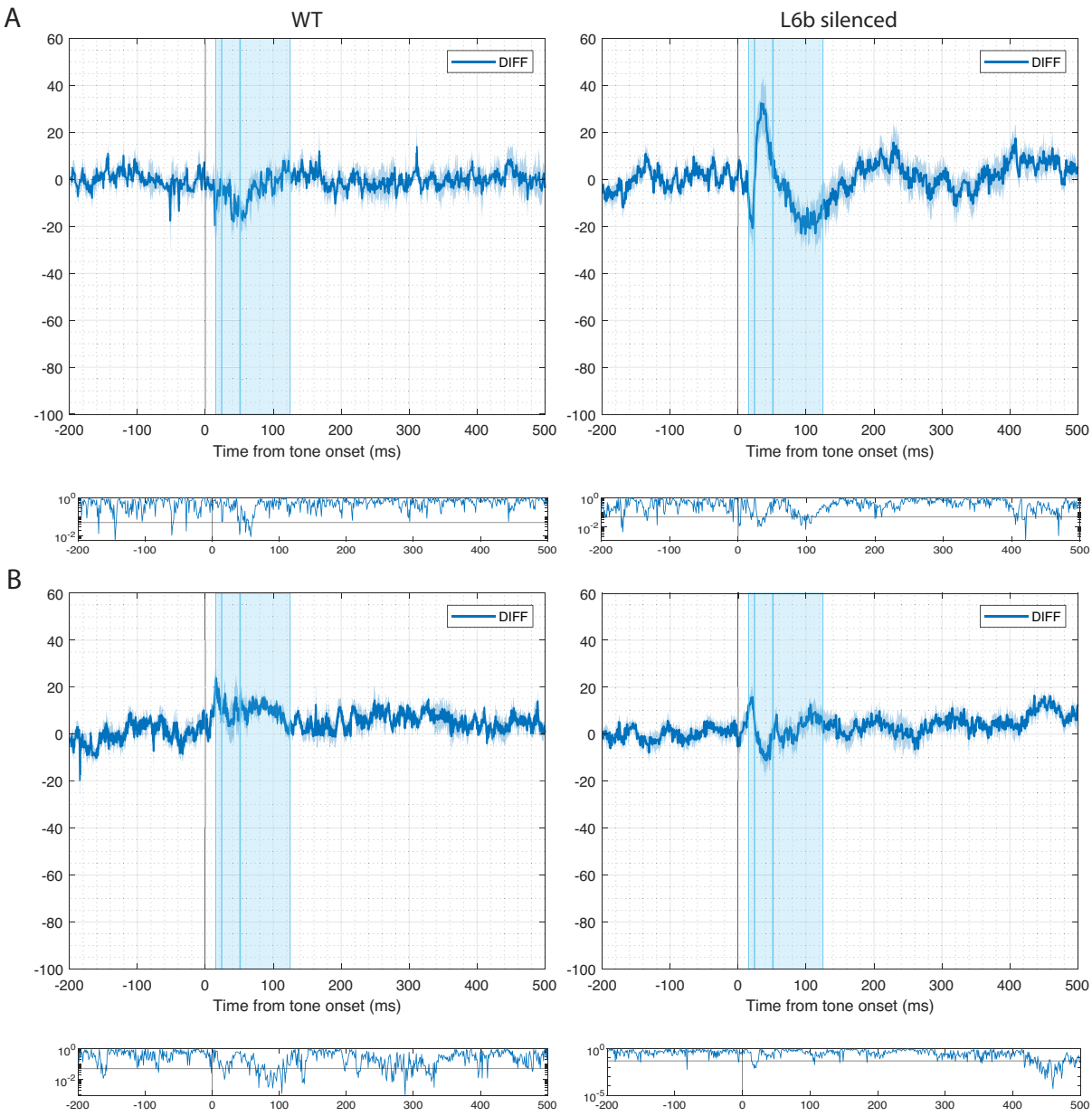

Supplementary Figure S5.1 Difference waves oddball paradigms.
Differences waves are calculated by subtraction of the response to the standard tone from the response to the deviant tone (STD-DEV) for individual animals. Traces show mean ± SEM for genotype groups. The lower graphs show the p values for the comparison of the difference to 0 per sample number with multiple t tests, with the horizontal line indicating p=0.05.
(A) Ascending oddball paradigm ($f_{DEV}>f_{STD}$). Wildtype animals (n=6) show a difference in response in the early phase of N2. L6b silenced animals (n=8) also show this effect but they show and additional increase in P1 and N1 ampltiudes. No clear effect of deviant tone presentation is visible in the time range after P2 in either genotype.
(B) Descending oddball paradigm ($f_{DEV}<f_{STD}$). Wildtype animals (n=6) show a difference in response in the P1 and P2 time ranges. L6b silenced animals (n=7) show a difference in response mostly in the N1 time range. There is no late (after P2) effect of deviant tone presentation in either genotype.

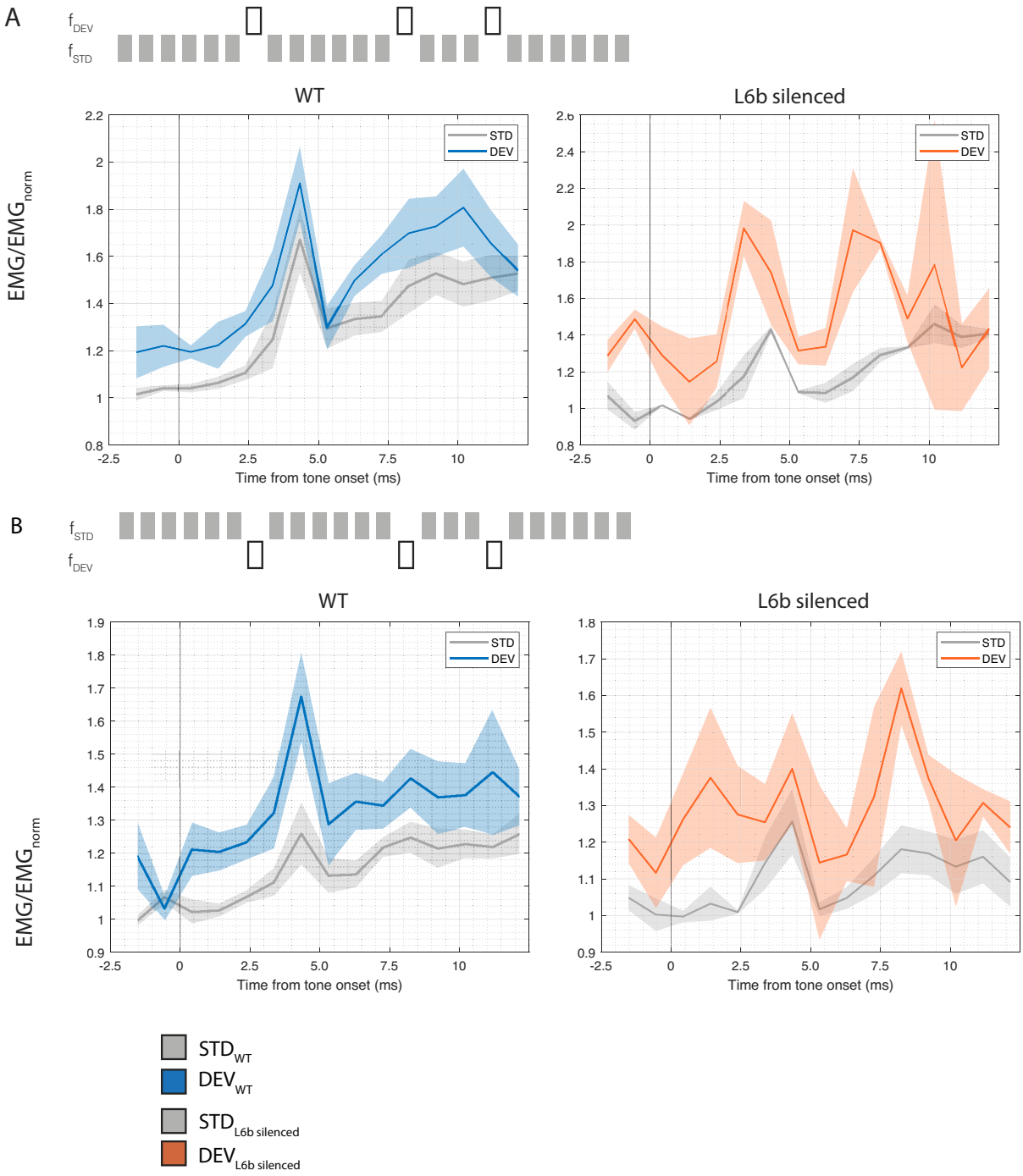

Supplementary Figure S5.2: Acoustic startle response.
(A) Ascending oddball paradigm, EMG responses to deviant tones and standard tones in wildtype and L6b silenced animals.
(B) Descending oddball paradigm, EMG responses to standard and deviant tones.
WT n=7, L6b silenced n=9.
The acoustic startle response seems to appear just before 5ms in WT animals. In L6b silenced animals, a peak appears around the same time, but a peak is less clearly distinguishable because of technical issues with the EMG signals in L6b silenced animals.

Bibliography

1. Achermann, P., and Borbély, A. a (2003). Mathematical models of sleep regulation. Front. Biosci. 683–693.
2. Adamantidis, A., and de Lecea, L. (2009). The hypocretins as sensors for metabolism and arousal. J. Physiol. *587*, 33–40.
3. Adamantidis, A.R., Zhang, F., Aravanis, A.M., Deisseroth, K., and De Lecea, L. (2007). Neural substrates of awakening probed with optogenetic control of hypocretin neurons. Nature *450*, 420–424.
4. Adamantidis, A.R., Gutierrez Herrera, C., and Gent, T.C. (2019). Oscillating circuitries in the sleeping brain. Nat. Rev. Neurosci. *20*, 746–762.
5. Adamantidis, A.R., Schmidt, M.H., Carter, M.E., Burdakov, D., Peyron, C., and Scammell, T.E. (2020). A circuit perspective on narcolepsy. Sleep *43*, 1–9.
6. Adler, L.E., Pachtman, E., Franks, R.D., Pecevich, M., Waldo, M.C., and Freedman, R. (1982). Neurophysiological evidence for a defect in neuronal mechanisms involved in sensory gating in schizophrenia. Biol. Psychiatry *17*, 639–654.
7. Aerde, K.I.V., Qi, G., and Feldmeyer, D. (2015). Cell type-specific effects of adenosine on cortical neurons. Cereb. Cortex *25*, 772–787.
8. Akanmu, M.A., and Honda, K. (2005). Selective stimulation of orexin receptor type 2 promotes wakefulness in freely behaving rats. Brain Res. *1048*, 138–145.
9. Akbarian, S., Kim, J.J., Pothin, S.G., Hetrick, W.P., Bunney, W.E., and Jones, E.G. (1996). Maldistribution of Interstitial neurons in prefrontal white matter of the brains of schizophrenic patients. Arch. Gen. Psychiatry *53*, 425–436.
10. Allendoerfer, K.L., and Shatz, C.J. (1994). The subplate, a transient neocortical structure: Its role in the development of connections between thalamus and cortex. Annu. Rev. Neurosci. *17*, 185–218.
11. Amzica, F., and Steriade, M. (2002). The functional significance of K-complexes. Sleep Med. Rev. *6*, 139–149.
12. Anafi, R.C., Kayser, M.S., and Raizen, D.M. (2019). Exploring phylogeny to find the function of sleep. Nat. Rev. Neurosci. *20*, 109–116.
13. Ansorge, J., Humanes-Valera, D., Pauzin, F.P., Schwarz, M.K., and Krieger, P. (2020). Cortical layer 6 control of sensory responses in higher-order thalamus. J. Physiol. *598*, 3973–4001.
14. Antunes, F.M., and Malmierca, M.S. (2021). Corticothalamic Pathways in Auditory Processing: Recent Advances and Insights From Other Sensory Systems. Front. Neural Circuits *15*, 1–25.
15. Antunes, F.M., Nelken, I., Covey, E., and Malmierca, M.S. (2010). Stimulus-specific adaptation in the auditory thalamus of the anesthetized rat. PLoS One *5*.
16. Arimatsu, Y., Ishida, M., Kaneko, T., Ichinose, S., and Omori, A. (2003). Organization and development of corticocortical associative neurons expressing the orphan nuclear receptor Nurr1. J. Comp. Neurol. *466*, 180–196.
17. Auksztulewicz, R., and Friston, K. (2016). Repetition suppression and its contextual determinants in predictive coding. Cortex *80*, 125–140.
18. Ayala, Y.A., and Malmierca, M.S. (2012). Stimulus-specific adaptation and deviance detection in the inferior colliculus. Front. Neural Circuits *6*, 1–16.
19. Bailey, A., Luthert, P., Dean, A., Harding, B., Janota, I., Montgomery, M., Rutter, M., and Lantos, P. (1998). A clinicopathological study of autism. Brain *121*, 889–905.
20. Bajo, V.M., Rouiller, E.M., Welker, E., Clarke, S., Villa, A.E.P., Ribaupierre, Y. De, and Ribaupierre, F. De (1995). Morphology and spatial distribution of corticothalamic terminals originating from the cat auditory cortex. Hear. Res. *83*, 161–174.
21. Bandarabadi, M., Herrera, C.G., Gent, T.C., Bassetti, C., Schindler, K., and Adamantidis, A.R.

(2020). A role for spindles in the onset of rapid eye movement sleep. Nat. Commun. *11*.
22. Banks, G., Heise, I., Starbuck, B., Osborne, T., Wisby, L., Potter, P., Jackson, I.J., Foster, R.G., Peirson, S.N., and Nolan, P.M. (2015). Genetic background influences age-related decline in visual and nonvisual retinal responses, circadian rhythms, and sleep. Neurobiol. Aging *36*, 380–393.
23. Banks, G.T., Guillaumin, M.C.C., Heise, I., Lau, P., Yin, M., Bourbia, N., Aguilar, C., Bowl, M.R., Esapa, C., Brown, L.A., et al. (2020). Forward genetics identifies a novel sleep mutant with sleep state inertia and REM sleep deficits. Sci. Adv. *6*, 1–13.
24. Bargiello, T.A., Jackson F. R., and Young, M.W. (1984). Restoration of circadian behavioural rhythms by gene transfer in Drosophila bargiello, jackson, young 1984 paper. 8. Stuiver, M. Radiocarb. *301*, 427–430.
25. Bassetti, C.L.A., Adamantidis, A., Burdakov, D., Han, F., Gay, S., Kallweit, U., Khatami, R., Koning, F., Kornum, B.R., Lammers, G.J., et al. (2019). Narcolepsy — clinical spectrum, aetiopathophysiology, diagnosis and treatment. Nat. Rev. Neurol. *15*, 519–539.
26. Bastianini, S., Lo Martire, V., Berteotti, C., Silvani, A., Ohtsu, H., Lin, J.S., and Zoccoli, G. (2016). High-amplitude theta wave bursts characterizing narcoleptic mice and patients are also produced by histamine deficiency in mice. J. Sleep Res. *25*, 591–595.
27. Bastos, A.M., Usrey, W.M., Adams, R.A., Mangun, G.R., Fries, P., and Friston, K.J. (2012). Canonical Microcircuits for Predictive Coding. Neuron *76*, 695–711.
28. Bayer, L., Eggermann, E., Saint-Mleux, B., Machard, D., Jones, B.E., Mühlethaler, M., and Serafin, M. (2002). Selective action of orexin (hypocretin) on nonspecific thalamocortical projection neurons. J. Neurosci. *22*, 7835–7839.
29. Bayer, L., Serafin, M., Eggermann, E., Saint-Mleux, B., Machard, D., Jones, B.E., and Mühlethaler, M. (2004). Exclusive postsynaptic action of hypocretin-orexin on sublayer 6b cortical neurons. J. Neurosci. *24*, 6760–6764.
30. Bazanova, O.M., and Vernon, D. (2014). Interpreting EEG alpha activity. Neurosci. Biobehav. Rev. *44*, 94–110.
31. Beglopoulos, V., Montag-Sallaz, M., Rohlmann, A., Piechotta, K., Ahmad, M., Montag, D., and Missler, M. (2005). Neurexophilin 3 Is Highly Localized in Cortical and Cerebellar Regions and Is Functionally Important for Sensorimotor Gating and Motor Coordination. Mol. Cell. Biol. *25*, 7278–7288.
32. Ben-Simon, Y., Kaefer, K., Velicky, P., Csicsvari, J., Danzl, J.G., and Jonas, P. (2022). A direct excitatory projection from entorhinal layer 6b neurons to the hippocampus contributes to spatial coding and memory. Nat. Commun. *13*.
33. Berger, B. (1991). Dopaminergic Innervation of the Cerebral Cortex: Developmental and Organizational Differences in Primates as Compared to Rodents. In Developmental Neuropathology of Schizophrenia., (Springer), p.
34. Berger, H. (1929). Über das Elektrenkephalogramm des Menschen. Arch. Psychiatr. Nervenkr.
35. Bhagwandin, A., Debipersadh, U., Kaswera-Kyamakya, C., Gilissen, E., Rockland, K.S., Molnár, Z., and Manger, P.R. (2020). Distribution, number, and certain neurochemical identities of infracortical white matter neurons in the brains of three megachiropteran bat species. J. Comp. Neurol. 1–16.
36. Bickel, S., Lipp, H.P., and Umbricht, D. (2008). Early auditory sensory processing deficits in mouse mutants with reduced NMDA receptor function. Neuropsychopharmacology *33*, 1680–1689.
37. Biskamp, J., Bartos, M., and Sauer, J.F. (2017). Organization of prefrontal network activity by respiration-related oscillations. Sci. Rep. *7*, 1–11.
38. Blanco-Duque, C., Bond, S.A., Krone, L.B., Dufour, J.-P., Gillen, E.C.P., Kahn, M.C., Purple, R.J., Bannerman, D.M., Mann, E.O., Achermann, P., et al. (2023). Oscillatory-Quality of sleep spindles: from properties to function. BioRxiv *44*, 2023.06.28.546981.
39. Le Bon-Jego, M., and Yuste, R. (2007). Persistently Active, Pacemaker-Like Neurons in Neocortex. Front. Neurosci. *1*, 123–129.
40. Bonjean, M., Baker, T., Lemieux, M., Timofeev, I., Sejnowski, T., and Bazhenov, M. (2011).

Corticothalamic feedback controls sleep spindle duration in vivo. J. Neurosci. *31*, 9124–9134.
41. Boon, J., Clarke, E., Kessaris, N., Goffinet, A., Molnár, Z., and Hoerder-Suabedissen, A. (2019). Long-range projections from sparse populations of GABAergic neurons in murine subplate. J. Comp. Neurol. *527*, 1610–1620.
42. Borbély, A.A. (1982). A two process model of sleep regulation. Hum. Neurobiol. *1*, 195–204.
43. Borbély, A.A., Daan, S., Wirz-Justice, A., and Deboer, T. (2016). The two-process model of sleep regulation: A reappraisal. J. Sleep Res. *25*, 131–143.
44. Bortone, D.S., Olsen, S.R., and Scanziani, M. (2014). Translaminar inhibitory cells recruited by layer 6 corticothalamic neurons suppress visual cortex. Neuron *82*, 474–485.
45. Bourassa, J., and Deschênes, M. (1995). Corticothalamic projections from the primary visual cortex in rats: a single fiber study using biocytin as an anterograde tracer. Neuroscience *66*, 253–263.
46. Boutros, N.N., Korzyukov, O., Jansen, B., Feingold, A., and Bell, M. (2004). Sensory gating deficits during the mid-latency phase of information processing in medicated schizophrenia patients. Psychiatry Res. *126*, 203–215.
47. Boyce, R., Glasgow, S.D., Williams, S., and Adamantidis, A. (2016). Sleep research: Causal evidence for the role of REM sleep theta rhythm in contextual memory consolidation. Science (80-.). *352*, 812–816.
48. Bragin, A., Jandó, G., Nádasdy, Z., Hetke, J., Wise, K., and Buzsáki, G. (1995). Gamma (40-100 Hz) oscillation in the hippocampus of the behaving rat. J. Neurosci. *15*, 47–60.
49. Bronk, P., Deák, F., Wilson, M.C., Liu, X., Südhof, T.C., and Kavalali, E.T. (2007). Differential effects of SNAP-25 deletion on Ca2+-dependent and Ca2+-independent neurotransmission. J. Neurophysiol. *98*, 794–806.
50. Burdakov, D., Gerasimenko, O., and Verkhratsky, A. (2005). Physiological changes in glucose differentially modulate the excitability of hypothalamic melanin-concentrating hormone and orexin neurons in situ. J. Neurosci. *25*, 2429–2433.
51. Busch, N.A., Dubois, J., and VanRullen, R. (2009). The phase of ongoing EEG oscillations predicts visual perception. J. Neurosci. *29*, 7869–7876.
52. Buszáki, G. (2002). Theta Oscillations in the Hippocampus. Neuron *33*, 1–16.
53. Buzsáki, G., Anastassiou, C.A., and Koch, C. (2012). The origin of extracellular fields and currents-EEG, ECoG, LFP and spikes. Nat. Rev. Neurosci. *13*, 407–420.
54. Bystron, I., Blakemore, C., and Rakic, P. (2008). Development of the human cerebral cortex: Boulder Committee revisited. Nat. Rev. Neurosci. *9*, 110–122.
55. Campbell, S.S., and Tobler, I. (1984). Animal sleep: A review of sleep duration across phylogeny. Neurosci. Biobehav. Rev. *8*, 269–300.
56. Carroll, B.J., Sampathkumar, V., Kasthuri, N., and Sherman, S.M. (2022). Layer 5 of cortex innervates the thalamic reticular nucleus in mice. Proc. Natl. Acad. Sci. U. S. A. *119*, 1–7.
57. Carter, M.E., Adamantidis, A., Ohtsu, H., Deisseroth, K., and De Lecea, L. (2009). Sleep homeostasis modulates hypocretin-mediated sleep-to-wake transitions. J. Neurosci. *29*, 10939–10949.
58. Casado-Román, L., Carbajal, G. V., Pérez-González, D., and Malmierca, M.S. (2020). Prediction error signaling explains neuronal mismatch responses in the medial prefrontal cortex. PLoS Biol. *18*, 1–29.
59. Casanova, M.F. (2015). The neuropathology of autism. Mol. Basis Autism *2012*, 153–171.
60. Case, L., Lyons, D.J., and Broberger, C. (2017). Desynchronization of the rat cortical network and excitation of white matter neurons by neurotensin. Cereb. Cortex *27*, 2671–2685.
61. Chemelli, R.M., Willie, J.T., Sinton, C.M., Elmquist, J.K., Scammell, T., Lee, C., Richardson, J.A., Clay Williams, S., Xiong, Y., Kisanuki, Y., et al. (1999). Narcolepsy in orexin knockout mice: Molecular genetics of sleep regulation. Cell *98*, 437–451.
62. Chi, V.N., Müller, C., Wolfenstetter, T., Yanovsky, Y., Draguhn, A., Tort, A.B.L., and

Brankačk, J. (2016). Hippocampal respiration-driven rhythm distinct from theta oscillations in awake mice. J. Neurosci. *36*, 162–177.
63. Chou, T.C., Bjorkum, A.A., Gaus, S.E., Lu, J., Scammell, T.E., and Saper, C.B. (2002). Afferents to the ventrolateral preoptic nucleus. J. Neurosci. *22*, 977–990.
64. Chung, L., Moore, S.D., and Cox, C.L. (2009). Cholecystokinin action on layer 6b neurons in somatosensory cortex. Brain Res. *1282*, 10–19.
65. Cirelli, C., and Tononi, G. (2008). Is sleep essential? PLoS Biol. *6*, 1605–1611.
66. Clancy, B., and Cauller, L.J. (1999). Widespread projections from subgriseal neurons (layer VII) to layer I in adult rat cortex. J. Comp. Neurol. *407*, 275–286.
67. Colrain, I.M., and Campbell, K.B. (2007). The use of evoked potentials in sleep research. Sleep Med. Rev. *11*, 277–293.
68. Costa-Faidella, J., Baldeweg, T., Grimm, S., and Escera, C. (2011). Interactions between "what" and "when" in the auditory system: Temporal predictability enhances repetition suppression. J. Neurosci. *31*, 18590–18597.
69. Crunelli, V., Cope, D.W., and Hughes, S.W. (2006). Thalamic T-type Ca 2 + channels and NREM sleep. Cell Calcium *40*, 175–190.
70. Csercsa, R., Dombovári, B., Fabó, D., Wittner, L., Erss, L., Entz, L., Sólyom, A., Rásonyi, G., Szcs, A., Kelemen, A., et al. (2010). Laminar analysis of slow wave activity in humans. Brain *133*, 2814–2829.
71. Daan, S., Beersma, D.G.M., and Borbely, A.A. (1984). Timing of human sleep: Recovery process gated by a circadian pacemaker. Am. J. Physiol. - Regul. Integr. Comp. Physiol. *15*.
72. Dagani, F., and D'Angelo, E. (1992). Glutamate metabolism, release, and quantal transmission at central excitatory synapses: implications for neural plasticity. Funct Neurol. *7*, 315–336.
73. Dauvilliers, Y., Mignot, E., del Río Villegas, R., Du, Y., Hanson, E., Inoue, Y., Kadali, H., Koundourakis, E., Meyer, S., Rogers, R., et al. (2023). Oral Orexin Receptor 2 Agonist in Narcolepsy Type 1. N. Engl. J. Med. *389*, 309–321.
74. David, F., Schmiedt, J.T., Taylor, H.L., Orban, G., Di Giovanni, G., Uebele, V.N., Renger, J.J., Lambert, R.C., Leresche, N., and Crunelli, V. (2013). Essential thalamic contribution to slow waves of natural sleep. J. Neurosci. *33*, 19599–19610.
75. Debener, S., Kranczioch, C., Herrmann, C.S., and Engel, A.K. (2002). Auditory novelty oddball allows reliable distinction of top-down and bottom-up processes of attention. Int. J. Psychophysiol. *46*, 77–84.
76. Dehaene-Lambertz, G. (1997). Electrophysiological correlates of categorical phoneme perception in adults. Neuroreport *8*, 919–924.
77. Delgado-Martínez, I., Nehring, R.B., and Sørensen, J.B. (2007). Differential abilities of SNAP-25 homologs to support neuronal function. J. Neurosci. *27*, 9380–9391.
78. Deurveilher, S., and Semba, K. (2005). Indirect projections from the suprachiasmatic nucleus to major arousal-promoting cell groups in rat: Implications for the circadian control of behavioural state. Neuroscience *130*, 165–183.
79. DIng, C., Emmenegger, V., Schaffrath, K., and Feldmeyer, Di. (2021). Layer-Specific Inhibitory Microcircuits of Layer 6 Interneurons in Rat Prefrontal Cortex. Cereb. Cortex *31*, 32–47.
80. Duchatel, R.J., Shannon Weickert, C., and Tooney, P.A. (2019). White matter neuron biology and neuropathology in schizophrenia. Npj Schizophr. *5*.
81. Duque, D., and Malmierca, M.S. (2015). Stimulus-specific adaptation in the inferior colliculus of the mouse: anesthesia and spontaneous activity effects. Brain Struct. Funct. *220*, 3385–3398.
82. Duque, A., Krsnik, Z., Kostović, I., and Rakic, P. (2016). Secondary expansion of the transient subplate zone in the developing cerebrum of human and nonhuman primates. Proc. Natl. Acad. Sci. U. S. A. *113*, 9892–9897.
83. Dzirasa, K., Santos, L.M., Ribeiro, S., Stapleton, J., Gainetdinov, R.R., Caron, M.G., and Nicolelis, M.A.L. (2009). Persistent hyperdopaminergia decreases the peak frequency of hippocampal theta oscillations during quiet waking and REM sleep. PLoS One *4*.

84. Eastwood, S.L., and Harrison, P.J. (2003). Interstitial white matter neurons express less reelin and are abnormally distributed in schizophrenia: Towards an integration of molecular and morphologic aspects of the neurodevelopmental hypothesis. Mol. Psychiatry *8*, 821–831.
85. Edwards, C.M.B., Abusnana, S., Sunter, D., Murphy, K.G., Ghatei, M.A., and Bloom, S.R. (1999). The effect of the orexins on food intake: Comparison with neuropeptide Y, melanin-concentrating hormone and galanin. J. Endocrinol. *160*, 3–8.
86. Ehlers, C.L., and Somes, C. (2002). Long latency event-related potentials in mice: Effects of stimulus characteristics and strain. Brain Res. *957*, 117–128.
87. Engel, A.K., and Fries, P. (2010). Beta-band oscillations-signalling the status quo? Curr. Opin. Neurobiol. *20*, 156–165.
88. Estabrooke, I. V., McCarthy, M.T., Ko, E., Chou, T.C., Chemelli, R.M., Yanagisawa, M., Saper, C.B., and Scammell, T.E. (2001). Fos expression in orexin neurons varies with behavioral state. J. Neurosci. *21*, 1656–1662.
89. Evans, R., Kimura, H., Nakashima, M., Ishikawa, T., Yukitake, H., Suzuki, M., Hazel, J., Faessel, H., Wu, J., Hang, Y., et al. (2023). Orexin 2 receptor-selective agonist danavorexton (TAK-925) promotes wakefulness in non-human primates and healthy individuals. J. Sleep Res. 1–13.
90. Featherstone, R.E., Melnychenko, O., and Siegel, S.J. (2018). Mismatch negativity in preclinical models of schizophrenia. Schizophr. Res. *191*, 35–42.
91. Feldmeyer, D. (2023). Structure and function of neocortical layer 6b. Front. Cell. Neurosci. 1–16.
92. Fellous, J.M., and Sejnowski, T.J. (2000). Cholinergic induction of oscillations in the hippocampal slice in the slow (0.5-2 Hz), theta (5-12 Hz), and gamma (35-70 Hz) bands. Hippocampus *10*, 187–197.
93. Fendt, M., and Koch, M. (2013). Translational value of startle modulations. Cell Tissue Res. *354*, 287–295.
94. Ferrarelli, F., and Tononi, G. (2017). Reduced sleep spindle activity point to a TRN-MD thalamus-PFC circuit dysfunction in schizophrenia. Schizophr. Res. *180*, 36–43.
95. Fischer, C., Morlet, D., Bouchet, P., Luaute, J., Jourdan, C., and Salord, F. (1999). Mismatch negativity and late auditory evoked potentials in comatose patients. Clin. Neurophysiol. *110*, 1601–1610.
96. Fitzgerald, K., and Todd, J. (2020). Making Sense of Mismatch Negativity. Front. Psychiatry *11*, 1–19.
97. Flores, Á., Saravia, R., Maldonado, R., and Berrendero, F. (2015). Orexins and fear: Implications for the treatment of anxiety disorders. Trends Neurosci. *38*, 550–559.
98. Garrido, M.I., Kilner, J.M., Stephan, K.E., and Friston, K.J. (2009a). The mismatch negativity: A review of underlying mechanisms. Clin. Neurophysiol. *120*, 453–463.
99. Garrido, M.I., Kilner, J.M., Kiebel, S.J., and Friston, K.J. (2009b). Dynamic causal modeling of the response to frequency deviants. J. Neurophysiol. *101*, 2620–2631.
100. Gent, T.C., Bandarabadi, M., Herrera, C.G., and Adamantidis, A.R. (2018). Thalamic dual control of sleep and wakefulness. Nat. Neurosci. *21*, 974–984.
101. Gerfen, C.R., Paletzki, R., and Heintz, N. (2013). GENSAT BAC cre-recombinase driver lines to study the functional organization of cerebral cortical and basal ganglia circuits. Neuron *80*, 1368–1383.
102. Guidi, L., Korrell, K., Hoerder-Suabedissen, A., Oliver, P., Wilson, Mi., O'Kanold, P., Bannerman, D., and Molnár, Z. (2016). The role of cortical layer VIb in mouse behaviour. Soc. Neurosci. Poster Present.
103. Guillaumin, M.C.C., McKillop, L.E., Cui, N., Fisher, S.P., Foster, R.G., De Vos, M., Peirson, S.N., Achermann, P., and Vyazovskiy, V. V. (2018a). Cortical region-specific sleep homeostasis in mice: Effects of time of day and waking experience. Sleep *41*, 1–16.
104. Guillaumin, M.C.C., McKillop, L.E., Cui, N., Fisher, S.P., Foster, R.G., De Vos, M., Peirson, S.N., Achermann, P., and Vyazovskiy, V. V. (2018b). Cortical region-specific sleep homeostasis in mice: Effects of time of day and waking experience. Sleep *41*, 1–16.

105. Guo, W., Clause, A.R., Barth-Maron, A., and Polley, D.B. (2017). A Corticothalamic Circuit for Dynamic Switching between Feature Detection and Discrimination. Neuron *95*, 180-194.e5.
106. Hádinger, N., Bősz, E., Tóth, B., Vantomme, G., Lüthi, A., and Acsády, L. (2023). Region-selective control of the thalamic reticular nucleus via cortical layer 5 pyramidal cells. Nat. Neurosci. *26*, 116–130.
107. Hagan, J.J., Leslie, R.A., Patel, S., Evans, M.L., Wattam, T.A., Holmes, S., Benham, C.D., Taylor, S.G., Routledge, C., Hemmati, P., et al. (1999). Orexin A activates locus coeruleus cell firing and increases arousal in the rat. Proc. Natl. Acad. Sci. USA *96*, 10911–10916.
108. Hahn, M., Joechner, A.K., Roell, J., Schabus, M., Heib, D.P.J., Gruber, G., Peigneux, P., and Hoedlmoser, K. (2019). Developmental changes of sleep spindles and their impact on sleep-dependent memory consolidation and general cognitive abilities: A longitudinal approach. Dev. Sci. *22*, 1–16.
109. Hall, R.D., and Borbely, A.A. (1970). Acoustically evoked potentials in the rat during sleep and waking. Exp. Brain Res. *11*, 93–110.
110. Hanson, P.I., Roth, R., Morisaki, H., Jahn, R., and Heuser, J.E. (1997). Structure and conformational changes in NSF and its membrane receptor complexes visualized by quick-freeze/deep-etch electron microscopy. Cell *90*, 523–535.
111. Hara, J., Beuckmann, C.T., Nambu, T., Willie, J.T., Chemelli, R.M., Sinton, C.M., Sugiyama, F., Yagami, K.I., Goto, K., Yanagisawa, M., et al. (2001). Genetic ablation of orexin neurons in mice results in narcolepsy, hypophagia, and obesity. Neuron *30*, 345–354.
112. Hardin, P.E., Hall, J.C., and Rosbash, M. (1990). Feedback of the Drosophila period gene product on circadian cycling of its messenger RNA levels. Nature *343*, 536–540.
113. Harms, L., Fulham, W.R., Todd, J., Budd, T.W., Hunter, M., Meehan, C., Penttonen, M., Schall, U., Zavitsanou, K., Hodgson, D.M., et al. (2014). Mismatch negativity (MMN) in freely-moving rats with several experimental controls. PLoS One *9*.
114. Harms, L., Michie, P.T., and Näätänen, R. (2016). Criteria for determining whether mismatch responses exist in animal models: Focus on rodents. Biol. Psychol. *116*, 28–35.
115. Harris, K.D., and Shepherd, G.M.G. (2015). The neocortical circuit: Themes and variations. Nat. Neurosci. *18*, 170–181.
116. Harris, K.D., and Thiele, A. (2011). Cortical state and attention. Nat. Rev. Neurosci. *12*, 509–523.
117. Hassani, O.K., Lee, M.G., and Jones, B.E. (2009). Melanin-concentrating hormone neurons discharge in a reciprocal manner to orexin neurons across the sleep-wake cycle. Proc. Natl. Acad. Sci. U. S. A. *106*, 2418–2422.
118. Hay, Y.A., Andjelic, S., Badr, S., and Lambolez, B. (2015). Orexin-dependent activation of layer VIb enhances cortical network activity and integration of non-specific thalamocortical inputs. Brain Struct. Funct. *220*, 3497–3512.
119. Haynes, A.C., Jackson, B., Chapman, H., Tadayyon, M., Johns, A., Porter, R.A., and Arch, J.R.S. (2000). A selective orexin-1 receptor antagonist reduces food consumption in male and female rats. Regul. Pept. *96*, 45–51.
120. Haynes, A.C., Chapman, H., Taylor, C., Moore, G.B.T., Cawthorne, M.A., Tadayyon, M., Clapham, J.C., and Arch, J.R.S. (2002). Anorectic, thermogenic and anti-obesity activity of a selective orexin-1 receptor antagonist in ob/ob mice. Regul. Pept. *104*, 153–159.
121. Helfrich, R.F., Mander, B.A., Jagust, W.J., Knight, R.T., and Walker, M.P. (2018). Old Brains Come Uncoupled in Sleep: Slow Wave-Spindle Synchrony, Brain Atrophy, and Forgetting. Neuron *97*, 221-230.e4.
122. Henning, T., Bandiera, S., and Molnár, Z. (2023). Towards the Transcriptionally based Classification of L6b in the Adult Mouse Brain. Neocortical Neurogenes. Dev. Evol. *6*, 317–330.

123. Herring, W.J., Roth, T., Krystal, A.D., and Michelson, D. (2019). Orexin receptor antagonists for the treatment of insomnia and potential treatment of other neuropsychiatric indications. J. Sleep Res. *28*, 1–15.
124. Heuer, H., Christ, S., Friedrichsen, S., Brauer, D., Winckler, M., Bauer, K., Raivich, G., Heur, H., Christ, S., Friedrichsen, S., et al. (2003). Connective tissue growth factor: a novel marker of VII neurons in the rat cerebral cortex. Neuroscience *119*, 43–52.
125. Hoerder-Suabedissen, A., and Molnár, Z. (2013). Molecular diversity of early-born subplate neurons. Cereb. Cortex *23*, 1473–1483.
126. Hoerder-Suabedissen, A., and Molnár, Z. (2015). Development, evolution and pathology of neocortical subplate neurons. Nat. Rev. Neurosci. *16*, 133–146.
127. Hoerder-Suabedissen, A., Wang, W.Z., Lee, S., Davies, K.E., Goffinet, A.M., Rakić, S., Parnavelas, J., Reim, K., Nicolić, M., Paulsen, O., et al. (2009). Novel markers reveal subpopulations of subplate neurons in the murine cerebral cortex. Cereb. Cortex *19*, 1738–1750.
128. Hoerder-Suabedissen, A., Hayashi, S., Upton, L., Nolan, Z., Casas-Torremocha, D., Grant, E., Viswanathan, S., Kanold, P.O., Clasca, F., Kim, Y., et al. (2018). Subset of cortical layer 6b neurons selectively innervates higher order thalamic nuclei in mice. Cereb. Cortex *28*, 1882–1897.
129. Hoerder-Suabedissen, A., Korrell, K. V., Hayashi, S., Jeans, A., Ramirez, D.M.O., Grant, E., Christian, H.C., Kavalali, E.T., Wilson, M.C., and Molnár, Z. (2019). Cell-specific loss of SNAP25 from cortical projection neurons allows normal development but causes subsequent neurodegeneration. Cereb. Cortex *29*, 2148–2159.
130. Hong, J., Lozano, D.E., Beier, K.T., Chung, S., and Weber, F. (2023). Prefrontal cortical regulation of REM sleep. Nat. Neurosci.
131. Horvath, T.L., Peyron, C., Diano, S., Ivanov, A., Aston-Jones, G., Kilduff, T.S., and Van Den Pol, A.N. (1999). Hypocretin (orexin) activation and synaptic innervation of the locus coeruleus noradrenergic system. J. Comp. Neurol. *415*, 145–159.
132. Http://www.gensat.org, 1 (2023). The Gene Expression Nervous System Atlas (GENSAT) Project, NINDS Contracts N01NS02331 & HHSN271200723701C to The Rockefeller University (New York, NY).
133. Huang, Z.L., Qu, W.M., Li, W.D., Mochizuki, T., Eguchi, N., Watanabe, T., Urade, Y., and Hayaishi, O. (2001). Arousal effect of orexin A depends on activation of the histaminergic system. Proc. Natl. Acad. Sci. U. S. A. *98*, 9965–9970.
134. Huber, R., Ghilardi, M.F., Massimini, M., and Tononi, G. (2004). Local sleep and learning. Nature *430*, 78–81.
135. Hutchison, I.C., and Rathore, S. (2015). The role of REM sleep theta activity in emotional memory. Front. Psychol. *6*, 1–15.
136. Ikeno, T., and Yan, L. (2018). A comparison of the orexin receptor distribution in the brain between diurnal Nile grass rats (Arvicanthis niloticus) and nocturnal mice (Mus musculus). Brain Res. *1690*, 89–95.
137. Irukayama-Tomobe, Y., Ogawa, Y., Tominaga, H., Ishikawa, Y., Hosokawa, N., Ambai, S., Kawabe, Y., Uchida, S., Nakajima, R., Saitoh, T., et al. (2017). Nonpeptide orexin type-2 receptor agonist ameliorates narcolepsy-cataplexy symptoms in mouse models. Proc. Natl. Acad. Sci. U. S. A. *114*, 5731–5736.
138. Ison, J.R., and Allen, P.D. (2003). Low-Frequency Tone Pips Elicit Exaggerated Startle Reflexes in C57BL/6J Mice with Hearing Loss. JARO - J. Assoc. Res. Otolaryngol. *4*, 495–504.
139. Jääskeläinen, I.P., Ahveninen, J., Bonmassar, G., Dale, A.M., Ilmoniemi, R.J., Levänen, S., Lin, F.H., May, P., Melcher, J., Stufflebeam, S., et al. (2004). Human posterior auditory cortex gates novel sounds to consciousness. Proc. Natl. Acad. Sci. U. S. A. *101*, 6809–6814.
140. Jacobs, E.C., Campagnoni, C., Kampf, K., Reyes, S.D., Kalra, V., Handley, V., Xie, Y.Y., Hong-Hu, Y., Spreur, V., Fisher, R.S., et al. (2007). Visualization of corticofugal projections during early cortical development in a τ-GFP-transgenic mouse. Eur. J. Neurosci. *25*, 17–

30.
141. Jessberger, J., Zhong, W., Brankačk, J., and Draguhn, A. (2016). Olfactory Bulb Field Potentials and Respiration in Sleep-Wake States of Mice. Neural Plast. *2016*.
142. Jodo, E., Inaba, H., Narihara, I., Sotoyama, H., Kitayama, E., Yabe, H., Namba, H., Eifuku, S., and Nawa, H. (2019). Neonatal exposure to an inflammatory cytokine, epidermal growth factor, results in the deficits of mismatch negativity in rats. Sci. Rep. *9*, 1–14.
143. Johnson, P.L., Truitt, W., Fitz, S.D., Minick, P.E., Dietrich, A., Sanghani, S., Träskman-Bendz, L., Goddard, A.W., Brundin, L., and Shekhar, A. (2010). A key role for orexin in panic anxiety. Nat. Med. *16*, 111–115.
144. Johnson, S.L., Safieddine, S., Mustapha, M., and Marcotti, W. (2019). Hair cell afferent synapses: Function and dysfunction. Cold Spring Harb. Perspect. Med. *9*, 1–24.
145. Jouvet, M.F. (1959). Corrélations électromyographiques du sommeil chez le Chat décortiqué et mésencéphalique chronique. C. R. Seances Soc. Biol. Fil. *153*, 422–425.
146. Kanold, P.O., and Luhmann, H.J. (2010). The subplate and early cortical circuits. Annu. Rev. Neurosci. *33*, 23–48.
147. Katz, B.Y.B., and Miledi, R. (1963). of Biophysics, University College. 389–422.
148. Keller, G.B., and Mrsic-Flogel, T.D. (2018). Predictive Processing: A Canonical Cortical Computation. Neuron *100*, 424–435.
149. Khodagholy, D., Gelinas, J.N., and Buzsáki, G. (2017). Learning-enhanced coupling between ripple oscillations in association cortices and hippocampus. Science (80-.). *372*, 369–372.
150. Kirkpatrick, B., Messias, N.C., Conley, R.R., and Roberts, R.C. (2003). Interstitial cells of the white matter in the dorsolateral prefrontal cortex in deficit and nondeficit schizophrenia. J. Nerv. Ment. Dis. *191*, 563–567.
151. Kodani, S., Soya, S., and Sakurai, T. (2017). Excitation of gabaergic neurons in the bed nucleus of the stria terminalis triggers immediate transition from non-rapid eye movement sleep to wakefulness in mice. J. Neurosci. *37*, 7164–7176.
152. Koelsch, S., Heinke, W., Sammler, D., and Olthoff, D. (2006). Auditory processing during deep propofol sedation and recovery from unconsciousness. Clin. Neurophysiol. *117*, 1746–1759.
153. Korrell, K. V., Disser, J., Parley, K., Vadisiute, A., Requena-Komuro, M.C., Fodder, H., Pollart, C., Knott, G., Molnár, Z., and Hoerder-Suabedissen, A. (2019). Differential effect on myelination through abolition of activity-dependent synaptic vesicle release or reduction of overall electrical activity of selected cortical projections in the mouse. J. Anat. *235*, 452–467.
154. Kostovic, I., and Rakic, P. (1980). Cytology and time of origin of interstitial neurons in the white matter in infant and adult human and monkey telencephalon. J. Neurocytol. *9*, 219–242.
155. Kostovic, I., and Rakic, P. (1990). Developmental history of the transient subplate zone in the visual and somatosensory cortex of the macaque monkey and human brain. J. Comp. Neurol. *297*, 441–470.
156. Kostović, I. (2020). The enigmatic fetal subplate compartment forms an early tangential cortical nexus and provides the framework for construction of cortical connectivity. Prog. Neurobiol. *194*, 101883.
157. Kostović, I., and Judaš, M. (2010). The development of the subplate and thalamocortical connections in the human foetal brain. Acta Paediatr. Int. J. Paediatr. *99*, 1119–1127.
158. Krone, L.B., Yamagata, T., Blanco-Duque, C., Guillaumin, M.C.C., Kahn, M.C., Akerman, C.J., Hoerder-Suabedissen, A., Molnár, Z., and Vyazovskiy, V. V (2020). A role for the cortex in sleep-wake regulation. BioRxiv *44*, 2020.03.17.996090.
159. Krone, L.B., Yamagata, T., Blanco-Duque, C., Guillaumin, M.C.C., Kahn, M.C., van der Vinne, V., McKillop, L.E., Tam, S.K.E., Peirson, S.N., Akerman, C.J., et al. (2021). A role for the cortex in sleep–wake regulation. Nat. Neurosci. *24*, 1210–1215.

160. Krueger, J., and Obál, F. (1993). A neuronal group theory of sleep function. J. Sleep Res *2*, 63–69.
161. Krueger, J.M., Rector, D.M., Roy, S., Van Dongen, H.P.A., Belenky, G., and Panksepp, J. (2008). Sleep as a fundamental property of neuronal assemblies. Nat. Rev. Neurosci. *9*, 910–919.
162. Kurkela, J.L.O., Lipponen, A., Kyläheiko, I., and Astikainen, P. (2018). Electrophysiological evidence of memory-based detection of auditory regularity violations in anesthetized mice. Sci. Rep. *8*, 1–9.
163. Lakatos, P., O'Connell, M.N., Barczak, A., McGinnis, T., Neymotin, S., Schroeder, C.E., Smiley, J.F., and Javitt, D.C. (2020). The Thalamocortical Circuit of Auditory Mismatch Negativity. Biol. Psychiatry *87*, 770–780.
164. Lambe, E.K., and Aghajanian, G.K. (2003). Hypocretin (orexin) induces calcium transients in single spines postsynaptic to identified thalamocortical boutons in prefrontal slice. Neuron *40*, 139–150.
165. Lambe, E.K., Olausson, P., Horst, N.K., Taylor, J.R., and Aghajanian, G.K. (2005). Hypocretin and nicotine excite the same thalamocortical synapses in prefrontal cortex: Correlation with improved attention in rat. J. Neurosci. *25*, 5225–5229.
166. Laposky, A., Easton, A., Dugovic, C., Walisser, J., Bradfield, C., and Turek, F. (2005). Deletion of the mammalian circadian clock gene BMAL1/Mop3 alters baseline sleep architecture and the response to sleep deprivation. Sleep *28*, 395–409.
167. Lecci, S., Fernandez, L.M.J., Weber, F.D., Cardis, R., Chatton, J.-Y., Born, J., and Lüthi, A. (2017). Coordinated infraslow neural and cardiac oscillations mark fragility and offline periods in mammalian sleep. Sci. Adv. *3*.
168. Lecea, D., Ilduff, T.S.K., Eyron, C.P., Ao, X.G., Oye, P.E.F., Anielson, P.E.D., and Ukuhara, C.F. (1998). The hypocretins : Hypothalamus-specific peptides with neuroexcitatory activity. *95*, 322–327.
169. De Lecea, L., Kilduff, T.S., Peyron, C., Gao, X.B., Foye, P.E., Danielson, P.E., Fukuhara, C., Battenberg, E.L.F., Gautvik, V.T., Bartlett, F.S., et al. (1998). The hypocretins : Hypothalamus-specific peptides with neuroexcitatory activity. Proc. Natl. Acad. Sci. U. S. A. *95*, 322–327.
170. Ledderose, J.M., Zolnik, T.A., Toumazou, M., Trimbuch, T., Rosenmund, C., Eickholt, B.J., Jaeger, D., Larkum, M.E., and Sachdev, R.N. (2023). Layer 1 of somatosensory cortex: An important site for input to a tiny cortical compartment. BioRxiv 1–49.
171. Lee, M.G., Hassani, O.K., and Jones, B.E. (2005). Discharge of identified orexin/hypocretin neurons across the sleep-waking cycle. J. Neurosci. *25*, 6716–6720.
172. Leemburg, S., Vyazovskiy, V. V., Olcese, U., Bassetti, C.L., Tononi, G., and Cirelli, C. (2010). Sleep homeostasis in the rat is preserved during chronic sleep restriction. Proc. Natl. Acad. Sci. U. S. A. *107*, 15939–15944.
173. Li, X., Zhou, W., and Yi, Z. (2022). A glimpse of gender differences in schizophrenia. Gen. Psychiatry *35*, 2–4.
174. Li, Y., Li, S., Wei, C., Wang, H., Sui, N., and Kirouac, G.J. (2010). Orexins in the paraventricular nucleus of the thalamus mediate anxiety-like responses in rats. Psychopharmacology (Berl). *212*, 251–265.
175. Lin, L., Faraco, J., Li, R., Kadotani, H., Rogers, W., Lin, X., Qiu, X., Jong, P.J. de, Nishino, S., and Mignot, E. (1999). The sleep disorder canine narcolepsy is caused by a Mutation in the Hypocretin (Orexin) Receptor 2 Gene. Cell *98*, 365–376.
176. Lindín, M., Zurrón, M., and Díaz, F. (2005). Stimulus intensity effects on P300 amplitude across repetitions of a standard auditory oddball task. Biol. Psychol. *69*, 375–385.
177. Liu, X., Zwiebel, L.J., Hinton, D., Benzer, S., Hall, J.C., and Rosbash, M. (1992). The period gene encodes a predominantly nuclear protein in adult Drosophila. J. Neurosci. *12*, 2735–2744.
178. Loomis, A.L., Harvey, E.N., and Hobart, G. (1935). Further observationson the

potential rhythms of the cerebral cortex during sleep. Science (80-.). *82*, 198–200.
179. Lorente de Nó, R. (1922). La corteza cerebral del ratón (Primera contribución: la corteza acústica). Trab. Lab. Invest. Biol. 41–78.
180. Lu, J., Greco, M.A., Shiromani, P., and Saper, C.B. (2000). Effect of lesions of the ventrolateral preoptic nucleus on NREM and REM sleep. J. Neurosci. *20*, 3830–3842.
181. Lu, J., Zhang, Y.H., Chou, T.C., Gaus, S.E., Elmquist, J.K., Shiromani, R., and Saper, C.B. (2001). Contrasting effects of ibotenate lesions of the paraventricular nucleus and subparaventricular zone on sleep-wake cycle and temperature regulation. J. Neurosci. *21*, 4864–4874.
182. Lu, J., Bjorkum, A.A., Xu, M., Gaus, S.E., Shiromani, P.J., and Saper, C.B. (2002). Selective Activation of the Extended Ventrolateral Preoptic Nucleus during Rapid Eye Movement Sleep. J. Neurosci. *22*, 4568–4576.
183. Mao, B.Q., Hamzei-Sichani, F., Aronov, D., Froemke, R.C., and Yuste, R. (2001). Dynamics of spontaneous activity in neocortical slices. Neuron *32*, 883–898.
184. Marcus, J.N., Aschkenasi, C.J., Lee, C.E., Chemelli, R.M., Saper, C.B., Yanagisawa, M., and Elmquist, J.K. (2001). Differential expression of Orexin receptors 1 and 2 in the rat brain. J. Comp. Neurol. *435*, 6–25.
185. Marques-Smith, A., Lyngholm, D., Kaufmann, A.K., Stacey, J.A., Hoerder-Suabedissen, A., Becker, E.B.E., Wilson, M.C., Molnár, Z., and Butt, S.J.B. (2016). A Transient Translaminar GABAergic Interneuron Circuit Connects Thalamocortical Recipient Layers in Neonatal Somatosensory Cortex. Neuron *89*, 536–549.
186. Marx, M., and Feldmeyer, D. (2013). Morphology and physiology of excitatory neurons in layer 6b of the somatosensory rat barrel cortex. Cereb. Cortex *23*, 2803–2817.
187. Marx, M., Qi, G., Hanganu-Opatz, I.L., Kilb, W., Luhmann, H.J., and Feldmeyer, D. (2017). Neocortical Layer 6B as a Remnant of the Subplate - A Morphological Comparison. Cereb. Cortex *27*, 1011–1026.
188. Massimini, M., Huber, R., Ferrarelli, F., Hill, S., and Tononi, G. (2004). The sleep slow oscillation as a traveling wave. J. Neurosci. *24*, 6862–6870.
189. May, P.J.C., and Tiitinen, H. (2010). Mismatch negativity (MMN), the deviance-elicited auditory deflection, explained. Psychophysiology *47*, 66–122.
190. Maywood, E.S., Chesham, J.E., Winsky-Sommerer, R., and Hastings, M.H. (2021). Restoring the molecular clockwork within the suprachiasmatic hypothalamus of an otherwise clockless mouse enables circadian phasing and stabilization of sleep-wake cycles and reverses memory deficits. J. Neurosci. *41*, 8562–8576.
191. McConnell, S.K., Ghosh, A., and Shatz, C.J. (1989). Subplate neurons pioneer the first axon pathway from the cerebral cortex. Science (80-.). *245*, 978–982.
192. McGinley, M.J., Vinck, M., Reimer, J., Batista-Brito, R., Zagha, E., Cadwell, C.R., Tolias, A.S., Cardin, J.A., and McCormick, D.A. (2015). Waking State: Rapid Variations Modulate Neural and Behavioral Responses. Neuron *87*, 1143–1161.
193. McKillop, L.E., Fisher, S.P., Cui, N., Peirson, S.N., Foster, R.G., Wafford, K.A., and Vyazovskiy, V. V. (2018). Effects of aging on cortical neural dynamics and local sleep homeostasis in mice. J. Neurosci. *38*, 3911–3928.
194. McKillop, L.E., Fisher, S.P., Milinski, L., Krone, L.B., and Vyazovskiy, V. V. (2021). Diazepam effects on local cortical neural activity during sleep in mice. Biochem. Pharmacol. *191*, 114515.
195. Meyer, H.S., Wimmer, V.C., Hemberger, M., Bruno, R.M., De Kock, C.P.J., Frick, A., Sakmann, B., and Helmstaedter, M. (2010). Cell type-specific thalamic innervation in a column of rat vibrissal cortex. Cereb. Cortex *20*, 2287–2303.
196. Miano, S., and Ferri, R. (2010). Epidemiology and Management of Insomnia in Children with Autistic Spectrum Disorders. Pediatr. Drugs *12*, 75–84.
197. Michanski, S., Smaluch, K., Maria Steyer, A., Chakrabarti, R., Setz, C., Oestreicher, D., Fischer, C., Möbius, W., Moser, T., Vogl, C., et al. (2019). Mapping developmental maturation of inner hair cell ribbon synapses in the apical mouse cochlea. Proc. Natl.

Acad. Sci. U. S. A. *116*, 6415–6424.
198. Mieda, M., Willie, J.T., Hara, J., Sinton, C.M., Sakurai, T., and Yanagisawa, M. (2004). Orexin peptides prevent cataplexy and improve wakefulness in an orexin neuron-ablated model of narcolepsy in mice. Proc. Natl. Acad. Sci. U. S. A. *101*, 4649–4654.
199. Mieda, M., Hasegawa, E., Kisanuki, Y.Y., Sinton, C.M., Yanagisawa, M., and Sakurai, T. (2011). Differential roles of orexin receptor-1 and -2 in the regulation of Non-REM and REM sleep. J. Neurosci. *31*, 6518–6526.
200. Mileykovskiy, B.Y., Kiyashchenko, L.I., and Siegel, J.M. (2005). Behavioral correlates of activity in identified hypocretin/orexin neurons. Neuron *46*, 787–798.
201. Milinski, L., Fisher, S.P., Cui, N., McKillop, L.E., Blanco-Duque, C., Ang, G., Yamagata, T., Bannerman, D.M., and Vyazovskiy, V. V. (2021). Waking experience modulates sleep need in mice. BMC Biol. *19*, 1–14.
202. Mobarakeh, J.I., Takahashi, K., Sakurada, S., Nishino, S., Watanabe, H., Kato, M., Naghdi, N., and Yanai, K. (2005). Enhanced antinociception by intracerebroventricularly administered orexin A in histamine H1 or H2 receptor gene knockout mice. Pain *118*, 254–262.
203. Modi, M.E., and Sahin, M. (2017). Translational use of event-related potentials to assess circuit integrity in ASD. Nat. Rev. Neurol. *13*, 160–170.
204. Molnár, Z. (2019). Cortical layer with no known function. Eur. J. Neurosci. *49*, 957–963.
205. Molnár, Z., and Blakemore, C. (1995). How do thalamic axons find their way to the cortex? Cortex *18*, 389–397.
206. Molnár, Z., Adams, R., and Blakemore, C. (1998). Mechanisms underlying the early establishment of thalamocortical connections in the rat. J. Neurosci. *18*, 5723–5745.
207. Morlet, D., and Fischer, C. (2014). MMN and novelty P3 in coma and other altered states of consciousness: A review. Brain Topogr. *27*, 467–479.
208. Moruzzi, G., and Magoun, H. (1949). Brain stem reticular formation and activation of the EEG. EEG Clin Neurophysiol. *1*, 455–473.
209. Mueller, M., Meijer, E., Brown, L., Vyazovskiy, V., Peirson, S., and Molnár, Z. (2022). AUTOMATED AND CONTINUOUS FOOD-INTAKE MEASUREMENT WITH AN OPEN-ACCESS, USER-FRIENDLY, AND COST-EFFECTIVE DEVICE: THE SNACKERTRACKER. LASA Conf. *November 3*.
210. Mukhametov, L.M., Supin, A.Y., and Polyakova, I.G. (1977). Interhemispheric asymmetry of the electroencephalographic sleep patterns in dolphins. Brain Res. *134*, 581–584.
211. Näätänen, R., and Michie, P.T. (1979). Early selective-attention effects on the evoked potential: A critical review and reinterpretation. Biol. Psychol. *8*, 81–136.
212. Näätänen, R., Gaillard, A.W.K., and Mäntysalo, S. (1978). Early selective-attention effect on evoked potential reinterpreted. Acta Psychol. (Amst). *42*, 313–329.
213. Näätänen, R., Paavilainen, P., Rinne, T., and Alho, K. (2007). The mismatch negativity (MMN) in basic research of central auditory processing: A review. Clin. Neurophysiol. *118*, 2544–2590.
214. Nashida, T., Yabe, H., Sato, Y., Hiruma, T., Sutoh, T., Shinozaki, N., and Kaneko, S. (2000). Automatic auditory information processing in sleep. Sleep *23*, 821–828.
215. Naumann, A., Bierbrauer, J., Przuntek, H., and Daum, I. (2001). Attentive and preattentive processing in narcolepsy as revealed by event-related potentials (ERPs). Neuroreport *12*, 2807–2811.
216. Nir, Y., Vyazovskiy, V. V., Cirelli, C., Banks, M.I., and Tononi, G. (2015). Auditory responses and stimulus-specific adaptation in rat auditory cortex are preserved across NREM and REM sleep. Cereb. Cortex *25*, 1362–1378.
217. Nishino, S., Ripley, B., Overeem, S., Lammers, G.J., and Mignot, E. (2000). Hypocretin (orexin) deficiency in human narcolepsy. Lancet *355*, 39–40.

218. O'Reilly, J.A., and Angsuwatanakul, T. (2021). More evidence for a long-latency mismatch response in urethane-anaesthetised mice. Hear. Res. *408*, 108296.
219. O'Reilly, J.A., and Conway, B.A. (2021). Classical and controlled auditory mismatch responses to multiple physical deviances in anaesthetised and conscious mice. Eur. J. Neurosci. *53*, 1839–1854.
220. Obál, F., and Krueger, J.M. (2003). Sleep function. Front. Biosci. 520–550.
221. Olsen, S.R., Bortone, D.S., Adesnik, H., and Scanziani, M. (2012). Gain control by layer six in cortical circuits of vision. Nature *483*, 47–54.
222. Pantoni, M.M., Herrera, G.M., Van Alstyne, K.R., and Anagnostaras, S.G. (2020). Quantifying the Acoustic Startle Response in Mice Using Standard Digital Video. Front. Behav. Neurosci. *14*, 1–9.
223. Park, J., Render, K.P., and Cates, D.W. (2023). Daridorexant: Comprehensive Review of A New Oral Agent for the Treatment of Insomnia. Ann. Pharmacother.
224. Parras, G.G., Casado-Román, L., Schröger, E., and Malmierca, M.S. (2021). The posterior auditory field is the chief generator of prediction error signals in the auditory cortex. Neuroimage *242*, 118446.
225. Patke, A., Young, M.W., and Axelrod, S. (2020). Molecular mechanisms and physiological importance of circadian rhythms. Nat. Rev. Mol. Cell Biol. *21*, 67–84.
226. Paxinos, G., and Franklin, K.B.J. (2003). The mouse brain in stereotaxic coordinates (Academic Press).
227. Pérez-González, D., and Malmierca, M.S. (2014). Adaptation in the auditory system: An overview. Front. Integr. Neurosci. *8*, 1–10.
228. Perrenoud, Q., Rossier, J., Geoffroy, H., Vitalis, T., and Gallopin, T. (2013). Diversity of gabaergic interneurons in layer VIa and VIb of mouse barrel cortex. Cereb. Cortex *23*, 423–441.
229. Petrovich, G.D., Ross, C.A., Holland, P.C., and Gallagher, M. (2007). Medial prefrontal cortex is necessary for an appetitive contextual conditioned stimulus to promote eating in sated rats. J. Neurosci. *27*, 6436–6441.
230. Peyron, C., Tighe, D.K., Van Den Pol, A.N., De Lecea, L., Heller, H.C., Sutcliffe, J.G., and Kilduff, T.S. (1998). Neurons containing hypocretin (orexin) project to multiple neuronal systems. J. Neurosci. *18*, 9996–10015.
231. Peyron, C., Faraco, J., Rogers, W., Ripley, B., Overeem, S., Charnay, Y., Nevsimalova, S., Aldrich, M., Reynolds, D., Albin, R., et al. (2000). A mutation in a case of early onset narcolepsy and a generalized absence of hypocretin peptides in human narcoleptic brains. Nat. Med. *6*, 991–997.
232. Piper, D.C., Upton, N., Smith, M.I., and Hunter, A.J. (2000). The novel brain neuropeptide, orexin-A, modulates the sleep-wake cycle of rats. Eur. J. Neurosci. *12*, 726–730.
233. Poirier, M.A., Xiao, W., Macosko, J.C., Chan, C., Shin, Y.-K., and Bennett, M.K. (1998). The synaptic SNARE complex is a parallel four-stranded helical bundle. Nat. Struct. Biol. *5*, 765–769.
234. Van Den Pol, A.N. (1999). Hypothalamic hypocretin (orexin): Robust innervation of the spinal cord. J. Neurosci. *19*, 3171–3182.
235. Porkka-Heiskanen, T., Kalinchuk, A., Alanko, L., Huhtaniemi, I., and Stenberg, D. (2004). Orexin A and B levels in the hypothalamus of female rats: The effects of the estrous cycle and age. Eur. J. Endocrinol. *150*, 737–742.
236. Poulet, J.F.A., and Petersen, C.C.H. (2008). Internal brain state regulates membrane potential synchrony in barrel cortex of behaving mice. Nature *454*, 881–885.
237. Price, D.J., Aslam, S., Tasker, L., and Gillies, K. (1997). Fates of the earliest generated cells in the developing murine neocortex. J. Comp. Neurol. *377*, 414–422.
238. Price, J., Blau, J., Rothenfluh, A., Abodeely, M., Kloss, B., and Young, M. (1998). double-time Is a Novel Drosophila Clock Gene that Regulates PERIOD Protein Accumulation Jeffrey. Cell *94*, 83–95.
239. Prieto, J.J., and Winer, J.A. (1999). Layer VI in cat primary auditory cortex: Golgi

study and sublaminar origins of projection neurons. J. Comp. Neurol. *404*, 332–358.
240. Radnikow, G., and Feldmeyer, D. (2018). Layer- and cell type-specific modulation of excitatory neuronal activity in the neocortex. Front. Neuroanat. *12*.
241. Ramon Y Cajál, S. (1904). Textura del sistema nervioso del hombre y de los vertebrados : estudios sobre el plan estructural y composición histológica de los centros nerviosos adicionados de consideraciones fisiológicas fundadas en los nuevos descubrimientos. (Santiago).
242. Rechtschaffen, A., and Bergmann, B.M. (2002). Sleep deprivation in the rat: An update of the 1989 paper. Sleep *25*, 18–24.
243. Reep, R.L. (2000). Cortical layer VII and persistent subplate cells in mammalian brains. Brain. Behav. Evol. *56*, 212–234.
244. Reppert, S.M., and Weaver, D.R. (2002). Coordination of circadian clocks in mammals. Nature *418*, 935–941.
245. Rieger, M., Mayer, G., and Gauggel, S. (2003). Attention deficits in patients with narcolepsy. Sleep *26*, 36–43.
246. Rizo, J., and Südhof, T.C. (2012). The membrane fusion enigma: SNAREs, Sec1/Munc18 proteins, and their accomplices guilty as charged?
247. Rodriguez, R.A., Bussière, M., Froeschl, M., and Nathan, H.J. (2014). Auditory-evoked potentials during coma: Do they improve our prediction of awakening in comatose patients? J. Crit. Care *29*, 93–100.
248. Rolls, E.T. (2023). The orbitofrontal cortex, food reward, body weight and obesity. Soc. Cogn. Affect. Neurosci. *18*, 1–19.
249. Ruhnau, P., Herrmann, B., and Schröger, E. (2012). Finding the right control: The mismatch negativity under investigation. Clin. Neurophysiol. *123*, 507–512.
250. Ruusuvirta, T., Penttonen, M., and Korhonen, T. (1998). Auditory cortical event-related potentials to pitch deviances in rats. Neurosci. Lett. *248*, 45–48.
251. Sakurai, T. (2007). The neural circuit of orexin (hypocretin): Maintaining sleep and wakefulness. Nat. Rev. Neurosci. *8*, 171–181.
252. Sakurai, T. (2014). The role of orexin in motivated behaviours. Nat. Rev. Neurosci. *15*, 719–731.
253. Sakurai, T., Amemiya, A., Ishii, M., Matsuzaki, I., Chemelli, R.M., Tanaka, H., Williams, S.C., Richardson, J.A., Kozlowski, G.P., Wilson, S., et al. (1998). Orexins and orexin receptors: A family of hypothalamic neuropeptides and G protein-coupled receptors that regulate feeding behavior. Cell *92*, 573–585.
254. Sakurai, T., Nagata, R., Yamanaka, A., Kawamura, H., Tsujino, N., Muraki, Y., Kageyama, H., Kunita, S., Takahashi, S., Goto, K., et al. (2005). Input of orexin/hypocretin neurons revealed by a genetically encoded tracer in mice. Neuron *46*, 297–308.
255. Sambeth, A., Maes, J.H.R., Van Luijtelaar, G., Molenkamp, I.B.S., Jongsma, M.L.A., and Van Rijn, C.M. (2003). Auditory event-related potentials in humans and rats: Effects of task manipulation. Psychophysiology *40*, 60–68.
256. Santos, T.C., Wierda, K., Broeke, J.H., Toonen, R.F., and Verhage, M. (2017). Early golgi abnormalities and neurodegeneration upon loss of presynaptic proteins munc18-1, syntaxin-1, or SNAP-25. J. Neurosci. *37*, 4525–4539.
257. Saper, C., Scammell, T., and Lu, J. (2005). Hypothalamic regulation of sleep and circadian rhythms. Nature *437*, 1257–1263.
258. Saper, C.B., Chou, T.C., and Scammell, T.E. (2001). The sleep switch: hypothalamic control of sleep and wakefulness. Trends Neurosci. *24*, 726–731.
259. Saper, C.B., Fuller, P.M., Pedersen, N.P., Lu, J., and Scammell, T.E. (2010). Sleep State Switching. Neuron *68*, 1023–1042.
260. Sasaki, K., Suzuki, M., Mieda, M., Tsujino, N., Roth, B., and Sakurai, T. (2011). Pharmacogenetic modulation of orexin neurons alters sleep/wakefulness states in mice. PLoS One *6*.
261. Satoh, K., and Fibiger, H.C. (1986). Cholinergic neurons of the laterodorsal tegmental nucleus: Efferent and afferent connections. J. Comp. Neurol. *253*, 277–302.

262. Schabus, M., Dang-Vu, T.T., Albouy, G., Balteau, E., Boly, M., Carrier, J., Darsaud, A., Degueldre, C., Desseilles, M., Gais, S., et al. (2007). Hemodynamic cerebral correlates of sleep spindles during human non-rapid eye movement sleep. Proc. Natl. Acad. Sci. U. S. A. *104*, 13164–13169.
263. Scheffzük, C., Kukushka, V.I., Vyssotski, A.L., Draguhn, A., Tort, A.B.L., and Brankačk, J. (2011). Selective coupling between theta phase and neocortical fast gamma oscillations during REM-sleep in mice. PLoS One *6*, 1–9.
264. Schröger, E., and Wolff, C. (1996). Mismatch response of the human brain to changes in sound location. Neuroreport 3005–3008.
265. Schwartz, W.J., and Zimmerman, P. (1990). Circadian timekeeping in BALB/c and C57BL/6 inbred mouse strains. J. Neurosci. *10*, 3685–3694.
266. Shelley, A.M., Silipo, G., and Javitt, D.C. (1999). Diminished responsiveness of ERPs in schizophrenic subjects to changes in auditory stimulation parameters: Implications for theories of cortical dysfunction. Schizophr. Res. *37*, 65–79.
267. Sherin, J.E., Shiromani, P.J., McCarley, R.W., and Saper, C.B. (1996). Activation of ventrolateral preoptic neurons during sleep. Science (80-.). *271*, 216–219.
268. Sherin, J.E., Elmquist, J.K., Torrealba, F., and Saper, C.B. (1998). Innervation of histaminergic tuberomammillary neurons by GABAergic and galaninergic neurons in the ventrolateral preoptic nucleus of the rat. J. Neurosci. *18*, 4705–4721.
269. Sherman, S.M., and Guillery, R.W. (1996). Functional organization of thalamocortical relays. J. Neurophysiol. *76*, 1367–1395.
270. Sherman, S.M., Guillery, R.W., Sherman, S.M., and Guillery, R.W. (2014). An Introduction to Thalamocortical Pathways. Funct. Connect. Cortical Areas 1–16.
271. Shinba, T. (1997). Event-related potentials of the rat during active and passive auditory oddball paradigms. Electroencephalogr. Clin. Neurophysiol. - Evoked Potentials *104*, 447–452.
272. Shipp, S. (2016). Neural elements for predictive coding. Front. Psychol. *7*, 1–21.
273. Siegel, C., Waldo, M., Mizner, G., Adler, L.E., and Freedman, R. (1984). Deficits in Sensory Gating in Schizophrenic Patients and Their Relatives: Evidence Obtained With Auditory Evoked Responses. Arch. Gen. Psychiatry *41*, 607–612.
274. Siegel, S.J., Connolly, P., Liang, Y., Lenox, R.H., Gur, R.E., Bilker, W.B., Kanes, S.J., and Turetsky, B.I. (2003). Effects of strain, novelty, and NMDA blockade on auditory-evoked potentials in mice. Neuropsychopharmacology *28*, 675–682.
275. Siwicki, K.K., Eastman, C., Petersen, G., Rosbash, M., and Hall, J.C. (1988). Antibodies to the period gene product of drosophila reveal diverse tissue distribution and rhythmic changes in the visual system. Neuron *1*, 141–150.
276. Söllner, T., Bennett, M.K., Whiteheart, S.W., Scheller, R.H., and Rothman, J.E. (1993). A protein assembly-disassembly pathway in vitro that may correspond to sequential steps of synaptic vesicle docking, activation, and fusion. Cell *75*, 409–418.
277. Song, C. hui, Chen, X. wei, Xia, J. xia, Yu, Z. ping, and Hu, Z. an (2006). Modulatory effects of hypocretin-1/orexin-A with glutamate and γ-aminobutyric acid on freshly isolated pyramidal neurons from the rat prefrontal cortex. Neurosci. Lett. *399*, 101–105.
278. Steriade, M., Nunez, A., and Amzica, F. (1993a). A novel slow (< 1 Hz) oscillation of neocortical neurons in vivo: Depolarizing and hyperpolarizing components. J. Neurosci. *13*, 3252–3265.
279. Steriade, M., McCormick, D.A., and Sejnowski, T.J. (1993b). Thalamocortical oscillations in the sleeping and aroused brain. Science (80-.). *262*, 679–685.
280. Steriade, M., Contreras, D., Dossi, R.C., and Nunez, A. (1993c). The slow (<1 Hz) oscillation in reticular thalamic and thalamocortical neurons: Scenario of sleep rhythm generation in interacting thalamic and neocortical networks. J. Neurosci. *13*, 3284–3299.
281. Steriade, M., Timofeev, I., and Grenier, F. (2001). Natural waking and sleep states: A view from inside neocortical neurons. J. Neurophysiol. *85*, 1969–1985.
282. Strauss, M., Sitt, J.D., King, J.R., Elbaz, M., Azizi, L., Buiatti, M., Naccache, L., Van Wassenhove, V., and Dehaene, S. (2015). Disruption of hierarchical predictive coding

during sleep. Proc. Natl. Acad. Sci. U. S. A. *112*, E1353–E1362.
283. Südhof, T.C., and Rothman, J.E. (2009). Membrane fusion: Grappling with SNARE and SM proteins. Science (80-.).
284. Sulaman, B.A., Wang, S., Tyan, J., and Eban-Rothschild, A. (2023). Neuro-orchestration of sleep and wakefulness. Nat. Neurosci. *26*, 196–212.
285. Sutton, R.B., Fasshauer, D., Jahn, R., and Brunger, A.T. (1998). Crystal structure of a SNARE complex involved in synaptic exocytosis at 2.4 A resolution. Nature *395*, 347–353.
286. Suzuki, M., Beuckmann, C.T., Shikata, K., Ogura, H., and Sawai, T. (2005). Orexin-A (hypocretin-1) is possibly involved in generation of anxiety-like behavior. Brain Res. *1044*, 116–121.
287. Swiegers, J., Bhagwandin, A., Sherwood, C.C., Bertelsen, M.F., Maseko, B.C., Hemingway, J., Rockland, K.S., Molnár, Z., and Manger, P.R. (2019). The distribution, number, and certain neurochemical identities of infracortical white matter neurons in a lar gibbon (Hylobates lar) brain. J. Comp. Neurol. *527*, 1633–1653.
288. Swiegers, J., Bhagwandin, A., Williams, V.M., Maseko, B.C., Sherwood, C.C., Hård, T., Bertelsen, M.F., Rockland, K.S., Molnár, Z., and Manger, P.R. (2021a). The distribution, number, and certain neurochemical identities of infracortical white matter neurons in a chimpanzee (Pan troglodytes) brain. J. Comp. Neurol. *529*, 3429–3452.
289. Swiegers, J., Bhagwandin, A., Maseko, B.C., Sherwood, C.C., Hård, T., Bertelsen, M.F., Spocter, M.A., Molnár, Z., and Manger, P.R. (2021b). The distribution, number, and certain neurochemical identities of infracortical white matter neurons in the brains of a southern lesser galago, a black-capped squirrel monkey, and a crested macaque.
290. Tabuchi, S., Tsunematsu, T., Black, S.W., Tominaga, M., Maruyama, M., Takagi, K., Minokoshi, Y., Sakurai, T., Kilduff, T.S., and Yamanaka, A. (2014). Conditional ablation of orexin/hypocretin neurons: A new mouse model for the study of narcolepsy and orexin system function. J. Neurosci. *34*, 6495–6509.
291. Tafoya, L.C.R., William, C.W., Yanagawa, Y., Obata, K., and Wilson, M.C. (2008). The role of the t-SNARE SNAP-25 in action potential-dependent calcium signaling and expression in GABAergic and glutamatergic neurons. BMC Neurosci. *9*.
292. Tantirigama, M.L.S., Zolnik, T., Judkewitz, B., Larkum, M.E., and Sachdev, R.N.S. (2020). Perspective on the Multiple Pathways to Changing Brain States. *14*, 1–10.
293. Ten-Blanco, M., Flores, Á., Cristino, L., Pereda-Pérez, I., and Berrendero, F. (2023). Targeting the orexin/hypocretin system for the treatment of neuropsychiatric and neurodegenerative diseases: From animal to clinical studies. Front. Neuroendocrinol. *69*.
294. Tervaniemi, M., Maury, S., and Näätänen, R. (1994). Neural representations of abstract stimulus features in the human brain as reflected by the mismatch negativity. Neuroreport *5*, 844–846.
295. Thakkar, M.M., Ramesh, V., Strecker, R.E., and McCarley, R.W. (2001). Microdialysis perfusion of orexin-A in the basal forebrain increases wakefulness in freely behaving rats. Arch. Ital. Biol. *139*, 313–328.
296. Thannickal, T.C., Moore, R.Y., Nienhuis, R., Ramanathan, L., Gulyani, S., Aldrich, M., Cornford, M., and Siegel, J.M. (2000). Reduced number of hypocretin neurons in human narcolepsy. Neuron *27*, 469–474.
297. Thomas, C.W., Guillaumin, M.C.C., McKillop, L.E., Achermann, P., and Vyazovskiy, V. V. (2020). Global sleep homeostasis reflects temporally and spatially integrated local cortical neuronal activity. Elife *9*, 1–25.
298. Thomas, C.W., Blanco-Duque, C., Bréant, B.J., Goodwin, G.M., Sharp, T., Bannerman, D.M., and Vyazovskiy, V. V. (2022). Psilocin acutely alters sleep-wake architecture and cortical brain activity in laboratory mice. Transl. Psychiatry *12*, 1–13.
299. Thomson, A.M. (2010). Neocortical layer 6, a review. Front. Neuroanat. *4*, 1–14.
300. Timofeev, I., Grenier, F., Bazhenov, M., Sejnowski, T.J., and Steriade, M. (2000). Origin of slow cortical oscillations in deafferented cortical slabs. Cereb. Cortex *10*, 1185–

1199.
301. Tone, D., Ode, K.L., Zhang, Q., Fujishima, H., Yamada, R.G., Nagashima, Y., Matsumoto, K., Wen, Z., Yoshida, S.Y., Mitani, T.T., et al. (2022). Distinct phosphorylation states of mammalian CaMKIIβ control the induction and maintenance of sleep.
302. Torres-Reveron, J., and Friedlander, M.J. (2007). Properties of persistent postnatal cortical subplate neurons. J. Neurosci. *27*, 9962–9974.
303. Tossell, K., Yu, X., Giannos, P., Anuncibay Soto, B., Nollet, M., Yustos, R., Miracca, G., Vicente, M., Miao, A., Hsieh, B., et al. (2023). Somatostatin neurons in prefrontal cortex initiate sleep-preparatory behavior and sleep via the preoptic and lateral hypothalamus. Nat. Neurosci.
304. Traut, J., Mengual, J.P., Meijer, E.J., McKillop, L.E., Alfonsa, H., Hoerder-Suabedissen, A., Song, S.H., Fehér, K.D., Riemann, D., Molnar, Z., et al. (2023). Effects of clozapine-N-oxide and compound 21 on sleep in laboratory mice. Elife *12*, 1–23.
305. Trivedi, P., Yu, H., MacNeil, D.J., Van Der Ploeg, L.H.T., and Guan, X.M. (1998). Distribution of orexin receptor mRNA in the rat brain. FEBS Lett. *438*, 71–75.
306. Tsujino, N., and Sakurai, T. (2013). Role of orexin in modulating arousal, feeding and motivation. Front. Behav. Neurosci. *7*, 1–14.
307. Ulanovsky, N., Las, L., and Nelken, I. (2003). Processing of low-probability sounds by cortical neurons. Nat. Neurosci. *6*, 391–398.
308. Umbricht, D., Vyssotky, D., Latanov, A., Nitsch, R., Brambilla, R., D'Adamo, P., and Lipp, H.P. (2004). Midlatency auditory event-related potentials in mice: Comparison to midlatency auditory ERPs in humans. Brain Res. *1019*, 189–200.
309. Umbricht, D., Vyssotki, D., Latanov, A., Nitsch, R., and Lipp, H.P. (2005). Deviance-related electrophysiological activity in mice: Is there mismatch negativity in mice? Clin. Neurophysiol. *116*, 353–363.
310. Vadisiute, A., Meijer, E., Szabó, F., Hoerder-Suabedissen, A., Kawashita, E., Hayashi, S., and Molnár, Z. (2022). The role of snare proteins in cortical development. Dev. Neurobiol. *82*, 457–475.
311. Valente, M., Castiñeiras-De Saa, J.R., Renart, A., and Pardo-Vazquez, J.L. (2023). Ratphones: An Affordable Tool for Highly Controlled Sound Presentation in Freely Moving Rats. ENeuro *10*, 1–5.
312. Valverde, F., Facal-valverde, M.V., Santacana, M., and Heredia, M. (1989). Development and differentiation of early generated cells of sublayer VIb in the somatosensory cortex of the rat: A correlated Golgi and autoradiographic study. J. Comp. Neurol. *290*, 118–140.
313. Vandevelde, I.L., Duckworth, E., and Reep, R.L. (1996). Layer VII and the gray matter trajectories of corticocortical axons in rats. Anat. Embryol. (Berl). *194*, 581–593.
314. Vassalli, A., and Franken, P. (2017). Hypocretin (orexin) is critical in sustaining theta/gamma-rich waking behaviors that drive sleep need. Proc. Natl. Acad. Sci. U. S. A. *114*, E5464–E5473.
315. Velluti, R.A. (1997). Interactions between sleep and sensory physiology. J. Sleep Res. *6*, 61–77.
316. Viswanathan, S., Sheikh, A., Looger, L.L., and Kanold, P.O. (2017). Molecularly Defined Subplate Neurons Project Both to Thalamocortical Recipient Layers and Thalamus. Cereb. Cortex *27*, 4759–4768.
317. Vosshall, L.B., Price, J.L., Sehgal, A., Saez, L., and Young, M.W. (1994). Block in nuclear localization of period protein by a second clock mutation, timeless. Science (80-.). *263*, 1606–1609.
318. Vyazovskiy, V. V., and Harris, K.D. (2013). Sleep and the single neuron: The role of global slow oscillations in individual cell rest. Nat. Rev. Neurosci. *14*, 443–451.
319. Vyazovskiy, V. V., and Tobler, I. (2005). Theta activity in the waking EEG is a marker of sleep propensity in the rat. Brain Res. *1050*, 64–71.
320. Vyazovskiy, V. V., Olcese, U., Lazimy, Y.M., Faraguna, U., Esser, S.K., Williams, J.C., Cirelli, C., and Tononi, G. (2009). Cortical Firing and Sleep Homeostasis. Neuron *63*, 865–

878.
321. Vyazovskiy, V. V., Olcese, U., Hanlon, E.C., Nir, Y., Cirelli, C., and Tononi, G. (2011). Local sleep in awake rats. Nature *472*, 443–447.
322. Waite, F., Myers, E., Harvey, A.G., Espie, C.A., Startup, H., Sheaves, B., and Freeman, D. (2016). Treating Sleep Problems in Patients with Schizophrenia. Behav. Cogn. Psychother. *44*, 273–287.
323. Wang, W.Z., Hoerder-Suabedissen, A., Oeschger, F.M., Bayatti, N., Ip, B.K., Lindsay, S., Supramaniam, V., Srinivasan, L., Rutherford, M., Møllgård, K., et al. (2010). Subplate in the developing cortex of mouse and human. J. Anat. *217*, 368–380.
324. Washbourne, P., Thompson, P.M., Carta, M., Costa, E.T., Mathews, J.R., Lopez-Benditó, G., Molnár, Z., Becher, M.W., Valenzuela, C.F., Partridge, L.D., et al. (2002). Genetic ablation of the t-SNARE SNAP-25 distinguishes mechanisms of neuroexocytosis. Nat. Neurosci. *5*, 19–26.
325. Wenger Combremont, A.L., Bayer, L., Dupré, A., Mühlethaler, M., and Serafin, M. (2016a). Slow bursting neurons of mouse cortical layer 6b are depolarized by hypocretin/orexin and major transmitters of arousal. Front. Neurol. *7*, 1–9.
326. Wenger Combremont, A.L., Bayer, L., Dupré, A., Mühlethaler, M., and Serafin, M. (2016b). Effects of Hypocretin/Orexin and Major Transmitters of Arousal on Fast Spiking Neurons in Mouse Cortical Layer 6B. Cereb. Cortex *26*, 3553–3562.
327. Werling, D.M., and Geschwind, D.H. (2013). Sex differences in autism spectrum disorders. Curr. Opin. Neurol. *26*, 146–153.
328. Willie, J.T., Chemelli, R.M., Sinton, C.M., Tokita, S., Williams, S.C., Kisanuki, Y.Y., Marcus, J.N., Lee, C., Elmquist, J.K., Kohlmeier, K.A., et al. (2003). Distinct narcolepsy syndromes in orexin receptor-2 and orexin null mice: Molecular genetic dissection of non-REM and REM sleep regulatory processes. Neuron *38*, 715–730.
329. Willie, J.T., Takahira, H., Shibahara, M., Hara, J., Nomiyama, M., Yanagisawa, M., and Sakurai, T. (2011). Ectopic overexpression of orexin alters sleep/wakefulness states and muscle tone regulation during REM sleep in mice. J. Mol. Neurosci. *43*, 155–161.
330. Wimmer, V.C., Bruno, R.M., De Kock, C.P.J., Kuner, T., and Sakmann, B. (2010). Dimensions of a projection column and architecture of VPM and POm axons in rat vibrissal cortex. Cereb. Cortex *20*, 2265–2276.
331. Wisor, J.P., O'Hara, B.F., Terao, A., Selby, C.P., Kilduff, T.S., Sancar, A., Edgar, D.M., and Franken, P. (2002). A role of cryptochromes in sleep regulation. BMC Neurosci. *3*, 1–14.
332. Xia, J.X., Chen, X.W., Cheng, S.Y., and Hu, Z.A. (2005). Mechanisms of orexin A-evoked changes of intracellular calcium in primary cultured cortical neurons. Neuroreport *16*, 783–786.
333. Yamagata, T., Kahn, M.C., Prius-Mengual, J., Meijer, E., Sabanovi, M., Guillaumin, M.C.C., van der Vinne, V., Huang, Y.G., McKillop, L.E., Jagannath, A., et al. (2021). The hypothalamic link between arousal and sleep homeostasis in mice. Proc. Natl. Acad. Sci. U. S. A. *118*, 1–12.
334. Yamaguchi, S., Globus, H., and Knight, R.T. (1993). P3-like potential in rats. Electroencephalogr. Clin. Neurophysiol. Evoked Potentials *88*, 151–154.
335. Yamanaka, A., Beuckmann, C.T., Willie, J.T., Hara, J., Tsujino, N., Mieda, M., Tominaga, M., Yagami, K.I., Sugiyama, F., Goto, K., et al. (2003). Hypothalamic orexin neurons regulate arousal according to energy balance in mice. Neuron *38*, 701–713.
336. Yan, J., He, C., Xia, J.X., Zhang, D., and Hu, Z.A. (2012a). Orexin-A excites pyramidal neurons in layer 2/3 of the rat prefrontal cortex. Neurosci. Lett. *520*, 92–97.
337. Yan, J., He, C., Xia, J.X., Zhang, D., and Hu, Z.A. (2012b). Orexin-A excites pyramidal neurons in layer 2/3 of the rat prefrontal cortex. Neurosci. Lett. *520*, 92–97.
338. Yoshida, K., McCormack, S., España, R.A., Crocker, A., and Scammell, T.E. (2006). Afferents to the orexin neurons of the rat brain. J. Comp. Neurol. *494*, 845–861.
339. Yoshida, Y., Fujiki, N., Nakajima, T., Ripley, B., Matsumura, H., Yoneda, H., Mignot, E., and Nishino, S. (2001). Fluctuation of extracellular hypocretin-1 (orexin A) levels in

the rat in relation to the light-dark cycle and sleep-wake activities. Eur. J. Neurosci. *14*, 1075–1081.

340. Zehring, W.A., Wheeler, D.A., Reddy, P., Konopka, R.J., Kyriacou, C.P., Rosbash, M., and Hall, J.C. (1984). P-element transformation with period locus DNA restores rhythmicity to mutant, arrhythmic drosophila melanogaster. Cell *39*, 369–376.

341. Zolnik, T.A., Ledderose, J., Toumazou, M., Trimbuch, T., Oram, T., Rosenmund, C., Eickholt, B.J., Sachdev, R.N.S., and Larkum, M.E. (2020). Layer 6b Is Driven by Intracortical Long-Range Projection Neurons. Cell Rep. *30*, 3492-3505.e5.

342. Zolnik, T.A., Bronec, A., Ross, A., Staab, M., Sachdev, R.N.S., Molnár, Z., Eickholt, B.J., and Larkum, M.E. (2023). Layer 6b controls brain state via apical dendrites and the higher-order thalamocortical system. Neuron 1–16.